CEDR
Conférence Européenne des Directeurs des Routes
Conference of European Directors of Roads

# CEDR TRANSNATIONAL ROAD RESEARCH PROGRAMME 2018


# D2.2 – Final report on the main results of WP2 (including M2.1, M2.2. and M2.3) – Acoustic assessment of the intrinsic performances of noise barriers

| | |
|---|---|
| **Document** | 20210408_spnWP2_D2.2.docx |
| **Main Editor(s)** | Marco Conter (AIT), all contributors will be mentioned on the title page of each task report |
| **Due Date** | February 2021 |
| **Delivery Date** | April 2021 |
| **Work Package** | WP2 - State of the art on the intrinsic acoustic performance assessment of noise barriers |
| **Tasks** | T2.1 - Review of the physical significance of EN1793-1, -2, -5 and -6<br>T2.2 - Update and analysis of noise barrier database including new current measurements<br>T2.3 - Influence of acoustic degradation of noise barriers on the total noise reduction |
| **Dissemination Level** | Public |

A-tech AIT bast ERF

# Introduction and structure of deliverable report D2.2

The present document summarises all findings achieved in the frame of work package 2 (WP2) of the SOPRANOISE project. This work package was started in January 2020 and was completed in February 2021 and was structured in the following tasks:

- T2.1 - Review of the physical significance of EN1793-1, -2, -5 and -6;
- T2.2 - Update and analysis of noise barrier database including new current measurements;
- T2.3 - Influence of acoustic degradation of noise barriers on the total noise reduction.

The general objective of WP2 was to provide both theoretical and practical background information on measurement methods of the acoustic performance of noise barriers.

Therefore, first a systematic research on the State of the Art regarding available correlations in the literature and trends between measurement results of methods under diffuse sound field conditions and methods under direct sound field conditions was performed. The results of this work have been summarised in the report D2.1, delivered in June 2020, which also represents the achievements of milestone M2.1 (*State of the Art on the physical significance of the different measurement methods*) as a final output of task T2.1. This task report has been included in this document as a final output of task T2.1 and it is the first part of the present deliverable D2.2.

Secondly, as the main objective of task T2.2 was the update and analysis of noise barrier database including new current measurements, the WP2 activities was focused on extending the relevant database of European noise barriers developed within the QUIESST project, including single-number ratings and third-octave band spectra from manufactured products and already installed noise barriers. This updated database aims to show facts and figures about acoustic performances obtained from measurements performed under diffuse sound field as well as direct sound field conditions, together with a better understanding of the respective significance, similarities and differences of these standardized methods. The results of the analysis performed within this task are summarised in the second part of the present document, showing the achievement of milestone M2.2 (*Update and analysis of the noise barrier database including new measurements*).

Finally, within task T2.3, the effect of acoustic degradation on the global acoustic performance of noise barriers was considered in detail. The results of this work are reported in the task report T2.3, which shows the achievement of milestone M2.3 (*Influence of acoustic degradation of noise barriers on the total noise reduction*) and represents the third and last part of the present document D2.2.

CEDR
Conférence Européenne des Directeurs des Routes
Conference of European Directors of Roads

## CEDR TRANSNATIONAL ROAD RESEARCH PROGRAMME 2018

SOPRANOISE

# T2.1 report – Review of the physical significance of EN 1793-1, EN 1793-2, EN 1793-5 and EN 1793-6

## June 2020

| | |
|---|---|
| **Document** | 20210408_spnWP2_T2.1_D2.1.docx |
| **Main Editor(s)** | Paul Reiter, Andreas Fuchs (AIT) with the contribution of Massimo Garai (UNIBO), Wolfram Bartolomaeus (BASt) and Marco Conter (AIT) |
| **Due Date** | June 2020 |
| **Delivery Date** | June 2020, revised in April 2021 |
| **Work Package** | WP2 – State of the Art on the intrinsic acoustic performance assessment of NB |
| **Task** | T2.1 - Review of the physical significance of EN 1793-1, -2, -5 -6 |
| **Dissemination Level** | Public |

Atech AIT bast

# Table of Contents

# Table of Figures

# 1 Overview of SOPRANOISE WP2

The objective of work package 2 of SOPRANOISE is to provide theoretical and practical background information on the measurement of the acoustic performance of noise barriers.

This report shows the achievement of milestone M2.1 (State of the Art on the physical significance of the different measurement methods) and is the final output of task 2.1 (Review of the physical significance of EN1793-1, -2, -5 and -6), providing the state of the art regarding correlations and possible trends between diffuse and direct sound field methods. A database of the EU noise barrier market, including manufactured products and already installed noise barriers has been created. This database aims to show facts and figures about acoustic performances obtained from both the diffuse sound field and direct sound field methods, together with a better understanding of the respective significance, similarities and differences of these standardized methods. The final results will be presented in the report T2.2, which is the second part of deliverable report D2.2.

Moreover, in WP2, the effect of acoustic degradation on the global noise barrier performance will be carefully considered and documented to objectively understand the long-term ability of noise barriers to reduce noise immissions. The results of this work are reported in the report T2.3, which is the third and last part of D2.2.

This deliverable presents the current state of the art of the standardized measurement methods for assessing the intrinsic acoustic performances of noise reducing devices.

It starts with short summaries of the diffuse sound field measurement methods for sound absorption [1] and for airborne sound insulation [2], followed by descriptions of the direct sound field measurement methods for sound reflection [3] and for airborne sound insulation [4]. These descriptions are not complete manuals for the measurement methods, but they contain the general measurement procedures as well as some physical background information.

Subsequently, the differences between the diffuse sound field methods, requiring (laboratory) reverberant rooms, and the direct sound field methods, which can be applied everywhere the direct sound field conditions are met, including alongside roads, are investigated. This will be done first in general, and then specifically for the sound absorption under diffuse sound field conditions and the sound reflection under direct sound field conditions, as well as for the diffuse and direct sound field measurement methods for airborne sound insulation.

Finally, a short conclusion about the presented information is given.

# 2 Current methods for assessing the acoustic performance of European NRD

There are four standardized methods for assessing the intrinsic properties of sound absorption and airborne sound insulation of NRD. They can be categorised into two classes: the diffuse sound field methods and the direct sound field methods.

Diffuse sound field measurement methods were the first used to determine the intrinsic acoustic properties of NRD: at the early stages (the seventies), they were the only measurement methods available, but the sound field used by those methods does not correspond to the effective sound field for noise barriers (except for closed field and tunnels).

Since 2015, with the final publication of the respective standards describing measurement methods for sound reflection and airborne sound insulation under direct sound field conditions, a clear distinction is made on the scope of application for those different methods.

It is now mandatory to characterize the NRD with the appropriate sound field that corresponds to their effective intended use, i.e.: direct or diffuse sound field.

In the following sections, an overview of the existing diffuse sound field and direct sound field measurement methods for intrinsic NRD properties is given and their possible relations to each other is explained.

## *2.1 Acoustic properties of NRD*

The acoustic properties of NRD can be divided into two categories:

- intrinsic properties of NRD
- extrinsic properties of NRD

Intrinsic properties are inherent to the (product) NRD and are independent of the environment. Examples of intrinsic properties are the sound absorption and the airborne sound insulation, which depend only on the specific make-up of the NRD itself.

Extrinsic properties, on the other hand, depend on the specific environment in which the NRD is used. An example of an extrinsic property is the insertion loss, which can depend on the terrain or even on meteorological circumstances, but also the dimensions of the NRD: it compares the sound immissions at specific points with and without the NRD.

This state-of-the-art report is only addressing the measurement methods for intrinsic properties, i.d., sound absorption/reflection and airborne sound insulation.

EN 1793-4 describes a measurement procedure for testing the intrinsic property of sound diffraction at the top of the NRD [5]; however, as sound diffraction is not in the focus of SOPRANOISE, the measurement procedure is not addressed in this report.

## *2.2 Diffuse sound field measurement methods*

Diffuse sound field measurement methods require special infrastructure, i.e., reverberation rooms, to be performed, as well as test-specimen which must be mounted inside these rooms. The main property of a diffuse sound field is that it has no privileged direction of the energy, i.d. for a NRD the incident sound energy is equally spread over all angles of the hemisphere.

The following two subsections summarise the standards EN 1793-1 for sound absorption and EN 1793-2 for airborne sound insulation to describe their measurement principles.

### 2.2.1 Diffuse sound field method for testing sound absorption (EN 1793-1)

The diffuse sound field measurement method for sound absorption is based on the change of the reverberation time inside a reverberation chamber (as measured with ISO 354 [6]) after installation of a test sample of the NRD at the surface of the room.

The reverberation time of a room can be calculated with Sabine's law.

$$T = k\frac{V}{cA} \tag{1}$$

With the constant $k = 24\ln(10) \approx 55.3$, the volume of the reverberation room $V$, the speed of sound $c$ and the effective absorption area $A$. Inversion of this law allows the calculation of the effective absorption area from the reverberation time.

To calculate the absorptance $\alpha$ of the test sample, the reverberation time before ($T_1$) and after ($T_2$) its installation in the room must be measured. From these reverberation times the effective absorption areas $A_1$ and $A_2$ can be calculated. Each effective absorption area $A$ depends on all individual surfaces $S_i$ of the room and their absorptances $\alpha_i$. Additionally, a term for the sound absorption of air itself ($m$ according to ISO 9613-1 [7]) must be considered.

$$A = \sum_{i=1}^{N} S_i\,\alpha_i + 4mV \tag{2}$$

The effective absorption area ($A_T$) of the test specimen can therefore be calculated with the following equation:

$$A_T = A_2 - A_1 = 55.3V\left(\frac{1}{c_2T_2} - \frac{1}{c_1T_1}\right) - 4V(m_2 - m_1) \tag{3}$$

The absorptance of the NRD ($\alpha_{NRD}$) with the surface $S$ is then given by

$$\alpha_{NRD} = \frac{A_T}{S} \tag{4}$$

Finally, a single number rating $\mathrm{DL}_{\alpha,\mathrm{NRD}}$ can be calculated by averaging over all third-octave band values of the absorptance weighted with the third-octave band values of the standardised traffic noise spectrum ($L_i$) according to EN 1793-3 [8].

$$\mathrm{DL}_{\alpha,\mathrm{NRD}} = -10\log_{10}\left[1 - \frac{\sum_{i=1}^{18}\alpha_{\mathrm{NRD},i}\,10^{0.1L_i}}{\sum_{i=1}^{18}10^{0.1L_i}}\right] \tag{5}$$

### 2.2.2 Diffuse sound field method for testing airborne sound insulation (EN 1793-2)

The diffuse sound field measurement method for airborne sound insulation according to EN 1793-2 is based on EN ISO 10140-2 [9] and requires two adjacent reverberation rooms, the "source room" and the "receiving room". The "source room" contains one or multiple loudspeakers which generate a diffuse sound field and the "receiving room" contains one or multiple microphones. The rooms are linked by a window in which the test-specimen is placed.

The comparison of the averaged sound pressure levels in the source ($L_1$) and the receiving ($L_2$) room then yields the airborne sound insulation $R$ of the specimen.

$$R = L_1 - L_2 + 10\log_{10}\left(\frac{S}{A}\right) \tag{6}$$

The quantities $S$ and $A$ are the size of the connecting window (about 10 m$^2$) containing the test specimen and the effective sound absorption area in the receiving room, respectively.

The airborne sound insulation in third-octave bands can also be summarised in a single number rating $\mathrm{DL}_R$ by a weighted average using the third-octave band values of the standardised traffic noise spectrum $L_i$ from EN 1793-3 [8].

$$\mathrm{DL}_R = -10\log_{10}\left[\frac{\sum_{i=1}^{18} 10^{0.1L_i}\, 10^{-0.1R_i}}{\sum_{i=1}^{18} 10^{0.1L_i}}\right] \tag{7}$$

## 2.3 Direct sound field measurement methods

The direct sound field measurement methods for airborne sound insulation and sound reflection are based on the measurement of impulse responses between the loudspeaker and dedicated microphone positions. Since a loudspeaker emits a spherical wave in the first approximation, the incident sound energy on the NRD is concentrated in distinct directions. Impulse response measurement techniques (MLS, Sweeps) [10] are able to omit disturbing sound sources, hence these methods can be performed also in environments with acoustic harsh conditions, e.g. alongside roads under traffic. The most limiting requirement of the methods is sufficient dimensions of the NRD under test, to allow the removal of spurious reflections (on the ground, at the top, and on lateral edges) outside the time window used for the post-processing (signal analysis).

The directional sound field used in these measurement methods also better emulates the directional sound of traffic noise in open area, which makes the results more relevant to real-world conditions for noise barriers.

### 2.3.1 Direct sound field method for testing sound reflection (EN 1793-5)

The direct sound field measurement method for sound reflection according to EN 1793-5 is based on a comparison between the sound energy reflected from the NRD and the sound energy emitted towards it.

The sound is generated by a loudspeaker positioned 1.5m in front of the NRD at half of its height. The corresponding microphones are positioned in-between, in a 3x3 grid with a distance of 0.25m to the NRD and with a spacing of 0.4m to neighbouring ones. Multiple impulse response measurements are performed with this setup to average out noise from the environment.

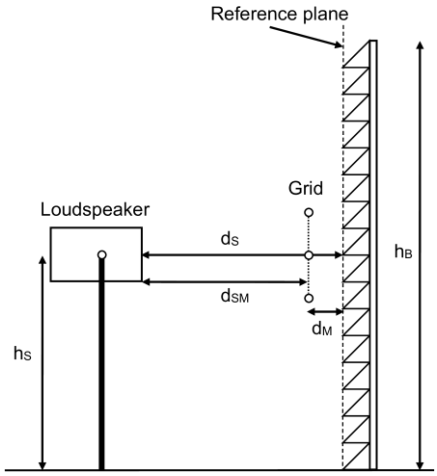


Figure 1: Setup of a direct sound field reflection measurement

The measured signal of the actual measurement comprises the impulses of the sound towards the NRD and the reflection coming back (Figure 2, left). To separate the reflected sound from the received signal of the actual measurement, an additional free-field measurement has to be performed. The subtraction of the free-field measurement from the actual measurement results in only the reflected component of the impulse response, as well as spurious reflections from the surroundings which can be removed by time-windowing (Figure 2, right).

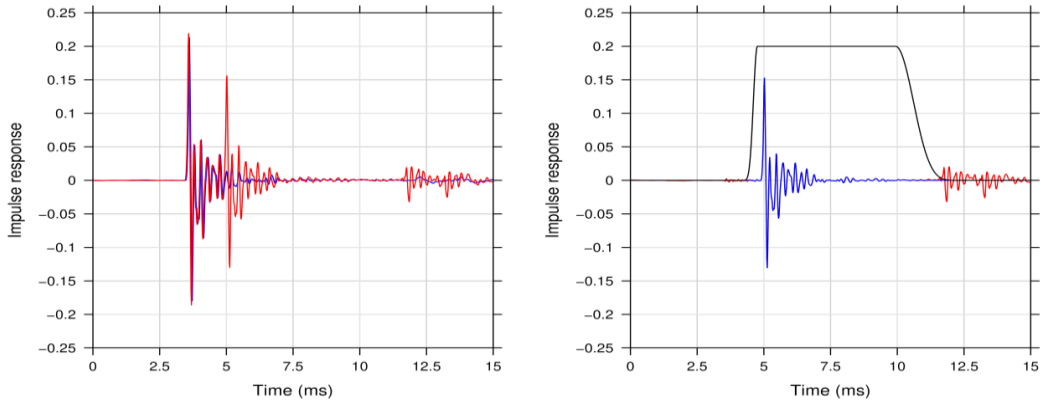


Figure 2: Impulse responses before and after subtraction and time-windowing. Left: free-field (blue) and actual (red) impulse response. Right: reflected component before (red) and after (blue) time windowing.

When comparing the energy content of the reflected and the impinging sound several influences have to be considered. The main one is the longer propagation path of the reflected sound, which causes a decrease of the sound pressure approximately equal to $1/r$ (for point sources), which is corrected by the factor $c_{\mathrm{geo},k}$. Additionally, correction factors for the directivity of the loudspeaker ($c_{\mathrm{dir},k}(\Delta f_j)$) and a possible change of the gain settings ($c_{\mathrm{gain},k}(\Delta f_g)$) between the actual and the free-field measurements are taken into account.

With these correction factors, the reflectance in third-octave bands ($RI_j$), can be calculated as follows:

$$RI_j = \frac{1}{n_j}\sum_{k=1}^{n_j}\left[\frac{\int_{\Delta f_j}\left|F[h_{r,k}(t)w_{r,k}(t)]\right|^2 \mathrm{d}f}{\int_{\Delta f_j}\left|F[h_{i,k}(t)w_{i,k}(t)]\right|^2 \mathrm{d}f}\; c_{\mathrm{geo},k}\; c_{\mathrm{dir},k}(\Delta f_j)\; c_{\mathrm{gain},k}(\Delta f_g)\right] \tag{8}$$

Here, $F$ denotes the Fourier transform, $h_{r,k}(t)$ and $h_{i,k}(t)$ are the reflected and the incident components of the measured impulse responses, $w_{r,k}(t)$ and $w_{r,k}(t)$ are window functions (specific windows, having Blackman-Harris leading and trailing edges and a flat central part are used), $n$ is the number of microphones and $j$ is the index of the third-octave bands.

It has to be noted that the currently valid EN 1793-5:2016+AC:2018, also called QUIESST method after the project in which it was developed, is the successor of the former CEN/TS 1793-5 also known as Adrienne method, which was similar but not identical. The main differences between the methods are the microphone positions and the handling of the correction factors. While the centre microphone position was identical, instead of using a measurement grid, the centre microphone was attached to the loudspeaker with a cantilever and the whole microphone – loudspeaker construction was rotated around the loudspeaker position in 10° increments, in the horizontal and vertical plane, from -40° to +40°, for 17 independent microphone positions in total. Additionally, instead of the correction factors mentioned above, a time multiplication was performed which counteracts the approximate $1/r$ decline in sound pressure.

$$RI_j = \frac{1}{n_j}\sum_{k=1}^{n_j}\left[\frac{\int_{\Delta f_j}\left|F[t\cdot h_{r,k}(t)w_{r,k}(t)]\right|^2 \mathrm{d}f}{\int_{\Delta f_j}\left|F[th_{i,k}(t)w_{i,k}(t)]\right|^2 \mathrm{d}f}\right] \tag{9}$$

For flat and homogenous noise barriers a very good correlation could be found between the QUIESST and the Adrienne method [11], where the values of the QUIESST method were found to be slightly smaller.

Similar to the diffuse sound field methods, the third-octave band values are then averaged and weighted according to the standardised traffic noise spectrum ($L_i$) in EN 1793-3, to get a single number rating for the NRD.

$$\mathrm{DL}_{RI} = -10\log_{10}\left[\frac{\sum_{i=1}^{18}\mathrm{RI}_i\, 10^{0.1L_i}}{\sum_{i=1}^{18} 10^{0.1L_i}}\right] \tag{10}$$

As $RI_j$, as well as $\alpha_{NRD}$ , is defined as an energy ratio, its meaningful range for a flat homogeneous surface is between 0 and 1. Nevertheless, for non-flat surfaces the $RI_j$ can take values larger than 1 at some frequencies, due to focusing and interferential effects. By contrast, for highly absorbing samples, $\alpha_{NRD}$ can take values larger than 1, due to the approximations underlaying the reverberation room method. Special care must be taken, as these two quantities are defined in a complementary way. A highly reflective NRD (e.g. transparent panels) will have an $\alpha_{NRD}$ close to 0 and a $RI_j$ close to 1. On the other hand, a highly absorptive NRD should reach an $\alpha_{NRD}$ close to 1 and a $RI_j$ close to 0.

Nevertheless, for the calculated single-number ratings $\mathrm{DL}_{\alpha,\mathrm{NRD}}$ and $\mathrm{DL}_{RI}$ a higher value denotes a higher sound absorption, the property which is generally desired for a NRD.

### 2.3.2 Direct sound field method for testing airborne sound insulation (EN 1793-6)

The measurement method for airborne sound insulation according to EN 1793-6 is based on a comparison between the sound energy arriving at the microphone positions with and without the NRD. The setup is comparable to the direct sound field measurement method for sound reflection, using a similar source position and the same microphone grid, but the grid is positioned on the opposite side of the NRD. Since the distance between the NRD and the grid

is the same as for testing sound reflection (0.25m), the absolute distance between the source and the microphones is now dependent on the thickness of the NRD. This has to be taken into account when performing the measurement under free-field conditions.

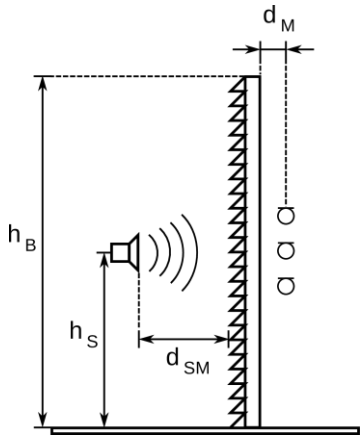


Figure 3: Setup of a direct sound field measurement of airborne sound insulation

The measured impulse response now consists of two major components: the first one is the sound that travelled through the NRD and the second is the sound that e.g. travelled over or around the NRD. To separate them and to get rid of spurious reflections from the ground, time windowing is used.

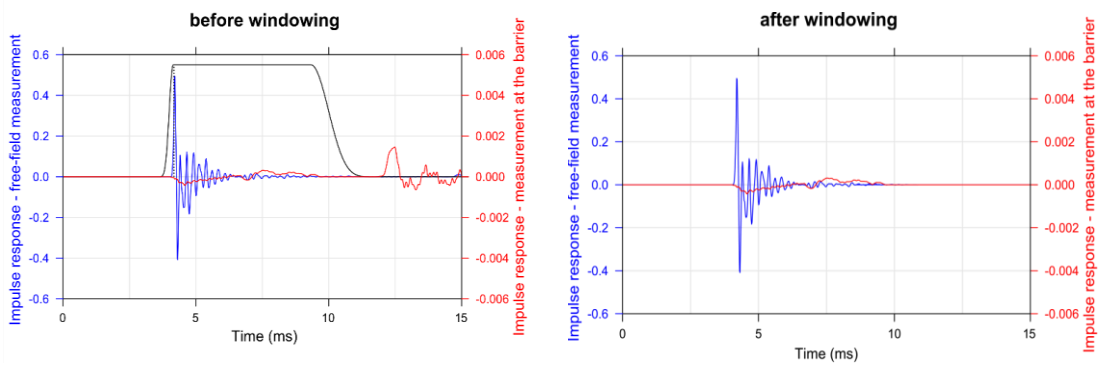


Figure 4: Impulse responses before (left) and after (right) time windowing; the blue curve depicts the free-field, the red curve the actual measurement at the NRD

The comparison between the sound energy of the direct component from the free-field measurement and the sound energy transmitted through the barrier from the measurement at the NRD is then performed similar to the reflection measurement method.

$$\mathrm{SI}_j = -10\ \log_{10}\left[\frac{1}{n}\sum_{k=1}^{n}\frac{\int_{\Delta f_j}\left|F[h_{t,k}(t)w_{r,k}(t)]\right|^2\,\mathrm{d}f}{\int_{\Delta f_j}\left|F[h_{i,k}(t)w_{i,k}(t)]\right|^2\,\mathrm{d}f}\right] \tag{11}$$

The resulting $\mathrm{SI}_j$ are then summarised as a single number rating by a weighted average with the standardised traffic noise spectrum ($L_i$) according to EN 1793-3.

$$\mathrm{DL_{SI}} = -10\log_{10}\left[\frac{\sum_{i=1}^{18}10^{0.1L_i}\,10^{-0.1\mathrm{SI}_i}}{\sum_{i=1}^{18}10^{0.1L_i}}\right] \tag{12}$$

# 3 Relation between the measurement methods

As the two kind of methods (diffuse and direct sound field) coexist, notwithstanding the fact that their correspond to different physics, it is interesting to investigate up to what extent they can be compared: this section highlights the main similarities and differences between the methods if pairwise comparisons are made. In the following subsections the state of the art of the relation between the measurement methods are presented.

**Scope of application**

The scope of application for each measurement method depends on the relevant sound field. The diffuse sound field measurement methods should be applied to describe the NRDs intrinsic properties if it is to be installed in a reverberating environment, e.g., tunnels, otherwise the direct sound field measurement methods should be used. In the respective standards reverberant conditions are defined based on geometric considerations. Figure 5 shows typical examples of where reverberant conditions of noise reducing devices alongside roads can occur, as they are given in the standards.

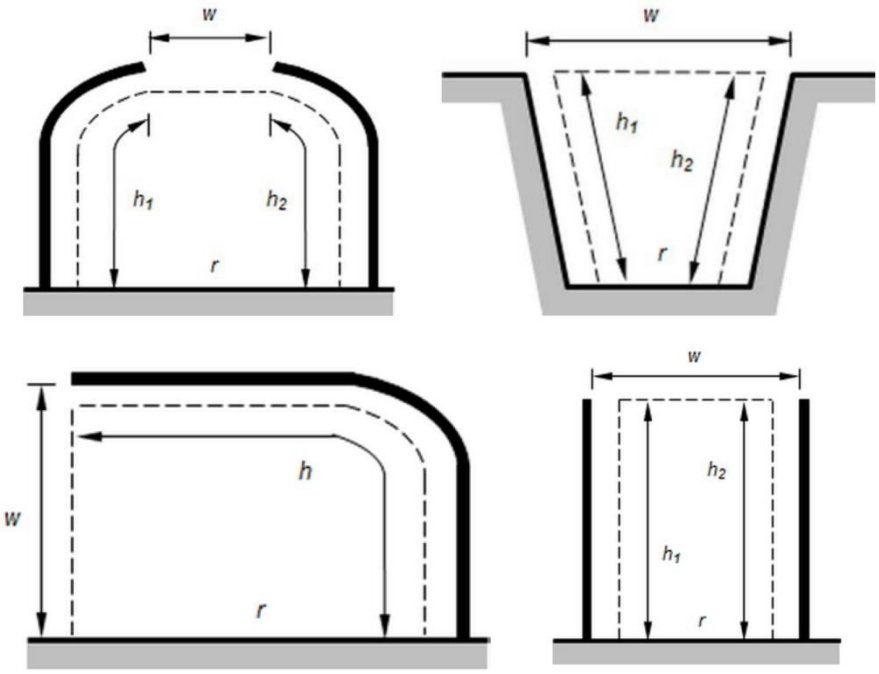


Figure 5: In natural reading order; Partial cover on both sides of the road; Deep trench envelope; Partial cover on one side of the road with $h = 2 * h1$; Tall barriers or buildings; from [3], [4]

An environment is considered reverberating, if $w/e \leq 0.25$, where $e = (w + h1 + h2)$. In other words, the non-enclosed length ($w$) must be at maximum 1/4 times the sum of the enclosing envelope ($e$, $h_1$ and $h_2$) without the road surface $r$. For the typical case where the two enclosing heights are equal, Figure 6 shows the relationship between the open width and the height of the noise reducing device for assessing reverberant conditions. It can be easily seen that even for a very small width of 5 meters (viz. less than two lanes), the noise reducing devices can be up to 7.5 meters high to be in a non-reverberant condition. Thus, for the most common conditions alongside roads, only the direct sound field methods according to EN 1793-5 and EN 1793-6 are applicable. Additionally, these methods have the advantage that they can assess the properties of already installed NRDs, which makes them suitable for the evaluation of recently installed NRDs, based on their predefined specification, and for the long-term monitoring and evaluation of NRDs.

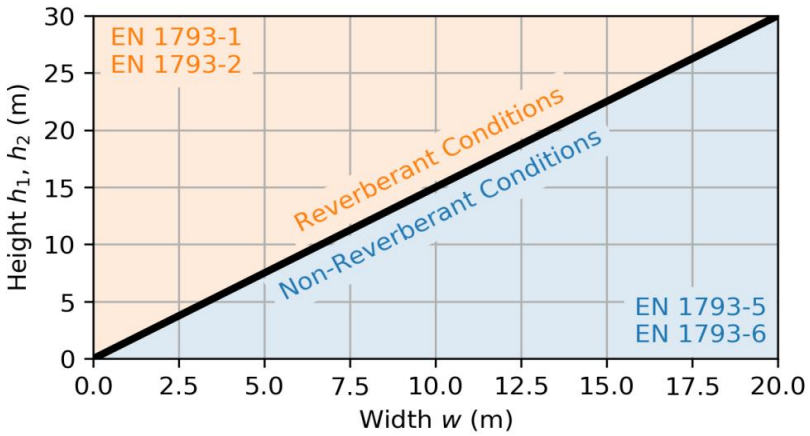


Figure 6: The boundary of reverberant conditions, separating the areas of application of the diffuse and direct sound field measurement method, based on the width and height of the enveloping geometry. For simplicity $h_1 = h_2$ is assumed.

### Type of the sound field: "diffuse" versus "direct"

The diffuse sound field methods, which are carried-out in reverberant rooms, give an averaged response of the performances at all angles of incidences and over the whole sample. In contrast, the direct sound field methods incorporate only incident angles close to normal incidences at specific points of the sample.

Therefore, if the intrinsic property of airborne sound insulation is measured both with the diffuse sound field method and with the direct sound field method, similar but not identical physical quantities are measured.

The importance of the angle of incidence is even bigger for sound absorption: that will lead to bigger differences between diffuse and direct sound field measurement.

### Artificial boundary conditions for diffuse sound field method

To highlight another difference between the measurement methods, consider the following equation for the ratios of the absorbed ($\alpha$), the reflected ($\rho$) and the transmitted ($\tau$) sound energy to the incident sound energy.

$$\alpha + \rho + \tau = 1 \tag{13}$$

Since energy is never lost, their sum must always be 1. In noise protection, only the reflected and the transmitted sound are relevant for the environment. The direct sound field measurement methods determine these quantities directly, while the diffuse sound field measurement methods determine $\tau$ directly, but not $\rho$.

In the sound absorption measurement method under diffuse sound field conditions the transmission path artificially set to zero as the transmitted energy is reflected at the floor and is remaining in the reverberant room after a second transmission through the barrier. The reflected sound is assumed and calculated with $\rho = 1 - \alpha$ (compare also Eq. (5)), see left part of Figure 7. In contrast to this, in the direct sound field method, the ratio of the reflected sound energy to the incident sound energy $\rho$ is measured directly, see right part of Figure 7. As the test setup artificially adds energy to the reflected sound for the diffuse sound field Figure 1method that would normally be transmitted, it is only a valid approximation for NRD where the energy of the transmitted sound is much lower than the reflected energy. Usually, this is a valid simplification to make, but for the extreme example of an acoustically almost fully

transparent NRD, the diffuse sound field methods would give an inconsistent picture of the properties of the NRD, with almost full transmission and full reflection at the same time.

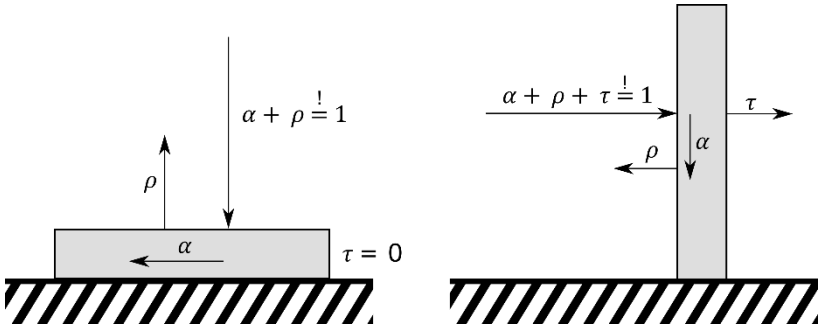


Figure 7: Relationship between the ratios of the absorbed ($\alpha$), the reflected ($\rho$) and the transmitted ($\tau$) sound energy for the measurement set-ups of the diffuse sound field method for measuring sound absorption (left) and the direct sound field method for sound reflection (and airborne sound insulation) (right).

### Condition of the test sample

As the diffuse sound field methods can only be performed inside of reverberation rooms, always distinct test samples are used, which are carefully prepared and mounted inside the test chambers. On the other hand, the direct sound field measurement methods have much lower demands on the acoustic environment during the test. If the NRD is mounted specifically for testing (e.g. inside a laboratory hall or outside), then approximately the same diligence of installation of the test sample as for the diffuse sound field methods can be assumed. Nevertheless, as one of the major advantages of the direct sound field methods is the possibility to test alongside roads under real-world conditions, the test sample might not be in perfect laboratory condition due to mounting errors, wear or contamination. Moreover, for the diffuse sound field method for sound absorption, the sample has free edges that give rise to the so-called “edge effect” artificially increasing the measured sound absorption (see [12]).

### Facilities used, and conditions for a measurement

The methods for measurements under diffuse sound field conditions are depending on reverberation rooms, where it is possible to generate a nearly diffuse sound field. The diffuse sound field measurement method for airborne sound insulation even requires two reverberation rooms that are linked by a window for the test sample. When a strongly absorbing sample is placed in a reverberation room, the sound field is not diffuse any longer, because the sound intensity vectors tend to flow towards the absorbing sample. This is one of the causes of the systematic overestimation of sound absorption with the diffuse sound field method (ISO 354).

For direct sound field measurements, the loudspeaker has to be capable of generating enough sound power to reliably detect the sound transmitted through a noise barrier over unwanted noise. This requirement is released considerably using deterministic signals, like MLS or ESS, which can get a very high signal-to-noise ratio even with a relatively low sound pressure level. Additionally, the direct sound field methods require a noise barrier that is high enough to enable time windowing for the removal of spurious reflections from the measured signal. When the noise barrier height is progressively lowered below 4m a progressive reduction of the valid frequency range applies (see EN 1793-5 and EN 1793-6). If measurements are taken outside with the direct sound field methods, naturally additional requirements regarding the environmental conditions for temperature, wind and humidity must be considered.

## 3.1 Relation between diffuse sound field and direct sound field methods concerning sound absorption/reflection

The correlation between the measurement method for sound reflection under a direct sound field and the measurement method for sound absorption under a diffuse sound field is generally low [13], [14].

Figure 8, taken from QUIESST report [14], shows a linear regression for the correlation of the single number ratings of the diffuse sound field absorption measurement method (horizontal) and the direct sound field reflection measurement method (vertical), for all NRDs in the QUIESST database, for which both measurement results exist.

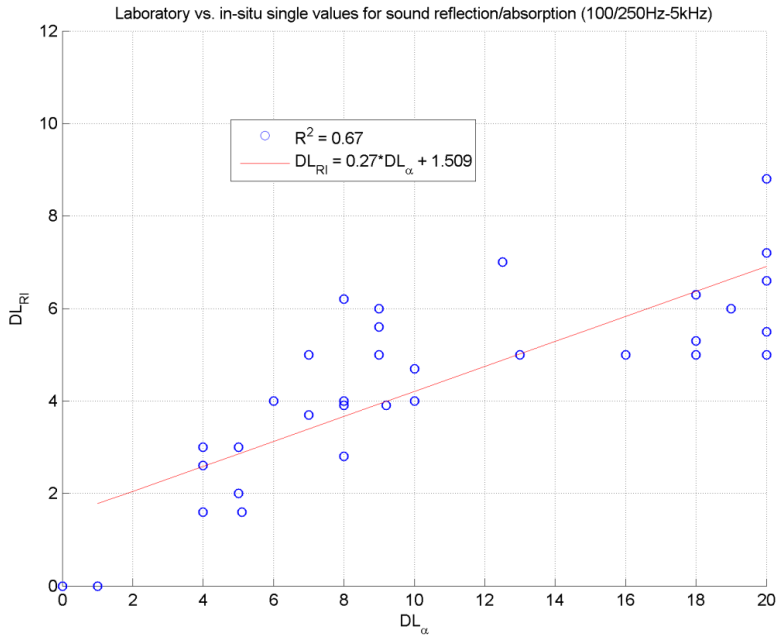


Figure 8: Correlation between the single-number ratings in dB of the diffuse sound field method for sound absorption (horizontal) and the direct sound field method for sound reflection (vertical) for all NRDs in the QUIESST database for which both measurement results exist; from [14].

It can be seen that the correlation is relatively poor and while it is slightly better when only looking at NRD consisting of concrete ($\mathrm{DL_{RI}} = 0.35\mathrm{DL_{\alpha}} - 0.86$ with $R^2 = 0.73$), it is even worse when only looking at metal barriers ($\mathrm{DL_{RI}} = 0.20\mathrm{DL_{\alpha}} - 2.27$ with $R^2 = 0.47$). The number of NRDs made of timber in the QUIESST database, for which measurement results of both methods are available, is only 4 which makes a linear regression not meaningful.

In [15] a theoretical approach for the relationship between the single number-ratings for sound absorption under diffuse sound field conditions ($DL_{\alpha}$) and sound reflection under direct sound field conditions ($DL'_{RI}$) is presented, where the absorption coefficient of the diffuse sound field is derived by integration of the absorption coefficient of a plane wave over the hemisphere. For calculating the $DL'_{RI}$ only the centre microphone according to CEN/TS 1793-5 is used. The result of both theoretical calculations is a good linear correlation (see Figure 9). For values not too high (up to 6 or 7 dB of the single-number rating for sound reflection $DL'_{RI}$) the theoretical estimation is

$$DL'_{RI} \approx \frac{2}{3} DL_{\alpha}. \tag{14}$$

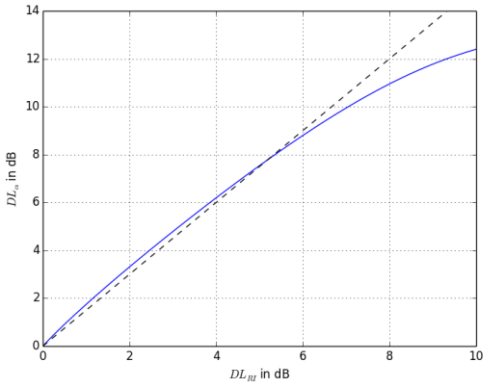


Figure 9: Theoretical curve for single number rating of absorption coefficient $DL_\alpha$ against single-number rating of sound reflection $DL'_{RI}$ (blue) and a linear slope of 3/2 (dashed); from [15]

In comparison to Figure 8 this simplified relationship only holds for NRDs with a low absorption, and even then mainly overestimates the $DL'_{RI}$. Beside the different correction method for geometric divergence in CEN/TS 1793-5, the omission of the non-perpendicular microphone positions is a significant deviation to the measurement results presented in Figure 8.

This means, that there is currently no accurate way of converting measurement results to make useful comparisons. The reasons for that are manifold, below are some of the probable causes listed for this disparity.

### Uncertainties measuring sound absorption under diffuse sound field conditions

One main cause for the poor correlation is the generally low repeatability of the diffuse sound field method, as described in [16], where a meta-analysis of several round-robin tests was performed. Especially the almost linear relationship between the standard deviation and the absorptance of the test sample, which moreover varies strongly by frequency, could cause sufficient variations to cause a low correlation to the direct sound field method. One reason for this is the curvature of the decay curve. For low frequencies (below the Schröder frequency), where the mode density is low, this curvature is caused by the different decay of axial, tangential and diagonal modes. For high frequencies the uneven absorption, which is usually the case for diffuse sound field absorption measurements where the sample is mounted on the ground, also causes a curvature. Since reverberation times are usually calculated with a linear regression, a curvature resp. nonlinearity of the decay curve can negatively influence the accuracy and repeatability of the method. [17] presents this curvature for multiple measurements and shows that it is even dependent on the placement and number of diffusors used in the reverberation room. To mitigate this problem, the use of a multi-exponential fit instead of a conventional linear regression is suggested.

### Limitation of $\mathrm{DL}_{\alpha,\mathrm{NRD}}$ to 20 dB

Another cause for the poor correlation could be the artificial limitation of the $\mathrm{DL}_{\alpha,\mathrm{NRD}}$ to a maximum value of 20dB. This limitation is performed in order to ensure the argument of the logarithm being positive, even when a slight measurement error would make it close to zero or even negative. In Figure 8 it can be seen that several measurement results have a $\mathrm{DL}_\alpha$ of exactly 20dB, while those same NRD have different $\mathrm{DL}_{RI}$ values. In combination with the faulty energy comparison as described after Equation 1, this has the effect that the diffuse sound field method might be inaccurate or at least not comparable to the direct sound field methods for very high values of $\mathrm{DL}_{\alpha,\mathrm{NRD}}$. This, of course, is a problem when calculating a linear regression.

### Non-linearity of single-number rating calculation

Additionally, the non-linearity of the logarithm for calculating the single-number ratings can cause a poor correlation between the methods. Figure 10 compares the measured third-octave band spectra of the direct sound field method (old method according to CENT/TS 1793-5) with $1 - \alpha$ of the diffuse sound field method for seven different NRD.

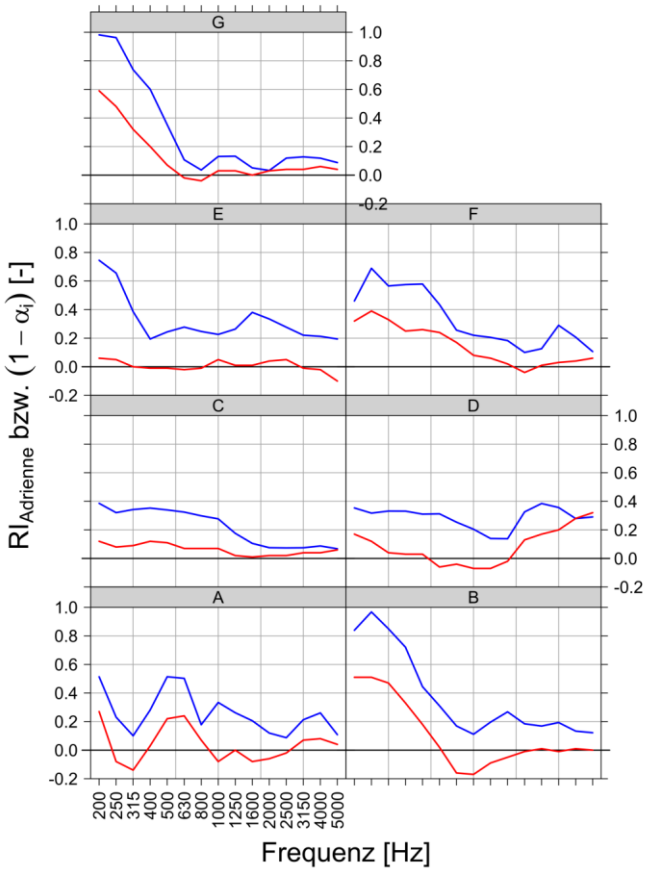


Figure 10: Spectra of seven different noise barriers measured with the CEN/TS 1793-5 (Adrienne) method (blue) and the diffuse sound field absorption method (red); from [11]

It is apparent that most of the spectra have a very similar shape, although they show a (possibly frequency-dependent) offset. An offset alone, even if the shape of the spectra would otherwise be identical, is enough to prevent a linear relationship between the results because of the non-linearity of the logarithm. Additionally, when looking at Figure 8, it is apparent that a non-linear log-shaped regression might fit the data more accurately. Although a correlation with a multi-variate non-linear model might be found for these seven NRD shown in Figure 10, the correlation would only be valid for these noise barriers, which are all considered to be flat and homogenous according to [3].

### Interference patterns for highly structured surfaces under direct sound field conditions

As mentioned before, the direct sound field method uses only one loudspeaker position, which essentially approximates a single point source (just one wave front) instead of the diffuse sound (infinite point sources and wave front). For direct sound field conditions, this can cause strong interference patterns for certain NRD shapes, and therefore an under- or overestimation of the reflected sound, which might be smoothened by the integration over all angles of the

diffuse sound field. For example, an NRD shape that focuses multiple reflected waves at one microphone position can even cause a sound reflection index larger than one. This effect is technically not a measurement error since it is a repeatable property of the method itself, but nevertheless it can cause over- or underestimations of the total reflected sound energy. This effect may be tackled by an increased number of microphone and/or reference positions.

Most of the mentioned reasons for the disparity between the direct sound field and the diffuse sound field method are based on possible inaccuracies of the diffuse sound field method, but there are also some physical differences between the measurement methods which make a comparison between them very difficult. Due to the mentioned differences a precise calculation from the results from one method to the other is not feasible, especially as measurement uncertainties must be considered. Nevertheless, road operators, civil engineers and the NRD industry itself are used to the range of values of the diffuse sound field method for sound absorption. As the range of values for the direct sound field for sound reflection differ significantly, Task 2.2 shall examine the relationship between these two measurement methods more closely as to support road operators and civil engineers in choosing appropriate minimum requirement values for NRDs for the direct sound field method for sound reflection, as it is the more precise and practical method to use for NRDs alongside roads.

## 3.2 Relation between diffuse sound field and direct sound field methods concerning airborne sound insulation

Generally, the results of the diffuse sound field measurement method and the direct sound field measurement method for airborne sound insulation have a good correlation, although, depending on the type of the NRD, the results can have quite a bit of an offset.

Figure 11 from [14], shows a linear regression between the single number ratings of the diffuse sound field method (horizontal axis) and the direct sound field method (vertical axis), for all NRDs in the QUIESST database for which both measurement results exist. It can be seen that the correlation coefficient ($R^2 = 0.954$) is very high, which indicates a very good accordance between the methods overall. However, when looking at different types of NRD separately, the parameters of the linear regression are not as clear. On page 60 of [14] the regression parameters and the correlation coefficients for multiple types of NRD consisting of concrete metal and timber are shown, see Table 1. While all results have a decent correlation coefficient ($R^2 \geq 0.52$), the parameters of the linear regression are clearly different. One caveat of these results is the relatively low number of NRDs in each category (e.g. only 7 for timber), so the statistics might not be very robust. Nevertheless, they show that there possibly are additional physical effects at play, whose magnitude depend on the material of the NRD. In the following, a few reasons for this disparity are listed.

Table 1: Linear correlation models between the single-number ratings for airborne sound insulation under diffuse sound field conditions ($DL_R$) and direct sound field conditions ($DL_{SI}$), [14]

| NRD MATERIAL | LINEAR REGRESSION | $R^2$ |
|---|---|---|
| **CONCRETE** | $DL_{SI} = 1.33DL_R - 7.53$ | 0.7 |
| **METAL** | $DL_{SI} = 0.75DL_R - 10.38$ | 0.52 |
| **TIMBER** | $DL_{SI} = 1.04DL_R - 7.38$ | 0.78 |

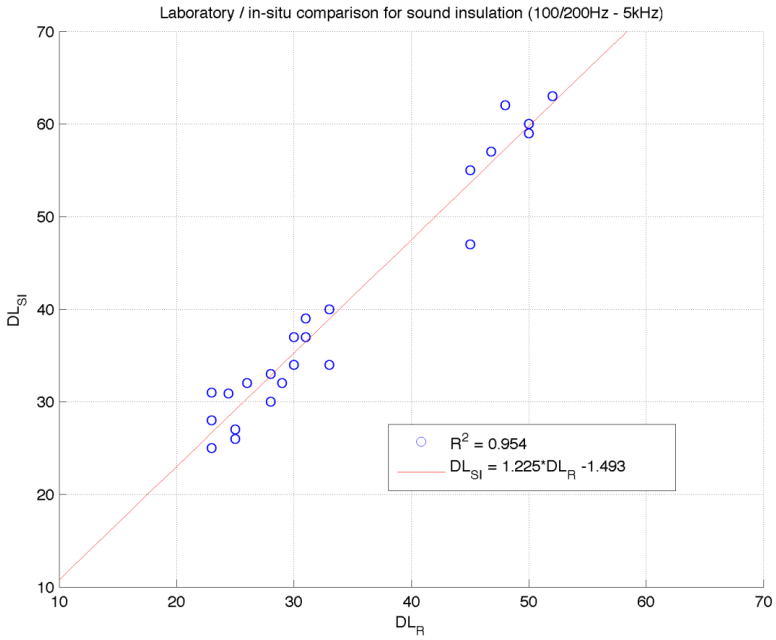


Figure 11: Correlation between the single-number ratings in dB of the diffuse sound field (horizontal) and the direct sound field (vertical) method for airborne sound insulation for all NRD in the QUIESST database for which both measurement results exist; from [14]

### Averaging of acoustic element and post measurement

The sensitivity to installation errors and spots of locally lower insulation is different, since the direct sound field method includes separate measurements at the posts, which are especially susceptible to mounting errors on site, whereas the diffuse sound field method always assesses the whole sample consisting of acoustic element and one post, carefully mounted and sealed in the laboratory. Using the energetic mean of the acoustic element and the post measurement for the global single-number rating of the direct sound field method, this value might not properly reflect the actual average over the whole NRD, as measured in the diffuse sound field method.

### Artificial set-up in reverberation room

The different boundary conditions regarding the fixation of the NRD elements can have an influence on the vibration modes and therefore the transmitted sound. In the measurement method under diffuse sound field conditions the sample is clamped at all four edges inside the reverberation room, while the noise barrier is clamped only at the two lateral edges, blocked by the gravity on the bottom edge and free on the top edge when measuring under direct sound field conditions.

### Maximum of sound transmission at coincidence frequency

Sound impinging under oblique angles can cause a maximum of sound transmission at the coincidence frequency, where the wavelength in air projected on the barrier and the wavelength in the material of the NRD are the same. This has been shown in [18], where the measurement results of both methods are compared for noise barriers consisting of thin acrylic sheets.

# 4 Conclusions

In this report, the state of the art regarding the measurement of intrinsic properties of NRD was presented. The main focus was on the methods for the measurement of sound absorption and airborne sound insulation under a diffuse sound field, as well as on the measurement methods for sound reflection and airborne sound insulation under a direct sound field. A brief summary of each measurement method was presented, before their differences were discussed in more detail.

Apart from the obvious different scope of application, the differences between the measurement procedures can be traced back to the used sound field (diffuse vs. direct), condition of the test sample (localized defects have different consequences) and the necessary facilities to perform the measurements (reverberation chambers vs portable loudspeaker/microphones).

These differences cause also a disparity in the measurement results, and while the results from the two different airborne sound insulation methods correlate quite well (compare Figure 11), the diffuse sound field absorption method and the direct sound field reflection method do not (compare Figure 8).

Several influencing factors were presented, where the main contributing factor is the difference in measuring the reflected component for specific (direct sound field) angles to artificially obtaining the reflected component by measuring the absorbed sound energy for all angles (diffuse sound field). Additional influences regarding the diffuse sound field absorption method are probably its bad repeatability overall [16], the clipping of the results for high absorptances at $\mathrm{DL}_{\alpha} = 20dB$ and the blockage of transmitted sound energy. Additionally, the logarithms used in the equations for the $\mathrm{DL}_{\mathrm{RI}}$ and the $\mathrm{DL}_{\alpha}$ cause a non-linear relationship between the results for offset but otherwise similar spectra and therefore a poor correlation.

Finally, as an outlook, these differences will be analysed in more detail in Task 2.2 of this project.

# 5 References


[1] *EN 1793-1, "Road traffic noise reducing devices - test method for determining the acoustic performance - part 1: Intrinsic characteristics of sound absorption under diffuse sound field conditions." 2017.*

[2] *EN 1793-2, "Road traffic noise reducing devices - part 2: Intrinsic characteristics of airborne sound insulation under diffuse sound field conditions." 2018.*

[3] *EN 1793-5, "Road traffic noise reducing devices. Test method for determining the acoustic performance. Intrinsic characteristics. In situ values of sound reflection under direct sound field conditions." 2018.*

[4] *EN 1793-6, "Road traffic noise reducing devices - test method for determining the acoustic performance - part 6: Intrinsic characteristics - in situ values of airborne sound insulation under direct sound field conditions." 2018.*

[5] *EN 1793-4, "Road traffic noise reducing devices - Test method for determining the acoustic performance - Part 4: Intrinsic characteristics - In situ values of sound diffraction.", 2015.*

[6] *EN ISO 354, "Acoustics - Measurement of sound absorption in a reverberation room.", 2003.*

[7] *ISO 9613-1, "Acoustics; attenuation of sound during propagation outdoors; part 1: calculation of the absorption of sound by the atmosphere.",* 1993.

[8] *EN 1793-3, "Road traffic noise reducing devices - Test method for determining the acoustic performance - Part 3: Normalised traffic noise spectrum.", 2018.*

[9] *EN ISO 10140-2, "Acoustics - Laboratory measurement of sound insulation of building elements - Part 2: Measuremem of airborne sound insulation.", 2010.*

[10] M. Garai and P. Guidorzi, "Impulse responses measured with MLS or swept-sine signals: A comparison between the two methods applied to noise barrier measurements," *Audio Engineering Society Convention 134,* 2013.

[11] M. Conter, R. Wehr, P. Reiter, H. Hoislbauer and G. Strohmayer, "REFLEX: Beurteilung der Reflexions- und Absorptionseigenschaften von Lärmschutzwänden," 2014.

[12] S. Thomasson, "On the absorption coefficient," *Acustica,* pp. 256-273, 1980.

[13] M. Conter and R. Wehr, "Comparison between laboratory and in-situ methods for measuring sound absorption properties of noise barriers," *Euronoise, Maastricht,* 2015.

[14] M. Conter, M. Czuka and S. Breuss, "Final procedural report on WP4 activities: Including public database of European NRD, data analysis and definition of NRD families," *QUIESST,* 2008.

[15] W. Bartolomaeus, "Reflexionsverlust vs Absorptionsgrad bei Lärmschutzwänden," *DAGA 2016 : 42. Jahrestagung für Akustik, Aachen, 2016,* 2016.

[16] V. Wittstock, "Unsicherheiten bei der Messung des Absorptionsgrades im Hallraum," *DAGA 2014 : 40. Jahrestagung für Akustik, Oldenburg,* 2014.

[17] J. Balint and G. Graber, “Gekrümmte Abklingkurven in Hallräumen,” *DAGA 2018 : 44. Jahrestagung für Akustik,* 2018.

[18] M. Garai and P. Guidorzi, “In situ measurements of the intrinsic characteristics of the acoustic barriers installed along a new high speed railway line,” *Noise Control Engineering Journal, vol. 56,* p. 342, 2008.

[19] M. Conter, “QUIESST D4.2 Report on use and structure of the database of NRD,” 2012.

[20] M. Garai and P. Guidorzi, “European methodology for testing the airborne sound insulation characteristics of noise barriers in situ: experimental verification and comparison with laboratory data,” *J. Acoust. Soc. Am., vol. 108,* pp. 1054-1067, 2000.

CEDR
Conférence Européenne des Directeurs des Routes
Conference of European Directors of Roads

## CEDR TRANSNATIONAL ROAD RESEARCH PROGRAMME 2018


# T2.2 report - Update and analysis of noise barrier database including new current measurements

## April 2021

| | |
|---|---|
| **Document** | 20210408_spnWP2_T2.2.docx |
| **Main Editor(s)** | Marco Conter, Andreas Fuchs (AIT) |
| **Due Date** | February 2021 |
| **Delivery Date** | February 2021 (revised in April 2021) |
| **Work Package** | WP2 – State of the Art on the intrinsic acoustic performance assessment of noise barriers |
| **Task** | T2.2 - Update and analysis of noise barrier database including new current measurements |
| **Dissemination Level** | Public |

A-tech AIT bast ERF

# Table of Contents

# Table of Figures

# Table of Tables

# 1 Introduction

The general objective of WP 2 of the SOPRANOISE project is to provide both theoretical and practical background information on measurement methods of the acoustic performance of noise barriers. First a systematic research on the State of the Art regarding available correlations in the literature and trends between measurement results of methods under diffuse sound field conditions and methods under direct sound field conditions was performed. The results of this work have been summarized in the report D2.1 [1], delivered in June 2020 as final output of task 2.1.

Second, as main objective of task 2.2, the work was focused on extending the relevant database of European noise barriers developed within the QUIESST project, including single-number ratings and third-octave band spectra from manufactured products and already installed noise barriers. This new SOPRANOISE database aims to show facts and figures about acoustic performances obtained from measurements performed under diffuse sound field as well as direct sound field conditions, together with a better understanding of the respective significance, similarities and differences of these standardized methods.

The results of the analysis performed within task 2.2 are summarised in the present report, as a second part of D2.2, which shows the achievement of milestone M2.2 on the update and analysis of the noise barrier database including new measurements. Moreover, in task 2.3, the effect of acoustic degradation on the global acoustic performance of noise barriers was considered in detail. The results of this work are reported in the report T2.3, which is the third and last part of D2.2.

The present report is structured as follows: after a short introduction explaining the structure of the document, in chapter 2 first the general structure of the database is briefly shown, then the data collection phase and the overall amount of data is described. Thereafter, a quick overview of the amount of data collected is given and finally the number of datasets after data selection, quality check and validation are presented.

Chapter 3 presents the single-number ratings of the measurement results collected for every method separately: first the results on sound absorption under diffuse sound field conditions (according to EN 1793-1 [2]), then the results on airborne sound insulation under diffuse sound field conditions (according to EN 1793-2 [3]), then on sound reflection under direct sound field conditions (according to EN 1793-5 [4] or CEN/TS 1793-5 [5]) and finally the results on airborne sound insulation under direct sound field conditions (according to EN 1793-6 [6]). For every method a first general statistical analysis was performed on the overall data collected, while in a further step each material was analysed separately.

Then, in chapter 4 the comparison between single-number ratings is performed: first the single-number rating results according to EN 1793-1 are compared to the results according to EN 1793-5, then the single-number rating results according to EN 1793-2 are compared to the results according to EN 1793-6, while chapter 5 presents the frequency spectra of the data collected in third-octave bands for every method separately.

Chapter 6 shows an empirical study on correlations between results of methods for measuring sound absorption under diffuse sound field conditions and sound reflection under direct sound field conditions (EN 1793-1 versus EN 1793-5), as well as for the methods for measuring airborne sound insulation under diffuse and direct sound field conditions (EN 1793-2 versus EN 1793-6) using several regression models, based not only on single-number ratings but also on third-octave band data. Finally, in the last chapter the conclusions and a possible outlook of the research are presented.

# 2 Data collection and data overview

In this chapter, first the general structure of the database is briefly shown, then the project phase when data collection was performed is described. Thereafter, a quick overview of the amount of data collected is given and finally the number of datasets after data selection, quality check and validation is presented.

## *2.1 Structure of the SOPRANOISE database*

Starting with the database available from the past QUIESST project, during the first months of SOPRANOISE WP 2 the database was completely re-designed to give a more consistent representation of the data obtained from the different measurement methods. This gives the ability for more detailed analysis with correct cross-references. The database was implemented in PostgreSQL using a locally hosted virtual machine running Ubuntu Linux 18.04. The data processing and statistical analysis were performed with the programming language Python.

The SOPRANOISE database is structured in the following tables:

- **manufacturer**: in this table all information available regarding the manufacturers of the collected noise barriers under test are inserted;
- **institute**: in this table the information on the test institution (laboratory) is inserted;
- **nrd**: here all information available on the noise barrier itself like name, type, material, homogeneity, inclination, roughness, shape, layer and possible additional remarks are inserted following the classification scheme of the QUIESST database;
- **nrd_attachments**: in this table possible additional attachments are linked to the nrd table;
- **measurements_attachments**: in this table possible additional attachments are linked to the respective measurement tables;
- **abstract_measurements**: (abstract) base table for all four measurement methods in the database with all the information available in all measurement methods. One row in a measurement table represents the data in one distinct measurement report;
- **absorption_measurement**: in this table measurements according to EN 1793-1 are stored;
- **insulation_diffuse_measurement**: in this table measurements according to EN 1793-2 are stored;
- **reflection_measurement**: in this table measurements according to EN 1793-5 or CEN/TS 1793-5 are stored;
- **insulation_measurement**: in this table measurements according to EN 1793-6 are stored;
- **dl_a**: in this table recalculated single-number ratings from the third-octave band values with the lowest possible third-octave band frequency for measurements according to EN 1793-1 are stored;
- **dl_r**: in this table recalculated single-number ratings from the third-octave band values with the lowest possible third-octave band frequency for measurements according to EN 1793-2 are stored;

- **dl_ri**: in this table recalculated single-number ratings from the third-octave band values with the lowest possible third-octave band frequency for measurements according to EN 1793-5 or CEN/TS 1793-5 are stored,
- **dl_si**: in this table recalculated single-number ratings from the third-octave band values with the lowest possible third-octave band frequency for measurements according to EN 1793-6 are stored;
- **abstract_tb_values**: (abstract) base table for the third-octave band values from 100 Hz to 5 kHz, which are linked to the respective measurement;
- **a_values**: in this table all third-octave band results from measurements according to EN 1793-1 are included;
- **r_values**: in this table all third-octave band results from measurements according to EN 1793-2 are included;
- **ri_values**: in this module all third-octave band results from measurements according to EN 1793-5 or CEN/TS 1793-5 are included (including every single reference position and every single rotation, if available);
- **si_values**: in this table all third-octave band results from measurements according to EN 1793-6 are included (including every post and element measurement separately).

The relations between the different modules are shown in Figure 1, where the different tables are shown with the relevant parameters considered.

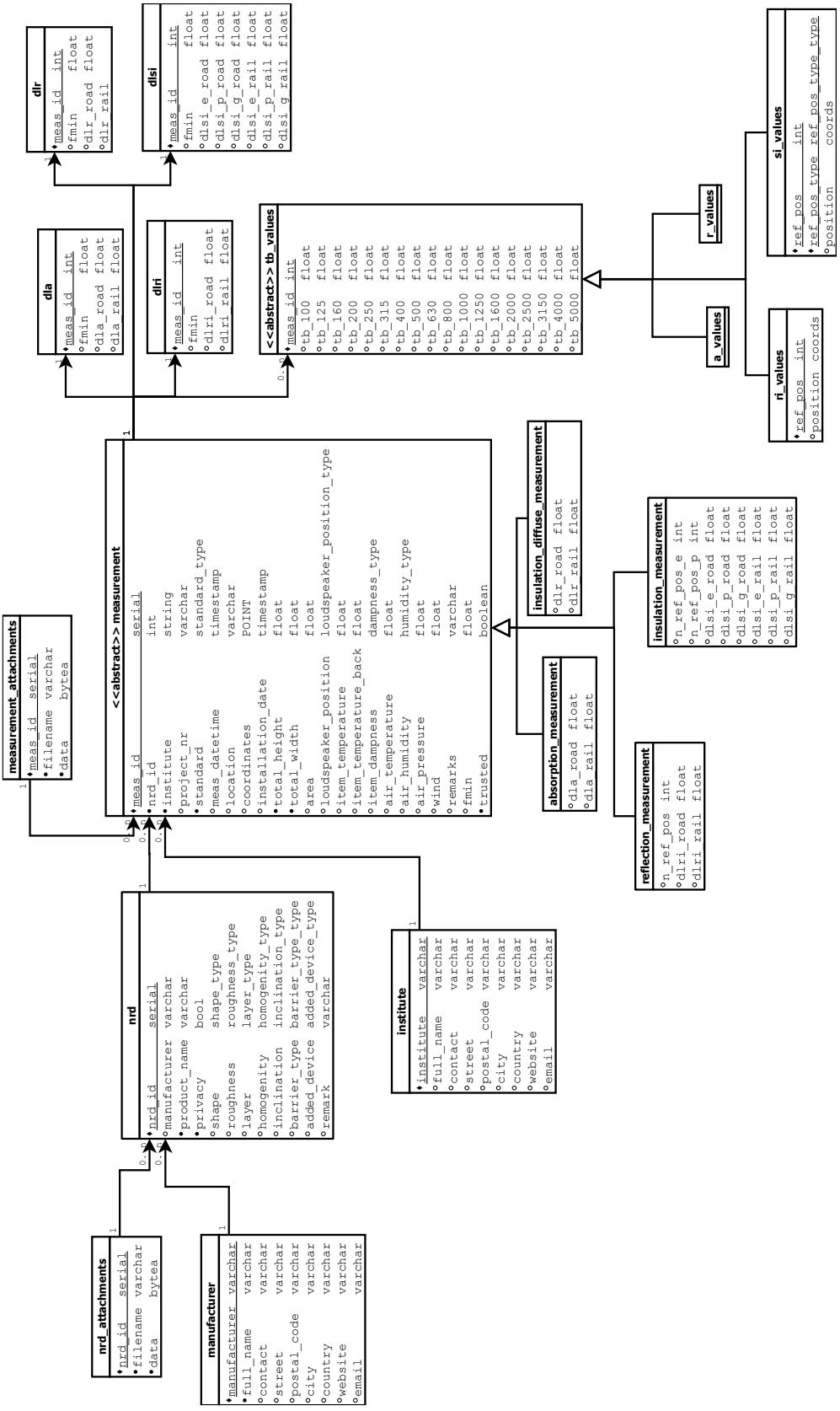


Figure 1: Structure of the SOPRANOISE database, showing the relation between the different modules and which parameters are considered in the tables.

## 2.2 Data collection

The second relevant step in order to achieve a meaningful database is the data collection: this has a relevant role in building consistent and statistically robust results. In fact, without a good and solid data basis, the data analysis would not lead to reasonable results, and from a statistical point of view a rather large amount of data is necessary to perform a sensible analysis.

In the frame of the QUIESST project a first European database on acoustic characteristics of noise barriers has been developed and data has been collected on this topic. Based on this database, the most recent data available within the consortium have been integrated, and further analyses on the relationships between the methods have been performed.

The data collection within the SOPRANOISE project started mid of January and ended in November 2020, after an extension of 3 months in order to collect more relevant data.

The work package leader AIT has prepared a Microsoft Office Excel template in order to facilitate the data collection and the insertion into the database. For every single measurement method (EN 1793-1, EN 1793-2, EN 1793-5 and EN 1793-6) a dedicated Excel template was prepared and circulated to the project consortium, to CEDR and other National Road Administrations, as well as noise barrier manufacturers and associations. Figure 2 presents an example of a filled template on measurements on airborne sound insulation under diffuse sound field conditions according to EN 1793-2.

Unfortunately, the most part of the collected data have been submitted in other formats, as for example simple datasheets, measurement reports in .pdf format and in some minor cases a simply scan of test reports, which caused additional effort in order to insert the data in the correct format for a correct implementation into the database.

## 2.3 General overview of the data collected

The work package leader AIT has received data, measurement results, product sheets, and general information from (1) project partners (AIT, A-Tech, UNIBO, BASt and ERF), (2) specific Road Administrations (the Austrian Road Administration ASFiNAG, the Transport Infrastructure Ireland TII, as well as the Road Administrations of Flanders and Wallonia), (3) other laboratories, (4) external test institutions (MFPA Leipzig, CEREMA), (5) noise barrier associations (ENBF, ANIPAR) and (6) from some noise barrier manufacturers.

For the sake of confidentiality, the noise barrier manufacturers will be not named in this report. Therefore, all analyses have been performed in an anonymous way and all results are shown with anonymised diagrams, so that neither the manufacturer nor the test institution can be identified from any analysis or diagram.

As mentioned before, the data collected during the QUIESST project [7] have been also considered, only the results according to the French method NFS 31089 have been discarded, as they lead to different overall results.

As of today, the SOPRANOISE database contains **448 different noise barriers** (meaning different test samples) manufactured by **58 noise barrier manufacturers** or construction companies, from **9 different European countries** (Austria, Belgium, France, Germany, Italy, Ireland, Spain, The Netherlands and United Kingdom) considering the country where the barrier was produced, and not where the barrier was tested or installed (which is obviously not necessarily the same country). The countries involved in the data collection were the following: Austria, Belgium, France, Italy, Ireland, Germany and Spain. The measurements collected have been performed by **39 different testing laboratories** from the European countries mentioned before.

| | A | B | C |
|---|---|---|---|
| 1 | Manufacturer ID | Woodworker | should match column Manufacturer ID in the Manufacturare table of the meta data |
| 2 | NRD ID | 1 | should match column NRD ID in the NRD table of the eta data |
| 3 | Institute | AIT | should match column Institute in the Institute table of the eta data |
| 4 | Project Nr. | 2.05.11111.1.0 | internal project number of the institute |
| 5 | Standard | EN 1793-2:2017 | measurement standard in the format: EN 1793-2:2019 |
| 6 | Measurement Datetime | 01.01.2019 00:00 | |
| 7 | Location | Giefinggasse 4, Vienna | location of the measurement site |
| 8 | Coordinates | 48.269134, 16.426587 | GPS coordinates, should be readable by Google Maps |
| 9 | Installation Date | 10.12.2018 00:00 | |
| 10 | Height | 4,00 | Height of the NRD in Meters |
| 11 | Width | 4,00 | Width of a typical element of the NRD in meters |
| 12 | Area | 16,00 | Surface area of the NRD under test in m² |
| 13 | Loudspeaker Position | Front | Position of the loudspeaker in reference to the typical application of the NRD: {Front, Back} |
| 14 | Item Temperature | 20 | in °C, surface temperature of the NRD at the front (traffic-faced) |
| 15 | Item Temperature Back | 20 | in °C, surface temperatur of the NRD at the back (not traffic-faced) |
| 16 | Item Dampness | dry | |
| 17 | Air Temperature | 20 | in °C |
| 18 | Air Humidity | < 30 % | |
| 19 | Air Pressure | 1005 | in hPa at measurement site |
| 20 | Wind | 0 | in m/s |
| 21 | f_min | 100 | in Hz |
| 22 | Attachments | | |
| 23 | Remarks | | |
| 24 | DL_R Road | 30 | in dB, weighted with spectrum from EN 1793-3 |
| 25 | DL_R Rail | 30 | in dB, weighted with spectrum from EN 16272-3-2 |
| 26 | R_100 | 30 | in dB |
| 27 | R_125 | 30 | in dB |
| 28 | R_160 | 30 | in dB |
| 29 | R_200 | 30 | in dB |
| 30 | R_250 | 30 | in dB |
| 31 | R_315 | 30 | in dB |
| 32 | R_400 | 30 | in dB |
| 33 | R_500 | 30 | in dB |
| 34 | R_630 | 30 | in dB |
| 35 | R_800 | 30 | in dB |
| 36 | R_1000 | 30 | in dB |
| 37 | R_1250 | 30 | in dB |
| 38 | R_1600 | 30 | in dB |
| 39 | R_2000 | 30 | in dB |
| 40 | R_2500 | 30 | in dB |
| 41 | R_3150 | 30 | in dB |
| 42 | R_4000 | 30 | in dB |
| 43 | R_5000 | 30 | in dB |

Figure 2: Example of the excel template prepared in order to facilitate the implementation of the data into the database: in this example a filled template on measurements on airborne sound insulation under diffuse sound field conditions according to EN 1793-2.

Table 1 presents the overall number of the entries inserted into the SOPRANOISE database in more detail. The overall amount of data collected was unexpectedly high, reaching a total of **2029 dataset** entries. For the sake of completeness, it should be noted that this number includes every single reference position (as it can be analysed separately), every single rotation (regarding CEN/TS 1793-5), and measurements performed in front of the element and measurements performed in front of the post separately (as in some cases only post or only element measurements were available). At the same time, the total number of different measurements reach the relevant value of **1503 entities**, which was much more than expected at the beginning of the project and is very promising from a statistical point of view.

Nevertheless, not all data were delivered with the same quality, and not all datasets have the same level of completeness. Therefore, in a further step all collected datasets have been checked and validated.

Table 1: Overall number of entries inserted in the SOPRANOISE database.

| Database Entry Type | Number of Entries |
|---|---|
| Total number of different **datasets** collected (considering post and element measurement, every reference position and every single rotation as a single dataset) | 2029 |
| Total number of different **test samples** of noise barriers represented | 448 |
| Total number of **manufacturers** or construction companies represented | 58 |
| Total number of testing **laboratories** represented | 39 |
| Total number of European **countries** delivered data in the frame of the SOPRANOISE project | 7 (AT, BE, DE, ES, FR, IT, IR) |
| Total number of European **countries** represented (considering the country where the barrier was produced, and not where the barrier was tested or installed) | 9 (AT, BE, DE, ES, FR, IT, IR, NL, UK) |
| Total number of different **measurements** collected (considering post and element measurement separately and different reference positions separately) | 1503 |
| Total number of different **measurements on EN 1793-1** collected | 179 |
| Total number of different **measurements on EN 1793-2** collected | 128 |
| Total number of **datasets on EN 1793-5 and CEN/TS 1793-5** collected (considering different reference positions and every single rotation separately) | 1028 |
| Total number of **measurements on EN 1793-5 and CEN/TS 1793-5** collected (combining different reference positions, which are part of a single measurement) | 695 |
| Total number of **datasets on EN 1793-6** collected (considering post and element separately) | 694 |
| Total number of **measurements on EN 1793-6** collected (combining post and element, which are part of a single measurement) | 501 |

Another interesting issue is the composition of the collected data regarding the measurement method available in order to get a first overview of the content. Figure 3 shows the total number of different measurements collected for each method: as today the SOPRANOISE database contains **179 entries on sound absorption according to EN 1793-1**, **128 entries on airborne sound insulation according to EN 1793-2**, **695 entries on sound reflection according to EN 1793-5 or CEN/TS 1793-5** (considering different reference positions separately) and **501 entries on airborne sound insulation according to EN 1793-6** (combining post and element, which are part of a single measurement).

Figure 4 shows the percentage of the data collected for every method separately, and it is interesting to note that 79% of the data collected are referring to measurements performed under direct sound field conditions, while only 21% of the data refers to measurements performed under diffuse sound field conditions. Therefore, based on these first rough figures it is evident that those measurement methods under direct sound field conditions (EN 1793-5 and EN 1793-6) have been applied several times during the last 15 years and are well established and frequently used in the European market.

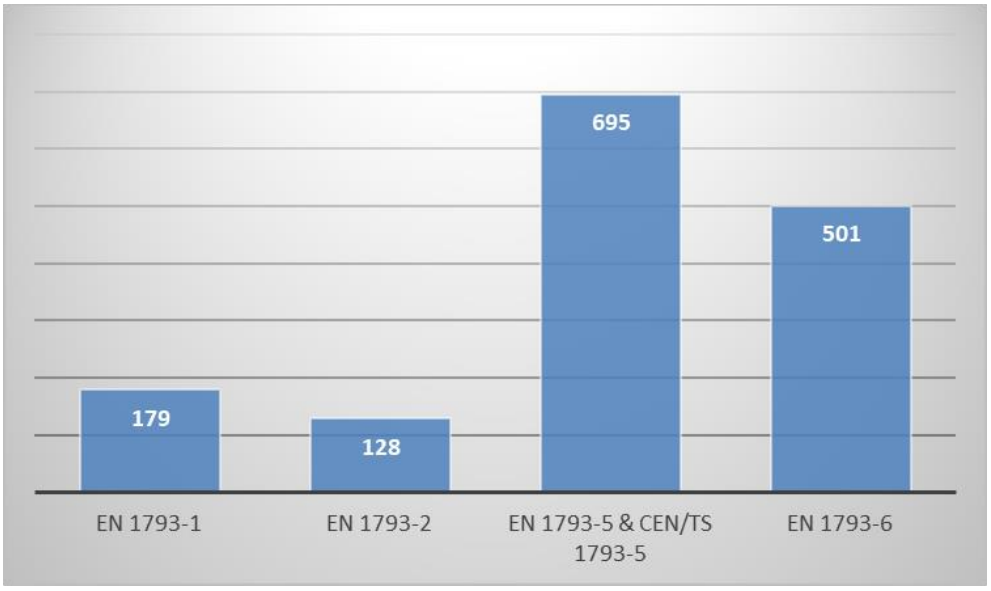


Figure 3: Total number of different measurements collected for each method: EN 1793-1, EN 1793-2, EN 1793-5 & CEN/TS 1793-5 (combining different reference positions, which are part of a single measurement) and EN 1793-6 (combining post and element, which are part of a single measurement).

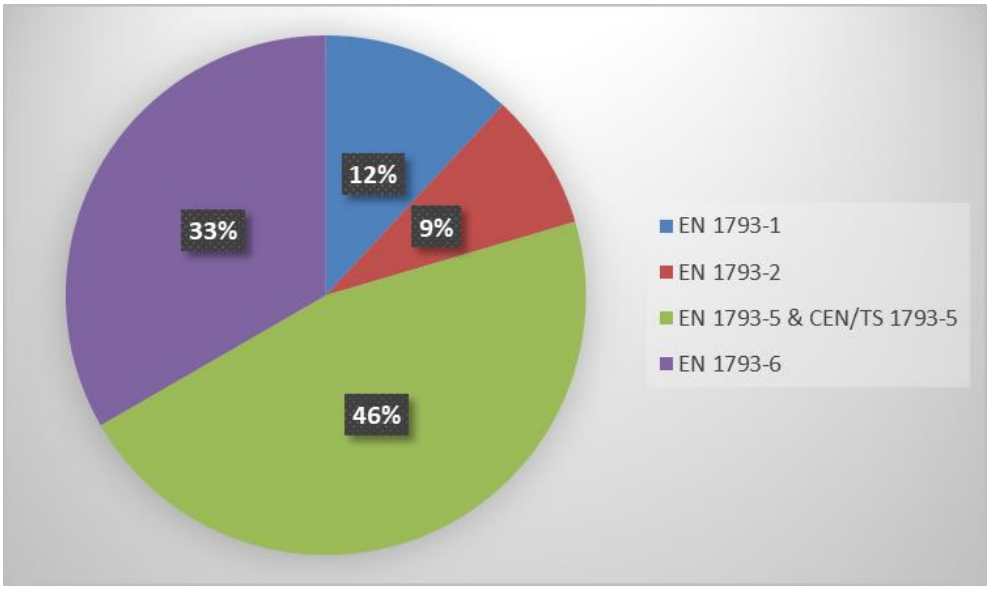


Figure 4: Percentage of the data collected for each methods: EN 1793-1, EN 1793-2, EN 1793-5 & CEN/TS 1793-5 (combining different reference positions, which are part of a single measurement) and EN 1793-6 (combining post and element, which are part of a single measurement).

## 2.4 Overview of the data collected after quality control and data validation

In order to perform a meaningful statistical analysis, the collected data has been evaluated in respect to:

- completeness of the datasets collected;
- plausibility of the results, mainly focusing on single-number ratings, but also considering effects in the third-octave band spectra;
- cross-checking in order to avoid repetitions of same data results coming from different sources;
- averaging of different reference positions and different rotations into one single-number rating (especially for EN 1793-5 and CEN/TS 1793-5);
- averaging of post and element measurements for data on EN 1793-6, in order to get the global value (if not available);
- re-calculating values of the single-number rating when all necessary frequencies were available, in order to avoid possible calculation mistakes;
- detecting outliers, task finally performed from a statistical point of view.

The quality check and the data validation / selection has been mainly performed in December 2020 after completing the data collection, which was closed in November 2020.

Figure 5 shows the number of different measurements validated after the quality control for each method separately: the **total number of validated data** reaches the considerable value of **1263 single-number ratings**. This amount of validated and high-quality data can be considered as a relevant basis for the further statistical analysis planned in this work package.

In more detail, the SOPRANOISE database contains after data validation and quality check the following relevant figures:

- 138 single-number ratings on sound absorption according to EN 1793-1;
- 72 single-number ratings on airborne sound insulation according to EN 1793-2;
- 359 single-number ratings on sound reflection according to EN 1793-5 or CEN/TS 1793-5;
- 267 single-number ratings on airborne sound insulation according to EN 1793-6 for elements;
- 244 single-number ratings on airborne sound insulation according to EN 1793-6 for posts;
- 183 single-number ratings of global values according to EN 1793-6.

Figure 6 shows the percentage of the data collected for every method separately: as mentioned before, it is relevant to note that also after quality control and data validation, circa 80% of the data collected are referring to measurements performed under direct sound field conditions, while only 20% of the data refers to measurements performed under diffuse sound field conditions.

All further statistical analyses have been performed based on those numbers.

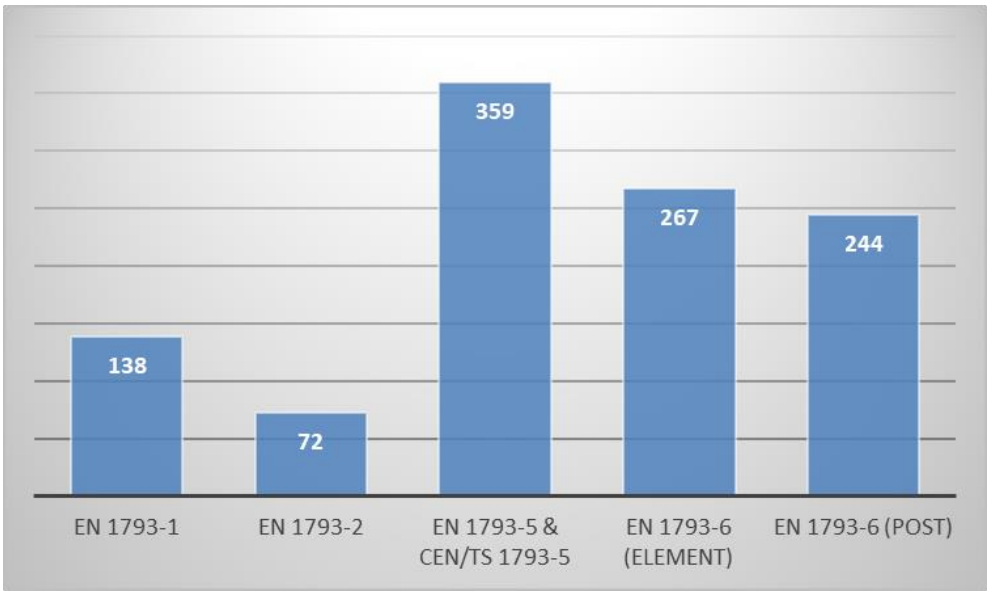


Figure 5: Total number of different measurements after quality check, data validation and averaging of different referent positions for EN 1793-1, EN 1793-2, EN 1793-5 & CEN/TS 1793-5 and EN 1793-6 (considering post and element measurements separately).

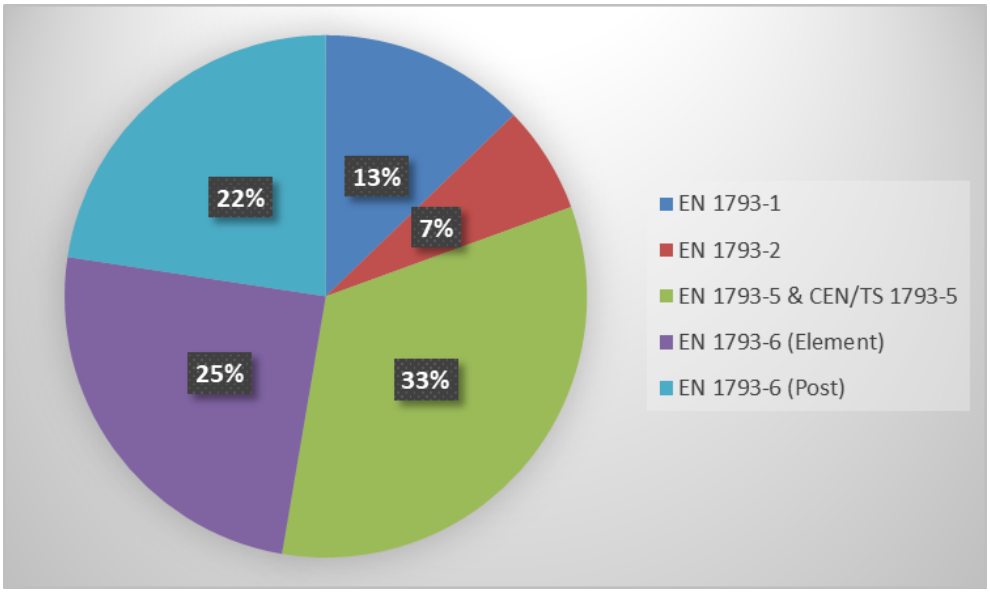


Figure 6: Percentage of the data collected for each method after quality check, data validation and averaging of different reference positions for EN 1793-1, EN 1793-2, EN 1793-5 & CEN/TS 1793-5 and EN 1793-6 (considering post and element measurements separately).

## 2.5 Classification of noise barrier types

The classification of the noise barriers tested is a relevant factor, which is influencing the further analysis performed in this work package. For this reason, attention was paid in order to check and classify the results of the collected tests to the correct noise barrier type.

Table 2 presents the classification of the noise barrier types according to the QUIESST project [7] and implemented in the original database. In order to be consistent to the data in the QUIESST database the same categorisation was used for the current work.

Table 2: Overview of barrier types according to the QUIESST classification [7].

| Barrier Type | Description |
|---|---|
| SM – Steel supporting structure + metallic panels | Most steel supporting structures have a H-shaped appearance. At least the surface layer consists of metallic material. |
| SC – Steel supporting structure + concrete panels | Structure of posts like in SM. At least the surface layer consists of concrete. Wood-fibre concrete barriers can also be assigned to this family. |
| ST – Steel supporting structure + Timber panels | Structure of posts like in SM. At least the surface layer consists of timber. |
| SG – Steel supporting structure + Transparent panels | Structure of posts like in SM. It is very highly probably that the noise barrier consists of only one transparent layer (e.g. acrylic glass). |
| C – Self-supporting concrete or brick system | NRD made of self-supporting construction. An example would be brick wall. |
| SP – Steel supporting structure + plastic panels | Structure of posts like in SM. At least the surface layer consists of plastic material. |
| CT – Tunnel concrete structure | Tunnel-structure, which surrounds the entire road to provide full noise screening. May be constructed self-supporting or with concrete beams supported by concrete pillars. |
| Stu – Tunnel steel structure | Tunnel-structure, which surrounds the entire road to provide full noise screening. Consists of steel supporting structure and metallic cassettes. |
| GT – Tunnel with transparent panels | Tunnel-structure, which surrounds the entire road to provide full noise screening. Consists of steel supporting structure and transparent panels. |
| GB – Green barrier | NRD type, which obtains its acoustic properties from soil with vegetation. A classic example would be a concrete structure with containers, filled with earth and plantings. |
| GA – Gabion with stones | NRD made of a gabion framework (solid metallic grid) filled with stones. |
| EB – Earth barrier | Artificial or natural earth wall – can be planted or unplanted. |
| PVNB – Photovoltaic noise barrier | Usually a conventional noise barrier with added photovoltaic elements. |

# 3 Overview of the overall results and statistical analysis

In this chapter the single-number ratings of the measurement results collected will be presented for every method separately: first the results on sound absorption under diffuse sound field conditions according to EN 1793-1, then the results on airborne sound insulation under diffuse sound field conditions according to EN 1793-2, then on sound reflection under direct sound field conditions according to EN 1793-5 or CEN/TS 1793-5 and finally the results on airborne sound insulation under direct sound field conditions according to EN 1793-6.

For all methods a first general statistical analysis on the overall data collected was performed using box plots, statistical distribution, probability function and the data results itself, while in a further step each material was analysed separately.

Based on the collected data the most represented materials[1] are **metal**[2], **timber** and **wood-fibre concrete**[3], followed by **concrete** (self-supported), **plastic**[4] and **transparent**[5] material. In addition to those materials under the material category **"other"** some special cases are represented, for which only few elements are present in the database, like prototypes (not available on the market), earth and green barriers, gabions (improved for their sound absorbing and / or airborne sound insulation performances), and noise barriers with integrated PV panels.

In this chapter, in order to have a better overview of the data, the analysis is presented in two different ways: (1) considering different frequency ranges and (2) considering data with full frequency range only. This differentiation is relevant in particular for the methods under direct sound field conditions (EN 1793-5 and EN 1793-6) as in several cases the measurements were performed under real-life conditions (e.g. on a motorways) where the barrier height or width was less than 4 meters, meaning that those measurements were not performed for certification purposes and not in the full frequency range from 200 Hz to 5 kHz to produce physically valid results. For the methods under diffuse sound field conditions (EN 1793-1 and EN 1793-2), as those methods were used for certification purpose only, the full frequency range from 100 Hz to 5 kHz was always available.

In general, all analyses have been performed for single-number ratings calculated with the road traffic noise spectrum according to EN 1793-3 [8], as those results are more common on the European market and the client of the research CEDR, being an Organisation of European Road Directors, is obviously more interested in those results. Nevertheless, for data where third-octave band spectra are available, the analysis can be repeated in a similar way with single-number ratings weighted with the railway noise spectrum according to EN 16272-1 [9] and EN 16272-3-2 [10].

[1] In general, the materials have been defined according to the QUIESST classification presented in table 2.

[2] In this material category at least the surface layer consists of metallic material.

[3] This material category includes all wood-fibre concrete barriers, only self-supported concrete barriers have been considered separately.

[4] In this material category at least the surface layer consists of plastic material. It is relevant to note that this material category should not be confused with transparent barriers.

[5] In this material category of transparent barriers also mixed barriers have been included, where at least 50% of the barrier was declared as transparent.

## 3.1 Overall results on sound absorption under diffuse sound field conditions according to EN 1793-1

In order to have a better comprehension of the data collected a detailed statistical analysis of single-number ratings of sound absorption under diffuse sound field conditions was performed. As the data collected were always delivered from 100 Hz to 5 kHz, the full frequency range was always considered as a basis for the further analysis.

On this point it is worth to note, that there is a difference in the formula for the volume calculation in the newest version of the standard (published 2017) in comparison to the older standard (published in 2012): this difference lead to a small reduction in the single-number rating $DL_{\alpha,NRD}$. On the other hand, the data collected was mostly measured according to older version of the standard (88% of the total) and the data measured with the newest standard are concerning flat products with small volume, where the difference between new and old standard is generally less than 0.5 dB. In addition, it should be considered that the measurement uncertainty of the method under diffuse sound conditions is considerably higher than the difference between older and newest standard ($U$ = ± 2.4 dB according to EN ISO 12999-2), therefore, during the further analysis the results will be considered together.

In a first analysis step all data were plotted in a single statistical graph divided into 3 specific diagrams (see Figure 7): here in the top diagram (1) a classical box-plot of the data is shown, representing minimum, median, maximum values as well as 25% and 75% percentile values; then in the middle diagram (2) the statistical distribution of the data is plotted using classical histograms first and the probability density function (blue line) at different values, smoothed by a kernel density estimator, is shown. In the bottom diagram (3) every single measurement result is plotted in order to have a clear view of the data, which are behind the statistical analysis and the probability distribution.

In the case of the single-number ratings on sound absorption in the diffuse sound field all data points are between 0 and 20 dB, with circa 50% of the data being between 8 and 13 dB. The **median value is around 9.6 dB** with a clear peak in the kernel density distribution around 9 dB, showing that the most relevant part of the data is placed between 8 and 12 dB, while a second less pronounced peak is at the maximum value of 20 dB. It should be mentioned that the single-number rating is artificially bound to the upper limit of 20 dB in the calculation procedure.

In a second step the single-number rating results have been divided into different material types according to the most common materials collected.

Figure 8 shows the statistical analysis of the data collected on the single-number ratings on sound absorption under diffuse sound field conditions according to EN 1793-1 for every material separately: the coloured dots represent the values of the single-number ratings measured; while the grey area shows the so-called violin plot, which represents the kernel density estimation of the probability density function of the data collected.

Metal and plastic barriers are in general between 8 and 20 dB, while timber barriers are between 4 and 12 dB, wood-fibre concrete and sound absorbing concrete (self-supporting) are more spread between 4 and 20 dB, while transparent barriers are naturally less absorptive and reach values between 0 and 4 dB, whereas the higher values are referring to mixed barriers with up to 50% of transparent material.

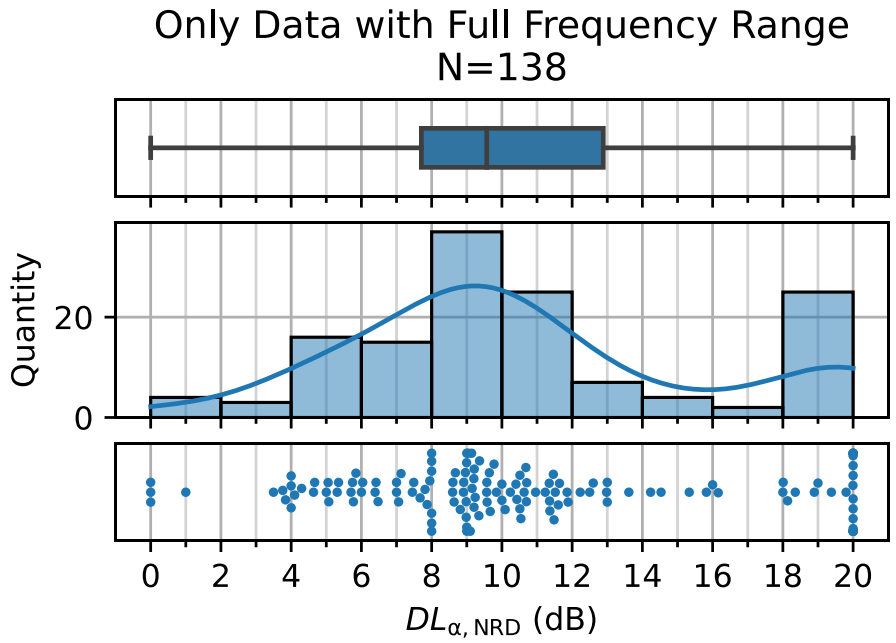


Figure 7: Statistical analysis of the single-number rating on sound absorption according to EN 1793-1: (1) box-plot of the data representing minimum, median, maximum value as well as 25% and 75% percentile values (top diagram); (2) histograms representing the statistical distribution of the data and the probability density function (blue line) at different values smoothed by a kernel density estimator (middle diagram); (3) single measurement results (bottom diagram). N is the number of data considered in total.

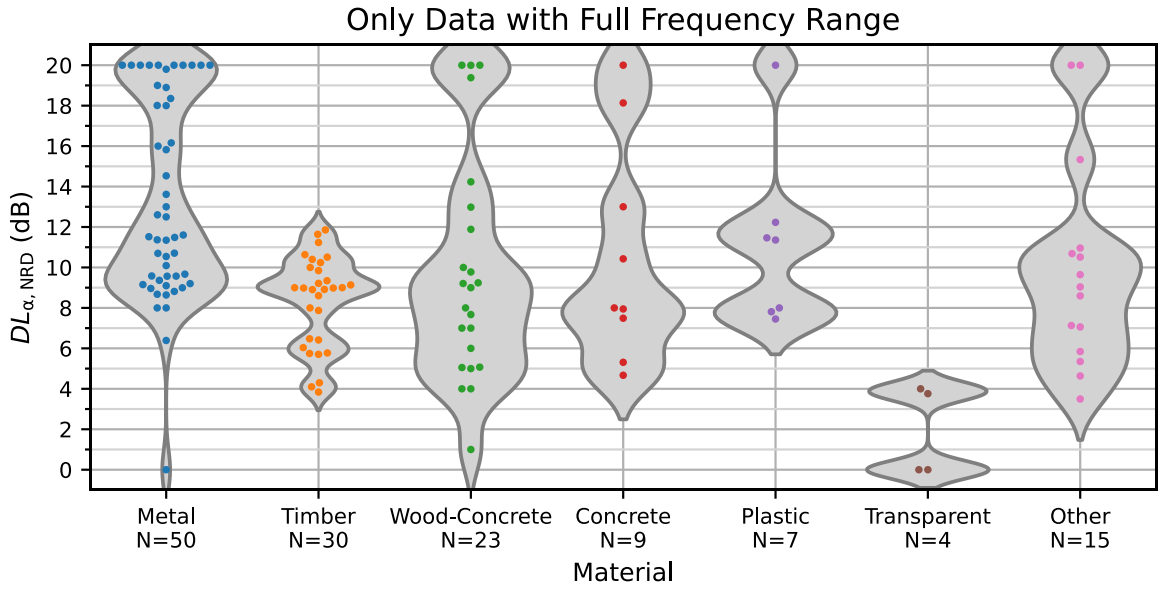


Figure 8: Statistical analysis of the data collected on the single-number rating on sound absorption according to EN 1793-1 for every material separately: the coloured dots represent the values of the single-number rating measured; while the grey area shows the violin plot, which represents the kernel density estimation of the probability density function of the data. N is the number of data considered for each material.

## 3.2 Overall results on airborne sound insulation under diffuse sound field conditions according to EN 1793-2

In order to have a better comprehension of the data collected a detailed statistical analysis of the data on single-number ratings of airborne sound insulation under diffuse sound field conditions was performed. As the data collected was always delivered from 100 Hz to 5 kHz, the full frequency range was always considered as a basis for the further analysis.

As mentioned before in a first step all data was plotted in a single statistical graph divided into three specific diagrams (see Figure 9).

In the case of the single-number rating on airborne sound insulation in the diffuse sound field all data points are in between 17 and 52 dB, with circa 50% of the data being between 24 and 33 dB. The **median value is around 28 dB**, with a peak in the kernel density distribution around 27 dB, showing that the most relevant part of the data is placed between 24 and 34 dB, while a second less pronounced peak is at the value of 47 dB.

In a second step the single-number rating results have been divided into different material types according to the most common materials collected.

Figure 10 shows the statistical analysis of the data collected on the single-number rating on airborne sound insulation under diffuse sound field conditions according to EN 1793-2 for every material separately: the coloured dots represent the values of the single-number ratings measured; while the grey area shows the violin plot, which represents the kernel density estimation of the probability density function of the data collected.

Metal, timber, plastic and transparent barriers are in general between 20 and 35 dB, while wood-fibre concrete and concrete barriers can reach higher values from 28 up to 52 dB.

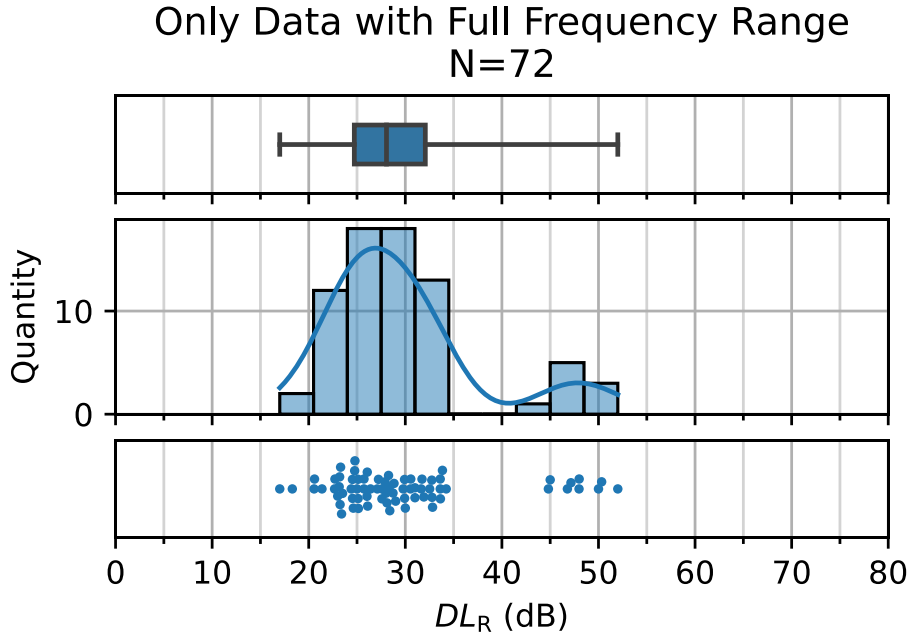


Figure 9: Statistical analysis of the single-number rating on airborne sound insulation according to EN 1793-2: (1) box-plot of the data representing minimum, median, maximum value as well as 25% and 75% percentile values (top diagram); (2) histograms representing the statistical distribution of the data and the probability density function (blue line) at different values smoothed by a kernel density estimator (middle diagram); (3) single measurement results (bottom diagram). N is the number of data considered in total.

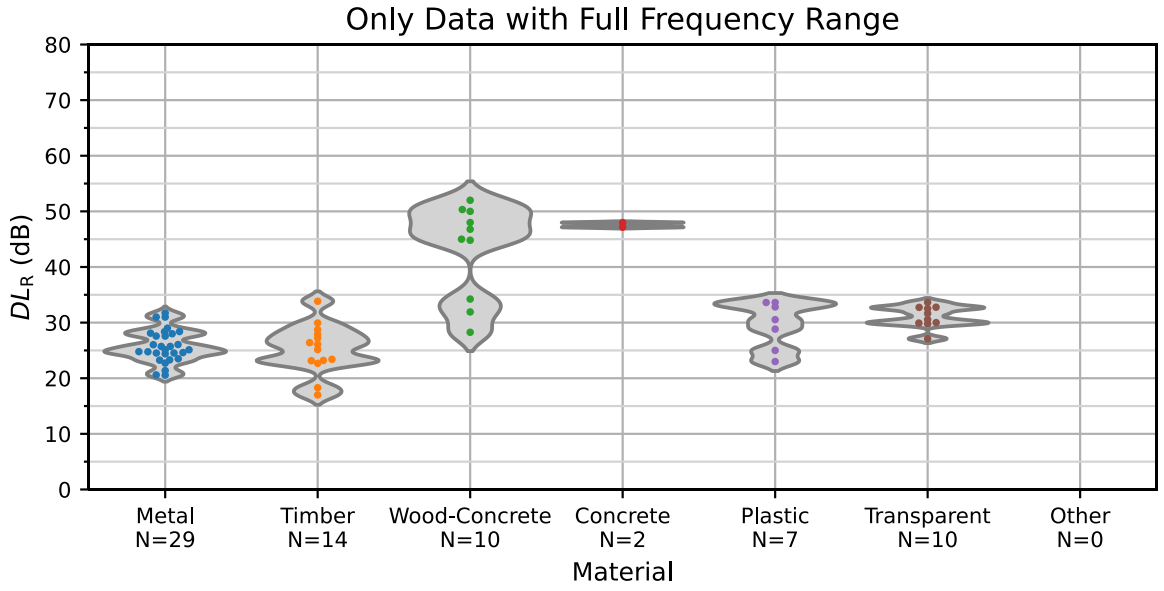


Figure 10: Statistical analysis of the data collected on the single-number rating on airborne sound insulation according to EN 1793-2 for every material separately: the coloured dots represent the values of the single-number rating measured; while the grey area shows the violin plot, which represents the kernel density estimation of the probability density function of the data. N is the number of data considered for each material.

## 3.3 Overall results on sound reflection under direct sound field conditions according to EN 1793-5 or CEN/TS 1793-5

In order to have a better comprehension of the data collected, a detailed statistical analysis of the data on single-number ratings of sound reflection under direct sound field has been performed.

In this special case it is worth to mention that the older data coming from the QUIESST database were mainly measured according to the old standard CEN/TS 1793-5 (also called Adrienne method), which was the only method published at the time of the project. Therefore, the results measured according to CEN/TS 1793-5 are marked with the label “Adrienne”, while the new results according to EN 1793-5 are marked with the label “QUIESST”.

As according to the Austrian project REFLEX [11] both methods are correlating very well ($R^2$ = 0.99) and the difference in terms of single-number ratings was between 0.5 and 0.9 dB, which is considerably less than the measurement uncertainty of the measurement method ($U$ = ±1.35 dB according to EN 1793-5), during the further analysis the results from EN 1793-5 and CEN/TS 1793-5 will not be separated anymore, but will be considered together.

Furthermore, as several data points according to EN 1793-5 were measured on site and not only for the purpose of certification, several data points were related to noise barriers smaller than 4 m height or width, meaning that those data points were valid only for a restricted frequency range. As a restricted frequency range generally leads to a significantly higher single-number rating (depending on the number of missing frequencies) the analyses have been performed always for both cases: (1) considering data with different frequency ranges (meaning that all validated data were included in the analysis) and (2) considering only data with valid results over the full frequency range from 200 Hz to 5 kHz (as specified in the EN 1793-5 for the purpose of certification).

Nevertheless, the results considering all frequency ranges should not be discarded as they represent meaningful and validated data of installed noise barriers. For this reason, both analyses will be shown in this chapter.

In a first step, all data were plotted in a single statistical diagram divided into 3 specific diagrams (see Figure 11): here the green line represents the probability density function of the data considering both methods (Adrienne and QUIESST), while the blue dots are the results according to EN 1793-5 (QUIESST method) and the orange dots are the results according to the CEN/TS 1793-5 (Adrienne method). The figure on the top (a) shows all validated data, including also data with different frequency ranges, while the figure on the bottom (b) shows only data where the full frequency range from 200 Hz to 5 kHz is available.

The results on sound reflection under direct sound field conditions are in general between 0 and 12 dB, with very few cases below 1 dB, and very few cases above 9 dB. The minimum results are by or very close to 0 dB, which is physically understandable in the case of full reflective barriers. The maximum values of 16 dB should be considered an “ideal” case, as this was not a real product placed on the market, but a special prototype, with full absorptive properties on the surface and very high surface structure. For this reason, **the best results representing real noise barriers should be considered in the range between 8 to 10 dB (excluding prototypes)**.

Furthermore, it is relevant to say that both diagrams (considering different frequency ranges and considering the full frequency range only) are showing a very similar statistical distribution, with a **prominent concentration of the results around 6 dB (median value)**, with circa 50% of data being between 4.6 and 6.8 dB (especially for the full frequency range). As expected, in the case of considering all frequency ranges the results tends to be slightly higher as the 50% of the data is placed between 4.9 and 6.7 dB. Nevertheless, in both cases the median value is placed around 6 dB. Due to the high amount of data considered, the statistical distribution and the probability function show a very consistent result.

In a further analysis step the single-number rating results have been divided into different material types according to the most common materials collected.

Figure 12 shows the statistical analysis of the data collected on the single-number rating on sound reflection for every material separately: the coloured dots represent the values of the single-number rating measured while the grey area shows the violin plot, which represents the kernel density estimation of the probability density function of the data collected. The figure on the top shows first all validated data, including also data with different frequency ranges, while the figure on the bottom shows only data where the full frequency range from 200 Hz to 5 kHz is available.

The statistical distribution for metal and timber barriers is rather similar, as the most part of the values are concentrated between 3 and 7 dB, but especially metal barriers can reach values around 8 dB or in some special cases even 10 to 12 dB. Other materials like concrete and wood-fibre concrete have a more widespread distribution, ranging from (close to) 0 to 10 or even 12 dB for special prototypes (for the full frequency range). For the other materials and for plastic the range can be also very different, from values close to 0, to values around 9 to 10 dB.

Transparent material barriers are naturally less absorptive and reach values between 0 and 4 dB, whereas the higher values are referring to mixed barriers with up to 50% of transparent material.

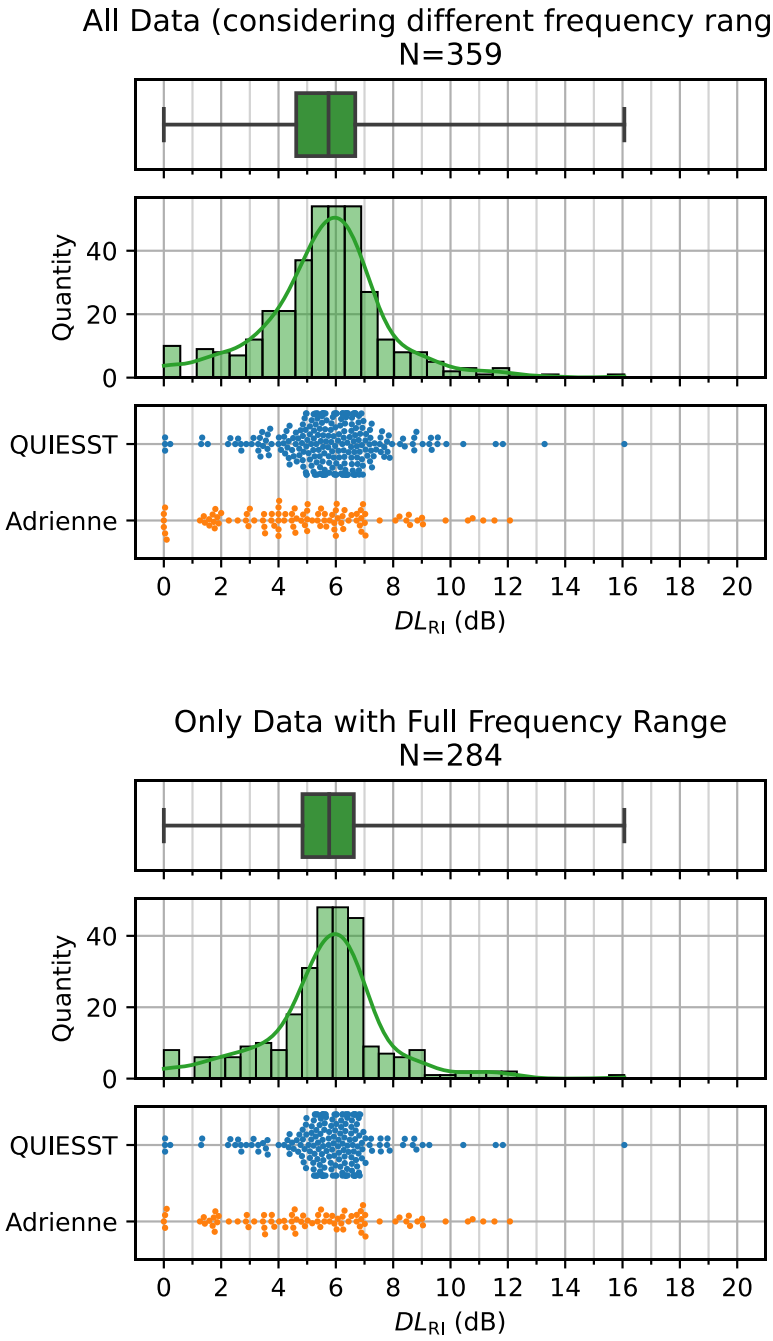


Figure 11: Statistical analysis of the single-number rating on sound reflection under diffuse sound field conditions according to EN 1793-5 or CEN/TS 1793-5: (1) box-plot of the data representing minimum, median, maximum value as well as 25% and 75% percentile values (top diagram); (2) histograms representing the statistical distribution of the data and the probability density function (green line) at different values smoothed by a kernel density estimator (middle diagram); (3) single measurement results (bottom diagram), the blue dots are the results according to EN 1793-5 (QUIESST method) and the orange dots are the results according to the CEN/TS 1793-5 (Adrienne method). The figure on the top (a) shows all validated data, including also data with different frequency ranges, while the figure on the bottom (b) shows only data where the full frequency range from 200 Hz to 5kHz is available. N is the number of data considered in total for both methods.

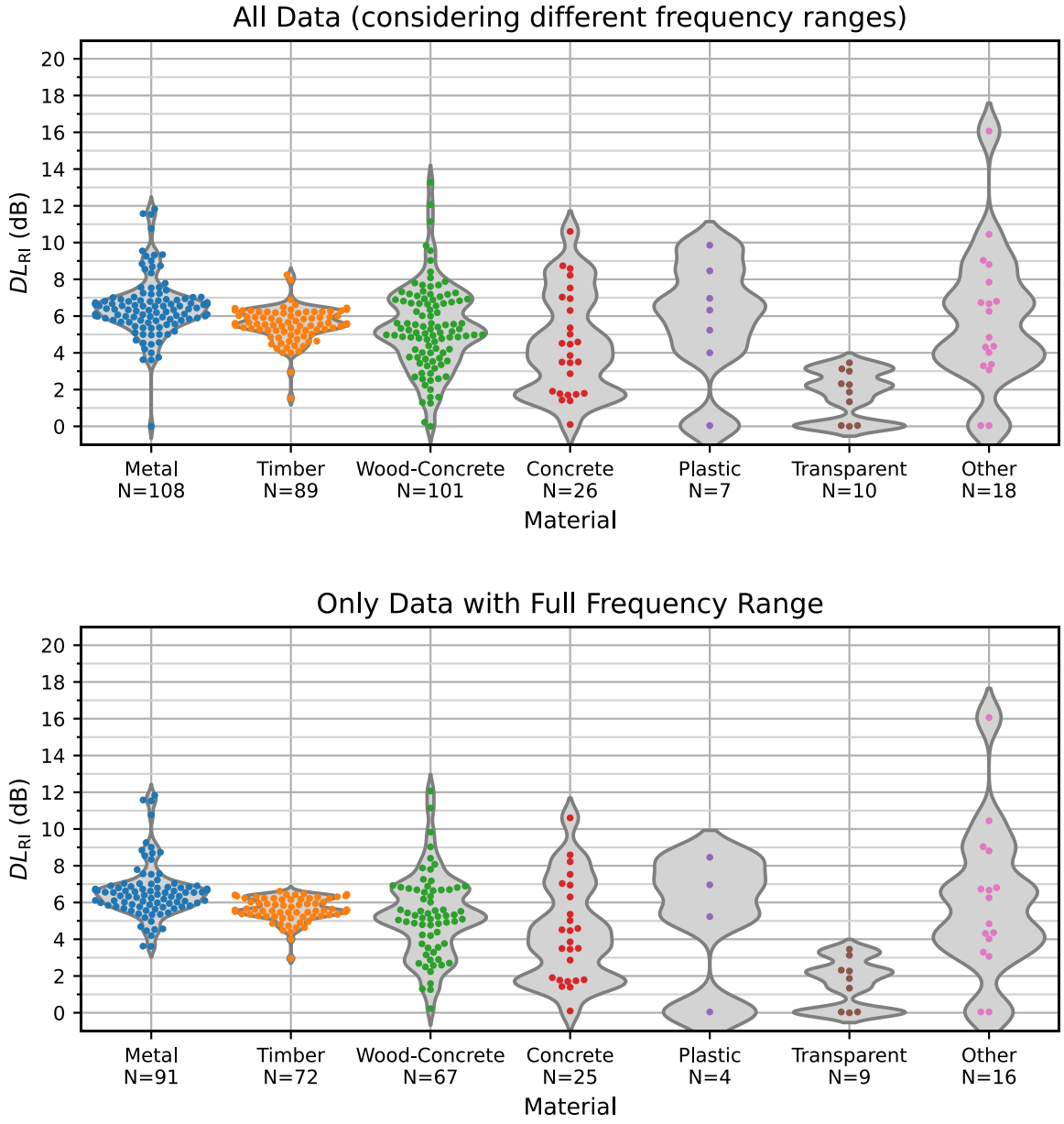


Figure 12: Statistical analysis of the data collected on the single-number rating on sound reflection according to EN 1793-5 or CEN/TS 1793-5 for every material separately: the coloured dots represent the values of the single-number rating measured; while the grey area shows the violin plot, which represents the kernel density estimation of the probability density function of the data. The figure on the top (a) shows all validated data, including also data with different frequency ranges, while the bottom figure (b) shows only data where the full frequency range from 200 Hz to 5kHz is available. N is the number of data considered for each material.

## 3.4 Overall results on airborne sound insulation under direct sound field conditions according to EN 1793-6

In order to have a better comprehension of the data collected a detailed statistical analysis of the data on single-number ratings of airborne sound insulation under direct sound field conditions has been performed.

Also in this case it relevant to say that several data points according to EN 1793-6 were measured on site and not only for certification purposes, several data points were related to noise barriers smaller than 4 m height or width, meaning that those data points were valid only for a restricted frequency range. As a restricted frequency range generally leads to a significantly higher single-number rating (depending on the number of missing frequencies) the analyses have been performed always for both cases: (1) considering data with different frequency ranges (meaning that all validated data were included in the analysis) and (2) considering only data with valid results over the full frequency range from 200 Hz to 5 kHz (as specified in the EN 1793-6 for the purpose of certification). Nevertheless, the results considering all frequency ranges should not be discarded as they represent meaningful and validated data of installed noise barriers. For this reason, both analyses will be shown in this chapter.

In a first step all data was plotted in a single statistical diagram divided into three specific diagrams (see Figure 13): the green line represents the probability density function of the data considering all data (element and post values), while the blue dots are the results measured in front of the element while the orange dots are the results measured in front of the post.

In the case of the single-number rating on airborne sound insulation under diffuse sound field conditions all data are in between 10 and 67 dB, with circa 50% of data being between 25 and 37 dB. The **median value of the data is around 32 dB**, with a peak in the kernel density distribution around 32 dB, showing that the most relevant part of the data is placed between 25 and 35 dB, while a second less pronounced peak is at the value of 55 dB.

In a further step the single-number ratings for “element”, “post” and “global” have been analysed separately: Figure 14 presents the statistical analysis of the single-number rating on airborne sound insulation according to EN 1793-6 for the three parameters: in blue, orange and green dots are the results respectively for “element”, “post” and “global” values. The figure on the top (a) shows all validated data, including also data with different frequency ranges, while the figure at bottom (b) shows only data where the full frequency range from 200 Hz to 5 kHz is available, while N is the number of data considered for each parameter.

It is relevant to note that the number of the element measurements is not equal to the number of post measurements and the global values, as some barriers have been measured only at the element or only at the post. So, the global values could only be calculated only in the cases where both measurements (acoustic element and post) were available.

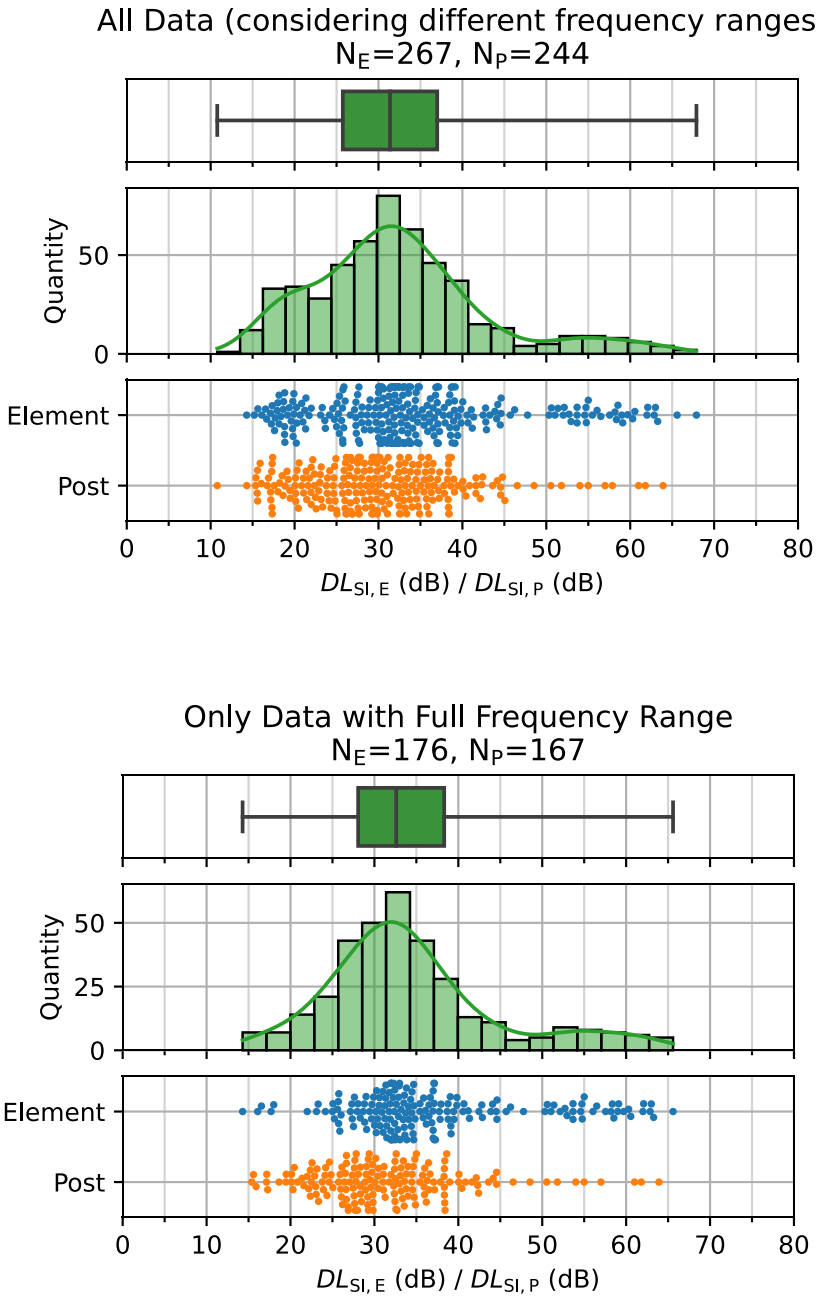


Figure 13: Statistical analysis of the single-number rating on airborne sound insulation according to EN 1793-6: (1) box-plot of the data representing minimum, median, maximum value as well as 25% and 75% percentile values for “element” and “post” merged together (top diagram); (2) histograms representing the statistical distribution of the data and the probability density function (for “element” and “post” merged) at different values smoothed by a kernel density estimator (middle diagram); (3) single measurement results (bottom diagram), the blue dots are the results “element” results, while the orange dots are the “post” results. The figure on the top (a) shows all validated data, including also data with different frequency ranges, while the figure at bottom (b) shows only data where the full frequency range from 200 Hz to 5kHz is available. N is the number of data considered for each parameter.

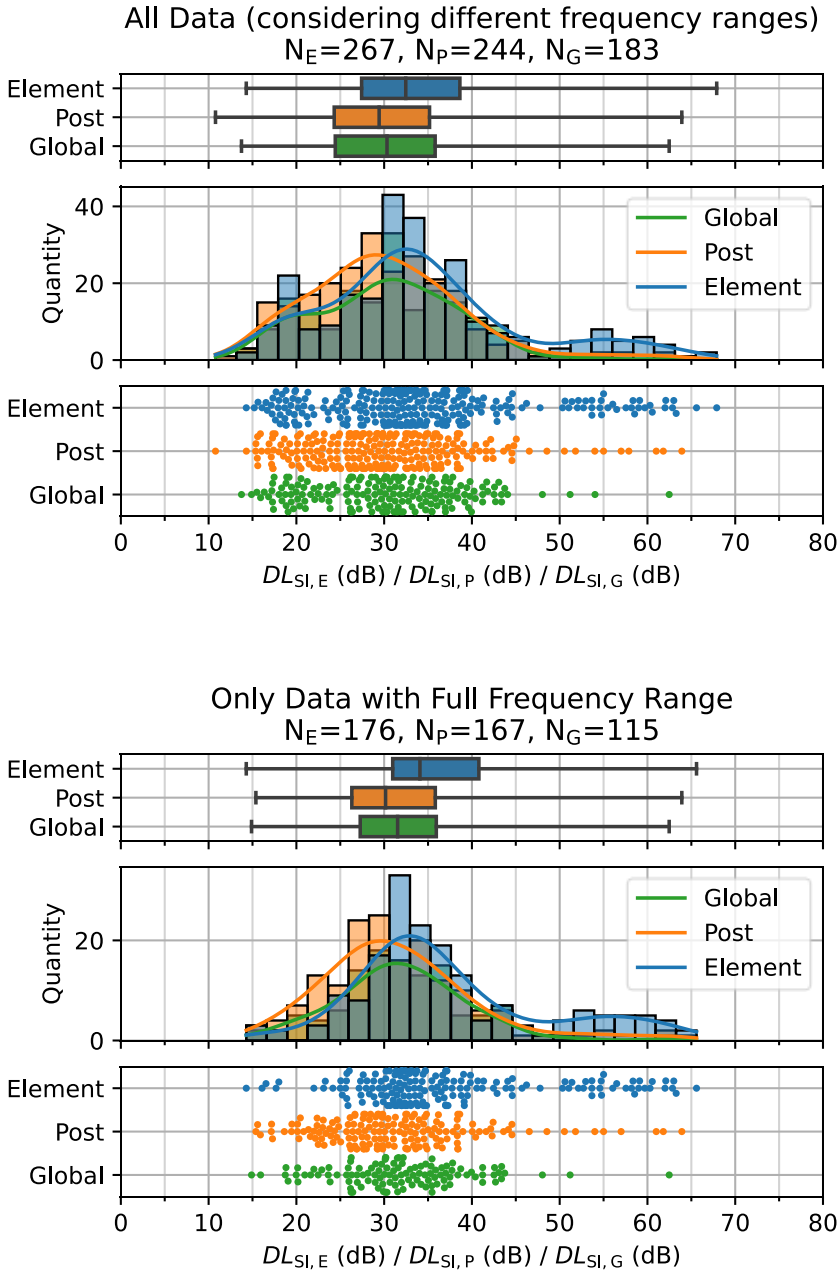


Figure 14: Statistical analysis of the single-number rating on airborne sound insulation according to EN 1793-6: (1) box-plot of the data representing minimum, median, maximum value as well as 25% and 75% percentile values respectively for “element”, “post” and “global” values (top diagram); (2) histograms representing the statistical distribution of the data and the probability density function (blue, orange and green lines respectively for “element”, “post” and “global” values) at different values smoothed by a kernel density estimator (middle diagram); (3) single measurement results (bottom diagram), the blue, orange and green dots are the results respectively for “element”, “post” and “global” values. The figure on the top (a) shows all validated data, including also data with different frequency ranges, while the figure at bottom (b) shows only data where the full frequency range from 200 Hz to 5kHz is available. N is the number of data considered for each parameter.

Again, the analysis performed with data considering the full frequency range lead to similar statistical distributions than considering data with different frequency ranges. **The median value is circa 34 dB for measurements performed in front of an element, while 30 dB for post and 31 dB** for the global value for the data considering the full frequency range. Due to the large amount of data considered, the statistical distribution and the probability function show a very consistent result.

In a further step the results on single-number ratings have been divided into different material types according to the most common materials collected.

Figure 15 shows the statistical analysis of the data collected on the single-number rating on airborne sound insulation under direct sound field conditions according to EN 1793-6 for every material separately for measurements performed in front of an element: the coloured dots represent the values of the single-number ratings measured while the grey area shows the violin plot, which represents the kernel density estimation of the probability density function of the data collected. Figure 16 shows the same analysis for results of measurements performed in front of post, while Figure 17 shows the results for the global value.

The single-number ratings for metal barriers (element) are in general quite narrow between 25 dB and 40 dB, while timber can be more spread between 15 dB and 42 dB. Transparent, plastic and concrete barriers reach in general higher values between 30 and 45 dB. Wood-fibre concrete are the most scattered material, as the values can range from a minimum of 15 dB up to very high values up to 66 dB. On this point, it is worth to remember that for the acoustic property of airborne sound insulation under direct sound field conditions the installation process is a relevant issue in order to have a noise barrier working properly, as several mistakes in the noise barrier installation can have a severe impact on the airborne sound insulation characteristic of the noise barrier on site.

In addition, a comparison between post and element measurements has been performed for every material. Figure 18 shows the statistical analysis of the data collected on the single-number rating on airborne sound insulation according to EN 1793-6 for every material separately comparing “element” and “post” values: the blue dots represent the values of the single-number rating measured in front of a noise barrier element, the orange dots the measurements performed in front of a post. The figure on the top (a) shows all validated data, including also data with different frequency ranges, while the figure on the bottom (b) shows only data where the full frequency range from 200 Hz to 5 kHz is available. N is the number of data considered for each material and each method. In general, the measurements in front of the post lead to a slightly lower value of around 2 to 3 dB in respect to the measurements at the acoustic element. Nevertheless, there are several cases where the values measured in front of the post are higher than the element values. This is often the case, when the noise barrier has some damages or leaks on the element.

Again, the analysis performed with data considering the full frequency range lead to similar statistical distributions than considering data with different frequency ranges.

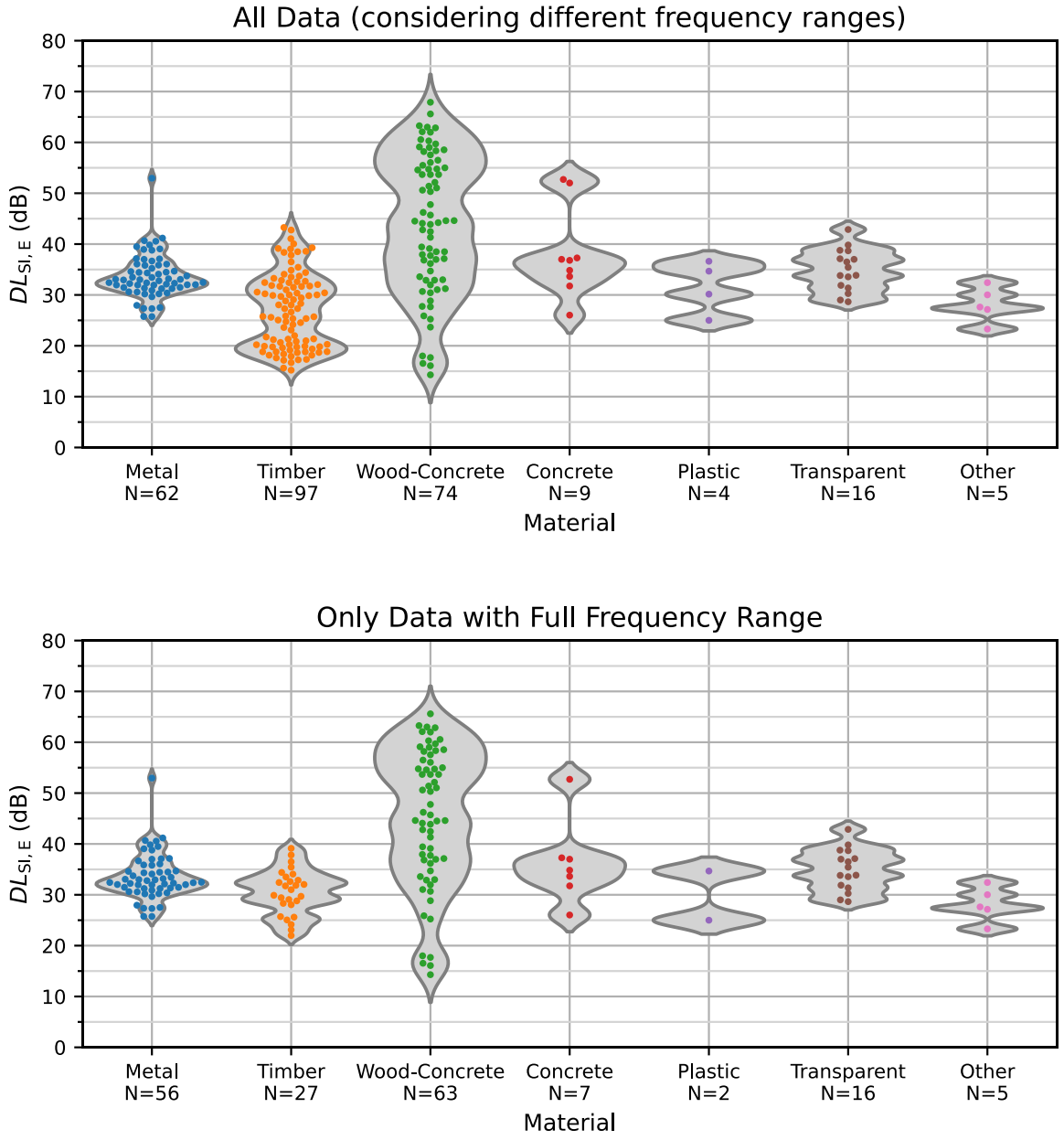


Figure 15: Statistical analysis of the data collected on the single-number rating on airborne sound insulation according to EN 1793-6 for every material separately (only measurements performed on the element): the coloured dots represent the values of the single-number rating measured; while the grey area shows the violin plot, which represents the kernel density estimation of the probability density function of the data. The figure on the top (a) shows all validated data, including also data with different frequency ranges, while the figure on the bottom (b) shows only data where the full frequency range from 200 Hz to 5kHz is available. N is the number of data considered for each material.

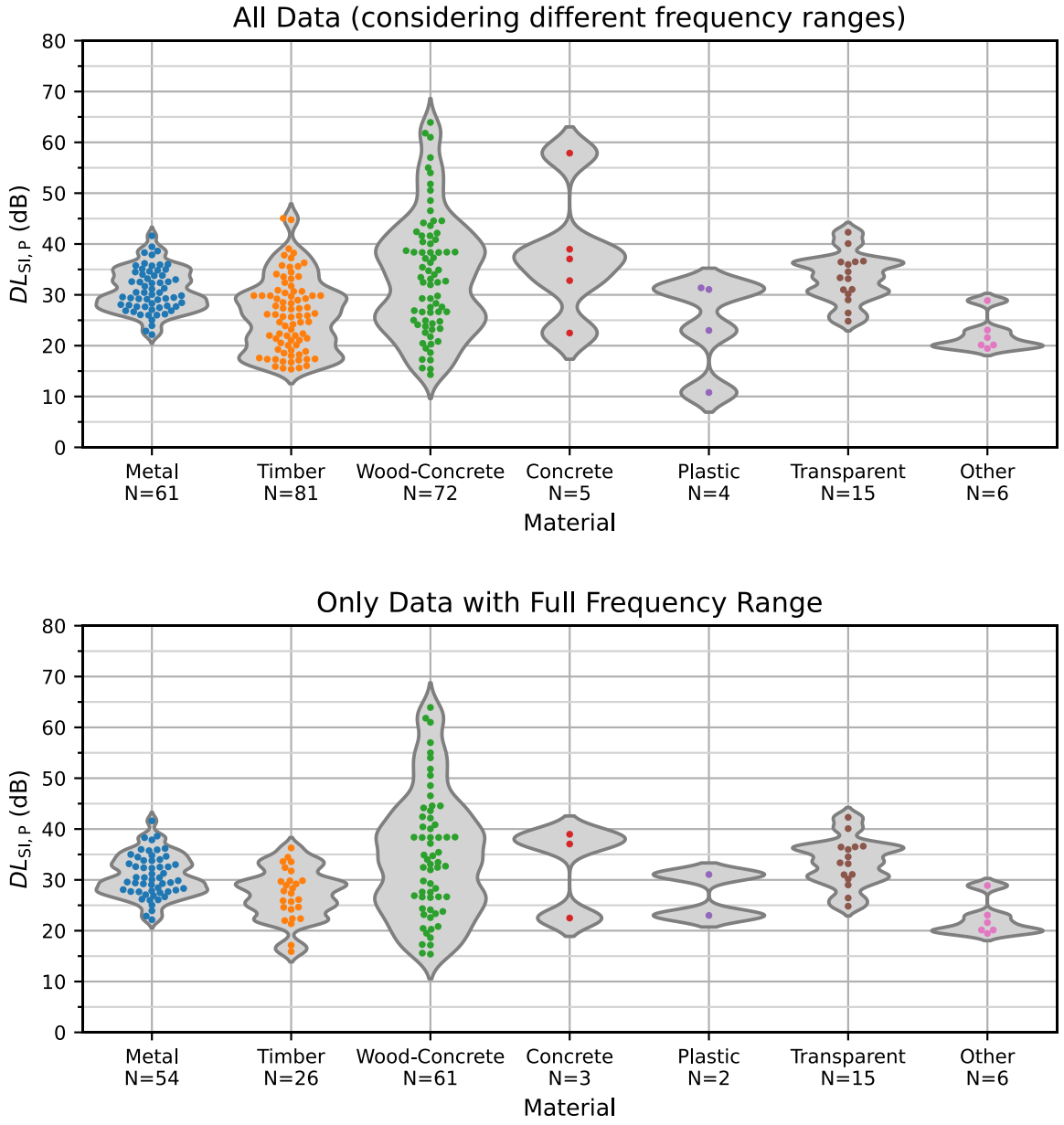


Figure 16: Statistical analysis of the data collected on the single-number rating on airborne sound insulation according to EN 1793-6 for every material separately (only measurements performed on the post): the coloured dots represent the values of the single-number rating measured; while the grey area shows the violin plot, which represents the kernel density estimation of the probability density function of the data. The figure on the top (a) shows all validated data, including also data with different frequency ranges, while the figure on the bottom (b) shows only data where the full frequency range from 200 Hz to 5kHz is available. N is the number of data considered for each material.

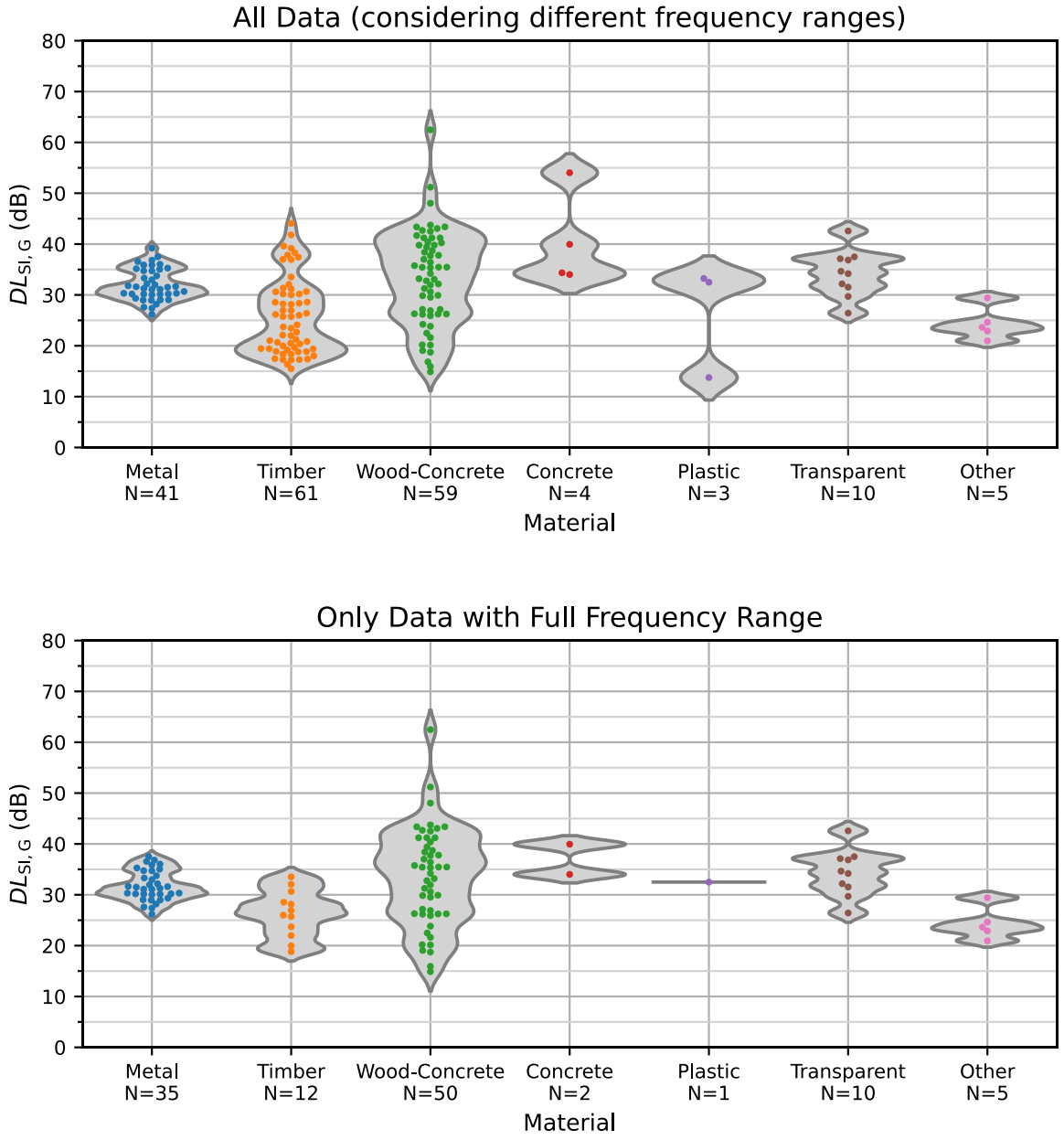


Figure 17: Statistical analysis of the data collected on the single-number rating on airborne sound insulation according to EN 1793-6 for every material separately (only global values, where both element and post was available): the coloured dots represent the values of the single-number rating measured; while the grey area shows the violin plot, which represents the kernel density estimation of the probability density function of the data. The figure on the top (a) shows all validated data, including also data with. different frequency ranges, while the figure on the bottom (b) shows only data where the full frequency range from 200 Hz to 5kHz is available. N is the number of data considered for each material.

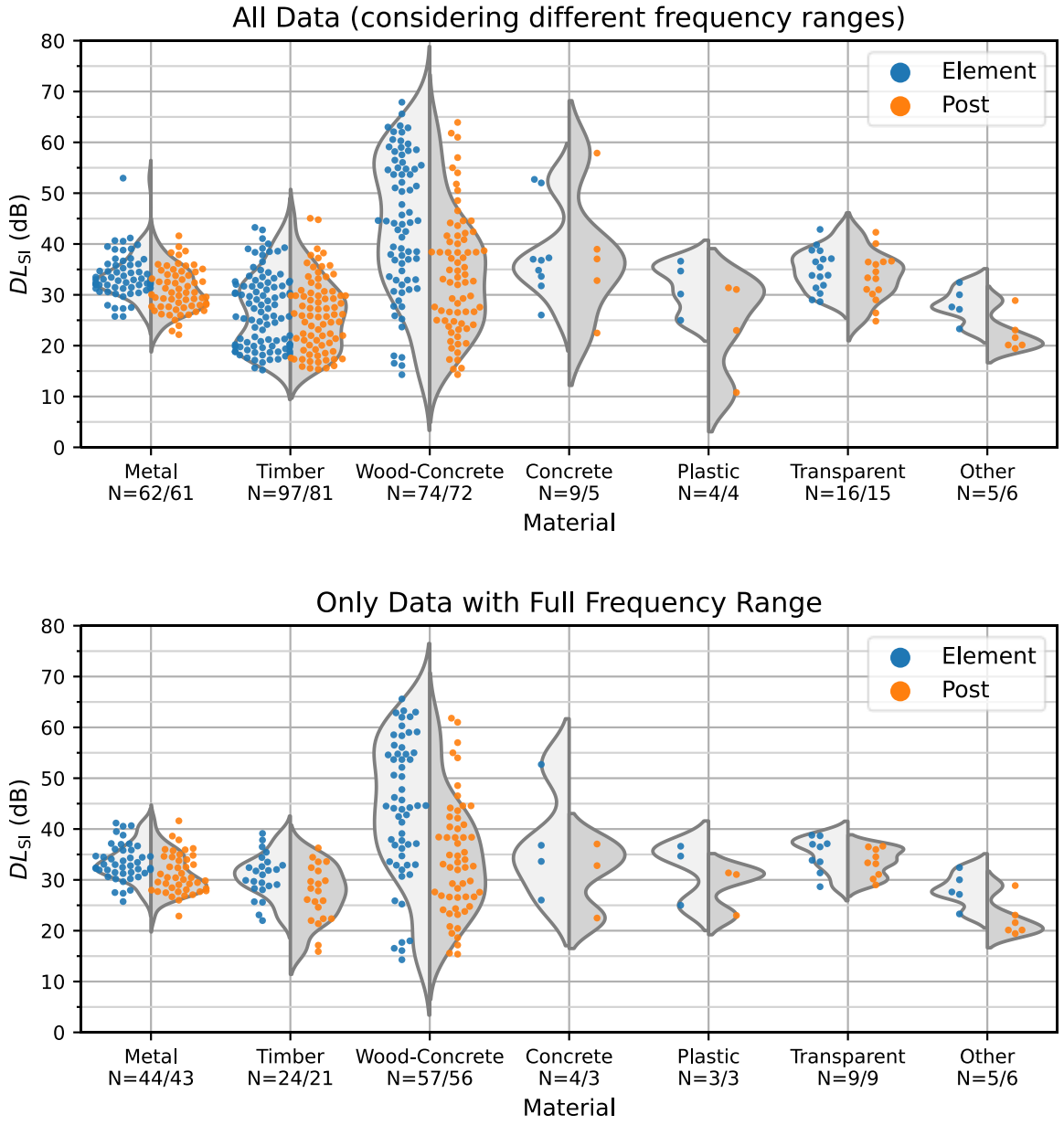


Figure 18: Statistical analysis of the data collected on the single-number rating on airborne sound insulation according to EN 1793-6 for every material separately: the blue dots represent the values of the single-number rating measured in front of a noise barrier element, the orange dots the measurements performed in front of a post; while the grey area shows the violin plot, which represents the kernel density estimation of the probability density function of the data. The figure on the top (a) shows all validated data, including also data with different frequency ranges, while the figure on the bottom (b) shows only data where the full frequency range from 200 Hz to 5kHz is available. N is the number of data considered for each material and each method.

# 4 Comparisons between single-number rating results measured under diffuse sound field conditions and results measured under direct sound field conditions

In this chapter a first comparison between single-number ratings of measurements collected is presented: first the results on sound absorption under diffuse sound field conditions (EN 1793-1) will be compared to the results on sound reflection under direct sound field conditions (EN 1793-5 or CEN/TS 1793-5), then the results on airborne sound insulation under diffuse sound field conditions (EN 1793-2) will be compared to the results on airborne sound insulation under direct sound field conditions (EN 1793-6).

For both comparisons, a first general statistical analysis on the overall data collected was performed using box plots, statistical distribution, probability function and the data results itself, while in a further step each material was analysed separately.

In order to have a better overview of the data, in chapter 3, the analysis have been presented both considering different frequency ranges and considering data with full frequency range only. As the statistical distribution of the data was very similar, in this chapter only data with full frequency range will be presented for the sake of simplicity. Nevertheless, the analysis considering all frequency ranges should not be discarded, those diagrams are shown in Annex A.

## *4.1 Comparison between results on sound absorption under diffuse sound field conditions and results on sound reflection under direct sound field conditions*

Figure 19 gives a first statistical overview of the data distribution for the single-number rating results according to EN 1793-1 and EN 1793-5 (or CEN/TS 1793-5). The blue area represents the statistical distribution of the single-number rating results on sound absorption in the diffuse field according to EN 1793-1, while the orange area represents the results on sound reflection according to EN 1793-5 or CEN/TS 1793-5. The box plot represents the minimum and the maximum values (discarding statistical outliers[6]), the 25% (Q1) and the 75% (Q3) percentile, while the white dot is the median value. The coloured areas show the violin plots, which represent the kernel density estimation of the probability density function of the data. This figure shows only data where the full frequency range from 200 Hz to 5 kHz is available. N is the number of datasets considered for each method.

The statistical distributions clearly show that values obtained with the method according to EN 1793-1 are in general considerably higher (in several cases up to maximum value of 20 dB) than the values obtained with the methods according to EN 1793-5 or CEN/TS 1793-5. The median value for the method according to EN 1793-1 is between 9 and 10 dB, while for the method according to EN 1793-5 the median value is around 6 dB. Also, the shape of the probabilistic functions is rather different, as in the first case the data is more spread and has a second peak on the maximum value, while in the second case the data is more focused between 4 and 8 dB.

On this point it is worth to mention that for sound absorption under diffuse sound field conditions, due to the calculation formula of the single-number rating the maximum reachable value is 20 dB. Therefore, applying the method according to EN 1793-1 several noise barriers reach the maximum value of 20 dB, while the values obtained with the method according to

[6] For additional information the whiskers of the boxplot were limited to the minimum and maximum value after outlier detection for these diagrams. If the interquartile range (Q3-Q1) is IQR, every data point smaller than Q1 – 1.5 IQR or greater than Q3 + 1.5 IQR is considered an outlier.

EN 1793-5 are generally lower with only few samples reaching values between 8 and 12 dB (only in one single case, a special prototype, not present on the market, reaches a single-number rating of 16 dB).

Again, due to the large amount of data considered, the statistical distribution and the probability function show a very consistent result.

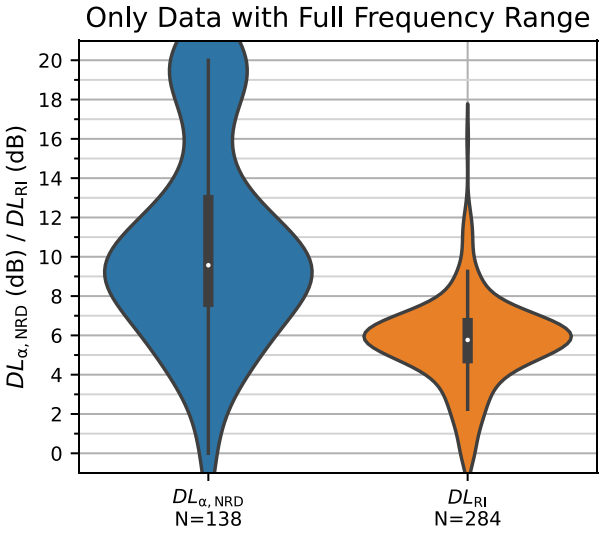


Figure 19: Comparison between the statistical distribution of the single-number rating results on sound absorption in the diffuse field according to EN 1793-1 (blue area) and the results on sound reflection according to EN 1793-5 or CEN/TS 1793-5 (orange area): the boxplot represents the minimum and the maximum value (discarding statistical outliers), the 25% and the 75% percentile, while the white dot is the median value. The coloured areas show the violin plots, which represent the kernel density estimation of the probability density function of the data. This figure shows only data where the full frequency range from 200 Hz to 5kHz is available. N is the number of datasets considered for each method.

Figure 20 shows the same probability functions as before, but in this case the coloured dots represent the measurement results, divided into different materials, while the grey areas are the probability density function of the data smoothed by a kernel density estimation. Again, this figure shows only data where the full frequency range from 200 Hz to 5 kHz is available.

In a further analysis step the single-number rating results of both methods have been compared for every material type separately. Figure 21 shows the comparison between single-number rating results on sound absorption according to EN 1793-1 (blue dots) and results on sound reflection according to EN 1793-5 or CEN/TS 1793-5 (green dots). The coloured dots represent the measurement results separated for every material, while the grey areas are the probability density function of the data smoothed by a kernel density estimation.

Therefore, the following first conclusion on the comparison between single-number ratings can be drawn: metal barriers reach values according to EN 1793-1 in general between 8 and 20 dB, while according to EN 1793-5 the values are between 4 and 11 dB, while the most part of those barriers reach values between 5.5 and 7.5 dB.

Regarding timber barriers the values according to EN 1793-1 are general between 4 and 12 dB, while according to EN 1793-5 the values are between 4 and 7 dB.

For concrete and wood-fibre concrete barriers the values are in general spread over the whole range between 0 and 20 dB according to EN 1793-1 and between 1 and 12 dB according to EN 1793-5, nevertheless the most part of the values are between 3 and 7 dB for direct sound field method.

For transparent barriers (including also mixed barriers) the results are very similar, as in both cases (EN 1793-1 and according to EN 1793-5) the results are between 0 and 4 dB, naturally dependent on the real amount of transparent material present in the test sample.

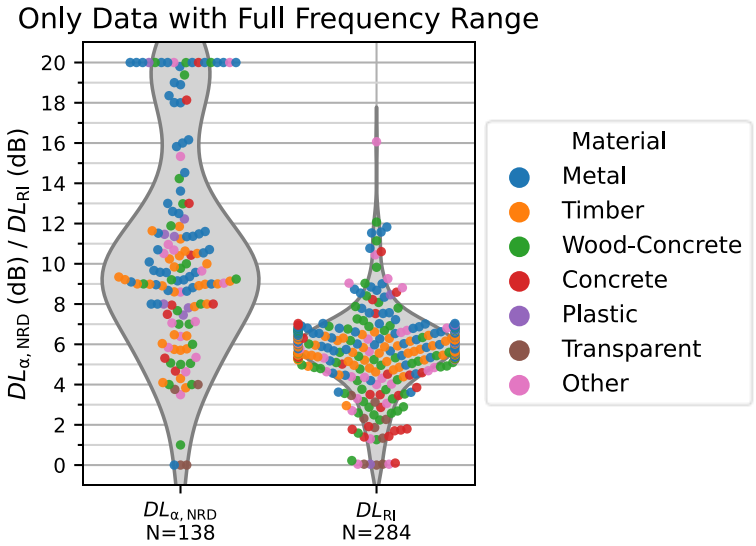


Figure 20: Comparison between single-number rating results on sound absorption according to EN 1793-1 (left) and results on sound reflection according to EN 1793-5 or CEN/TS 1793-5 (right). The coloured dots represent the measurement results, divided into different materials, while the grey areas are the probability density function of the data smoothed by a kernel density estimation. This figure shows only data where the full frequency range from 200 Hz to 5 kHz is available. N is the number of data considered for each method.

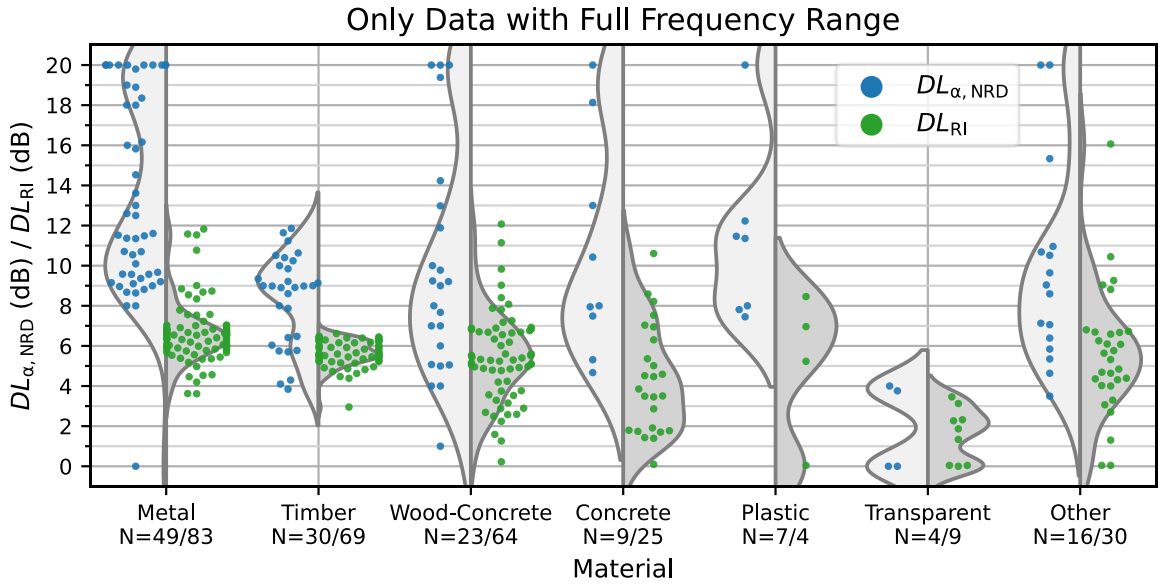


Figure 21: Comparison between single-number rating results on sound absorption according to EN 1793-1 (blue dots) and results on sound reflection according to EN 1793-5 or CEN/TS 1793-5 (green dots). The coloured dots represent the measurement results separated for every material, while the grey areas are the probability density function of the data smoothed by a kernel density estimation.

## 4.2 Comparison between results on airborne sound insulation under diffuse sound field conditions and results on airborne sound insulation under direct sound field conditions

In order to have a better understanding of the data the results on airborne sound insulation under direct sound filed conditions were analysed separately for their element, post and global values. Figure 22 gives a first statistical overview of the data distribution for the single-number rating results according to EN 1793-2 and EN 1793-6. The blue area represents the statistical distribution of the single-number rating results on airborne sound insulation in the diffuse field according to EN 1793-2, while the orange area represents the results on airborne sound insulation according to EN 1793-6 for the element. In green the values measured in front of the post and in red the global values are shown.

The statistical distributions show clearly that values obtained according to EN 1793-2 are in general slightly lower than the values obtained according to EN 1793-6. Element values are in general higher than the results on the post, while the global values are between those values. The median value for the method **according to EN 1793-2 is around 28 dB, while for the method according to EN 1793-6 the median values are around 34 dB for measurements at the acoustic element, 30 dB for measurements at the post and 31 dB for the global values**. Furthermore, the shape of the probability functions is rather similar, nevertheless the values according to EN 1793-6 can reach higher values up to 66 dB (especially at the element), while the values according to EN 1793-1 reach maximum values around 50 dB.

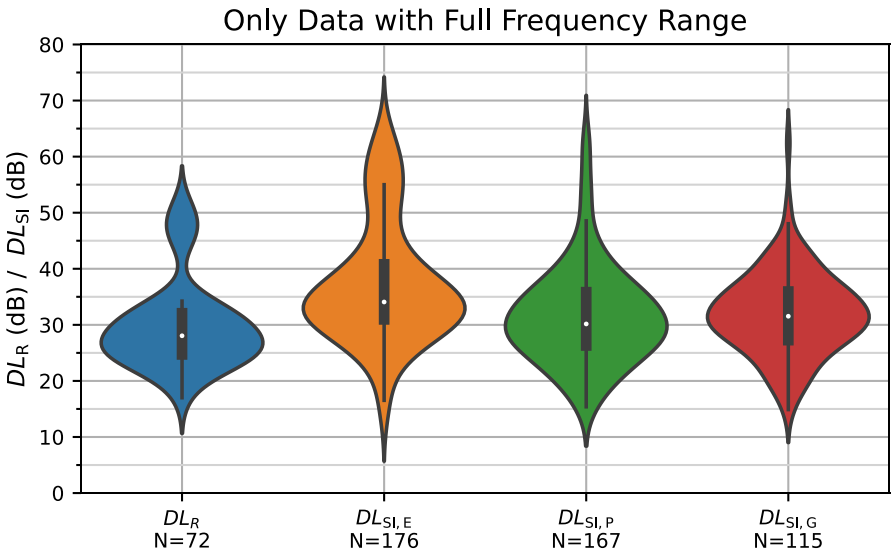


Figure 22: Comparison between the statistical distribution of the single-number rating results on airborne sound insulation according to EN 1793-2 (blue area) and the results on airborne sound insulation according to EN 1793-6 (orange area for “element”, green for “post” and red for “global” values): the box plot represents the minimum, the maximum value (discarding statistical outliers), and the 25% and the 75% percentile, while the white dot is the median value. The coloured areas show the violin plots, which represent the kernel density estimation of the probability density function of the data. This figure shows only data where the full frequency range from 200 Hz to 5 kHz is available. N is the number of data considered for each method.

Figure 23 shows the same probability functions as before, but in this case the coloured dots represent the measurement results, divided into different materials, while the grey areas are the probability density function of the data smoothed by a kernel density estimation. Again, this figure shows only data for which the full frequency range from 200 Hz to 5 kHz is available.

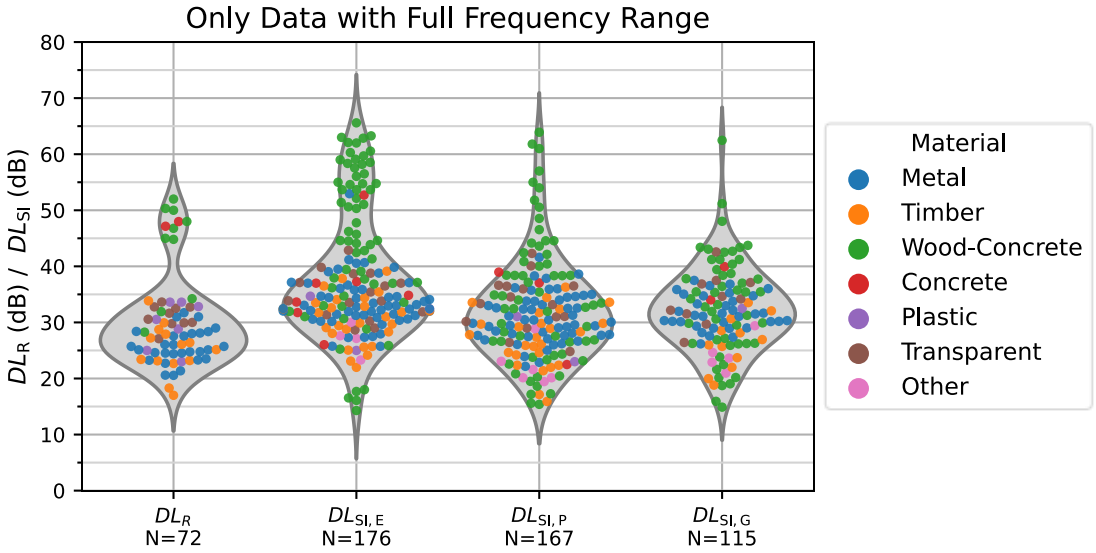


Figure 23: Comparison between single-number rating results on airborne sound insulation according to EN 1793-2 (left column) and results on airborne sound insulation according to EN 1793-6 (middle-left for “element”, middle-right for “post” and right for “global” values). The coloured dots represent the measurement results, divided into different materials, while the grey areas are the probability density function of the data smoothed by a kernel density estimation. This figure shows only data where the full frequency range from 200 Hz to 5 kHz is available. N is the number of data considered for each method.

In a further analysis step, the single-number rating results of both methods have been compared for every material type separately. Figure 24 shows the comparison between single-number rating results on airborne sound insulation according to EN 1793-2 (blue dots) and results on airborne sound insulation according to EN 1793-6 for values measured at the element (orange dots), for values measured at the post (green dots) and finally for global values (red dots). Also, in this case the results are shown for the full frequency range.

Therefore, the following first conclusion on the comparison between single-number ratings can be drawn: metal barriers reach values according to EN 1793-2 in general between 20 dB and 32 dB, while according to EN 1793-6 the values for global are between 22 and 42 dB.

Regarding timber barriers the values according to EN 1793-2 are very similar to the values according to EN 1793-6 (global values), for both methods between 16 and 36 dB.

For wood-fibre concrete barriers the values are in general more spread over the whole range, especially for the values according to EN 1793-6, as those measurements are performed under real life conditions and the installation process has an heavier impact on the results: The results are between 29 and 52 dB according to EN 1793-2 and between 15 and 65 dB according to EN 1793-6 (global values).

For transparent barriers (including also mixed barriers) the results are between 26 and 34 according to EN 1793-2, while the results according to EN 1793-6 can reach higher results between 26 and 43 dB (global values).

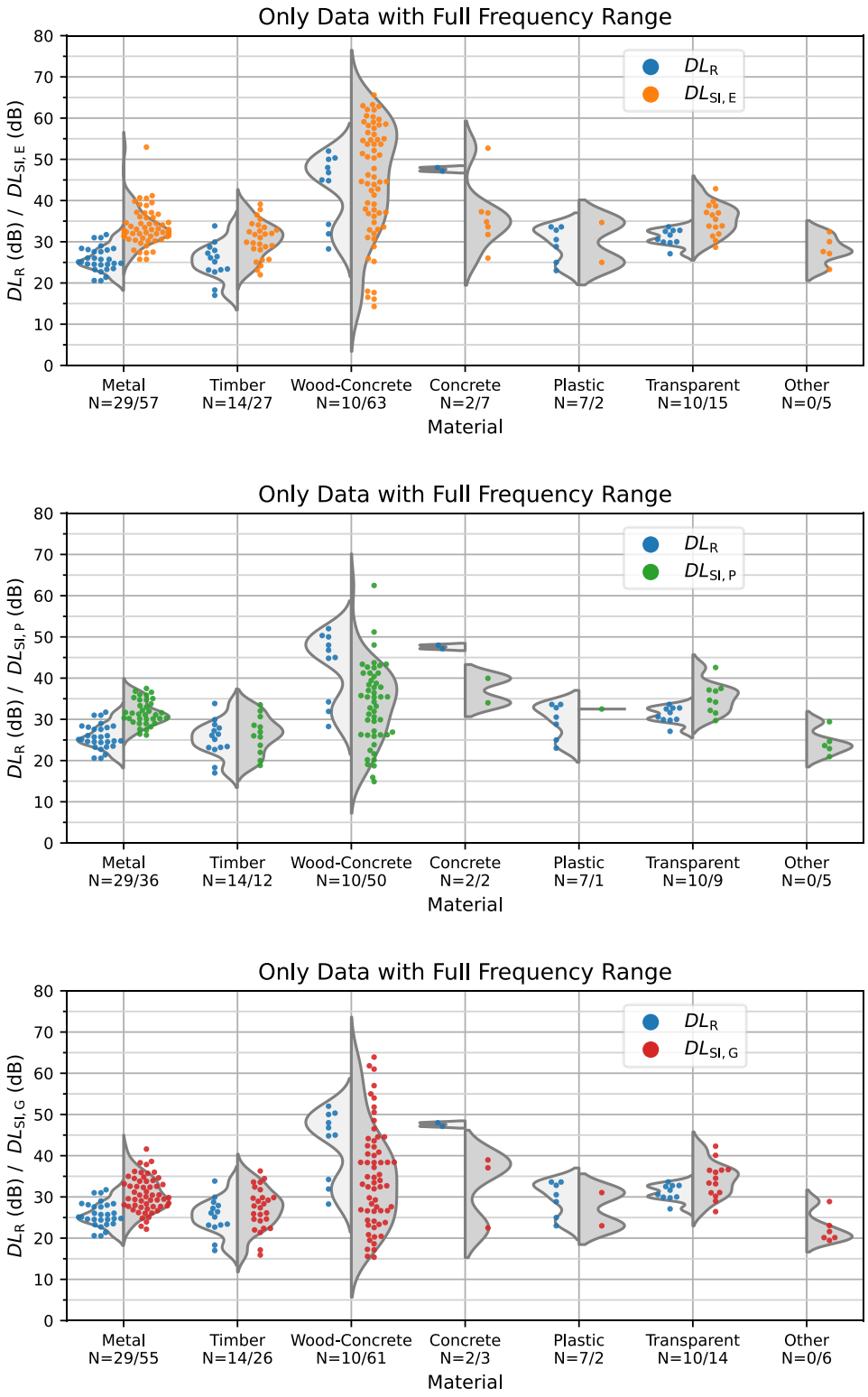


Figure 24: Comparison between single-number rating results on airborne sound insulation according to EN 1793-2 (blue dots) and results on airborne sound insulation according to EN 1793-6 (orange dots are values at the element, green dots at the post, while red dots represent global values). The coloured dots represent the measurement results separated for every material, while the grey areas are the probability density function of the data smoothed by a kernel density estimation. This figure shows only data where the full frequency range from 200 Hz to 5 kHz is available.

# 5 Overview of the third-octave band frequency spectra

In this chapter the in third-octave band frequency spectra of the measurements collected are presented for every method separately: first the results on sound absorption under diffuse sound field conditions according to EN 1793-1, then the results on airborne sound insulation under diffuse sound field conditions according to EN 1793-2, then the results on sound reflection under direct sound field conditions according to EN 1793-5 or CEN/TS 1793-5 and finally the results on airborne sound insulation under direct sound field conditions according to EN 1793-6.

The statistical analysis was performed for all validated datasets independent from the available frequency range for every material separately. Therefore, for the measurement methods for direct sound field conditions (EN 1793-5, CEN/TS 1793-5 and EN 1793-6) lower third-octave bands may contain less data points, due to a limited frequency range.

Nevertheless, only valid frequency ranges regarding the dimensions of the noise barrier under test have been included in the analysis. For the sake of simplicity, in this section, only diagrams with statistical significance are presented. Nevertheless, the analysis has been performed for all materials: these diagrams are shown in Annex B and Annex C.

## *5.1 Third-octave band results on sound absorption under diffuse sound field conditions according to EN 1793-1*

Figure 25 shows the frequency spectra in third-octave bands on sound absorption according to EN 1793-1 for metal, timber and wood-fibre concrete barriers. The dots are the measurement results; the blue line is the average spectrum for each noise barrier material, the grey area represents the 95% confidence interval of the average spectrum, while orange and blue areas represent respectively the 50% and 95% range of the data, while N is the number of data considered for the diagram presented.

In general the data on sound absorption under diffuse sound field conditions shows a clear trend for each barrier material: for some noise barrier materials like metal and timber a very homogeneous trend can be recognised. The coinfidence interval of the average and the 50% of the data are in a very narrow range. For wood-fibre concrete the values collected were more spread. For other materials, the amount of available data was not large enough to have a statistical robustness; nevertheless, those results are presented in Annex B.

The average spectrum of the metal barriers shows a very high absorption coefficient, reaching values higher than 0.9 between 250 Hz to 3.15 kHz, while for timber barriers similar values can be seen between 400 Hz and 1 kHz. The average spectrum of wood-fibre concrete barriers has a different shape, which is increasing with higher frequencies, reaching values above 0.9 between 400 Hz and 5 kHz.

## *5.2 Third-octave band results on airborne sound insulation under diffuse sound field conditions according to EN 1793-2*

Figure 26 shows the frequency spectra in third-octave bands on airborne sound insulation according to EN 1793-2 for metal, timber and wood-fibre concrete barriers.

In general, the data on airborne sound insulation under diffuse sound field conditions shows a clear and homogeneus trend for all shown barrier materials. The coinfidence interval of the average and the 50% of the data are in a very narrow range. For other materials like concrete, plastic and transparent barriers the available data were not enough in order to have a statistical robustness, nevertheless those results are presented in Annex B.

All average spectral values are increasing with higher frequencies. For metal barriers the values start around 15 dB at low frequencies, reaching more than 35 dB for higher frequencies, while timber barriers have values between 20 and 40 dB; wood-fibre concrete has as expected higher values starting from circa 35 dB at low frequencies and reaching values above 50 dB at high frequencies. Also, in this case wood-fibre concrete barriers are more scattered than metal and timber barriers, which have very consistent and homogeneous results.

## 5.3 Third-octave band results on sound reflection under direct sound field conditions according to EN 1793-5

Figure 27 presents the frequency spectra in third-octave bands on sound reflection according to EN 1793-5 or CEN/TS 1793-5 for metal, timber and wood-fibre concrete barriers.

In general the data on sound reflection under direct sound field conditions shows a very consistent trend for each barrier material. The coinfidence interval and the 50% of the data are in a very narrow range, especially for metal and timber barriers, while the frequency spectra of wood-fibre concrete barriers are again more spread. For other material the data available was not large enough in order to reach a statistical robustness, nevertheless those results are presented in Annex C.

The average spectrum of the metal barriers shows a clear minimum in the reflection index $RI$ at 1.6 kHz, while for timber barriers the minimum is reached between 350 Hz and 630 Hz, and a second local minimum is present around 1.6 kHz. The average spectrum of wood-fibre concrete barriers has again a different shape and shows a more scattered behaviour, having minimum values in the range between 630 Hz and 1.6 kHz. The 50% range of the reported $RI$ values is significantly higher than for the other materials. A cause might be, that generally wood-fibre concrete noise barriers have a distinct and often periodic surface roughness, which has a significant influence on the spectrum. It should also be noted that the high number of available samples gives a good estimate of the average spectrum with a relatively small confidence interval.

## 5.4 Third-octave band results on airborne sound insulation under direct sound field conditions according to EN 1793-6

Figure 28 and Figure 29 respectively show the frequency spectra in third-octave band on airborne sound insulation according to EN 1793-6 for metal, timber and wood-fibre concrete barriers.

In general the data on airborne sound insulation under direct sound field conditions shows a less homogeneus trend than for the other methods for all the materials, nevertheless it is possible to identify a clear trend for each material separetely. Again, for metal and timber barriers the data is rather homogeneous, especially at low frequency, while for wood-fibre concrete the results are more spread for the whole frequency spectrum. For other materials the amount of available data was not large enough in order to reach a statistical robustness, nevertheless those results are presented in Annex C.

All average spectra are increasing with higher frequencies. For metal barriers the values start around 20 dB at low frequencies, reaching more than 50 dB for higher frequencies, while timber barriers have values between 20 and 35 dB; wood-fibre concrete has as expected higher values starting from circa 40 dB at low frequencies and reaching values above 55 dB at high frequencies. The 50% range of the reported $SI$ values is significantly higher than for metal and timber barriers, which gives a clear indication of the wide spread of the third-octave band results for wood-fibre concrete barriers. The values at the post are in general slightly lower than at the acoustic element.

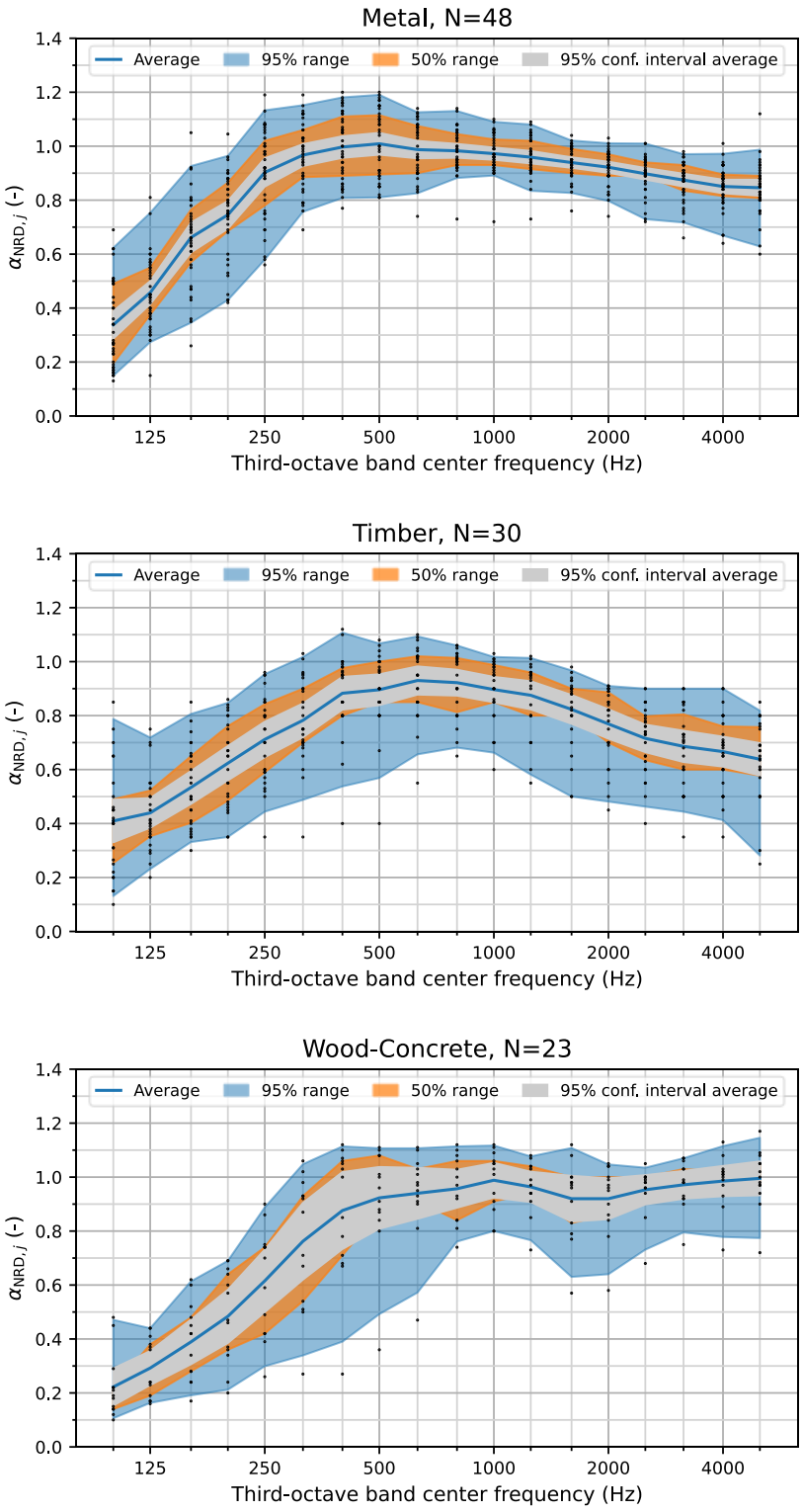


Figure 25: Frequency spectra in third-octave bands on sound absorption according to EN 1793-1 for metal (top), timber (middle) and wood-fibre concrete barriers (bottom). The dots are the measurement results; the blue line is the average spectrum for each noise barrier material, the grey area represents the 95% confidence interval of the average, while orange and blue areas represent respectively the 50% and 95% range of the data. N is the number of data considered for each material.

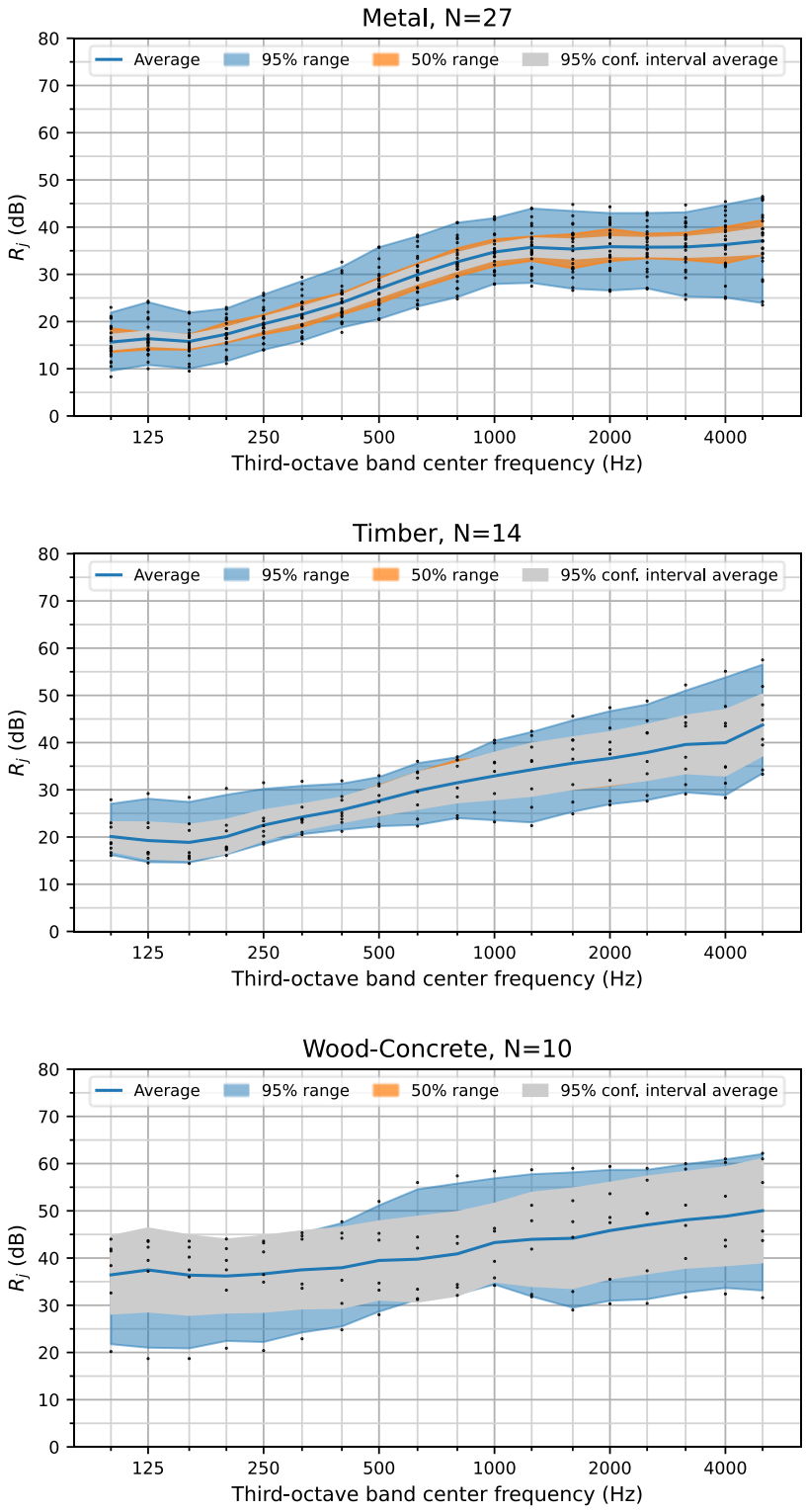


Figure 26: Frequency spectra in third-octave bands on airborne sound insulation according to EN 1793-2 for metal (top), timber (middle) and wood-fibre concrete barriers (bottom). The dots are the measurement results; the blue line is the average spectrum for each noise barrier material, the grey area represents the 95% confidence interval of the average, while orange and blue areas represent respectively the 50% and 95% range of the data. N is the number of data considered for each material.

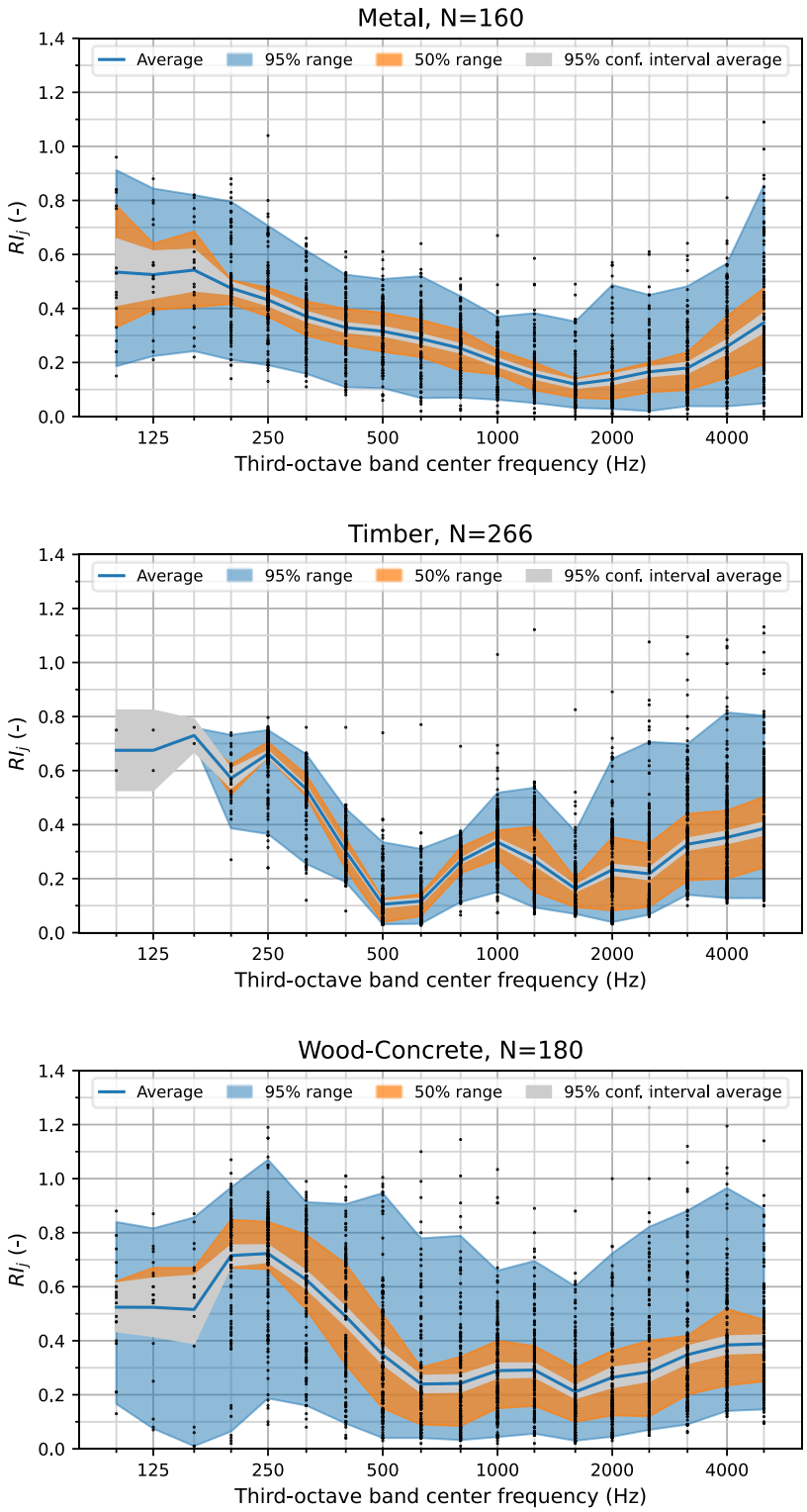


Figure 27: Frequency spectra in third-octave bands on sound reflection according to EN 1793-5 or CEN/TS 1793-5 for metal (top), timber (middle) and wood-fibre concrete barriers (bottom). The dots are the measurement results; the blue line is the average spectrum for each noise barrier material, the grey area represents the 95% confidence interval of the average, while orange and blue areas represent respectively the 50% and 95% range of the data. N is the number of data considered for each material.

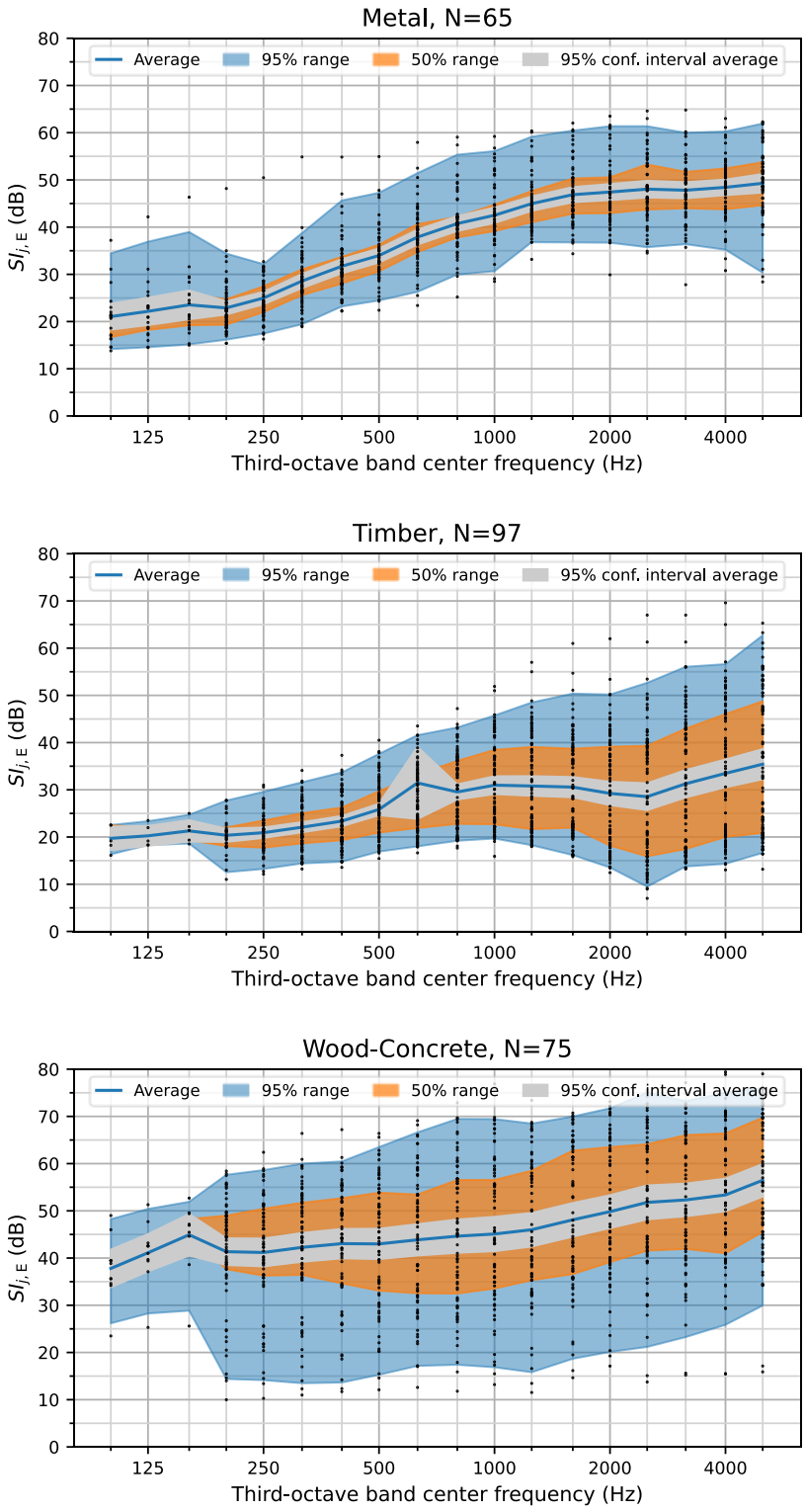


Figure 28: Frequency spectra in third-octave bands on airborne sound insulation according to EN 1793-6 for metal (top), timber (middle) and wood-fibre concrete barriers (bottom) measured before the acoustic element. The dots are the measurement results on the element; the blue line is the average spectrum for each noise barrier material, the grey area represents the 95% confidence interval of the average, while orange and blue areas represent respectively the 50% and 95% range of the data. N is the number of data considered for each material.

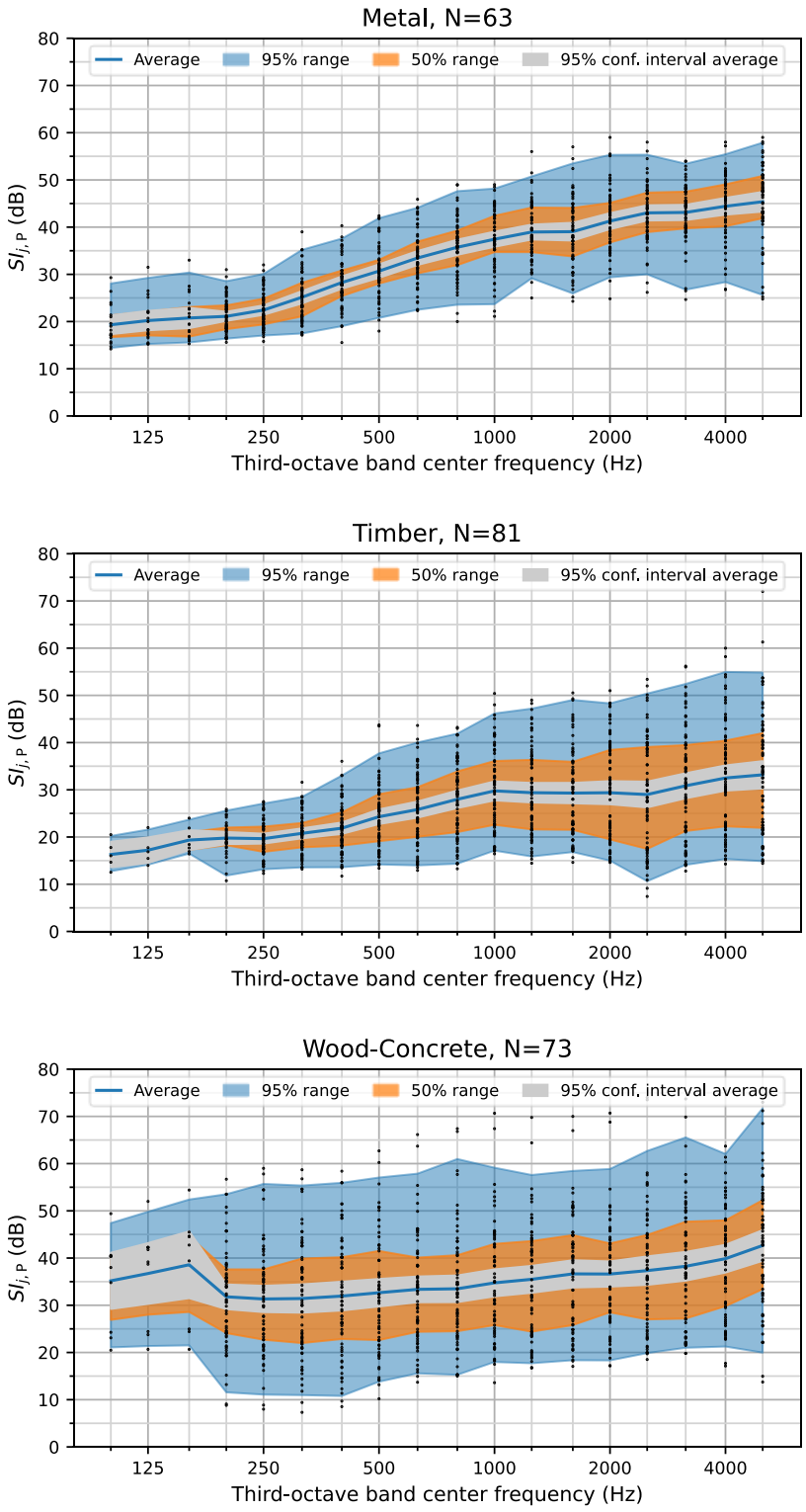


Figure 29: Frequency spectra in third-octave bands on airborne sound insulation according to EN 1793-6 for metal (top), timber (middle) and wood-fibre concrete barriers (bottom) measured before the post. The dots are the measurement results on the post; the blue line is the average spectrum for each noise barrier material, the grey area represents the 95% confidence interval of the average, while orange and blue areas represent respectively the 50% and 95% range of the data. N is the number of data considered for each material.

Figure 30 presents finally the frequency spectra in third-octave bands on airborne sound insulation according to EN 1793-6 for transparent barriers for the element (top) and for the post (bottom). Again, the results are very consistent, the values increase with higher frequencies. The difference between element and post measurements is rather small, as the element values start around 25 dB at low frequencies, reaching more than 45 dB at high frequencies, while measurements at the post show values between 20 and 40 dB.

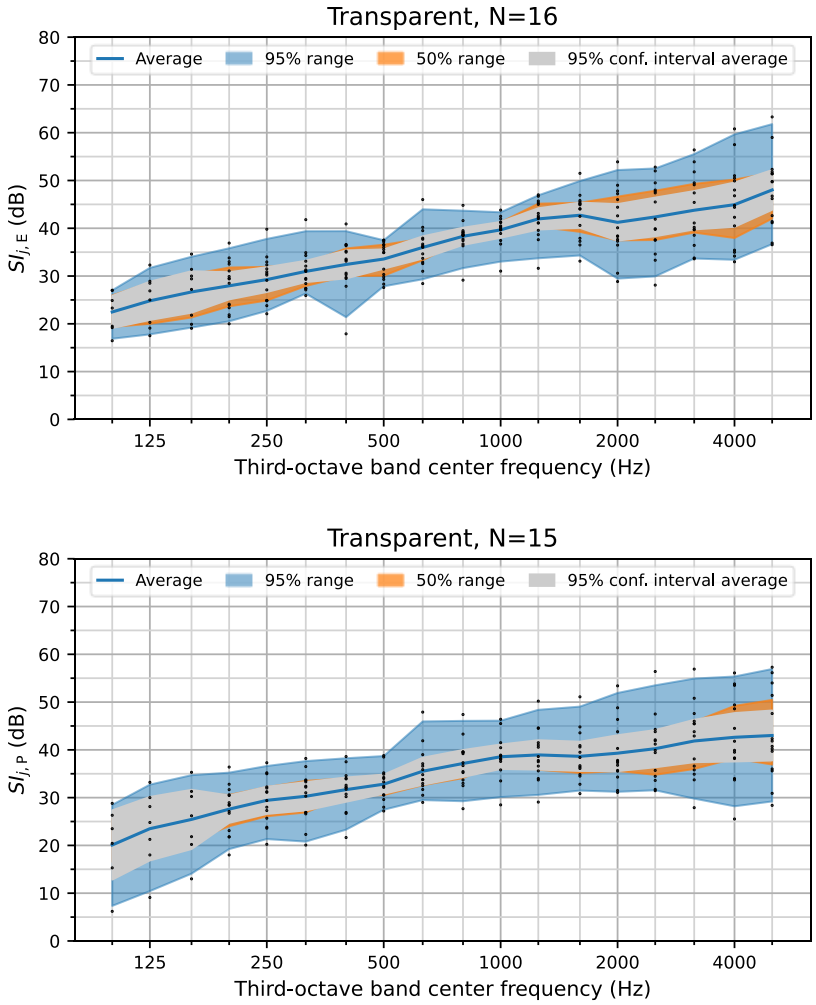


Figure 30: Frequency spectra in third-octave bands on airborne sound insulation according to EN 1793-6 for transparent barriers for the acoustic element (top) and for the post (bottom). The dots are the measurement results; the blue line is the average spectrum for each noise barrier material, the grey area represents the 95% confidence interval of the average, while orange and blue areas represent respectively the 50% and 95% range of the data. N is the number of data considered.

# 6 Empirical study on the correlation between measurement methods under diffuse sound field conditions and methods under direct sound filed conditions

The significant physical differences in the measurement methods for testing the intrinsic characteristics of noise barriers were explained in detail in deliverable D2.1 [1]. Nevertheless, the structural storage of the collected data in the database gives the opportunity to look back for more detailed empiric statistical correlations between the measurement methods for measuring sound absorption under diffuse field conditions (according to EN 1793-1) and the method for measuring sound reflection under direct sound field conditions according to EN 1793-5 as well as measuring airborne sound insulation under diffuse sound field conditions (according to EN 1793-2) and under direct sound field conditions (according to EN 1793-6).

Deliverable D4.3 of the QUIESST project [7] presented similar correlations of the available data at that time. With the extension of the QUIESST database in the SOPRANOISE project further insights can now be accomplished, although it should be noted that the amount of data, where results for both methods are available (under diffuse and under direct sound field conditions) is still limited and remains a crucial point. Therefore, the most challenging factor is the availability of reported measurement results to the SOPRANOISE partners of the same noise barrier for measurements under diffuse as well as under direct sound field conditions.

In this circumstance, "*same noise barriers"* refers to the same noise barrier product type, because most of the time not exactly the same noise barrier elements are tested in measurements under diffuse or direct sound field conditions. Nevertheless, in comparison to the QUIESST database the SOPRANOISE database has enough data points to perform the correlation analysis for the full frequency-range for the measurement methods, i.e. from 100 Hz to 5 kHz for the diffuse sound field methods and from 200 Hz to 5 kHz for the direct sound field methods respectively.[7]

Additionally, the correlation models are expanded to use third-octave band data instead of single-number ratings only. The goal of a regression model is to predict the single-number ratings based on the results originating from the complementary measurement method (e.g. calculating $DL_{\mathrm{RI}}$ from measurements of sound absorption under diffuse sound field conditions).

In order to find the best feasible correlation, different linear and non-linear models have been taken into consideration. The different regression models presented in this section will be evaluated by three performance measures, which are calculated from the measured values ($y$) and the predicted values ($\hat{y}$) and the total number of samples ($n$): (1) the coefficient of determination to give the proportion of the explained variance of the model, then (2) the mean absolute error and finally (3) the root mean squared error.

The definition of the performance measures, as well as the worst and best case, are given in Table 3. It should be noted that the coefficient of determination is a dimensionless number, whereas the two error measures are in the unit of the values. The mean absolute error *MAE* is an easy measure to understand, whereas the root mean squared error *RMSE* can be interpreted as the standard deviation of an unbiased estimator.

[7] In QUIESST D4.3 [7] for the correlation of the sound reflection values the frequency range was limited to 250 Hz to 5 kHz as this was the frequency range with the most data points available.

Table 3: Performance measures for evaluating the regression models.

| *Name* | *Formula* | *"Worst"* | *"Best"* |
|---|---|---|---|
| *Coefficient of Determination* | $R^2 = 1 - \frac{\sum_i (y_i - \bar{y})^2}{\sum_i (y_i - \hat{y})^2}$, with $\bar{y} = \frac{1}{n}\sum_{i=1}^{n} y_i$ | 0 | 1 |
| *Mean Absolute Error* | $MAE = \frac{\sum_{i=1}^{n} \lvert \hat{y}_i - y_i \rvert}{n}$ | ∞ | 0 |
| *Root Mean Squared Error* | $RMSE = \sqrt{\frac{\sum_{i=1}^{n} (\hat{y}_i - y_i)^2}{n}}$ | ∞ | 0 |

## 6.1 Correlation of the measurement methods for sound reflection under direct sound field conditions and sound absorption under diffuse field conditions

In this chapter, the prediction of the single-number rating for sound reflection under direct sound field conditions ($\widehat{DL_{\mathrm{RI}}}$) is presented. As predictors, the single-number rating for sound absorption under diffuse sound field conditions ($DL_{\alpha,\mathrm{NRD}}$) is used as well as the corresponding third-octave band values ($\alpha_{\mathrm{NRD},j}$). For using only single-number ratings, the database consists of 35 datasets, where the single-number rating is available for measurements on the same noise barrier for sound absorption under diffuse sound field conditions as well as for sound reflection under direct sound field conditions. For 20 of these datasets, the needed third-octave band values are available for use in the regression analysis.

The main challenge in this correlation is the significant difference in the physical quantity between sound absorption under diffuse sound field conditions and sound reflection under direct sound field conditions. As noise barriers tested for their sound absorbing qualities should ideally be highly absorptive, the test sample may alter the diffuse field in the reverberation room and the diffuse sound field method may systematically overestimate the sound absorption with the diffuse sound field method for highly absorbing test samples [1]. This may lead to a non-linear relationship between the results of the two measurement methods. In order to consider this possibility, two additional regression models are compared to a linear regression model in this section.

First, a linear regression model is presented between the natural logarithm of the $DL_{\alpha,\mathrm{NRD}}$ and the $DL_{\mathrm{RI}}$. Although, the natural logarithm is not suitable to predict small values (i.e. < 1) as it diverges to minus infinity for approaching 0, it gives for smaller values a steeper curve and flattens for higher values.

Secondly, a locally weighted linear regression model (so-called *lowess*[8] *regression*) is used to have an even more flexible model.

Although, by using the natural logarithm on the $DL_{\alpha,\mathrm{NRD}}$ a non-linear relationship can be examined, the underlaying regression model is still linear and therefore heavily constrained with only two degrees of freedom (in the univariate case). Therefore, for applying the *lowess* model more caution is necessary as it is a non-linear model. To avoid overfitting to the reduced sample size with third-octave band values, the *lowess* model is only used on the larger dataset available, where only the single-number rating is used as predictor.

[8] *lowess* is the abbreviation for **lo**cally **we**ighted **s**catterplot **s**moothing.

### 6.1.1 Predicting single-number rating $\widehat{DL_{\mathrm{RI}}}$ from single-number rating $DL_{\alpha,\mathrm{NRD}}$

The most intuitive approach in trying to predict the $\widehat{DL_{\mathrm{RI}}}$ is in using a univariate linear regression model[9] between the $DL_{\mathrm{RI}}$ and the $DL_{\alpha,\mathrm{NRD}}$. Figure 31 shows the three regression models between the single-number ratings for sound absorption under diffuse sound field conditions ($DL_{\alpha,\mathrm{NRD}}$) and sound reflection under direct sound field conditions ($DL_{\mathrm{RI}}$). The material of the respective noise barrier is color-coded into the scatter plot.

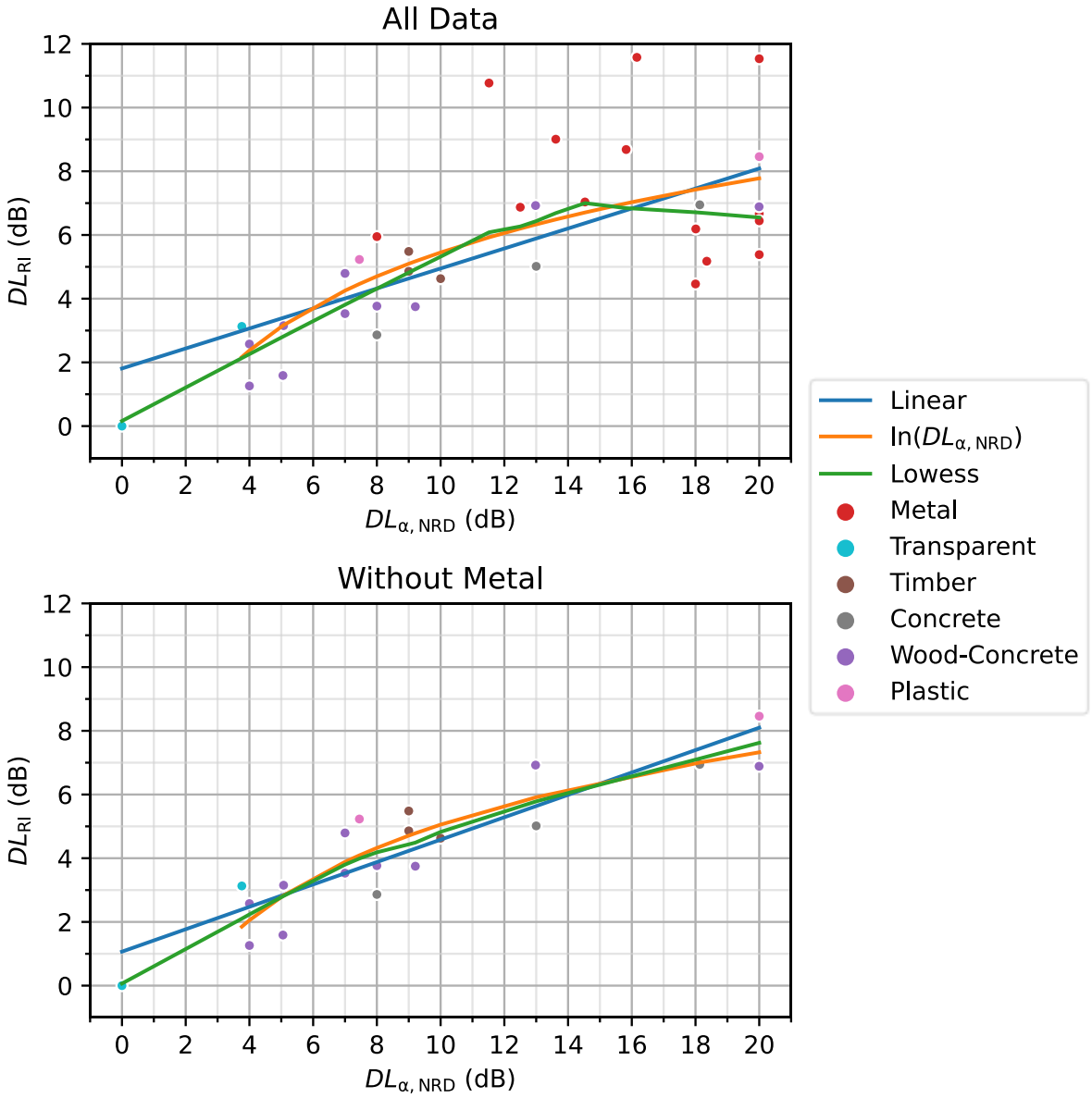


Figure 31: Result of the calculated fit for the three regression models considered between the single-number ratings for sound absorption under diffuse sound field conditions ($DL_{\alpha,\mathrm{NRD}}$) and sound reflection under direct sound field conditions ($DL_{\mathrm{RI}}$) for all available data (top diagram) and all available data without metal noise barriers (bottom diagram).

[9] Univariate linear regression focuses on determining relationship between one independent (explanatory variable) variable and one dependent variable.

In the top diagram the relationship is shown for all available data points. For values smaller than 10 dB of the $DL_{\alpha,\mathrm{NRD}}$ a nearly linear relationship can be seen, although the respective $DL_{\mathrm{RI}}$ is significantly smaller. For higher values of the $DL_{\alpha,\mathrm{NRD}}$ (> 10 dB) large deviations can be seen to this linear relationship. All models follow the strong support points of the small values, and only minor differences can be seen between the linear model and the logarithmic $\ln(\mathrm{DL}_{\alpha,NRD})$ model. The *lowess* model follows the $\ln(\mathrm{DL}_{\alpha,NRD})$ model, but can (in contrast to the logarithmic $\ln(\mathrm{DL}_{\alpha,NRD})$ model) extend to a single-number rating of zero and naturally sticks to the support point at 0. Also, for high values the *lowess* model deviates from the other models.

If the material of the noise barrier is considered, the larger deviations from the models can be attributed to metal noise barriers, although not all metal noise barriers deviate strongly from the regression model. As presented in the previous chapters, metal noise barriers have generally good sound absorption properties under diffuse sound field conditions and therefore in this dataset most of the high absorbing noise barriers are metal noise barriers. As mentioned at the beginning of this chapter, the diffuse sound field method tends to overestimate the sound absorption property especially for high-absorbing noise barrier types. This may be one explanation why mainly metal noise barriers diverge from the relationship models proposed.

On the other hand, it must be considered that the acoustic system of a metal noise barrier, which consists generally of a perforated metal sheet and a porous absorber material, differs clearly from most of the other absorptive noise barriers on the market and this may have significant differences in the angle-dependency of the absorption coefficient measured under diffuse sound field conditions than for other materials. As metal noise barriers are also considered light-weight, the placing of the noise barrier on the (acoustically hard) ground for the diffuse sound field method may also have an increased effect on the sound absorption, for example if compared to a wood-concrete noise barrier. Most of this description about metal noise barriers may also apply to plastic noise barriers. Nevertheless, the two plastic data points fit the models rather well, which may or may not be simply coincidence.

Therefore, in a second run of the analysis the metal noise barriers were discarded. The bottom diagram of Figure 31 shows the same scatter plot, but without the metal data points, as well as the newly fitted models. All models are very close for the intermediate values, at the edges some deviations occur. Due to the distribution of the data points univariate regression models for only the metal noise barriers show no meaningful relationship.

All regression models considered can be used to predict a single-number rating for sound reflection under direct sound field conditions ($\widehat{DL_{\mathrm{RI}}}$). Figure 32 compares these predictions for the available data to the measured values. In the upper part of the figure the models for all available data is shown, whereas in the lower part the models which were fitted without the metal barriers are depicted.

Due to the similarity of the models, the predictions are nearly the same, although smaller deviations for small values can be assed to the $\ln(\mathrm{DL}_{\alpha,NRD})$ and *lowess* model. Naturally the metal noise barriers show higher deviations. Due to the strong flattening of the *lowess* model, nearly all metal noise barriers have predicted $\widehat{DL_{\mathrm{RI}}}$ between 6 and 7 dB.

Table 4 shows the model formulations as well as the performance parameters for the regression models for all available data. It is relevant to note that the fitted *lowess* regression model cannot be represented by a mathematical formula. The strong deviations of the metal noise barriers are naturally reflected in the coefficient of determination, which ranges from 0.48 to 0.57. In respect to the range of the data (especially for the $DL_{\mathrm{RI}}$) the *MAE* and the *RMSE* are to be considered as significant errors.

If the metal noise barriers are discarded from the dataset (lower part of Figure 32) the prediction quality improves significantly. Also, there isn't much difference between the three regression models studied. This can also be seen in the performance measures shown in

Table 5, where the coefficient of determination ranges from 0.79 to 0.84, and also the two error measures are significantly lower.

By examining the best performing regression model, namely the *lowess* model, which in principle is rather close to the two other models, this univariate model can explain 84 % of the variance in the dataset. From the symmetric positions of the predictions values to the main diagonal in Figure 32, we can assume unbiased estimators for all the models and the *RMSE* can be interpreted as standard deviation. If we compare the *RMSE* values to the standard deviation of reproducibility of the measurement uncertainty according to EN 1793-5 [4] ($s_R$ = 0.68) the *RMSE* is in the same order of magnitude. Of course, this should be considered as an additional error, therefore, in order to quantify the total uncertainty the correct error propagation must be calculated, i.e. the measurement uncertainty of the original measurement (in this case for the $DL_{\alpha,\mathrm{NRD}}$) and the uncertainty of the regression model must be considered.

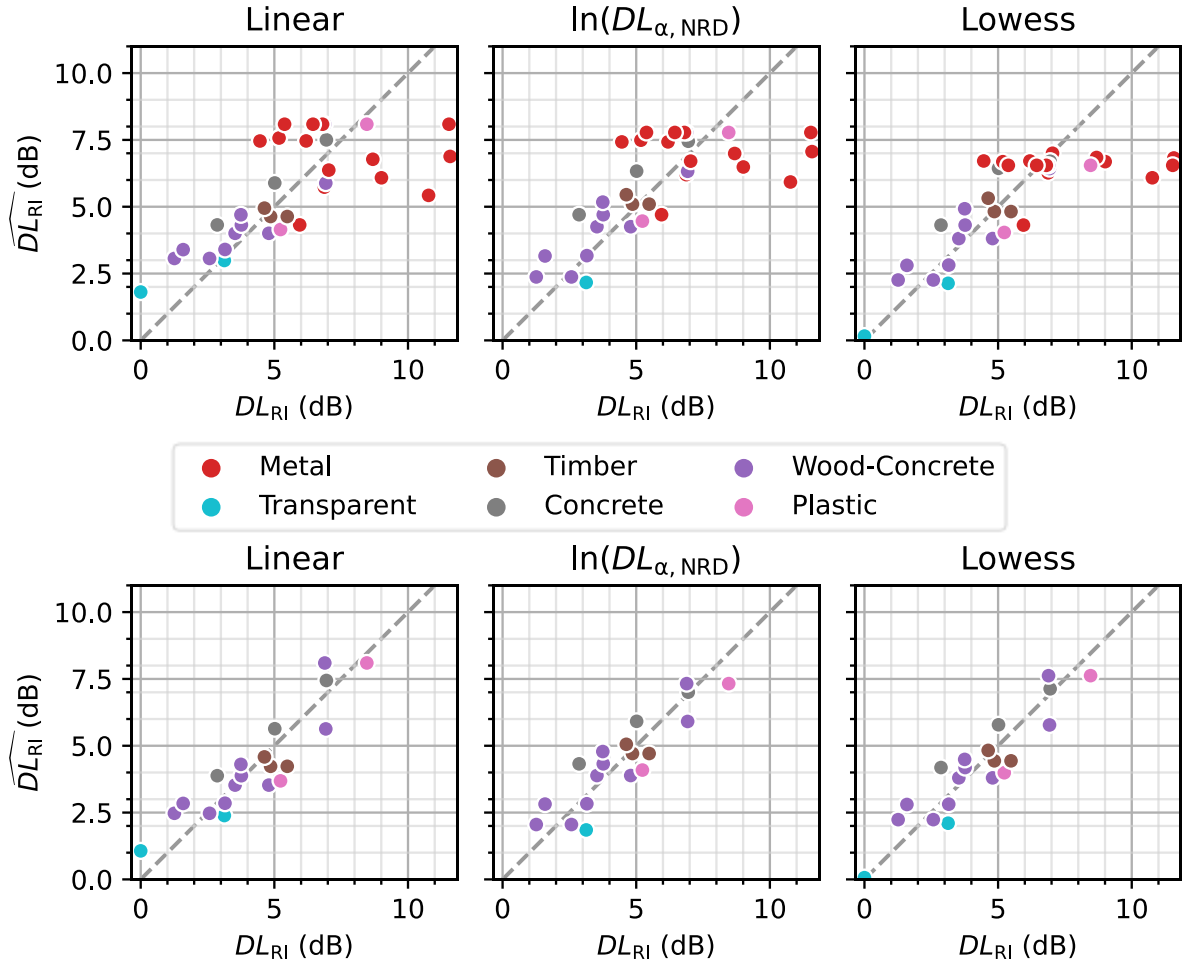


Figure 32: Prediction of the regression models for the single-number rating for sound reflection under direct sound field conditions ($\widehat{DL_{\mathrm{RI}}}$) against the measured value ($DL_{\mathrm{RI}}$) for all available data (upper diagrams) and all available data without metal noise barriers (lower diagrams).

Table 4:Model and performance parameters for the regression models between the single-number ratings for sound absorption under diffuse sound field conditions ($DL_{\alpha,\mathrm{NRD}}$) and sound reflection under direct sound field conditions ($DL_{\mathrm{RI}}$) for all available data.

| | *Model* | $R^2$ | $MAE$ *(dB)* | $RMSE$ *(dB)* |
|---|---|---|---|---|
| *Linear* | $\widehat{DL_{\mathrm{RI}}} = 0.31\,DL_{\alpha,\mathrm{NRD}} + 1.81$ | 0.48 | 1.50 | 1.92 |
| $ln(DL_{\alpha,\mathrm{NRD}})$ | $\widehat{DL_{\mathrm{RI}}} = 3.36\,ln(DL_{\alpha,\mathrm{NRD}}) - 2.28$ | 0.49 | 1.39 | 1.81 |
| *Lowess* | $LOWESS(DL_{\alpha,\mathrm{NRD}})$ | 0.57 | 1.21 | 1.75 |

Table 5:Model and performance parameters for the regression models between the single-number ratings for sound absorption under diffuse sound field conditions ($DL_{\alpha,\mathrm{NRD}}$) and sound reflection under direct sound field conditions ($DL_{\mathrm{RI}}$) for all available data without metal noise barriers.

| | *Model* | $R^2$ | $MAE$ *(dB)* | $RMSE$ *(dB)* |
|---|---|---|---|---|
| *Linear* | $\widehat{DL_{\mathrm{RI}}} = 0.35\,DL_{\alpha,\mathrm{NRD}} + 1.07$ | 0.81 | 0.75 | 0.89 |
| $ln(DL_{\alpha,\mathrm{NRD}})$ | $\widehat{DL_{\mathrm{RI}}} = 3.27\,ln(DL_{\alpha,\mathrm{NRD}}) - 2.49$ | 0.79 | 0.76 | 0.86 |
| *Lowess* | $LOWESS(DL_{\alpha,\mathrm{NRD}})$ | 0.84 | 0.71 | 0.81 |

### 6.1.2 Predicting single-number rating $\widehat{DL_{\mathrm{RI}}}$ from third-octave band values $\alpha_{\mathrm{NRD},j}$

As anticipated at the beginning of this chapter, for a total number of 20 test samples the database contains consistent third-octave band values related to the sound reflection under direct sound field conditions as well as to sound absorption under diffuse sound field conditions. This more detailed spectral information can be used to create a more accurate regression model to account for more complex correlations.

One approach might use the $\alpha_{\mathrm{NRD},j}$ third-octave band values in a multi-variate model[10] to directly predict the single-number rating for sound reflection $\widehat{DL_{\mathrm{RI}}}$. In respect to the sample size this approach is not feasible as it would require a non-linear model (to account for the logarithm in the calculation of the single-number rating) with 18 degrees of freedom and would lead to over-fitting the model. Therefore, the third-octave band values of the diffuse sound field method for sound absorption ($\alpha_{\mathrm{NRD},j}$) are used to predict the third-octave band values for sound reflection under direct sound field conditions ($\widehat{RI_j}$) but with constrained linear models to prevent overfitting. From the predicted $\widehat{RI_j}$ the $\widehat{DL_{\mathrm{RI}}}$ is finally predicted with the usual calculation based on the traffic noise spectrum according to EN 1793-3 [8].

To account for non-linear relationships different transformations of the predictor ($\alpha_{\mathrm{NRD},j}$) as well as for the target values ($\widehat{RI_j}$) have been tested. The most stable results were achieved by transforming the third-octave band values for sound absorption under diffuse sound field conditions in the same way as the single-number rating is calculated. The resulting value is a decibel value for the sound absorption under diffuse sound field conditions in third-octave bands and defined by:

[10] A Multi-variate model uses multiple variables to forecast outcomes instead of only one-variable in the univariate models

$$L_{\alpha,\mathrm{NRD},j} = -10\,log_{10}\left(1-\alpha_{\mathrm{NRD},j}\right)$$

where $\alpha_{\mathrm{NRD},j}$ is constrained to a maximum value of 0.99. Therefore $L_{\alpha,\mathrm{NRD},j}$ is constrained in the same way to a maximum value of 20 dB as the single-number rating $DL_{\alpha,\mathrm{NRD}}$.

Figure 33 shows the Pearson cross-correlation coefficient[11] between the $RI_j$ third-octave band values for sound reflection under direct sound field conditions and the $\alpha_{\mathrm{NRD},j}$ (left figure) as well the logarithmic $L_{\alpha,\mathrm{NRD},j}$ third-octave band values for sound absorption under diffuse sound field conditions (right figure). In the linear case the strongest correlations can be found upwards from the main diagonal (i.d. third-octave bands with the same centre frequency) as the values of the cross-correlation matrix are very close to the value -1. Therefore, high correlations were found between low frequency third-octave bands for the diffuse sound field method and higher frequencies of the direct sound field methods. Especially the $RI_j$ third-octave bands from 1 kHz to 2.5 kHz show a strong correlation to the $\alpha_{\mathrm{NRD},j}$ third-octave bands between 160 Hz and 800 Hz as well as from 1.6 kHz to 2.5 kHz.

In the logarithmic case (right figure) the correlation between the third-octave bands with different frequencies is even more prominent.

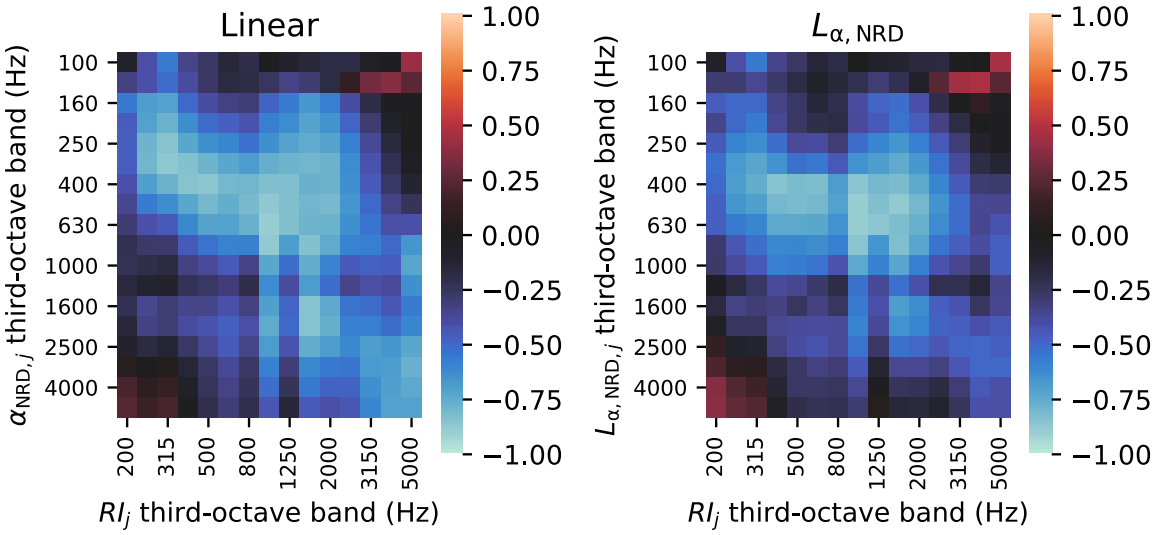


Figure 33: Cross-Correlation coefficient (Pearson) between the $RI_j$ third-octave band values for the direct sound field method and the $\alpha_{\mathrm{NRD},j}$ (left figure) and logarithmic $L_{\alpha,\mathrm{NRD},j}$ (right figure) third-octave band values for the diffuse sound field method.

As the main diagonal in the cross-correlation matrix doesn't show the strongest correlation, it is not the optimal strategy to build linear regression models between the third-octave bands with the same centre frequency. For this reason a sequential forward selection (SFS) algorithm[12] was used to search for each third-octave band of the sound reflection under direct

[11] The Pearson product-moment correlation coefficient is a measure of the strength and direction of the linear relationship between two variables that is defined as the covariance of the variables divided by the product of their standard deviations.

[12] From a set of regression parameters, the sequential forward selection (SFS) algorithm evaluates the performance of each parameter. For the best matching parameter, all possible combinations with the remaining parameters are evaluated. For this best matching set, again all possible combinations with the remaining parameters are evaluated. This process is repeated until the desired number of parameters are selected.

sound field conditions ($RI_j$) the best selection of two third-octave bands of sound absorption under diffuse sound field conditions ($L_{\alpha,\mathrm{NRD},j}$) for the multi-variate linear regression.

For the sequential forward selection SFS, the coefficient of determination of a linear regression model was used as metric. With these two best fitting third-octave bands for each third-octave band for the sound reflection index $RI_j$, these sound reflection indexes are predicted and the single-number rating $\widehat{DL_{\mathrm{RI}}}$ is calculated accordingly.

In order to show the high adaptability of this approach, the analysis was performed not only for all available data with third-octave band data (N=20), but also for all available third-octave band data without metal noise barriers (N=8) and for only the metal noise barriers (N=12). Although many parameters are fitted by this approach, the prediction for each third-octave band is independent from the other third-octave bands and limited to two parameters, as a linear regression model with two input parameters (i.e. third-octave bands) is used.

Figures 34, 35 and 36 give an overview of the resulting regression models for predicting the single-number rating for sound reflection under direct sound field conditions ($\widehat{DL_{\mathrm{RI}}}$) from the logarithmic $L_{\alpha,\mathrm{NRD},j}$ third-octave band values for sound absorption under diffuse sound field conditions for all the available third-octave band data (Figure 35), as well as for all the data without metal noise barriers and only for the metal noise barriers (Figure 36).

Table 6 summarised the performance measures of the regression models for the different data selections.

In the left part of the figures the cross-correlation matrices for the respective data selection are shown where the selected third-octave bands of the $L_{\alpha,\mathrm{NRD},j}$ are marked as green circles. In the right part of the figures the predicted $\widehat{DL_{\mathrm{RI}}}$ is compared to the measured $DL_{\mathrm{RI}}$.

The selection of third-octave bands in Figure 34 for all available data is only partly close to the main diagonal, therefore the algorithm preferred third-octave bands for the prediction which have not necessarily the same centre frequency. Naturally the algorithm also does not choose a co-linear third-octave band as the second choice (i.e. with a high correlation to the best fitting third-octave band), as more information is present in an ideally orthogonal direction. The final prediction of the $\widehat{DL_{\mathrm{RI}}}$ could be improved significantly in respect to the linear models for only the single-number ratings, as the values for the non-metal barriers are very close to the diagonal in the evaluation (right part of Figure 34). Nevertheless, the metal noise barriers show significant deviations from the regression model and therefore are handled separately.

If the metal noise barriers are omitted from the dataset, only 8 data points remain. Therefore, the analysis might not be generally robust and applicable to unknown noise barriers. Nevertheless, for the current dataset, a very strong correlation could be found with a coefficient of determination of 0.95 and a *RMSE* of 0.43, which is significantly lower than the standard deviation of reproducibility $s_R$ for the $DL_{\mathrm{RI}}$ as given in the standard. The chosen third-octave bands are close to the main diagonal. As the algorithm has *a priori* no preference of choosing third-octave bands with the same centre frequency for the prediction, this is an interesting fact that indicates a physical relationship between those third-octave bands. As already mentioned in the case of a prediction based on single-number ratings only, also in this data subset mostly noise barriers with lower sound absorption properties are present.

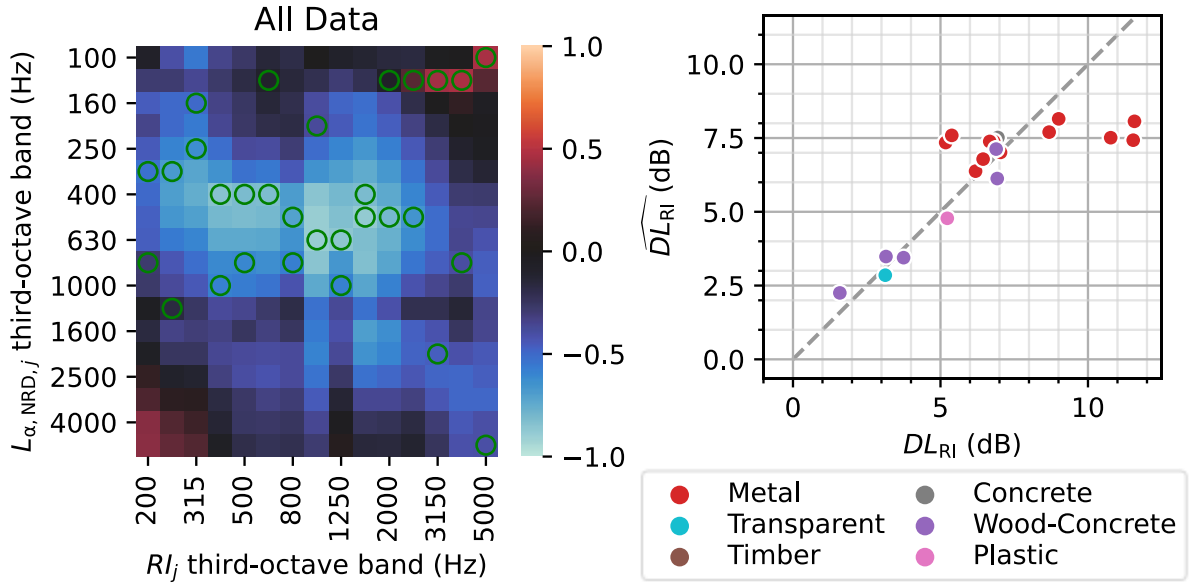


Figure 34: Selected third-octave bands (green circles) in the cross-correlation matrix (left figure) and model prediction for the $\widehat{DL_{\mathrm{RI}}}$ (right figure) from logarithmic $L_{\alpha,\mathrm{NRD},j}$ third-octave band values for all available data.

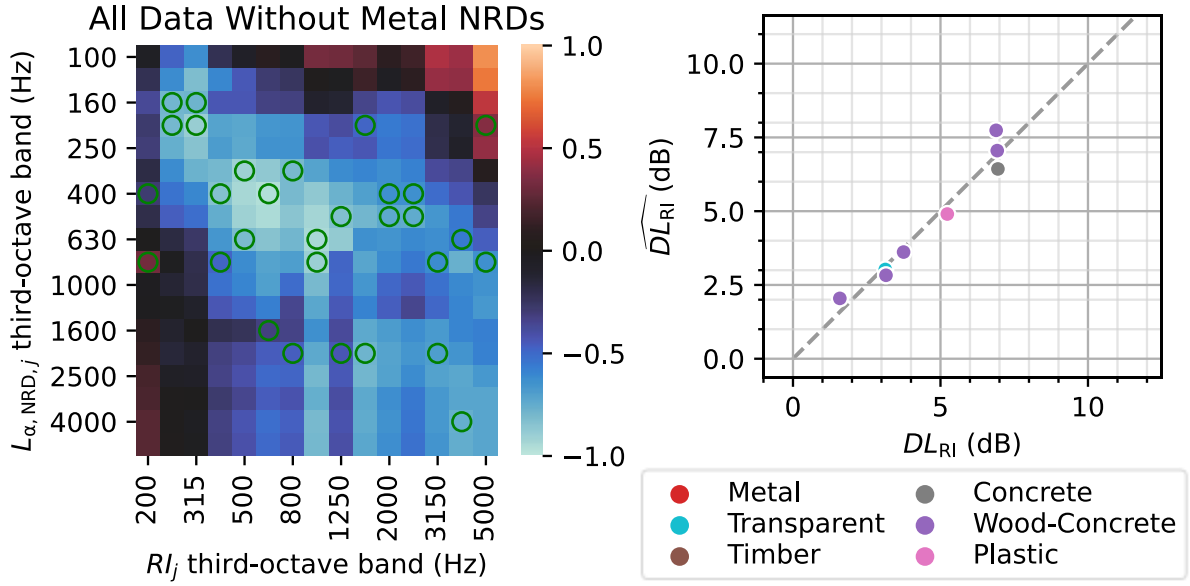


Figure 35: Selected third-octave bands (green circles) in the cross-correlation matrix (left figure) and model prediction for the $\widehat{DL_{\mathrm{RI}}}$ (right figure) from logarithmic $L_{\alpha,\mathrm{NRD},j}$ third-octave band values for all available data without metal noise barriers.

Regarding the prediction analysis on metal noise barriers only (Figure 36), no useful correlation could be performed based on the single-number ratings. With additional third-octave band information, the regression models are capable of roughly predicting the single-number rating $\widehat{DL_{\mathrm{RI}}}$ for metal noise barriers from the diffuse field method for sound absorption. The most interesting part in this context is the shown Pearson cross-correlation matrix, as most of the correlation coefficients are positive instead of negative as for the other subsets. As the logarithmic $L_{\alpha,\mathrm{NRD}}$ is higher for higher absorbing samples, this means for most of the third-octave bands a higher measured *absorption* with the diffuse sound field method corresponds to a higher *reflection* for the direct sound field method. It should be noted that the cross-

correlation matrix is directly derived from the reported data of 12 metal noise barriers with a significant range of values for each measurement method. Also, Spearman's rank correlation coefficients[13] show positive values between the reported third-octave bands for sound absorption under diffuse sound field conditions and sound reflection under direct sound field conditions respectively.

For a better understanding of this unexpected relationship the exact composition of the noise barriers as well as the conditions and the physical processes of the measurements must be examined, which is out of the scope of this project and may be done in further research. Nevertheless, this relationship confirms the significant physical differences between the two measurement methods, which were described in D2.1 [1], and points out that special attention is required, when the two methods are compared.

Therefore, for highly absorbing noise barriers (which metal noise barriers generally are), a robust prediction of a single-number rating for sound reflection under direct sound field conditions from measurements from the sound absorption under diffuse sound field conditions is not generally possible.

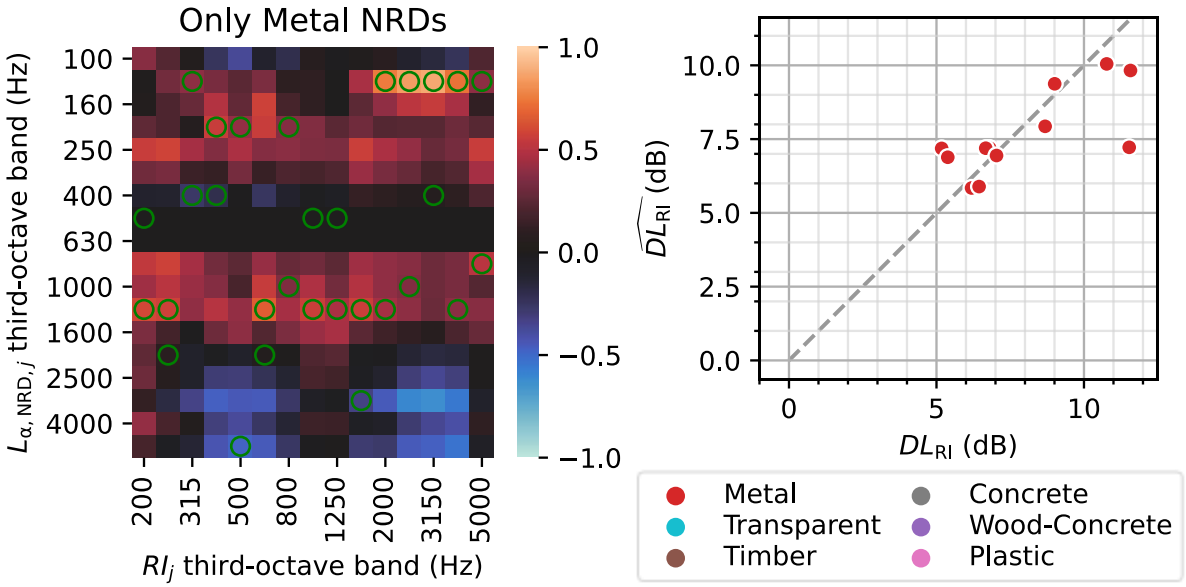


Figure 36: Chosen third-octave bands (green circles) in the cross-correlation matrix (left figure) and model prediction for the $\widehat{DL_{\mathrm{RI}}}$ (right figure) from logarithmic $L_{\alpha,\mathrm{NRD},j}$ third-octave band values for all metal noise barriers.

Table 6: Performance measures for predicting the $\widehat{DL_{\mathrm{RI}}}$ from logarithmic $L_{\alpha,\mathrm{NRD},j}$ third-octave band values for all data, all data without metal noise barriers and only metal noise barriers.

| *Data* | *Model* | $R^2$ | $MAE$ *(dB)* | $RMSE$ *(dB)* |
|---|---|---|---|---|
| *All data* | $RI_j \sim \left(L_{\mathrm{alpha,NRD},j}\right)_{2-best}$ | 0.61 | 1.19 | 1.64 |
| *All data without metal NRDs* | $RI_j \sim \left(L_{\mathrm{alpha,NRD},j}\right)_{2-best}$ | 0.95 | 0.36 | 0.43 |
| *Only Metal NRDs* | $RI_j \sim \left(L_{\mathrm{alpha,NRD},j}\right)_{2-best}$ | 0.49 | 1.11 | 1.58 |

[13] In contrast to Pearson's correlation coefficient, which assesses a linear relationship between the samples of two quantities, the Spearman's rank correlation coefficient assesses the order of the samples of the two quantities.

## 6.2 Correlation of the measurement methods for airborne sound insulation under direct sound field conditions and airborne sound insulation under diffuse field conditions

In this chapter the correlation between the measurement methods for airborne sound insulation under direct sound field conditions and airborne sound insulation under diffuse field conditions are presented. In [7] a good fit between the two methods between the single-number ratings could be found with a linear regression model, with a coefficient of determination of 0.95 based on 24 datasets.

For the correlation based on single-number ratings, a consistent dataset of 57 samples is available in the SOPRANOISE database, where the *same noise barrier* was tested with both measurement methods. For all results measured with the method under direct sound field conditions separate values for both the acoustic element and the post are available. For 27 of these samples also third-octave band data exists for both measurement methods. As the number of available samples is still limited and the relationship between the measurement methods appear to be linear [7], only linear regression models are shown in this section.

It should also be noted that the mathematical relationship between the third-octave band values and the single-number ratings is identical for the diffuse sound field and the direct sound field methods for measuring airborne sound insulation. As the third-octave band values as well as the single-number ratings are logarithmic measures, also regression models based on energetic relationships were tested, nevertheless, no improvement in comparison to the linear models where found.

Furthermore, no significant improvement in the regression model where found by using the values measured at the acoustic element, or values measured at the post for the direct sound field method in comparison to the regression model considering global values only. As in the diffuse sound field measurement method the acoustic element as well as the post are measured simultaneously, only the correlations which are performed between the values for airborne sound insulation under diffuse sound field conditions and the global values for airborne sound insulation under direct sound field conditions are presented in this section.

In the analysis of the SOPRANOISE database, good correlations were found for the single-number ratings, which could not be generally improved by using third-octave band data. These correlations are presented in the following section 6.2.1.

If the correlation is performed for metal noise barriers only, an improved fit could be found by using third-octave band data and is presented in section 6.2.2 for predicting the direct field single-number rating $\widehat{DL_{\mathrm{SI,P}}}$ from the third-octave band values $R_j$ from the diffuse sound field method.

### 6.2.1 Predicting single-number rating $\widehat{DL_{\mathrm{SI,G}}}$ from single-number rating $DL_{\mathrm{R}}$

As mentioned before, there are 57 test samples in the SOPRANOISE database, where single-number ratings exist for airborne sound insulation under diffuse sound field conditions as well as for airborne sound insulation under direct sound field conditions. Figure 37 shows the linear regression model based on these data points first applying the regression model for all datasets independently from the noise barrier material (i.e. one model for all the materials, black dashed line) and secondly applying the regression model fitting each noise barrier material separately (coloured dashed lines).

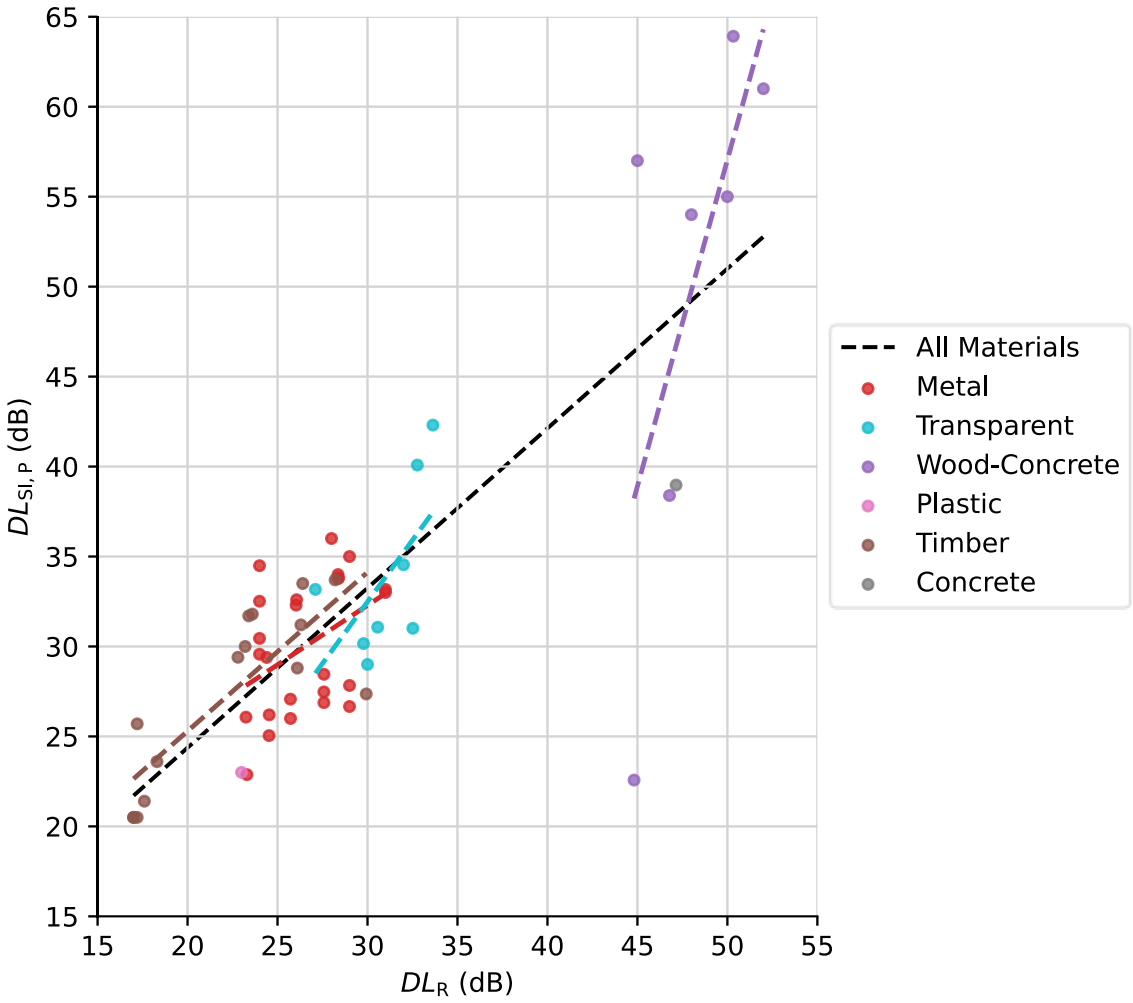


Figure 37: Fit for regression models between the single-number ratings for airborne sound insulation under diffuse sound field conditions ($DL_R$) and the global value for airborne sound insulation under direct sound field conditions ($DL_{SI,G}$) before outlier removal.

Three data points (one for concrete and two for wood-fibre concrete barriers) show significant deviations from the general trend with $DL_{SI,G}$values from 25 to 42 dB, where all the other wood-fibre concrete barriers show values above 55 dB. The lowest values for the direct sound field method are mostly caused by significant lower values measured at the post and may have been caused by a significantly different quality of installation. Therefore, these points were treated as outliers and discarded from the dataset.

Figure 38 and Figure 39 show the regression analysis between the single-number ratings for airborne sound insulation under diffuse sound field conditions and airborne sound insulation under direct sound field conditions after removal of the outliers. Figure 39 gives a detailed view of the regression lines and distribution of the data points for each material separately as well as the overall fitted regression line (blacked dashed line). Table 7 lists the respective model parameters as well as the performance parameters for the fitted linear regressions.

If the regression is fitted for all available data (i.e. all materials), the coefficient of determination shows a strong fit with a score of 0.87. This high score is significantly caused by the high values for the single-number ratings for the wood-fibre concrete noise barriers, as they serve as strong supporting points for the linear regression.

Nevertheless, in the intermediate range of 20 dB to 35 dB of the $DL_R$ significant deviations can be seen, which cause the *RMSE* of 3.36.

The timber noise barriers show a very similar fit to the overall fit in their respective data range and deviations with a *RMSE* of 2.08.

For the transparent and wood-fibre concrete noise barriers less than 10 samples are available in the database, so the correlations may not be very robust against new samples. Nevertheless, even in this small dataset and even considering the very different ranges of values available, the material-specific correlations are very close to the overall model.

Furthermore, it should be noted that a difference of 20 dB equals a factor of 1000, so even though the energy ratios for wood-fibre concrete are a 1000 times smaller than the ratios for the other materials, they still approximately show a similar relationship between the diffuse sound field and direct sound field method. On the other hand, the metal noise barriers show again no significant correlation between the single-number ratings having a poor coefficient of determination of 0.09.

For the sake of completeness, the linear regression models between the single-number ratings $DL_{\mathrm{R}}$ an $DL_{\mathrm{SI,E}}$ (acoustic element) and $DL_{\mathrm{SI,P}}$ (post) respectively are shown in Annex D.

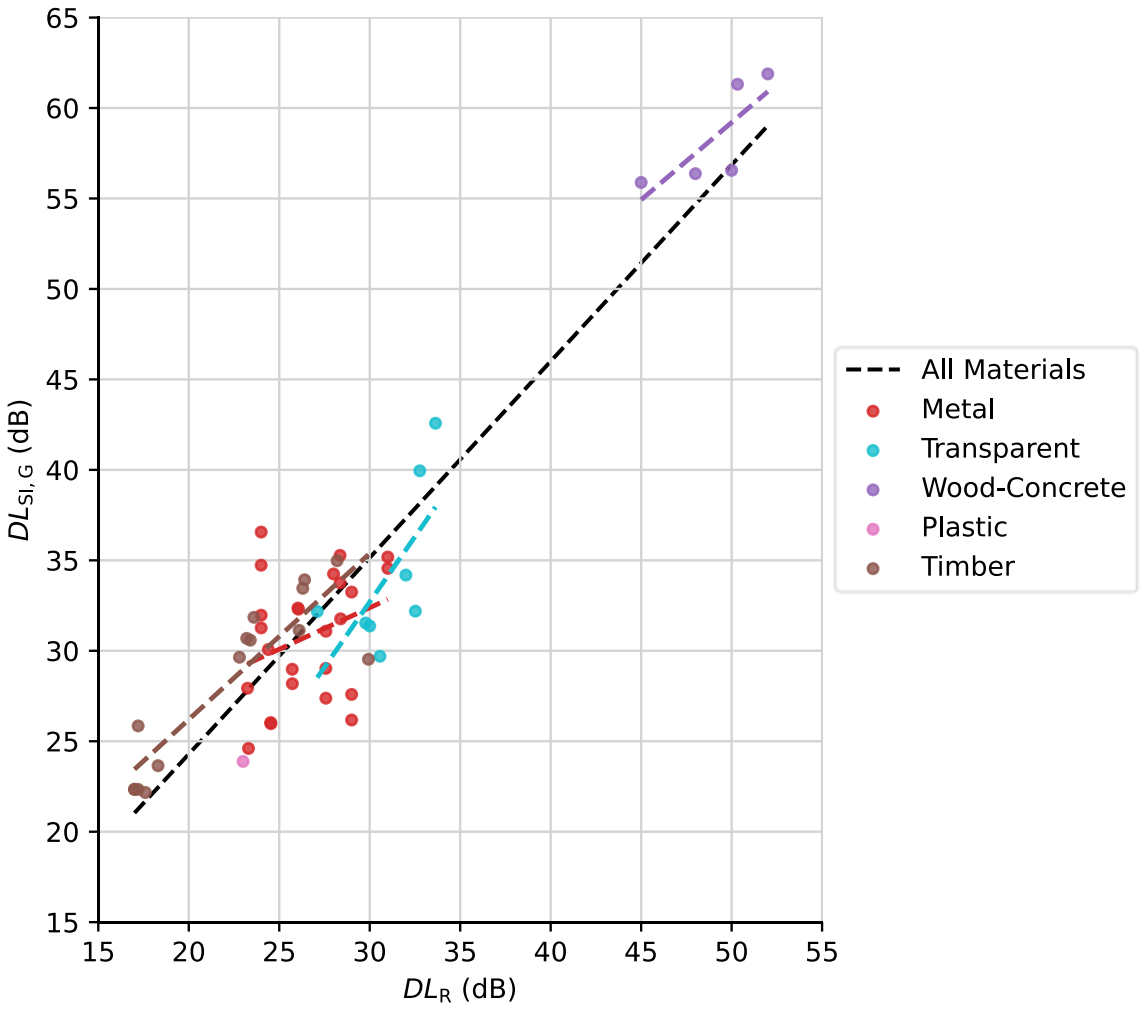


Figure 38: Fit for regression models between the single-number ratings for airborne sound insulation under diffuse sound field conditions ($DL_{\mathrm{R}}$) and the global value for airborne sound insulation under direct sound field conditions ($DL_{\mathrm{SI,G}}$) after outlier removal.

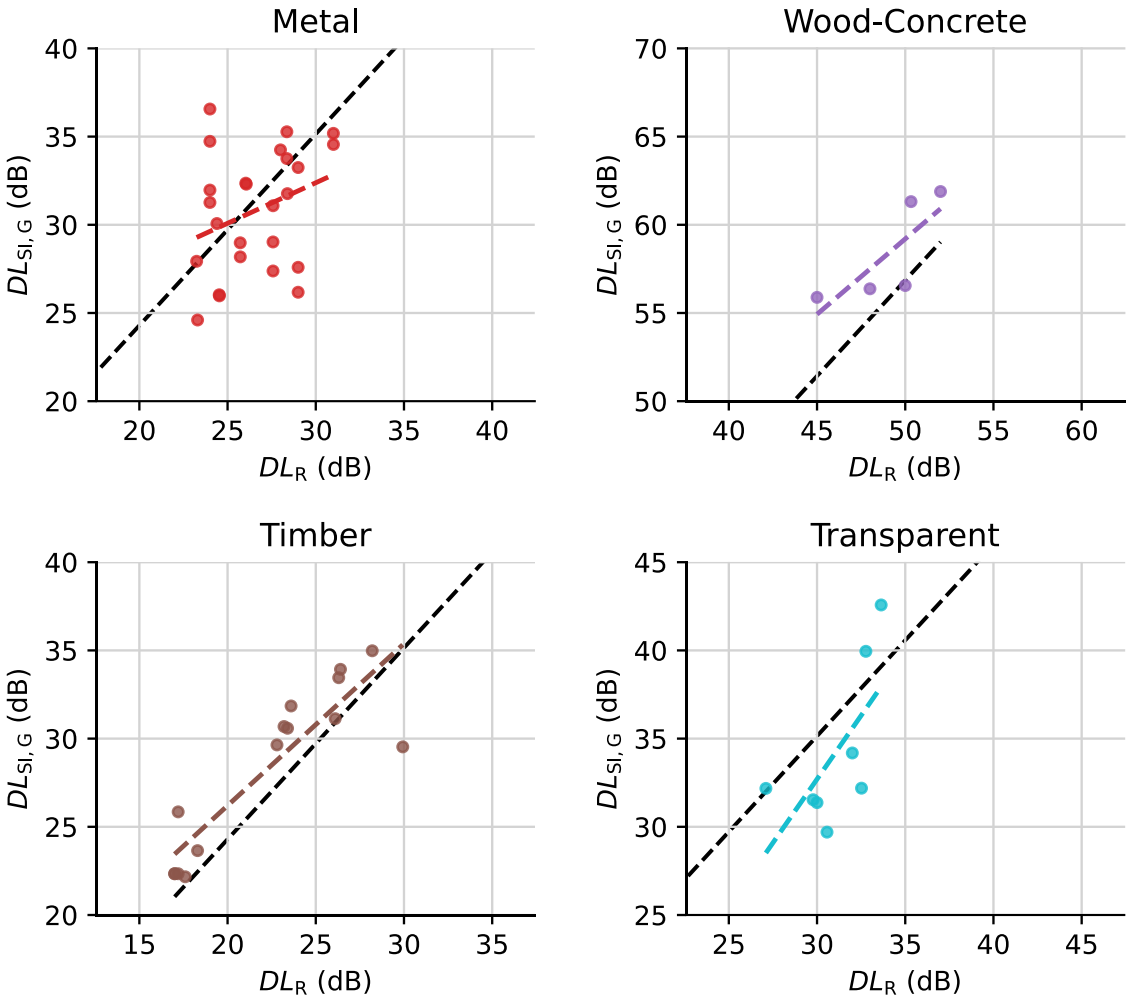


Figure 39: Fit for regression models between the single-number ratings for airborne sound insulation under diffuse sound field conditions ($DL_R$) and the global value for airborne sound insulation under direct sound field conditions ($DL_{SI,G}$) for each material (coloured dashed lines) and for the regression model for all available data (dashed black line) after outlier removal.

Table 7: Performance measures for predicting the $\widehat{DL_{SI,G}}$ from the $DL_R$ with a linear regression model for all materials and all the materials with minimum sample size N of 5.

| | *N* | *Model* | $R^2$ | $MAE$ *(dB)* | $RMSE$ *(dB)* |
|---|---|---|---|---|---|
| *All Materials* | 54 | $\widehat{DL_{SI,G}} = 1.09\,DL_R + 2.58$ | 0.87 | 2.77 | 3.36 |
| *Metal* | 25 | $\widehat{DL_{SI,G}} = 0.46\,DL_R + 18.60$ | 0.09 | 2.71 | 3.21 |
| *Transparent* | 8 | $\widehat{DL_{SI,G}} = 1.44\,DL_R - 10.59$ | 0.44 | 2.89 | 3.19 |
| *Wood-Concrete* | 5 | $\widehat{DL_{SI,G}} = 0.85\,DL_R + 16.47$ | 0.61 | 1.51 | 1.64 |
| *Timber* | 15 | $\widehat{DL_{SI,G}} = 0.92\,DL_R + 7.85$ | 0.79 | 1.71 | 2.08 |

### 6.2.2 Predicting single-number rating $\widehat{DL_{\mathrm{SI,G}}}$ from third-octave band values $R_j$

In order to improve the prediction accuracy of the correlations, the available third-octave band values have been used. For 27 noise barriers, the necessary third-octave band data for the diffuse and direct sound field method for airborne sound insulation are available, 16 of the noise barriers are metal noise barriers. As for the other materials, less than 10 samples exist: the third-octave band models are only applied to all the available data and to a subset of the data, which only contains the metal noise barriers.

Similar to section 6.1.2, the third-octave band values of the diffuse sound field method for sound insulation ($\mathrm{R_j}$) are used to predict the third-octave band values for sound reflection under direct sound field conditions ($\widehat{SI_{j,G}}$) but with constrained linear models to prevent overfitting. In contrast to section 6.1.2 three third-octave bands are used in the prediction instead of two as more data samples are available. From the predicted $\widehat{SI_{j,G}}$ the $\widehat{DL_{\mathrm{SI,G}}}$ is finally calculated with the usual calculation based on the traffic noise spectrum according to EN 1793-3 [8].

Figure 40 shows the relationship between the corresponding third-octave band values for airborne sound insulation under diffuse ($R_j$) and direct ($SI_{j,\mathrm{G}}$) sound field conditions for the same noise barriers for the centre frequencies 250 Hz, 500 Hz, 1 kHz, 2 kHz and 4 kHz with a pairwise linear regression model (dashed black line). Also, for third-octave bands with different centre frequencies a linear correlation could be found, although the model is heavily supported by the wood-fibre concrete data point with high values for the airborne sound insulation for both methods. Therefore, no additional transformation of the data was necessary in this case as the linear regression models can produce a good fit.

Similar to the prediction for sound reflection explained in the previous section, to improve the prediction quality significantly above the prediction by single-number ratings, a sequential forward selection (SFS) algorithm was used to search for each third-octave band of the airborne sound insulation under direct sound field conditions ($\mathrm{SI}_{j,G}$) the best selection of three third-octave bands of sound insulation under diffuse sound field conditions ($R_j$) for the regression. For the sequential forward selection SFS, the coefficient of determination of a linear regression model was used as a metric. With these three best fitting third-octave bands of the $R_j$ for each third-octave band of the $SI_{j,\mathrm{G}}$, the $\widehat{SI_{j,\mathrm{G}}}$ are predicted and the single-number rating $\widehat{DL_{\mathrm{SI,G}}}$ is calculated accordingly.

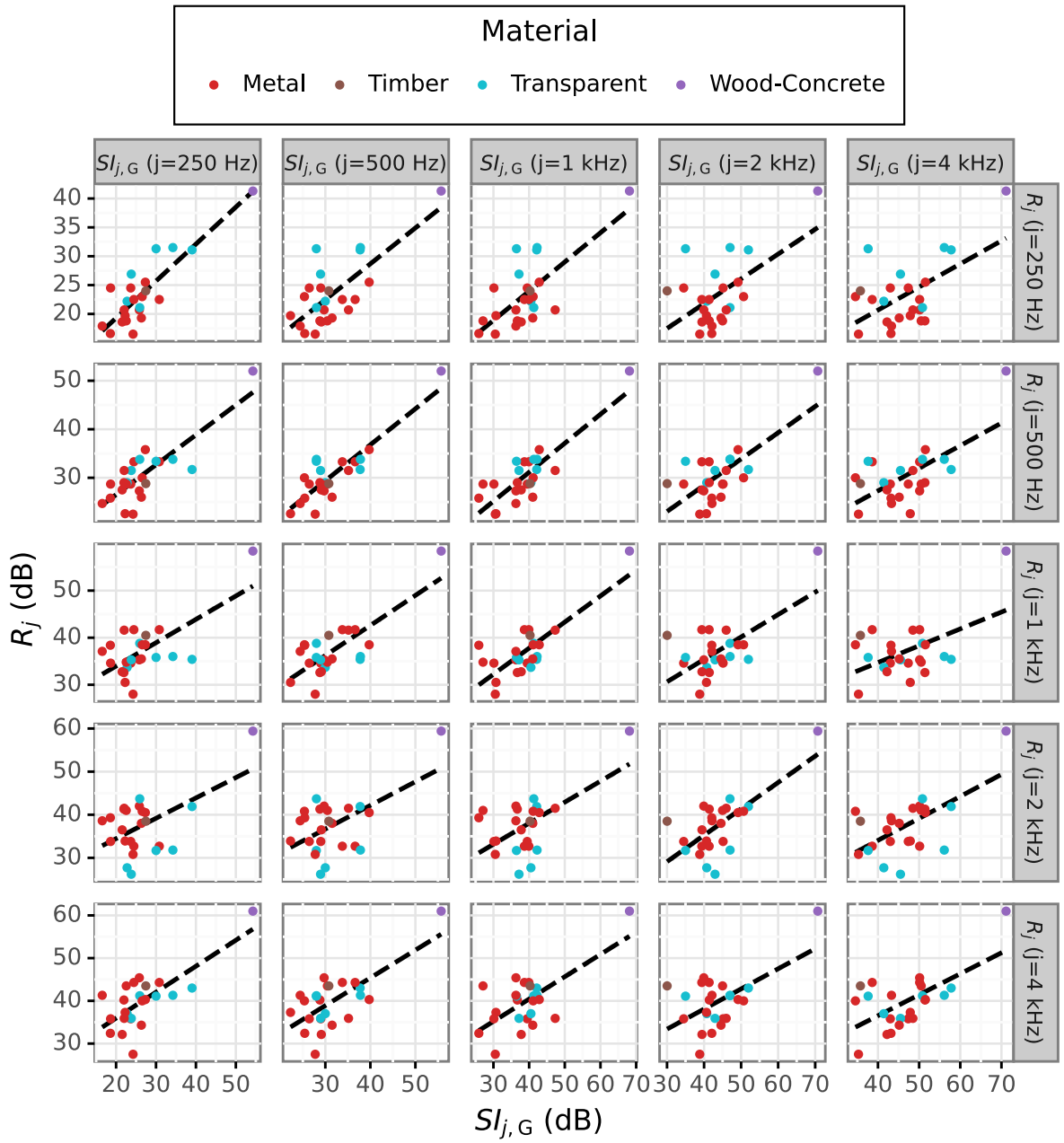


Figure 40: Corresponding third-octave band values for airborne sound insulation under diffuse ($R_j$) and direct ($SI_{j,G}$) sound field conditions for the same noise barriers for the centre frequencies 250 Hz, 500 Hz, 1 kHz, 2 kHz and 4 kHz with linear regression model (dashed black lines).

Figures 41 and 42 give an overview of the resulting regression models for predicting the global single-number rating for airborne sound insulation under direct sound field conditions ($\widehat{DL_{\mathrm{SI,G}}}$) from the $R_j$ third-octave band values for airborne sound insulation under diffuse sound field conditions. The analysis was performed both, (1) for all the available third-octave band data and (2) only for the metal noise barriers. In the left part of the figures the Pearson cross-correlation matrices for the respective data selection are shown where the selected third-octave bands of the $R_j$ are marked as green circles. In the right part of the figures the predicted $\widehat{DL_{\mathrm{SI,G}}}$ is compared to the measured $DL_{\mathrm{SI,G}}$.

Although the correlation matrix in Figure 41 shows strong correlations in the main diagonal (i.e. for the same third-octave band centre frequency), the cross correlations between the third-octave bands of the two methods are generally high. This is likely caused by strong support points of wood-fibre concrete noise barriers.

Nevertheless, the SFS algorithm chose many third-octave band values close to the main diagonal and was also able to find a robust correlation. Although the coefficient of determination is a bit lower than for the prediction with single-number ratings (0.83 instead of 0.87), the deviations from the ideal prediction are lower. This is well reflected in the lower error measures. The *RMSE* is 0.5 dB lower for the prediction with third-octave bands than for the prediction with single-number ratings and reaches a value of 2.78 dB. These deviations are significantly higher than the measurement uncertainties of the direct sound field method for airborne sound insulation, which are 1.06 dB for the acoustic element and 0.72 for the post. Due to the averaging in the calculation of the global value, the measurement uncertainty for the global value is according to the laws of error propagation generally lower than 1.06 dB.

Although the coefficient of determination shows a significant correlation, the uncertainties of the regression models must be considered additionally to the measurement uncertainty, if the regression models are used to predict values for airborne sound insulation under direct sound field conditions from values obtained with the measurement method under diffuse sound field conditions.

For the cross-correlation matrix in Figure 42, only the metal noise barriers where used, where third-octave band data was available for the measurement method for airborne sound insulation under diffuse sound field conditions as well as for airborne sound insulation under direct sound field conditions. The strongest components of the cross-correlation are in the main diagonal, so a high value in one third-octave band in the diffuse field method likely causes a high value in the same third-octave band for direct sound field method. The SFS algorithm used this likelihood by choosing many third-octave bands from the diagonal. But with the additional (orthogonal) information of two more third-octave bands, the prediction of the $\widehat{DL_{\mathrm{SI,G}}}$ improved significantly compared to the single-number rating correlation. From a nearly random relationship with $R^2$=0.09 for single-number rating correlation, the prediction with third-octave bands reaches a $R^2$ of 0.67 and a RMSE of 1.82 dB, which is still significantly higher than the measurement uncertainty of the direct sound field method. It is relevant to note that this is valid only for the data on metal noise barriers and special attention to the uncertainties is required if values are predicted.

Table 8 summarises the performance measures of the regression models for the different data selections.

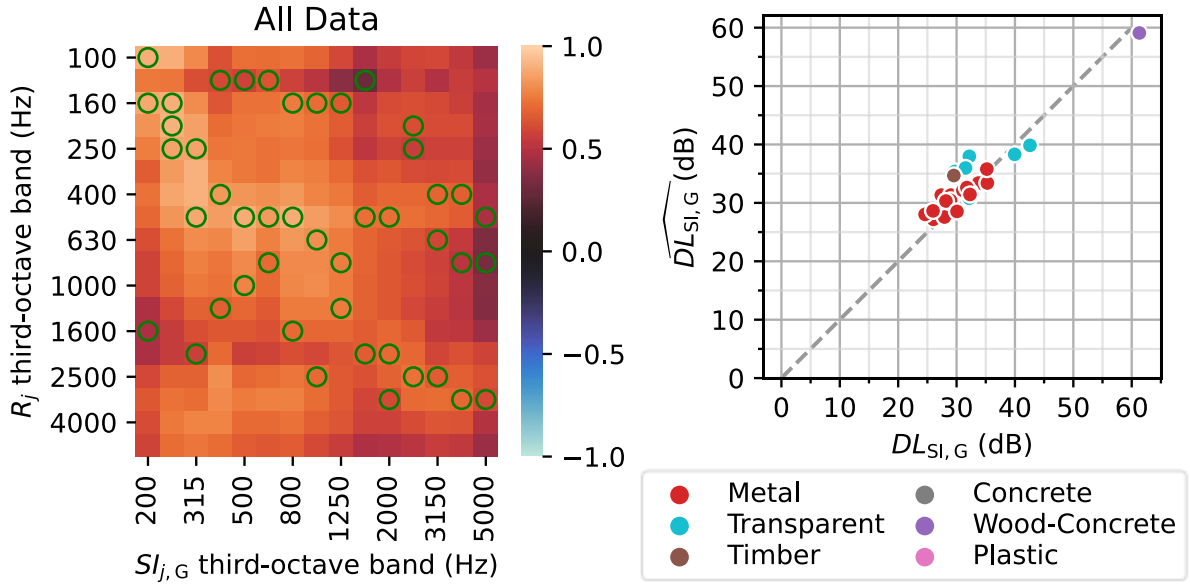


Figure 41: Chosen third-octave bands (green circles) in the cross-correlation matrix (left figure) and model prediction for the $\widehat{DL_{SI,G}}$ (right figure) from $R_j$ third-octave band values for all available data.

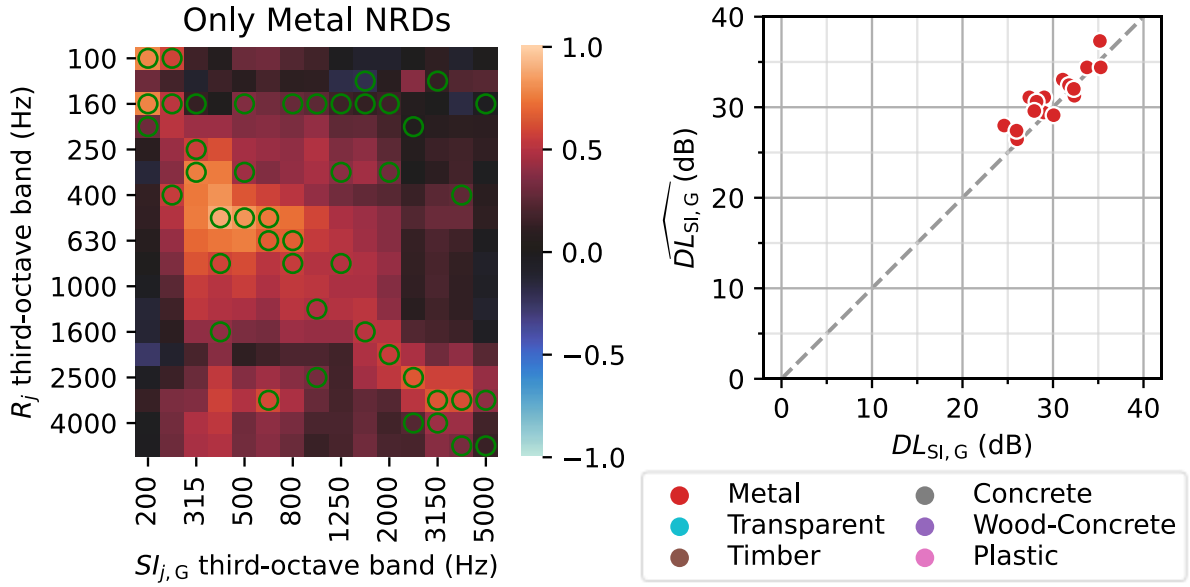


Figure 42: Chosen third-octave bands (green circles) in the cross-correlation matrix (left figure) and model prediction for the $\widehat{DL_{SI,G}}$ (right figure) from $R_j$ third-octave band values for all metal noise barriers.

Table 8: Performance measures for predicting the $\widehat{DL_{SI,G}}$ from $R_j$ third-octave band values for all data and only metal noise barriers.

| *Material* | *N* | *Model* | $R^2$ | $MAE$ *(dB)* | $RMSE$ *(dB)* |
|---|---|---|---|---|---|
| *All Data* | 27 | $SI_{j,G} \sim (Rj)_{3-best}$ | 0.83 | 2.56 | 2.78 |
| *Metal* | 16 | $SI_{j,G} \sim (Rj)_{3-best}$ | 0.67 | 1.51 | 1.82 |

# 7 Conclusions and outlook

The main objective of task 2.2 is to extend and update the database of the European noise barrier market that had been first developed within the QUIESST project, including single-number ratings as well as third-octave band spectra results. The SOPRANOISE database aims to show facts and figures about acoustic performances obtained from both the diffuse sound field and direct sound field methods, together with a better understanding of the respective significance, similarities and differences of these standardized methods, improving data analysis and correlations between these methods.

The SOPRANOISE database contains now results on 448 different noise barriers manufactured and installed by 58 different noise barrier manufacturers or construction companies, from 9 different European countries (Austria, Belgium, France, Germany, Ireland, Italy, Spain, The Netherlands, and United Kingdom). The measurements collected have been performed by 39 different testing laboratories from the European countries listed before.

The overall amount of data collected was unexpectedly high, reaching a total of 2029 dataset entries, while the total number of different measurements is equal to 1503 entities, and even after an accurate data selection for quality and validation purposes the total number of data considered reaches the relevant number of **1263 single-number ratings** considering the following measurement methods EN 1793-1, EN 1793-2, EN 1793-5 and EN 1793-6.

Regarding the correlations between the single-number rating of **sound absorption under diffuse sound field conditions** $\boldsymbol{DL_{\alpha,\mathrm{NRD}}}$ (EN 1793-1) and the single-number rating of **sound reflection under direct sound field conditions** $\boldsymbol{DL_{\mathrm{RI}}}$ (EN 1793-5), the statistical distribution shows clearly that values obtained with the method according to EN 1793-1 are in general considerably higher (in several cases up to maximum value of 20 dB) than the values obtained with the methods according to EN 1793-5 or CEN/TS 1793- 5. This is a **consequence of the overestimation occurring when testing highly sound absorbing elements with the measurement method under diffuse sound field conditions** (i.e.: in a assumed perfectly diffuse sound field, while it is not reached in a reverberant room).

Therefore, the median value for the method according to EN 1793-1 is between 9 and 10 dB, while for the method according to EN 1793-5 the median value is around 6 dB. Also, the shape of the probabilistic functions is rather different, as in the first case the data is more widespread and has a second peak at the maximum value, while in the second case the data is more focused between 4 and 8 dB.

On this point it is necessary to emphasize that, for sound absorption under diffuse sound field conditions, due to the calculation formula of the single-number rating, the maximum reachable value is 20 dB. Therefore, applying the method according to EN 1793-1 several noise barriers reach the maximum value of 20 B, while the values obtained with the method according to EN 1793-5 are generally lower and reach values between 8 and 10 dB (excluding special prototypes).

In order to more deeply analyse the data collected and to find a possible relevant relation between these methods, an **empirical study** was performed, in which several linear and non-linear regression models have been applied. This in-depth investigation was based on datasets where results on both methods were available. Thus, considering all available data complying with this requirement, a statistically stable regression model could not be found by considering all materials (i.e. without differentiating between different materials). Nevertheless, the prediction of a single-number rating from one method to the other is **possible for lower values of sound absorption**, where a coefficient of determination of 0.81 could be reached with a linear regression model between the single-number ratings with a reasonable root mean squared error of 0.89 dB and a robust sample size.

However, even for this strong fit an uncertainty of ±1.78 dB exists for applying the regression model under the theoretical and ideal assumption of no measurement uncertainty.

Nonetheless, for highly absorbing noise barriers, **a robust prediction** of a single-number rating for sound reflection under direct sound field conditions from measurements of sound absorption under diffuse sound field conditions **is not reliably possible** with acceptable error margins. A specific model for every single material was not found, mainly because of the low amount of data for every material separately.

In conclusion, for the **correlation** between measurement results for **sound absorption under diffuse sound field condition** and **sound reflection under direct sound field condition, only very rough estimates are possible**, which are **limited to low sound absorbing samples with no practical use for certification or quality assurance purposes**.

Regarding the correlations between the single-number rating of **airborne sound insulation under diffuse sound field conditions** $\boldsymbol{DL_R}$ (EN 1793-2) and the single-number rating of **airborne sound insulation under direct sound field conditions** $\boldsymbol{DL_{SI}}$ (EN 1793-6), the statistical distributions shows that values obtained according to EN 1793-2 are in general slightly lower than the values obtained according to EN 1793-6. Element values are in general higher than results at the post, while the global values are between these values. The median value for the method according to EN 1793-2 is around 28 dB, while for the method according to EN 1793-6 the median values are around 34 dB for element, 30 dB for post and 31 dB for global values. Furthermore, the shape of the probability functions is rather similar, nevertheless the values according to EN 1793-6 can reach higher values up to 66 dB (especially at the acoustic element), while the values according to EN 1793-1 reach maximum values around 50 dB.

In order to more deeply analyse the data collected and to try to find an empirical relation between these methods several linear regression models based on test samples where results on both methods were available have been analysed. In the statistical analysis performed, **good correlations were found for the single-number ratings**, which could not be generally improved by using third-octave band data.

If the regression is fitted for all available data (i.e. all materials), the coefficient of determination shows a strong fit with a score of 0.87, but with a root mean squared error of 3.36 dB. This high score is significantly caused by the high values for the single-number ratings for the wood-fibre concrete noise barriers, as they serve as strong supporting points for the linear regression. Nevertheless, even in this small dataset and even considering the different ranges of values available, the **material-specific correlations are very close to the general fit except for metal noise barriers**. These again show no significant correlation between the single-number ratings resulting and a poor coefficient of determination of 0.09. In contrast, by using the developed regression models on third-octave bands for airborne sound insulation only for metal noise barriers, the prediction could be improved to a coefficient of determination of 0.67 with a root mean squared error of 1.82.

For the **correlation** between measurement results for **airborne sound insulation** obtained under **diffuse sound field conditions and direct sound field conditions,** a **promising fit** could be achieved due to the wide data range. Nevertheless, the **significant uncertainties** of the regression models must be considered when predictions are made, which also **limits the practicality** of using prediction models for **certification or quality assurance purposes**.

Due to the tendency of the diffuse sound field method for sound absorption of **overestimating the sound absorbing qualities for highly absorptive samples** and the intrinsic property of the direct sound field methods of also **measuring the installation quality in-situ** (especially for airborne sound insulation), the **direct sound field methods have practical advantages**, beside the evident physical background of measuring under the relevant sound field conditions.

As **concluding outlook** of the research some specific questions emerged during the work performed, which could be analysed in further research:

- Can reliable **regression models** be found for different materials separately under the assumption of a large enough dataset **for each material**?
- Are the regression models between the measurement methods related and also applicable for different materials?
- What are the **physical or statistical reasons** behind the fact that some third-octave bands from one measurement method correlate better with third-octave bands from the other method with a different centre frequency?
- Is there a **better suitable classification for noise barriers especially regarding sound absorption/sound reflection** which focuses on the absorbing surface instead on the material of the noise barrier structure as does the QUIESST classification?

In SOPRANOISE WP2, the possibilities of finding correlations between the measurement methods were pushed to its limits regarding the use of external information and applying statistical linear and non-linear multi-variate regression models as an empirical approach.

Nonetheless, to answer the above questions a systematic and theoretical approach to this specific research questions is required, which includes an extensive gathering of specific data. For each measurement method, much more background information is inevitable, which normally cannot be gathered from external sources, as the required information is generally not present in datasheets or measurement reports. The measurement campaign shall include the acquisition of **measurement results for all measurement methods on a significant number of noise barriers for all relevant materials** (or absorbing surface types) if possible, **on the same noise barriers** and ideally even for the same noise barrier installation.

Furthermore, the exact physical processes during the measurements must be monitored and examined, like

- the diffusivity of the sound field,
- influence of the zero transmission for sound absorption measurements under diffuse sound field conditions,
- influence of roughness together with the number of reference positions for sound reflection measurements under direct sound field conditions,
- influence of the post on airborne sound insulation measurements under diffuse and under direct sound field conditions, etc.

Beside answering the above questions, this approach would result in an improved understanding of the measurement methods regarding the acoustic properties of noise barriers itself, leading to **possible reduction of the current measurement uncertainties**.

# 8 References


[1] A. Fuchs, P. Reiter, M. Garai and W. Bartolomaeus, “D2.1: State of the Art on the physical significance of the different measurement methods,” *SOPRANOISE project,* 2020.

[2] *EN 1793-1, “Road traffic noise reducing devices - test method for determining the acoustic performance - part 1: Intrinsic characteristics of sound absorption under diffuse sound field conditions.”,* CEN, 2017.

[3] *EN 1793-2, “Road traffic noise reducing devices - part 2: Intrinsic characteristics of airborne sound insulation under diffuse sound field conditions.”,* CEN, 2018.

[4] *EN 1793-5, “Road traffic noise reducing devices. Test method for determining the acoustic performance. Intrinsic characteristics. In situ values of sound reflection under direct sound field conditions.”,* CEN, 2018.

[5] *CEN/TS 1793-5 Road traffic noise reducing devices – Test method for determining the acoustic performance – Part 5: Intrinsic characteristics – In-situ values of sound reflection and airborne sound insulation,* CEN, 2003.

[6] *EN 1793-6, “Road traffic noise reducing devices - test method for determining the acoustic performance - part 6: Intrinsic characteristics - in situ values of airborne sound insulation under direct sound field conditions.”,* CEN, 2019.

[7] M. Conter, M. Czuka and S. Breuss, “D4.3 and MS 4.2 - Final procedural report on WP4 activities, including public database of European NRD, data analysis and definition of NRD falimies,” *QUIESST project,* 2012.

[8] *EN 1793-3, “Road traffic noise reducing devices - Test method for determining the acoustic performance - Part 3: Normalised traffic noise spectrum.”,* CEN, 1997.

[9] *EN 16272-3-1 - Noise barriers and related devices acting on airborne sound propagation - Test method for determining the acoustic performance - Part 3-1: Normalized railway noise spectrum and single number ratings for diffuse field,* CEN, 2012.

[10] *EN 16272-3-2 - Railway applications - Noise barriers and related devices acting on airborne sound propagation - Test method for determining the acoustic performance - Part 3-2: Normalized railway noise spectrum and single number ratings for direct field,* CEN, 2014.

[11] M. Conter and R. Wehr, “Comparison between laboratory and in-situ methods for measuring sound absorption properties of noise barriers,” *Euronoise, Maastricht,* 2015.

# Annex A: Comparisons between single-number rating measured under diffuse and under direct sound field conditions considering different frequency ranges

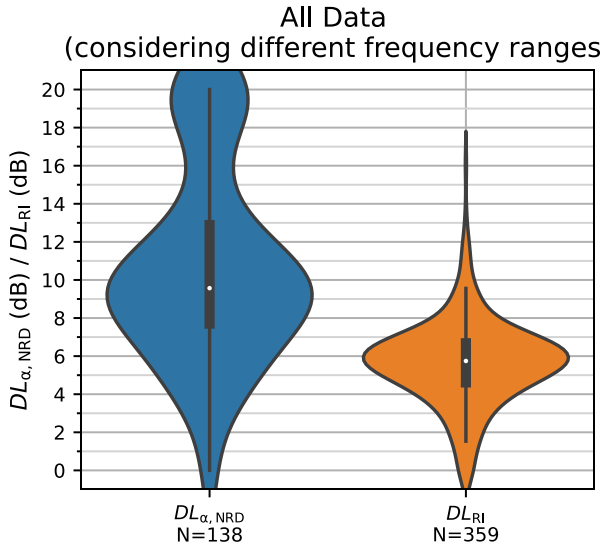


Figure 43: Comparison between the statistical distribution of the single-number rating results on sound absorption in the diffuse field according to EN 1793-1 (blue area) and the results on sound reflection according to EN 1793-5 or CEN/TS 1793-5 (orange area): the box-plot represents the minimum and the maximum value (discarding statistical outliers), and the 25% and the 75% percentile, while the white dot is the median value. The coloured areas show the so-called violin plots, which represent the kernel density estimation of the probability density function of the data. N is the number of data considered for each method.

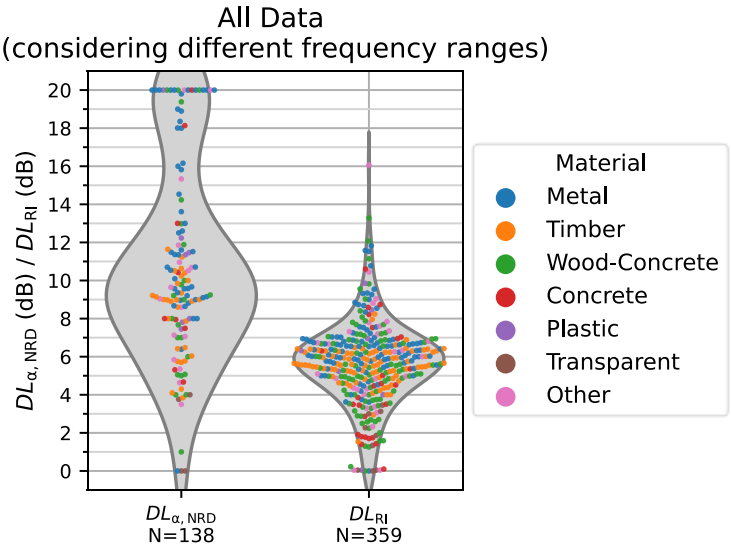


Figure 44: Comparison between single-number rating results on sound absorption according to EN 1793-1 (left) and results on sound reflection according to EN 1793-5 or CEN/TS 1793-5 (right). The coloured dots represent the measurement results, divided into different materials, while the grey areas are the probability density function of the data smoothed by a kernel density estimation.

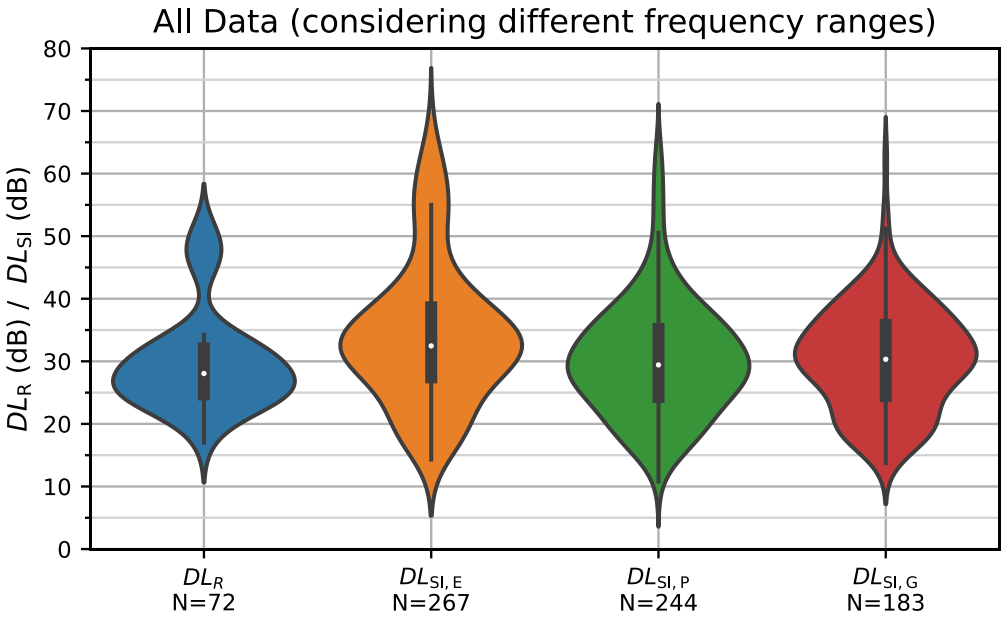


Figure 45: Comparison between the statistical distribution of the single-number rating results on airborne sound insulation according to EN 1793-2 (blue area) and the results on airborne sound insulation according to EN 1793-6 (orange area for “element”, green for “post” and red for “global” values): the box-plot represents the minimum and the maximum value (discarding statistical outliers), and the 25% and the 75% percentile, while the white dot is the median value. The coloured areas show the so-called violin plots, which represent the kernel density estimation of the probability density function of the data. This figure shows data considering different frequency ranges. N is the number of data considered for each method.

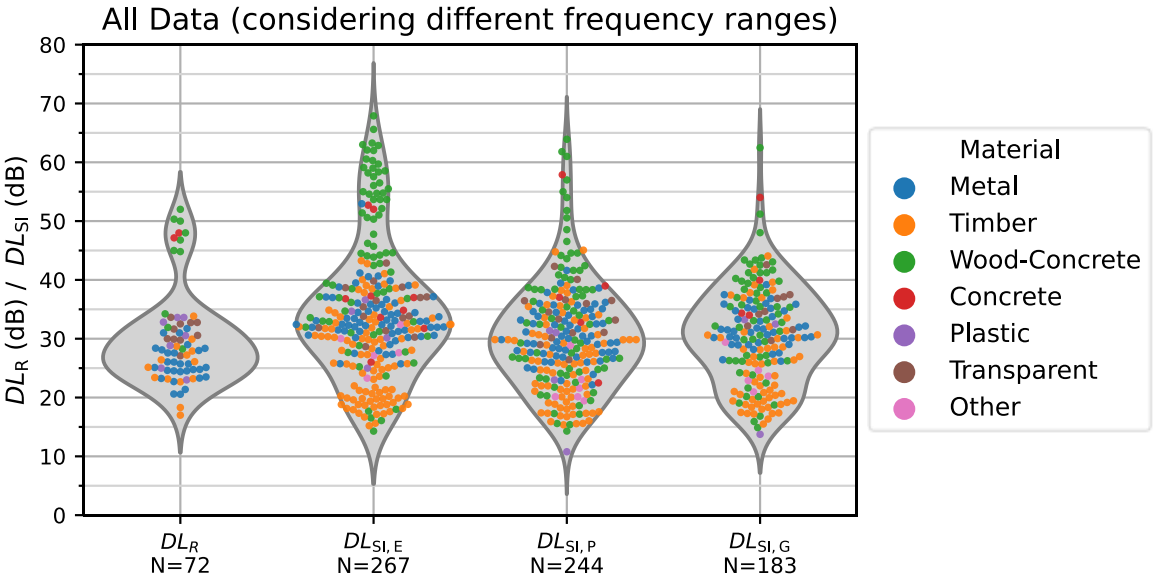


Figure 46: Comparison between single-number rating results on airborne sound insulation according to EN 1793-2 (left column) and results on airborne sound insulation according to EN 1793-6 (middle-left for “element”, middle-right for “post” and right for “global” values). The coloured dots represent the measurement results, divided into different materials, while the grey areas are the probability density function of the data smoothed by a kernel density estimation. This figure shows data considering different frequency ranges. N is the number of data considered for each method.

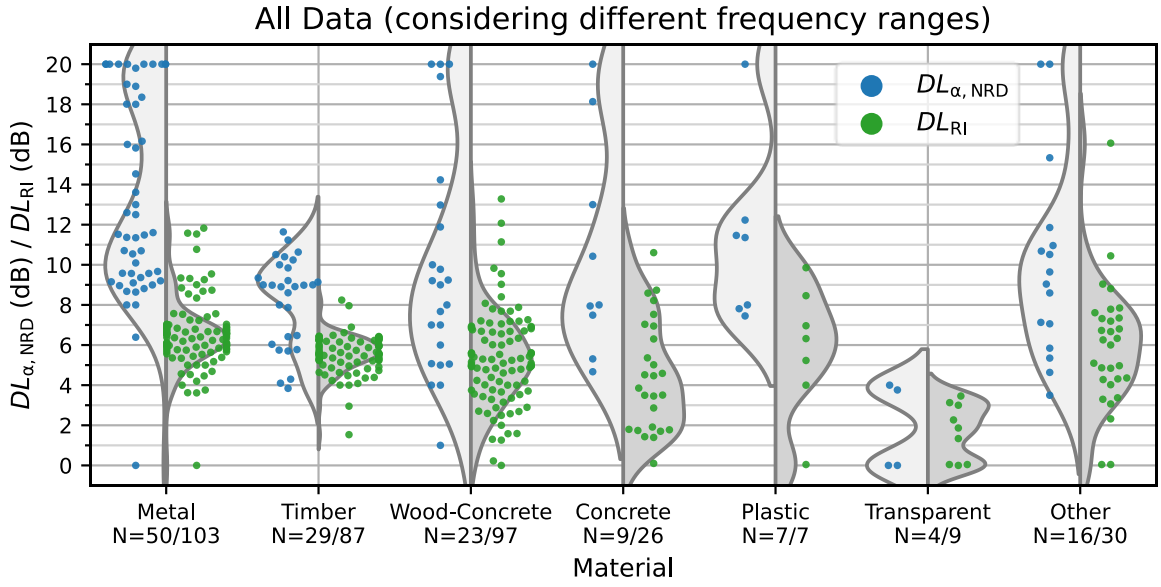


Figure 47: Comparison between single-number rating results on sound absorption according to EN 1793-1 (blue dots) and results on sound reflection according to EN 1793-5 or CEN/TS 1793-5 (green dots). The coloured dots represent the measurement results separated for every material, while the grey areas are the probability density function of the data smoothed by a kernel density estimation. This figure shows data considering different frequency ranges. N is the number of data considered for each method.

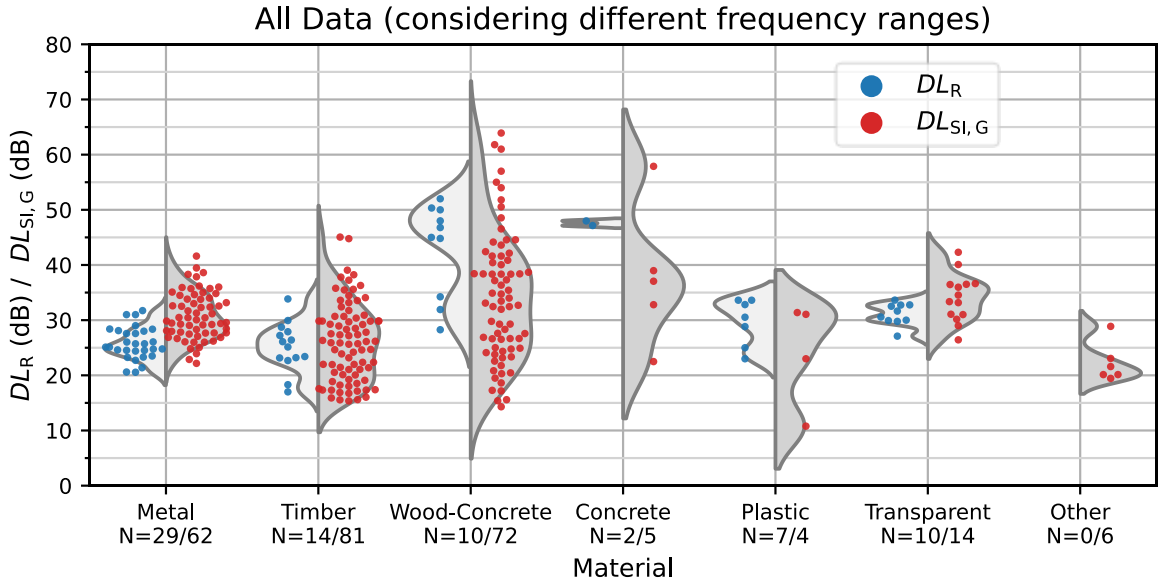


Figure 48: Comparison between single-number rating results on airborne sound insulation according to EN 1793-2 (blue dots) and results on airborne sound insulation according to EN 1793-6 (red dots, are global values). The coloured dots represent the measurement results separated for every material, while the grey areas are the probability density function of the data smoothed by a kernel density estimation. This figure shows data considering different frequency ranges. N is the number of data considered for each method.

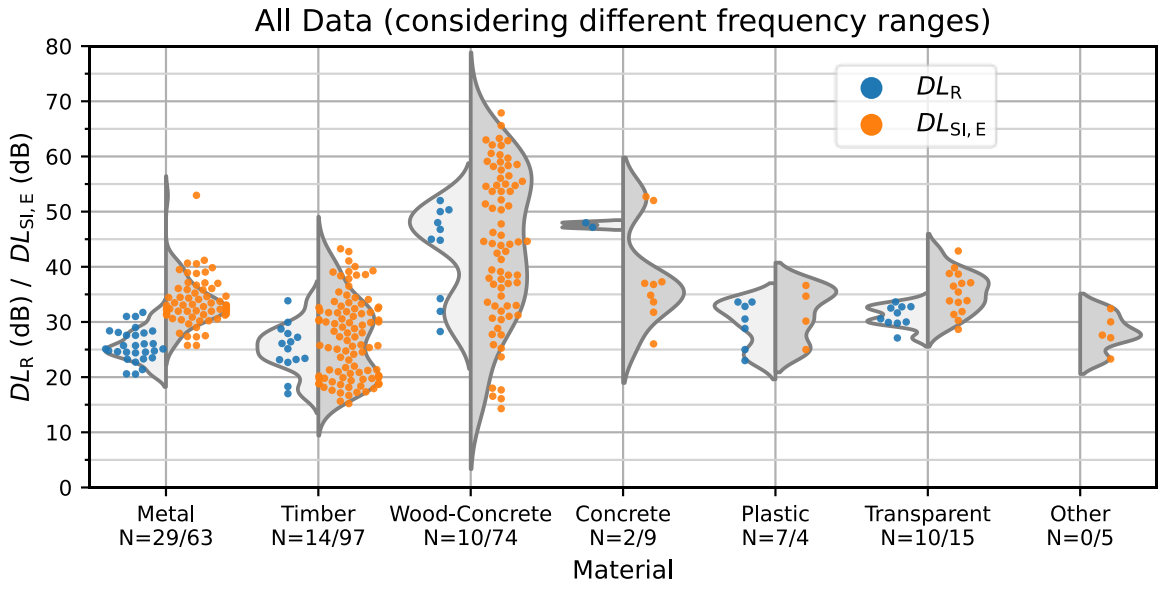


Figure 49: Comparison between single-number rating results on airborne sound insulation according to EN 1793-2 (blue dots) and results on airborne sound insulation according to EN 1793-6 (orange dots are values on the element). The coloured dots represent the measurement results separated for every material, while the grey areas are the probability density function of the data smoothed by a kernel density estimation. This figure shows data considering different frequency ranges. N is the number of data considered for each method.

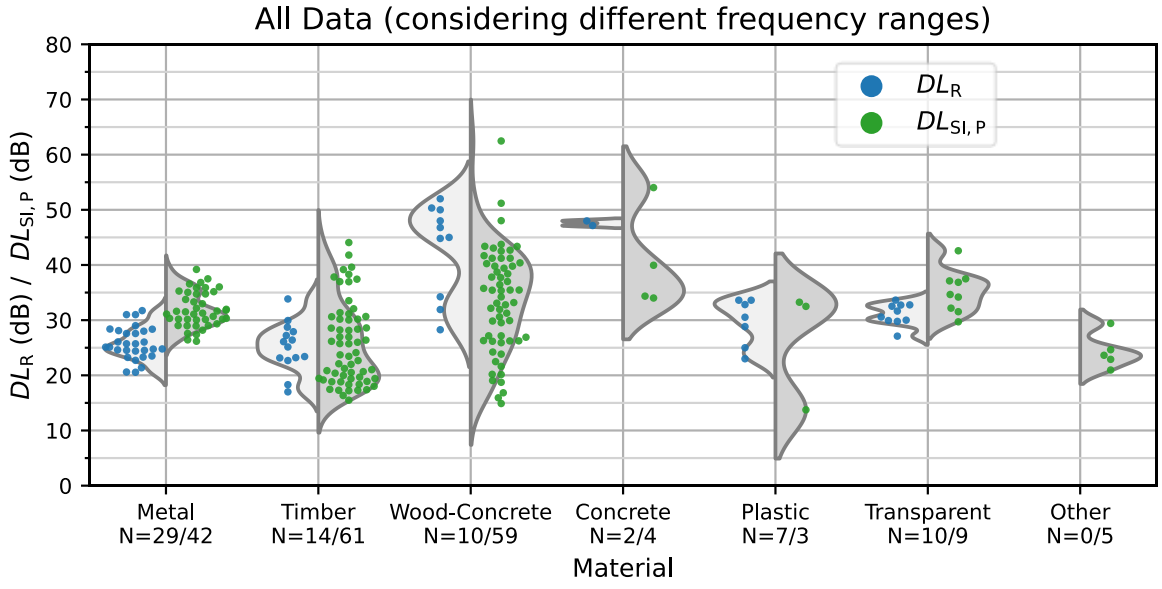


Figure 50: Comparison between single-number rating results on airborne sound insulation according to EN 1793-2 (blue dots) and results on airborne sound insulation according to EN 1793-6 (green dots are values on the post). The coloured dots represent the measurement results separated for every material, while the grey areas are the probability density function of the data smoothed by a kernel density estimation. This figure shows data considering different frequency ranges. N is the number of data considered for each method.

# Annex B: Third-octave band results measured under diffuse sound field conditions for less common materials

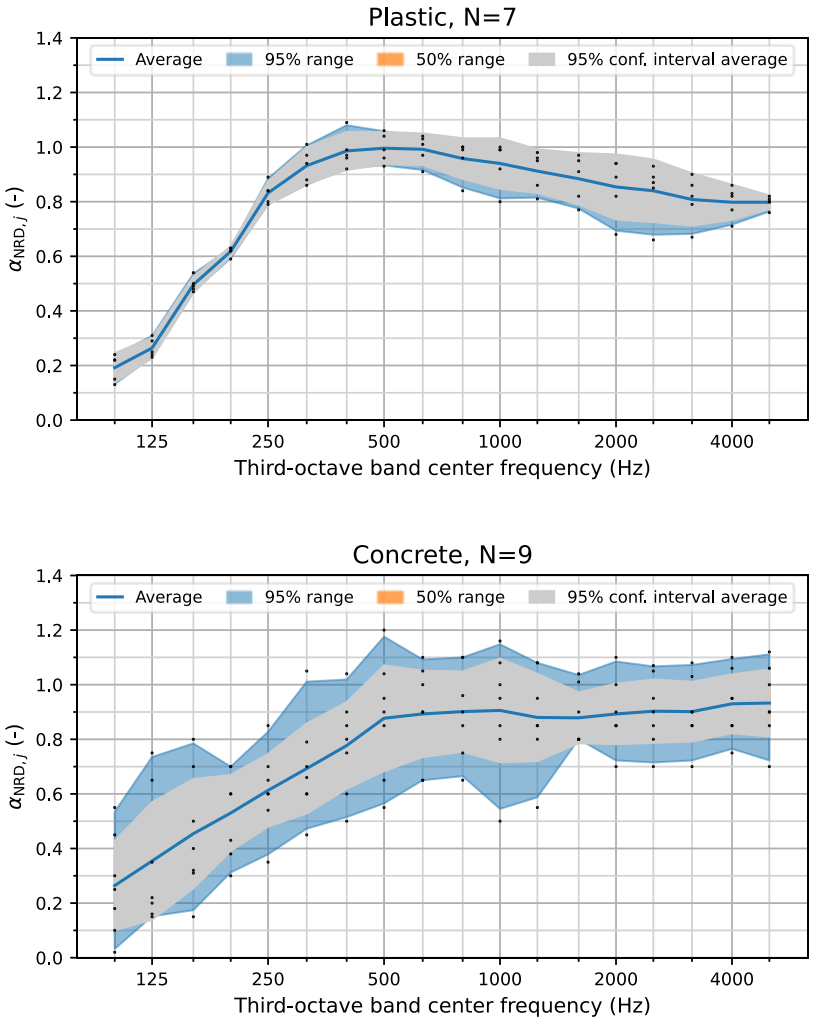


Figure 51: Frequency spectra in third-octave band on sound absorption according to EN 1793-1 for plastic (top) and concrete barriers (bottom) for data with full frequency range from 100 Hz to 5kHz available. The dots are the measurement results; the blue line is the average spectra for each noise barrier material, the grey area represents the 95% confidence interval, while orange and blue areas represent respectively the 50% and 95% range of the data. N is the number of data considered for each material.

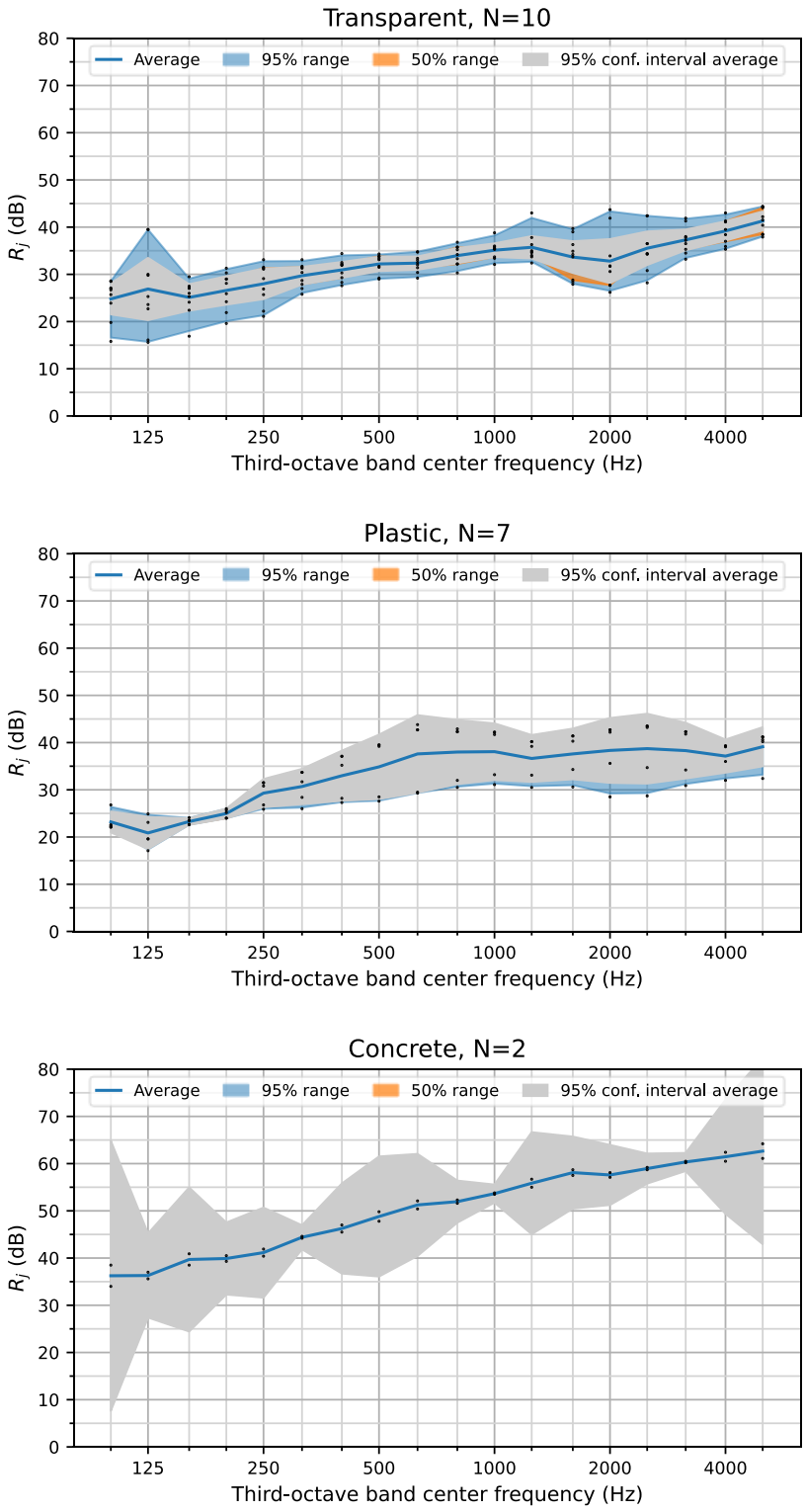


Figure 52: Frequency spectra in third-octave band on airborne sound insulation according to EN 1793-2 for transparent (top), plastic (middle) and concrete barriers (bottom) for data with full frequency range from 100 Hz to 5kHz available. The dots are the measurement results; the blue line is the average spectra for each noise barrier material, the grey area represents the 95% confidence interval, while orange and blue areas represent respectively the 50% and 95% range of the data. N is the number of data considered for each material.

# Annex C: Third-octave band results measured under direct sound field conditions for less common materials

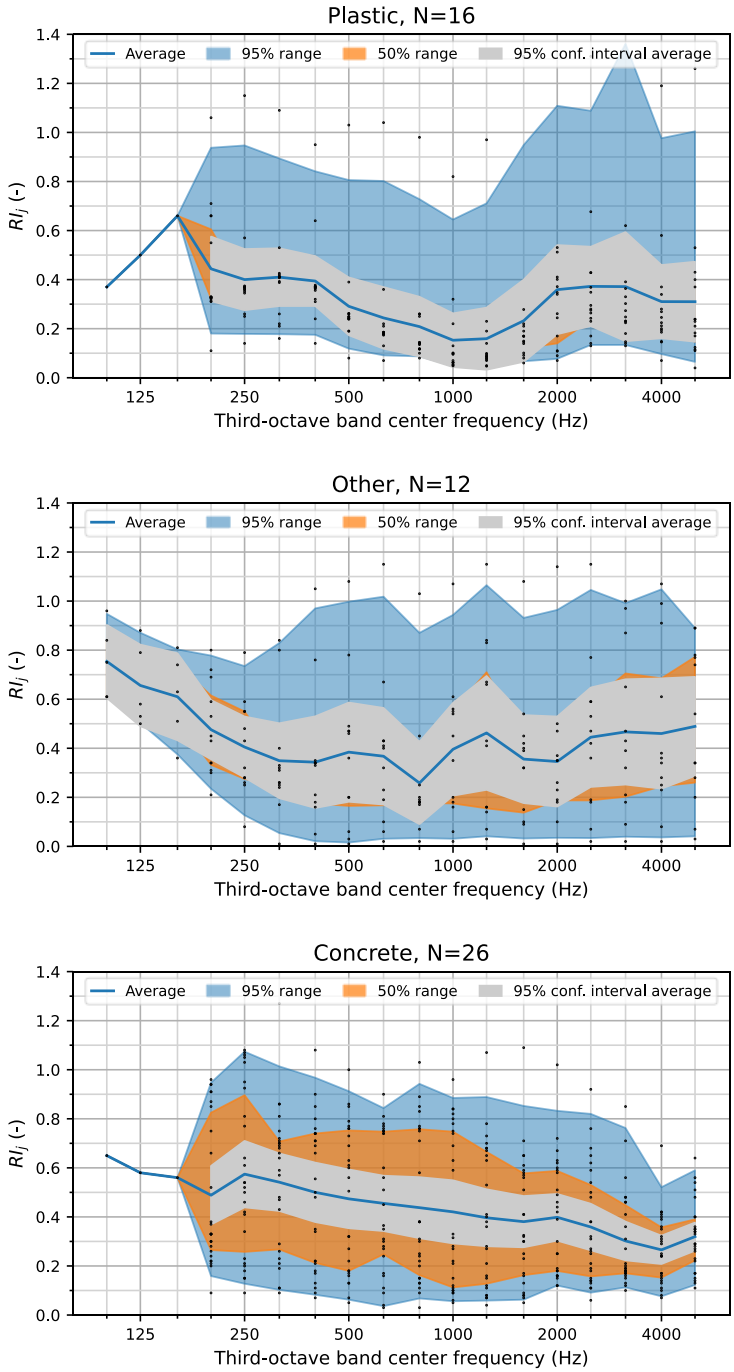


Figure 53: Frequency spectra in third-octave band on sound reflection according to EN 1793-5 or CEN/TS 1793-5 for plastic (top), other (middle) and concrete barriers (bottom) for data with full frequency range from at least 200 Hz to 5kHz available. The dots are the measurement results; the blue line is the average spectra for each noise barrier material, the grey area represents the 95% confidence interval, while orange and blue areas represent respectively the 50% and 95% range of the data. N is the number of data considered for each material.

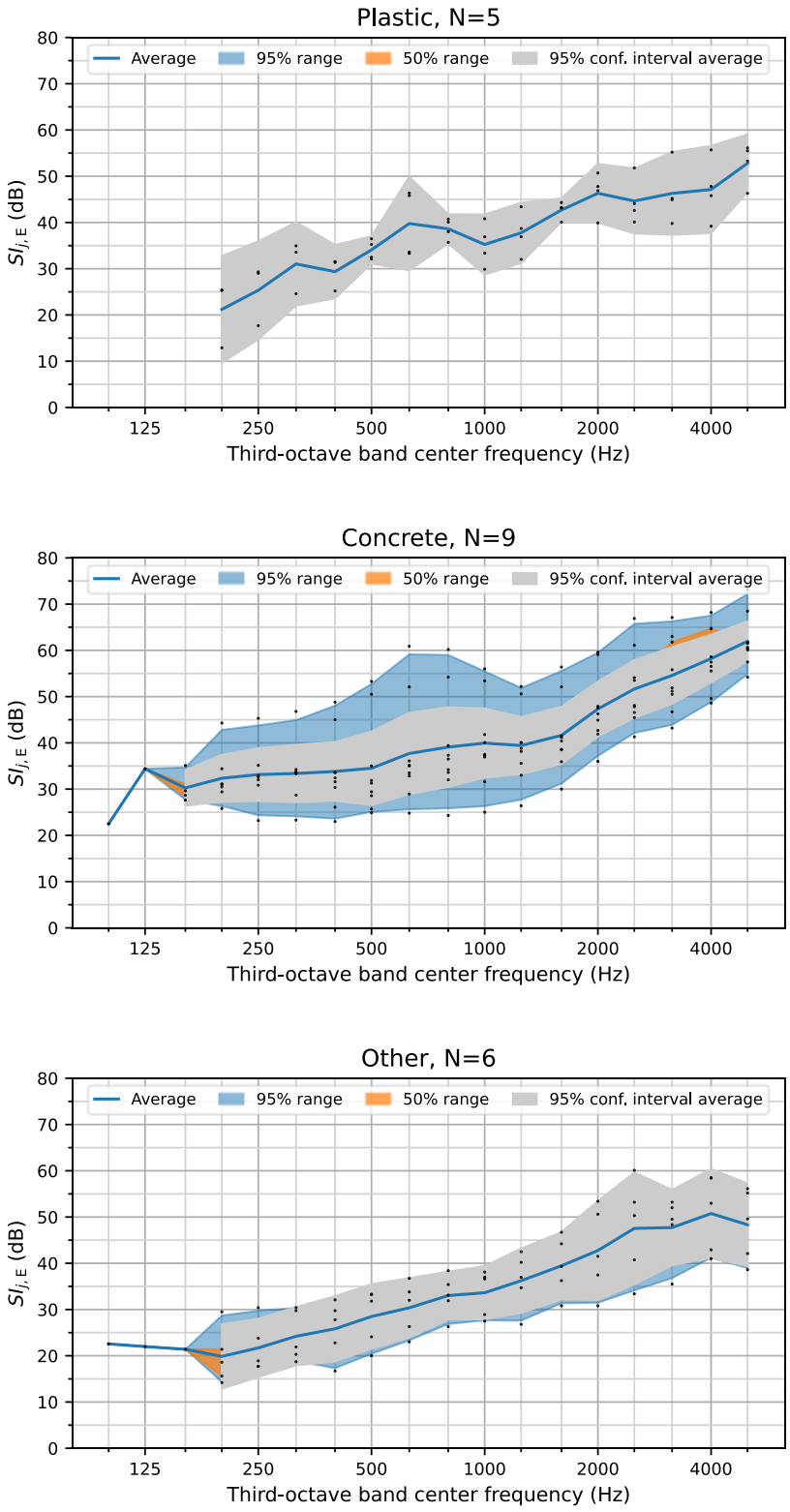


Figure 54: Frequency spectra in third-octave band on airborne sound insulation according to EN 1793-6 for plastic (top), concrete (middle) and other barriers (bottom) for data with full frequency range from at least 200 Hz to 5kHz available. The dots are the measurement results on the element; the blue line is the average spectra for each noise barrier material, the grey area represents the 95% confidence interval, while orange and blue areas represent respectively the 50% and 95% range of the data. N is the number of data considered for each material.

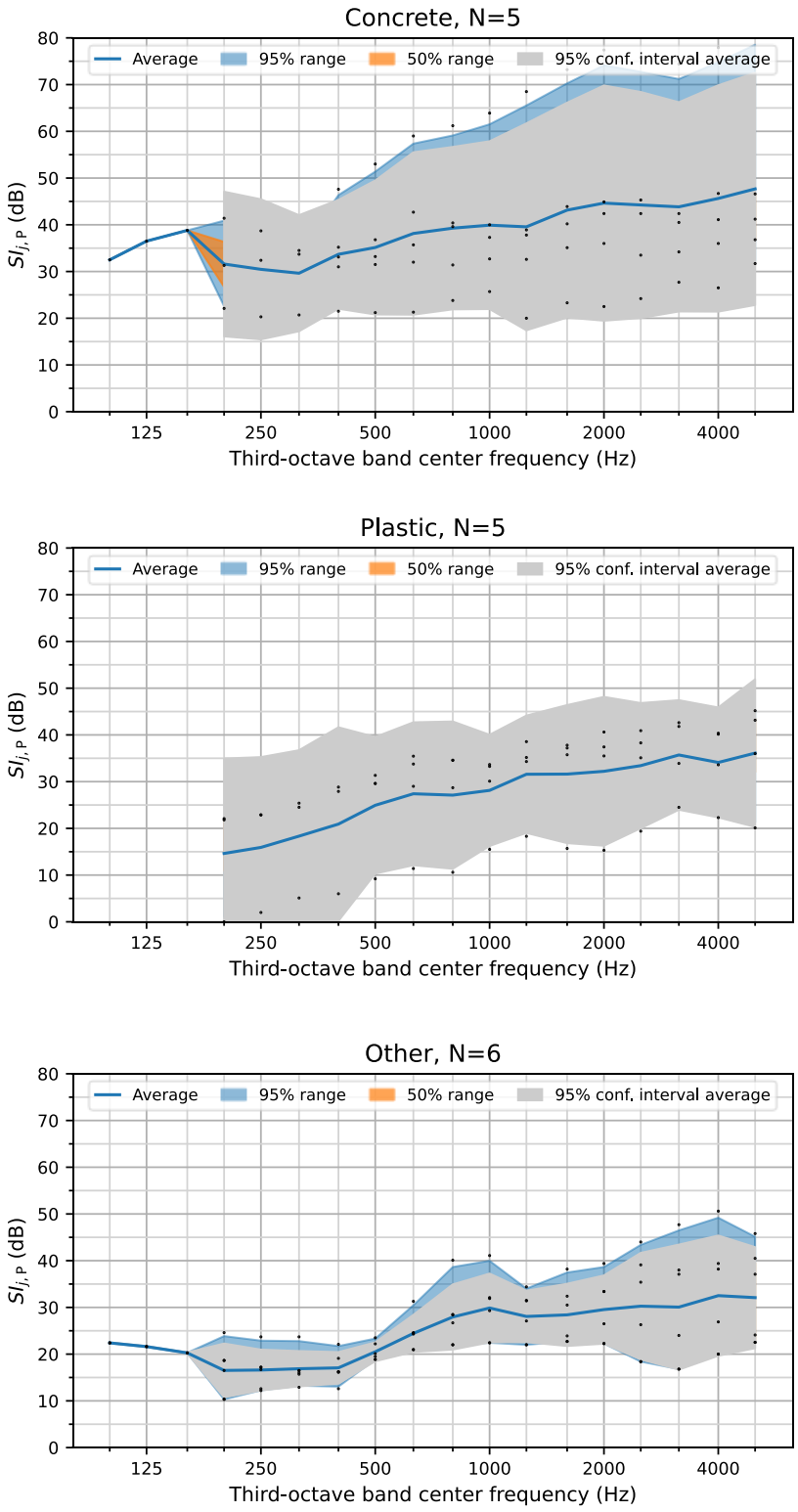


Figure 55: Frequency spectra in third-octave band on airborne sound insulation according to EN 1793-6 for concrete (top), other (middle) and plastic barriers (bottom) for data with full frequency range from at least 200 Hz to 5kHz available. The dots are the measurement results on the post; the blue line is the average spectra for each noise barrier material, the grey area represents the 95% confidence interval, while orange and blue areas represent respectively the 50% and 95% range of the data. N is the number of data considered for each material.

# Annex D: Linear regression model between single-number ratings of airborne sound insulation under diffuse and under direct sound field conditions

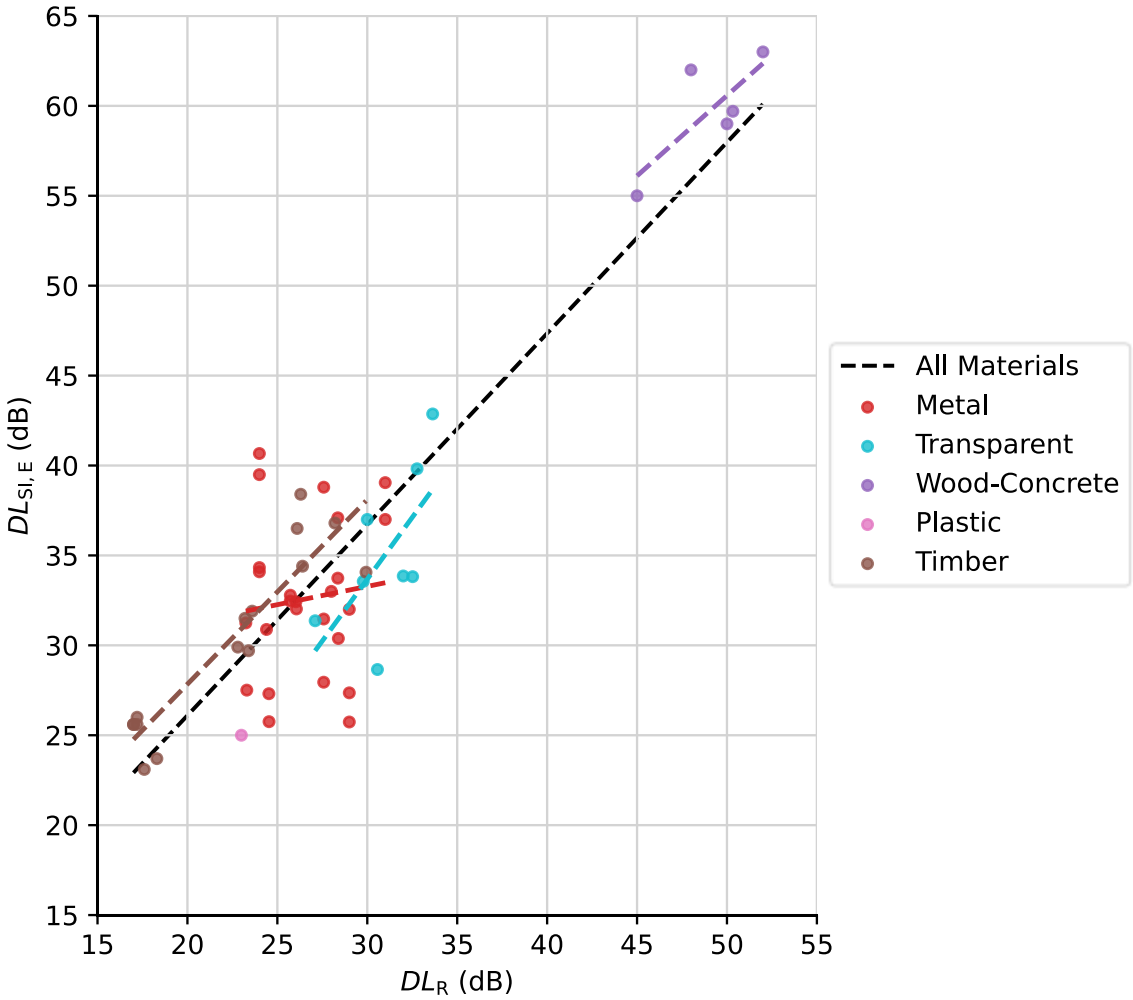


Figure 56: Fit for regression models between the single-number ratings for airborne sound insulation under diffuse sound field conditions ($DL_R$) and the single-number rating for airborne sound insulation under direct sound field conditions in front of the acoustic element ($DL_{SI,E}$) after outlier removal.

Table 9: Performance measures for predicting the $\widehat{DL_{SI,E}}$ from the $DL_R$ with a linear regression model for all materials and all the materials with minimum sample size N of 5.

| | *N* | *Model* | $R^2$ | *MAE (dB)* | *RMSE (dB)* |
|---|---|---|---|---|---|
| *All Materials* | 54 | $\widehat{DL_{SI,E}} = 1.06\ DL_R + 4.85$ | 0.81 | 3.07 | 4.01 |
| *Metal* | 25 | $\widehat{DL_{SI,E}} = 0.2\ DL_R + 27.18$ | 0.01 | 3.28 | 4.20 |
| *Transparent* | 8 | $\widehat{DL_{SI,E}} = 1.37\ DL_R - 7.55$ | 0.40 | 2.93 | 3.32 |
| *Wood-Concrete* | 5 | $\widehat{DL_{SI,E}} = 0.89\ DL_R + 15.9$ | 0.59 | 1.54 | 1.78 |
| *Timber* | 15 | $\widehat{DL_{SI,E}} = 1.03\ DL_R + 7.32$ | 0.84 | 1.48 | 1.93 |

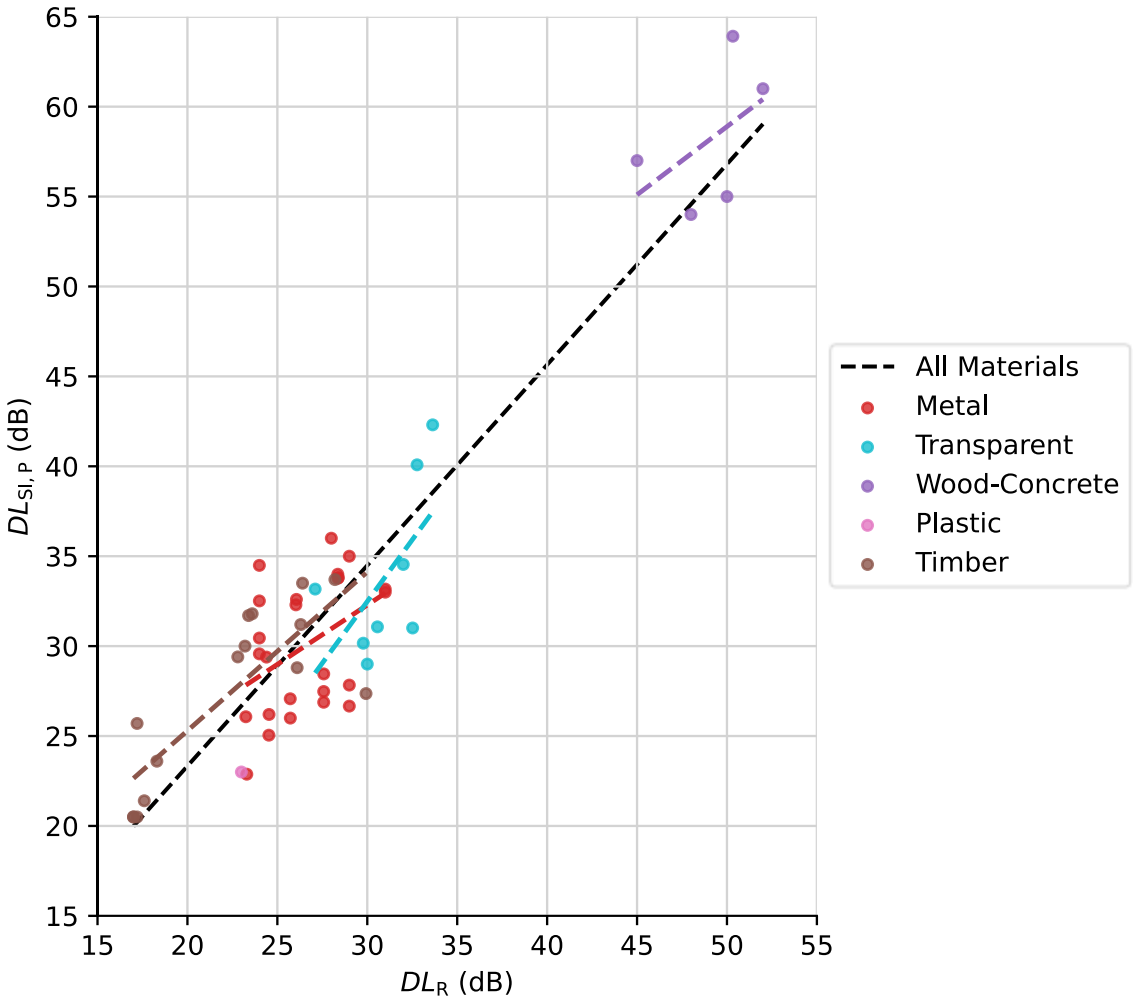


Figure 57: Fit for regression models between the single-number ratings for airborne sound insulation under diffuse sound field conditions ($DL_R$) and the single-number rating for airborne sound insulation under direct sound field conditions in front of the post ($DL_{SI,P}$) after outlier removal.

Table 10: Performance measures for predicting the $\widehat{DL_{SI,P}}$ from the $DL_R$ with a linear regression model for all materials and all the materials with minimum sample size N of 5.

| | *N* | *Model* | $R^2$ | *MAE (dB)* | *RMSE (dB)* |
|---|---|---|---|---|---|
| *All Materials* | 54 | $\widehat{DL_{SI,P}} = 1.12\ DL_R + 1.02$ | 0.86 | 3.08 | 3.59 |
| *Metal* | 25 | $\widehat{DL_{SI,P}} = 0.66\ DL_R + 12.48$ | 0.18 | 2.94 | 3.28 |
| *Transparent* | 8 | $\widehat{DL_{SI,P}} = 1.37\ DL_R - 8.65$ | 0.36 | 3.33 | 3.63 |
| *Wood-Concrete* | 5 | $\widehat{DL_{SI,P}} = 0.76\ DL_R + 20.97$ | 0.24 | 2.91 | 3.27 |
| *Timber* | 15 | $\widehat{DL_{SI,P}} = 0.88\ DL_R + 7.63$ | 0.67 | 2.29 | 2.72 |

CEDR
Conférence Européenne des Directeurs des Routes
Conference of European Directors of Roads

## CEDR TRANSNATIONAL ROAD RESEARCH PROGRAMME 2018

SOPRANOISE

# T2.3 report - Influence of acoustic degradation of noise barriers on the total noise reduction

## April 2021

| | |
|---|---|
| **Document** | 20210408_spnWP2_T2.3_BASt_final.docx |
| **Main Editor(s)** | Fabio Strigari and Wolfram Bartolomaeus, BASt |
| **Due Date** | January 2021 |
| **Delivery Date** | January 2021 (revised April 2021) |
| **Work Package** | WP2 – State of the Art on the intrinsic acoustic performance assessment of noise barriers |
| **Task** | T2.3 – Influence of acoustic degradation of noise barriers on the total noise reduction |
| **Dissemination Level** | Public |

A-tech AIT bast ERF

# Table of contents

# Table of Figures

# Table of Tables

# 1 Introduction

This report shows the achievement of milestone M2.3 and represents the third part of deliverable D2.2, which is the outcome of task T2.3 of the SOPRANOISE project.

Section 2 addresses the case of common simple sound leaks in noise barriers and gives the theoretical framework to understand the effect of those leaks on the sound insulation. Section 3 deals with the overall effect of changes in sound transmission and sound reflection of noise barriers on their noise reduction ability and the special case of multiple reflections between lorries and noise barriers.

By now, the consequences of degradations of the acoustic characteristics of noise barriers have not been investigated explicitly and in detail. However, since noise barriers shield sensitive immission sites from unwanted noise, it is important to be able to predict the decrease of their acoustic performance due to leaks – at best with the help of a practice-oriented and simple calculation. As resulting from the feedback to the SOPRANOISE questionnaire[1], such a theoretical model is lacking at present.

In Section 2, a theoretical model and exemplary calculations for several variations of leaks will be presented, which allow relating the changes of the intrinsic properties of noise barriers to the corresponding changes of their overall acoustic performance, in particular to the reduction of the sound insulation. This serves as a basis for a better understanding of the degradation of the acoustic performance of noise barriers throughout their lifetime and makes it possible to take specific and cost-efficient measures to recover the initial acoustic performance.

The results in this report are based on the research project “Acoustic effectivity of old noise barriers”, which has been carried out within the research program of the German Federal Ministry of Transport and Digital Infrastructure (BMVI) and is published in the in-house journal of the Federal Highway Research Institute (BASt) [1].

In Section 3, the overall effect of changes in the airborne sound insulation as well as in the sound absorption is examined. This is done for the case of traffic on a single lane nearby the noise barrier and for the case of a broad motorway with six lanes under the assumption of a realistic traffic distribution. Here the importance of a constant high value for the insertion loss of a noise barrier during its lifetime is underlined.

The effect of multiple reflections between a lorry and a noise barrier on the sound propagation is determined in Section 3.2.3 by using a simple mirror source model.

[1] Document title: “202001131433spnWP2WP3WP4_DOC_List of questions”, delivery date: 13 January 2020; Question *a*: “Are there, to your knowledge, theoretical models for noise barriers describing the impact of defects on sound insulation and absorption or any other investigations, which allow conclusions about the intrinsic properties of noise barriers based on the description of defects?”.

# 2 Theoretical model for simple sound leaks in noise barriers

During the lifetime of a noise barrier, a multitude of different sound leaks can occur due to ageing or external influences from e.g. traffic accidents. These leaks can have different sizes and geometries, and the degree of damage can vary considerably. In order to describe the sound propagation at noise barriers, the relevant propagation paths have to be considered: the diffraction over the barrier edge, the transmission through the non-damaged barrier and the transmission through the leak. A simple approach to do so is presented in Section 2.2, with the purpose to be implemented in the acoustical rating of the inspection procedure in WP 3.2. For a more detailed modelling, the degree of transmission of the leak is of central interest. Table 1 gives some examples for approaches to physically describe this contribution. For a more comprehensive review of existing models, the reader is referred to the publication by Sgard *et al.* [2].

Table 1: Approaches for the acoustic description of leaks

| Reference | Description | Drawbacks |
|---|---|---|
| Wilson *et al.* 1965 [3] | integral approach; modelling of sound field at round openings by assuming infinitely thin pistons (extended for rectangular openings by Sauter *et al.* [4]) | plane wave approximation with cut-off frequency depending on diameter of opening |
| Mechel 1986 [5] | integral approach; formulation for round and rectangular leaks which are filled with absorbing material and enclosed by rigid masses | prediction accuracy of detailed analytical description decreases for “non-ideal” leak geometry |
| Harrison *et al.* 1994 [6]<br>Watts 1999 [7] | discretisation of the surfaces via boundary element method (BEM), including coherence; incoherent calculation via sound intensity | computation time essentially limits the model size, usually two-dimensional with leak infinitely extended in horizontal direction |
| Wong 2000 [8] | geometric approach for horizontal slits; barrier is divided into three sub-barriers and the transmission is calculated by superposition of the diffracted sound fields | only applicable to slits of infinite extension in horizontal direction |
| Liu *et al.* 2006 [9] | modelling of noise barrier with interruption (vertical slit-like leak) by using the Traffic Noise Model [10] | only applicable to leaks which spread across the complete barrier height |

Table 1: (continued)

| Reference | Description | Drawbacks |
|---|---|---|
| Pfister *et al.* 2014 [11] | examination of the impact of gaps on the *in-situ* airborne sound insulation of noise barriers using three approaches: (1) measurements at a test facility with gaps of different sizes; (2) computer simulations of similar gaps using BEM; (3) comparison of the results according an analytical model | measured sound insulation tends to be higher than in simulation; one reason are symmetry constrictions in BEM to avoid unreasonable computation times |
| Reiter 2018 [12] | derivation of four mathematical models (analytical, BEM, FEM and transfer matrix method) for the prediction of the reflection index of acoustic layered systems, like noise barriers | no explicit treatment of leaks included.<br>NB: it should be noted that the presented models represent good tools for the prediction of the sound reflection index (RI) of noise barriers and allow an optimisation already during the design stage, with a certain computational effort |

## 2.1 Common types of leaks

In [1], a detailed investigation of sound leaks at noise barriers has been carried out to obtain an overview about which types of leaks occur in practice. Depending on the barrier material, different damage characteristics of different origins can be found:

- extensive deformations and sound leaks due to traffic collisions or fire damage
- slit-like sound leaks due to bad mounting, ageing processes or thermal effects
- leaks near the ground resulting from soil damages or bad foundation
- defects due to corrosion
- gaps due to missing sealing
- damages at the filling material within the insulation layer
- damages at the facing layer of concrete barriers
- elongated or net-like cracks with and without holes (e.g. due to stone chipping in transparent noise barriers)

In Figure 1 - Figure 6 some examples of different types of leaks and defects are given. In general, the geometry of a leak can be rather complex. However, it is not expedient and practical to aim for a full theoretical model which is able to capture all leak structures in all details. The research shows that in most cases a leak can be characterised by a **vertical or horizontal slit**. The more extensive damages usually are fairly described by a **hole-like structure**. For example, approximately round leaks are observed in wooden barriers caused by mechanical force or animals as well as in transparent barriers due to stone chipping. Missing sealings in concrete or aluminium barriers and leaks close to the ground can be well described by horizontal slits. Whereas vertical slits occur between single barrier elements or between a barrier beam and the adjoining element.

Figure 1: Damage at an aluminium noise barrier after traffic collision ©*BMVI, Germany*

Figure 2: Slit-like leak between an aluminium noise barrier and foundation ©*Walloon Road Administration, Belgium*

Figure 3: Holes in insulation layer of a wooden noise barrier ©*BMVI, Germany*

Figure 4: Missing sealing between two elements of a concrete noise barrier ©*BMVI, Germany*

Figure 5: Slit-like leak in an aluminium noise barrier due to corrosion ©*Walloon Road Administration, Belgium*

Figure 6: Net-like crack with a hole in a transparent barrier ©*BASt, Germany*

Thus, in order to cover the most common leak types, it is sufficient to formulate a theoretical model for the simplified cases of slits and holes. This simplification allows using the theoretical framework of Mechel (see Section 2.3) to assess the increase of sound transmission due to leaks in the noise barrier. The model by Mechel has been proven to be rather accurate in numerous publications. Furthermore, its parameter spectrum allows describing both fully and partially open leaks, which also can lead to a decrease of the noise barrier performance.

It should be emphasised that an inclusion of Mechel's model in the regular inspection procedure is not intended, since it involves rather elaborate calculations. The extended sound field simulations introduced below yield a sufficiently significant framework to classify a leak based on a visual *in-situ* inspection only. The modelling of slits and holes can be regarded as additional possibility in case a more detailed evaluation (going beyond worst-case assumptions) is required.

## 2.2 Extended sound field simulation

Calculations of sound propagation across a noise barrier can be carried out by applying a complex sound propagation model. However, such a model is not straightforward: a simplified and transferable description is much easier to use. Against this background, the *German guidelines for noise protection at roads* (RLS-90) [13] are used and extended to model the transmission through a noise barrier induced by a leak.

The geometry between source and receiver points is depicted in Figure 7 in top view. The emission height is chosen to be 0.5 m above the centre of the outer traffic lane according to the specifications in the RLS-90 [13]. The noise barrier is situated at a distance of 7.625 m from the centre of the first lane and its height is varied in the range from 3 m to 9 m. On the other side of the barrier, receiver positions $E_1, E_2 \dots E_k$ at 2.8 m above the ground and for distances up to 50 m from the centre of the first lane are considered. For the sound field calculation, the line source representing the traffic flow is divided into sections of length $l_i$ with single point sources $Q_1, Q_2 \dots Q_i$ according to the criteria in the German RLS-90 [13].

Please note that the specific assumptions for the road geometry and the positioning of source and receiver represent a non-general model case; however, the results obtained at the end are relative values for the insertion loss (IL). These values are not to be interpreted in an absolute sense, but the qualitative statements and conclusions remain valid.

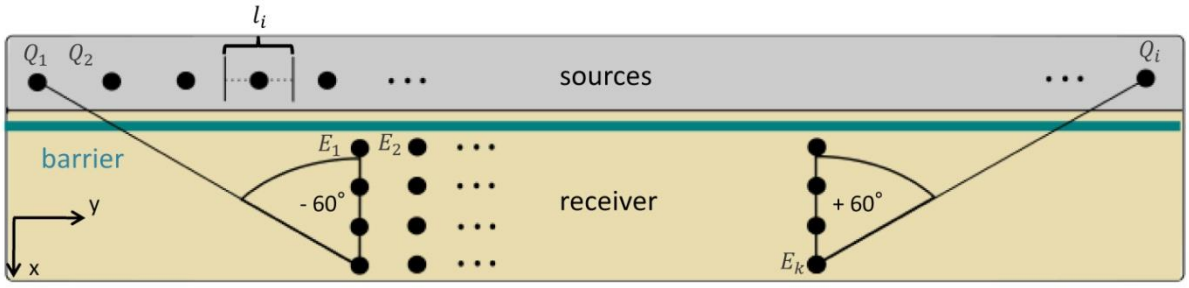


Figure 7: Schematic illustration of geometry between source and receiver points along the barrier in top view; the grey part represents the road with its single emission points $Q_i$, the green line represents the noise barrier, and the beige area contains the receiver positions $E_k$. ©BASt

In 2.2.1 and 2.2.2, the framework for calculating the influence of damages on the acoustic performance of the noise barrier will be set up. The idea is that a leak in the noise barrier acts as a point source emitting a hemispherical sound wave into the area behind the barrier. The sound power of its contribution is reduced according to the transmission loss caused when passing through the barrier.

Within this description the change of the barrier's insertion loss can be calculated for specific receiver points behind the barrier by comparing the power of the sound transmission with the sound diffraction across the top edge of the barrier. In 2.2.3 a definition of a simple criterion for the critical area behind a noise barrier, within which the impact of a leak is not negligible, is presented.

### 2.2.1 Sound propagation without considering sound transmission

In a first step, the sound propagation for an infinitely long noise barrier is calculated, including the diffraction effect at the top barrier edge but not considering airborne sound transmission through the barrier. The approach in the RLS-90 is based on the ISO 9613-2 [14] and works as follows:

For each receiver position $E_k$ the average (equivalent continuous) sound pressure level $L_{m,i}$ for the single point sources is calculated and eventually energetically summed up, so that the total sound immission level

$$L_{m,k} = 10\,\mathrm{lg}\left(\sum_i 10^{\frac{L_{m,i,k}}{10\ \mathrm{dB}}}\right)\ \mathrm{dB} \qquad (1)$$

at receiver position $k$ is obtained. The average sound pressure level $L_{m,i,k}$ induced by $Q_i$ at $E_k$ is now calculated once for free sound propagation and once in the presence of the barrier. Herein, the contributions which can be considered are the emission sound pressure level of the corresponding source section $L_{m,E}$, a correction for the source section length $D_l$, the attenuation due to atmospheric absorption and geometric divergence $D_{s_{i,k}}$, the attenuation due to ground and meteorological effects $D_{BM_{i,k}}$, and the screening attenuation due to the presence of the barrier $D_z$. In the case of free sound propagation, the average sound pressure level induced by $Q_i$ at $E_k$ then reads:

$$L_{m,i,k}{}^{\mathrm{free}} = L_{m,E} + D_l + D_{s_{i,k}} + D_{BM_{i,k}} \qquad (2)$$

In the presence of a barrier the average sound pressure level induced by $Q_i$ at $E_k$ is given by:

$$L_{m,i,k}{}^{\mathrm{NB}} = L_{m,E} + D_l + D_{s_{i,k}} - D_{z_{i,k}} \qquad (3)$$

The screening attenuation depends essentially on the so-called screening value

$$z_{i,k} = A_{i,k} + B_{i,k} + C - s_{i,k} \qquad (4)$$

which describes the detour of the sound passing via the barrier edge, see Figure 8. The barrier thickness $C$ is neglected here and set to zero. In general, the diffraction is frequency-dependent; however, the calculation of the screening attenuation is carried out without explicitly considering the frequency of the incident sound. Instead, the RLS-90 are valid for the energy range around the centre of the standardised traffic noise spectrum, see EN 1793-3 [15].

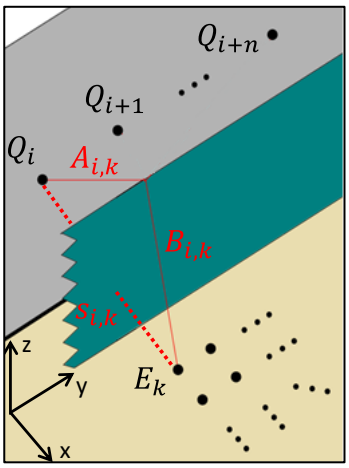


Figure 8: Schematic illustration of the geometrical parameters $A_{i,k}$, $B_{i,k}$ and $s_{i,k}$ for the determination of the screening value $z_{i,k}$ between source $Q_i$ and receiver $E_k$

Finally, the insertion loss $D_{E_0}$ of the noise barrier without transmission path through the barrier can be calculated by subtracting the total sound pressure level in the presence of screening from the total sound pressure level for free propagation:

$$D_{E_0} = 10\lg\left(\sum_i 10^{\frac{L_{m,i,k}{}^{\text{free}}}{10\,\text{dB}}}\right) - 10\lg\left(\sum_i 10^{\frac{L_{m,i,k}{}^{\text{NB}}}{10\,\text{dB}}}\right) = L_{m_k}{}^{\text{free}} - L_{m_k}{}^{\text{NB}} \quad (5)$$

### 2.2.2 Sound propagation considering sound transmission through a leak

The influence of a leak can be modelled by extending the description above and allowing additional transmission paths through the noise barrier. These additional propagation paths simulate the reduced sound insulation caused by the leak. The model assumes the noise barrier to be infinitely long with no airborne sound transmission occurring except the one through the leak.

As shown in Figure 9, the noise barrier is divided into segments of equal size. For each source-receiver pair a propagation path through each segment is assumed. Thus, the average sound pressure level $L_{m,i,k}$ induced by $Q_i$ at $E_k$ is a combination of the sound pressure level due to the diffraction at the top edge of the barrier ($L_{m,b_{i,k}}$; yellow path in Figure 9) and the transmission parts through the segments ($L_{m,t_{i,j,k}}$; red paths in Figure 9).

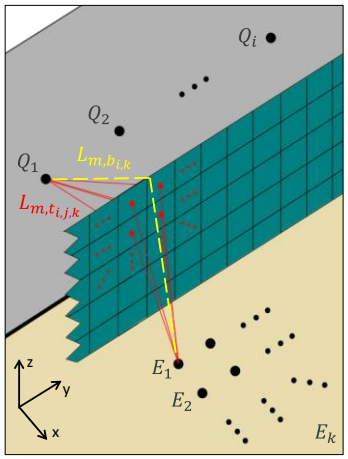


Figure 9: Schematic illustration of the propagation paths considered in the description of the sound propagation with transmission through the barrier ©*BASt*

The total sound immission level at receiver $E_k$ is then given by summing up over all sources and relevant segments:

$$L_{m_k}{}^{\mathrm{NB,leak}} = 10\,\mathrm{lg}\left[\sum_i \left(10^{\frac{L_{m,b_{i,k}}}{10\,\mathrm{dB}}} + \sum_j 10^{\frac{L_{m,t_{i,j,k}}}{10\,\mathrm{dB}}}\right)\right]\mathrm{dB} \qquad (6)$$

$L_{m,b_{i,k}}$ corresponds to Equation (3). For the calculation, the transmission path is divided into three sub-paths: $s_{i,j}$, starting from the source $Q_i$ and ending at the front centre of the barrier segment $j$; the transmission through the segment itself with the surface area $S_{\mathrm{seg}}$; and $s_{j,k}$, starting from the back centre of the barrier segment $j$ and ending at the receiver $E_k$. The sound propagation on the latter path is assumed to have a hemispherical characteristic. The contributions to the sound pressure level $L_{m,t_{i,j,k}}$ due to the transmission through segment $j$ are given by the following expression:

$$L_{m,t_{i,j,k}} = L_{m,E} + D_l + D_{s_{i,j}} + D_{S_j} - R_j + D_{s_{j,k}} \qquad (7)$$

As above, $L_{m,E}$ is the emission level of the source and $D_l$ is a correction for the source length and $D_{s_{i,j}}$ ($D_{s_{j,k}}$) the attenuation due to atmospheric absorption and geometric divergence on the sub-path in front of the barrier (behind the barrier). The transmission itself is modelled by the difference $D_{S_j} - R_j$, where $D_{S_j} = 10\,\mathrm{lg}\left(\frac{S_{Seg}}{1\,\mathrm{m}^2}\right)\mathrm{dB}$ represents the level change to calculate the sound power at the front side of the barrier segment $j$ with the surface area $S_{\mathrm{seg}}$, and $R_j = 10\mathrm{lg}\left(\frac{1}{\tau}\right)\mathrm{dB}$ represents the attenuation caused by the barrier segment $j$ with the transmission coefficient $\tau$ to calculate the sound power at the back side of the barrier segment $j$.

Analogous to Equation (5) the insertion loss of the noise barrier including transmission effects is given by

$$D_{E_{\mathrm{leak}}} = L_{m_k}{}^{\mathrm{free}} - L_{m_k}{}^{\mathrm{NB,leak}} \qquad (8)$$

with $L_{m_k}{}^{\mathrm{NB}}$ from Equation (6). The difference $\Delta D_E$ between the insertion losses for an undamaged noise barrier and a noise barrier with leak describes the impact of the leak on the total sound immission level:

$$\Delta D_E = D_{E_0} - D_{E_{\mathrm{leak}}} = L_{m_k}{}^{\mathrm{NB,leak}} - L_{m_k}{}^{\mathrm{NB}} \qquad (9)$$

### 2.2.3 Simulations and critical area

In the presence of a leak, an acoustical critical area behind the noise barrier is formed, in which the influence of the leak is dominant over the diffraction and the sound insulation of the barrier reduces significantly. At immission points beyond this area, the effect from the leak is negligible and the reduction of the sound insulation is not critical any more. We define the critical area by the criterion

$$L_{m,t} \leq L_{m,b} - 10\,\mathrm{dB} \qquad (10)$$

or by the criticality condition

$$\xi = L_{m,t} - L_{m,b} + 10\,\mathrm{dB} \qquad (11)$$

In these equations, $L_{m,b}$ describes the total immission at receiver point $E_k$ due to the diffraction across the top edge of the barrier and $L_{m,t}$ the total immission due to the transmission through the leak (compare first and second term of the sum in Equation (6), respectively). For $\xi > 0\,\mathrm{dB}$ the corresponding receiver point lies within the acoustical critical area, where the diminished

sound insulation due to the leak is relevant. For $\xi < 0\,\mathrm{dB}$ the presence of the leak has no significant influence on the sound immission. In other words, the condition $\xi = 0$ defines the border (or radius) of the critical area with dominant impact of the leak. See Figure 10.

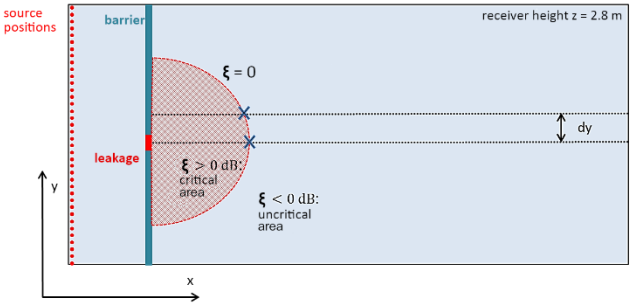


Figure 10: Illustration of the acoustical critical area behind a barrier with a leak ©*BASt*

Things can be simplified further by assuming the leak to be the size of a single segment *j* and the degree of transmission for the undamaged barrier to be approximately zero. As an example, the criticality condition is simulated for different parameters, shown in Figure 11.

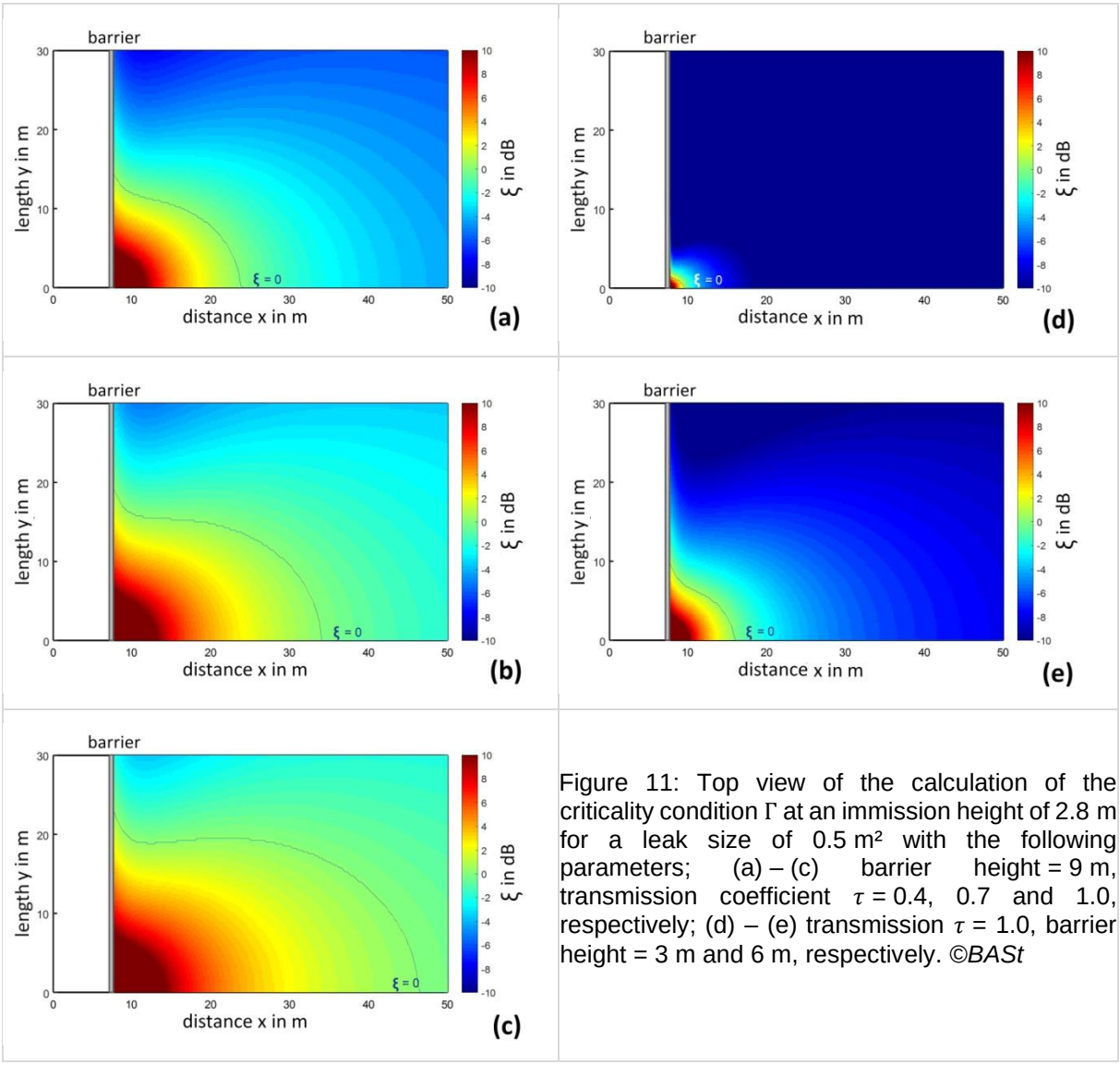


Figure 11: Top view of the calculation of the criticality condition Γ at an immission height of 2.8 m for a leak size of 0.5 m² with the following parameters; (a) – (c) barrier height = 9 m, transmission coefficient $\tau$ = 0.4, 0.7 and 1.0, respectively; (d) – (e) transmission $\tau$ = 1.0, barrier height = 3 m and 6 m, respectively. ©*BASt*

The colouring in the simulations represents the value for $\xi$, ranging from -10 to 10. The leak is positioned in the bottom left corner at x = 0 and y = 0 and at the height of 2.5 m above the ground. The border of the critical area ($\xi$ = 0) is shown as blue line.

It can be seen that the critical area has an axial symmetry and an elliptical form. The variation of the transmission coefficient $\tau$ shows an increase of the radius of influence by increasing the transmission (from ≈ 18 m for $\tau$ = 0.4 to ≈ 40 m for $\tau$ = 1.0), cf. Figure 11(a), (b) and (c).

On the other hand, the border of the critical area depends essentially on the barrier height, as can be seen by comparing Figure 11(c), (d) and (e). For a low barrier of only 3 m, the contribution of the diffracted sound dominates and the transmission through the leak has hardly any impact behind the barrier. This changes with increasing barrier height since the diffraction path becomes longer – accordingly, the critical area increases and the border with $\xi$ = 0 shifts to higher distances.

## *2.3 Theoretical framework for the degree of transmission*

The extended sound field simulations introduced in Section 2.2 allow to draw conclusions about the impact of a leak in a noise barrier for a given transmission coefficient. For an application to real-case scenarios, the next step is to describe the sound transmission depending on the characteristics of the leak. Some possibilities for the acoustic description of leaks have been listed at the beginning of Section 2. The most suitable and adaptable theoretical framework is the approach by Mechel [5]. It has been proven to give accurate results in the past and can be applied for different boundary conditions; e.g. for different incident angles, for diffuse sound fields, for front-to-back openings as well as for partial damages. And – as already pointed out in Section 2.1 – Mechel's model is defined for round and slit-like leaks, thereby covering most types which occur at noise barriers alongside roads.

In the following, the background of the theory by Mechel and the adaptation to the cases of interest is conveyed, in brief, both for round and rectangular leaks. For more details, the reader is referred to the original paper by Mechel [5] and the BASt report on the research "Acoustic Effectivity of Old Noise Barriers" [1]. Again, please note that Mechel's model is supposed to provide an additional theoretical framework to determine the transmission coefficient $\tau$ of a leak, depending on its properties and working as an input to the extended sound field model above. In general, the acoustic assessment of the *in-situ* inspection procedure works with a worst-case assumption for $\tau$. An inclusion of Mechel's model in the regular inspection procedure is not intended.

### 2.3.1 Round and rectangular leaks

In Figure 12(a) the underlying geometry and parameters for round leaks are depicted in a cross-sectional side view. The diameter of the leak is denoted by $2a$, its length by $d$ and the cross-sectional surface area by $S$. Both at the front and the back opening a surface-related mass $m_1$, respectively $m_2$, is assumed to cover the leak. These covering masses are considered to be inelastic and moving piston-like. The propagation within the leak is assumed to be one-dimensional along the $z$-axis, passing through a homogeneous, isotropic porous absorber with the normalised propagation constant $\Gamma_{an}$ and the normalised characteristic impedance $Z_{an}$.

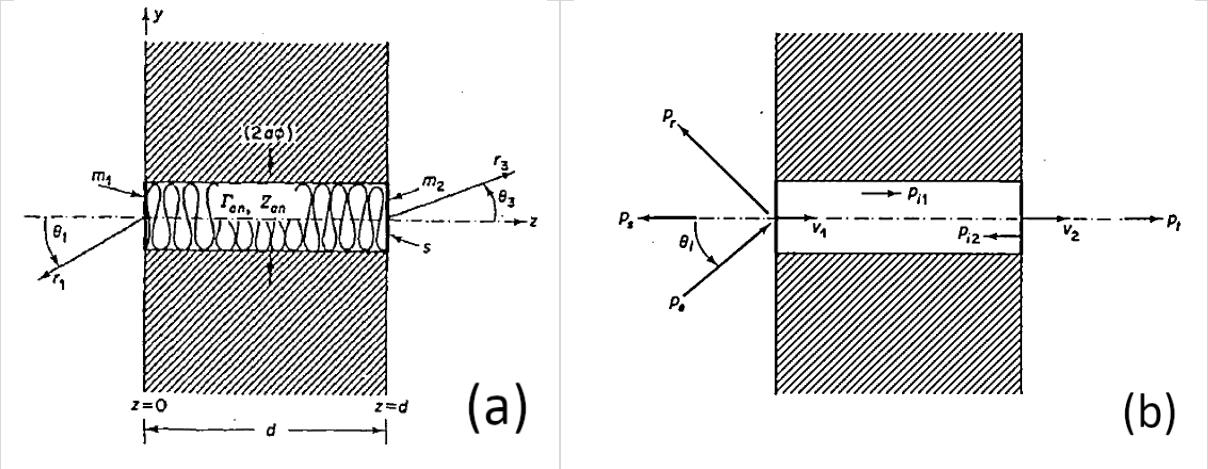


Figure 12: Schematic illustrations of the cross section of a barrier with round leak, taken from [5]; (a) geometrical dimensions and model parameters as described in the text; (b) partition of the sound field into single sound field components.

The sound field along the propagation path can be partitioned into its single components, as shown in Figure 12(b):

- $p_e$ is the incident plane wave;
- $p_r$ and $p_s$ are the partially reflected/scattered waves, respectively, at the front covering mass;
- $p_{i1}$ is the plane wave propagating within the leak towards the back opening;
- $p_{i2}$ is the returning wave which has been reflected at the back-covering mass;
- $p_t$ is the transmitted part of the wave behind the barrier;
- $v_1$ and $v_2$ denote the vibrational velocities of the front and back covering mass, respectively.

With the abovementioned inputs and assumptions, and by exploiting the force balance equation and continuity condition of the particle velocity at the leak openings, the degree of transmission in dependence of the incidence angle $\tau(\Theta)$ can be deduced (not shown here).

In the case of slit-like, rectangular leaks, the description has to be extended to two dimensions and two incidence angles ($\Theta_i$ and $\phi_i$, compare Figure 13) have to be used for the incoming sound wave (since the problem has no rotational symmetry any more). This leads to a band-like sound pressure level distribution at the slit surfaces, with varying pressure along *x* and constant pressure along *y*.

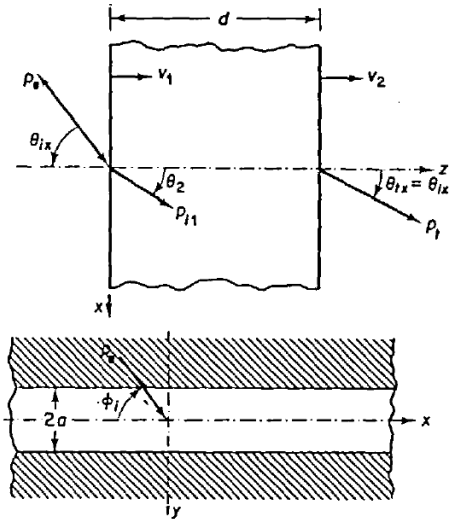


Figure 13: Schematic illustrations of the cross section in the z-x-plane (top) and x-y-plane (bottom) of a barrier with rectangular leak with the incidence angles $\Theta_i$ and $\phi_i$, taken from [5].

### 2.3.2 Validation and correction function

The theoretical descriptions of round and rectangular leaks as well as the sound field simulations (Section 2.2) have been validated experimentally within the BMVI project [1].

For this purpose, measurements were carried out *in situ* – in a first step at a noise barrier test stand with defined and variable slit and hole sizes and in a second step at damaged noise barriers alongside roads. The sound insulation and absorption were measured according to EN 1793-5 and -6 [16] [17], both at leaks and at non-damaged segments of the barrier.

Figure 14: Noise barrier test stand with defined and variable slit and hole size; used for the validation of the theoretical model developed by Mechel. ©*BASt*

In the first part, the comparison between the validation measurements and simulations revealed that a correction of the "illuminated" area is necessary. This means, that only the area which is actually "illuminated" by the incoming sound influences the measurement results. This effect must be considered by determining the relevant, frequency-dependent surface area of the leak with the concept of Fresnel zones. This correction function defines the surface ratio of the leak and the intact noise barrier within the total area that is effectively contributing in the measurements (see Figure 15).

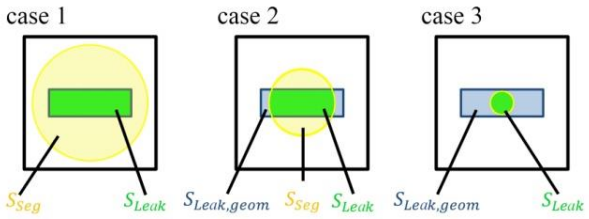


Figure 15: Illuminated area $S_{Seg}$, geometrical area of the leak $S_{Leak,geom}$ and the contributing area $S_{Leak}$ of the leak; three exemplary cases for a slit-like leak. ©*BASt*

When considering the correction function for the transmission loss of leaks, the simulation results of the sound insulation index (SI) are in good agreement with the measurement results obtained at the test stand – in particular for frequencies around 1000 Hz. Even measurements at non-standard positions close to the top edge of the barrier provide satisfactory results, but the results are more prone to errors due to the small delay between direct and diffracted sound. Since in real examinations the actual geometrical and acoustical material properties are not straightforward (e.g. absorber thickness, flow resistance, porosity etc.), in these cases it might be preferable to measure the transmission loss of the leak beforehand and use this value in the theoretical modelling instead (of course, here the above-mentioned correction of the "illuminated" area must be applied as well.)

The analysis of microphones in greater distance to the noise barrier allows the validation of the propagation model and the criticality condition $\xi$ (see Section 2.2): Within the experimental and theoretical accuracy, the results of the *in-situ* measurements according to the standard EN 1793-6 and the sound field simulations match rather well in first approximation. However, some deviations occur because of modifications in the simulations (made to fit the experimental setup) which are quite strong and not provided for by the original RLS-90 model. Moreover, usual experimental uncertainties due to temperature fluctuations and inaccurate positioning of the microphones and leak windows cannot be excluded. Regarding the criticality condition $\xi$, it can be seen that it changes only slowly with increasing distance when assuming a point source instead of a line source. In other words, the impact of a leak is less significant in the case of a line source.

The second part of the validation consisted of measurements at real noise barriers alongside roads with different leak types; namely, holes and cracks in a glass barrier, a vertical slit at the back side of a wooden barrier, and different damages at an aluminum barrier and its absorber material. All damages, except the fine cracks in the glass barrier, caused a significant reduction of the sound insulation index that could be measured *in situ*.

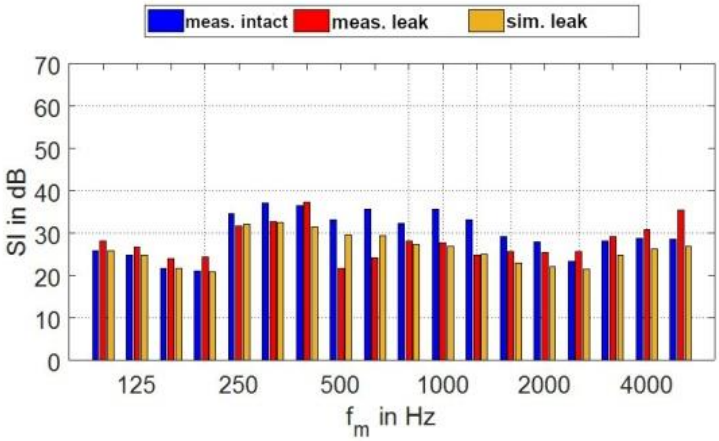


Figure 16: Sound insulation index SI of investigated glass noise barrier; blue: measurement of intact noise barrier (without leak); red: measurement of noise barrier with leak in situ; orange: simulation of noise barrier with leak. ©*BASt*

Although, as mentioned above, the correct determination of the model's inputs – i.e. material-specific and geometrical parameters of the leak – turned out to be difficult in some cases, the real-case leaks can be reproduced fairly well with the framework by Mechel. An example is shown in Figure 16, where the sound insulation index for a glass barrier measured with and without leak and simulated with the according leak parameters is plotted. The same good agreement between the simulation and measurement results can be seen for round leaks, for rectangular leaks with absorber filling, for the case with damaged absorber and even for missing absorber material. In all scenarios the correction of the frequency-dependent "illuminated" area is applied and apparently necessary for a satisfactory reproduction of the measurements. The simulations work quite well around 1000 Hz in particular, such that the use of the theoretical transmission coefficient resulting from the model by Mechel for the sound propagation model is justified in good approximation.

## 2.4 Impact of leaks

In the previous sections we have seen that the criticality condition of the extended sound propagation model, Equation (11), can be used to calculate the radius of influence for different leak dimensions and thereby obtain a measure for the impact of the leak on the overall acoustic performance of the barrier. In combination with the theoretical model for the transmission

coefficient, a comprehensive qualitative analysis can be carried out for a given leak in a noise barrier with mostly basic input parameters.

The calculated radius of influence for some exemplary leak dimensions is presented in Figure 17 to Figure 21.

Using the methods presented here, a wide-ranging “catalogue of leaks” can be set up, which can serve as first practical guidance when assessing the relevance of a leak. An exemplary catalogue of this sort is part of the original BMVI research report [1]. As previously explained, the considered geometries are round holes and horizontal and vertical rectangular slits – thereby covering the most common leak types.

For the sake of clarity, some general indications shall be pointed out:

- The geometry between source and receiver points is explained at the beginning of Section 2.2 and illustrated in Figure 7.
- The transmission through the non-damaged segments of the barrier is assumed to be zero (worst-case evaluation).
- The relevant model parameters for round leaks are the transmission coefficient $\tau_L$ within the barrier, the surface area $S_L$ and the average height $z_{Leak}$ of the leak.
- For rectangular shaped leaks the description comprises also the width $b_L$ and the length $l_{Leak}$.
- The height of the barrier is $h_{barrier}$.
- Since the variation of the leak surface has the same influence as the modification of the transmission (see definition of $\xi$ above), the use of the product $\tau_L \cdot S_L$ (effective area) and $\tau_L \cdot b_l$ (effective width) for round and rectangular leaks, respectively, is recommended.

The calculations in Figure 17 to Figure 21 visualise some general trends. Namely, the radius of influence of a leak increases for an increasing degree of transmission, for an increasing effective area, for an increasing barrier height and for a decreasing height of the leak. The latter effect can also be reversed, if the effective area is small enough and the average height of the leak comes closer to the emission height.

The catalogue can be extended and customised to cover the relevant cases and draw conclusions about when the impact of a leak is negligible – and when further actions are necessary. But of course, apart from the acoustic effects one should keep in mind that the visual impression of heavily damaged noise barriers can also negatively influence the acoustic perception of affected residents, even though there is no reduction of the overall acoustic performance of the barrier.

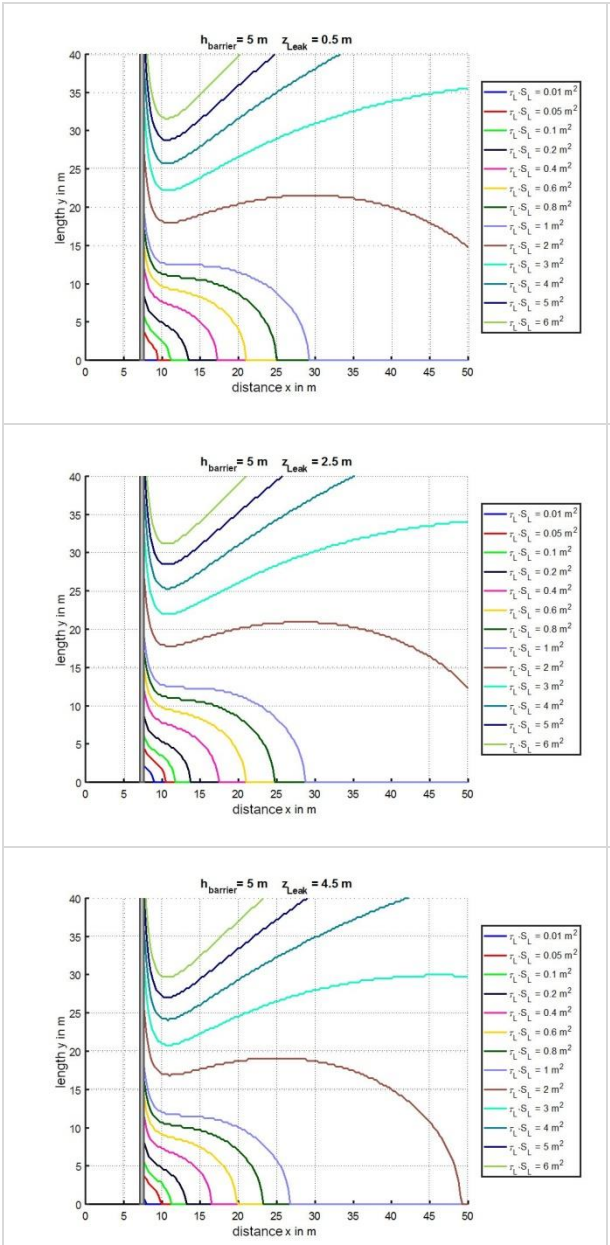


Figure 17: Calculated radius of influence for round leaks with different effective area $\tau_L \cdot S_L$; barrier height $h_{barrier}$ = 5 m; average leak height $z_{Leak}$ = 0.5 m, 2.5 m and 4.5 m. ©BASt

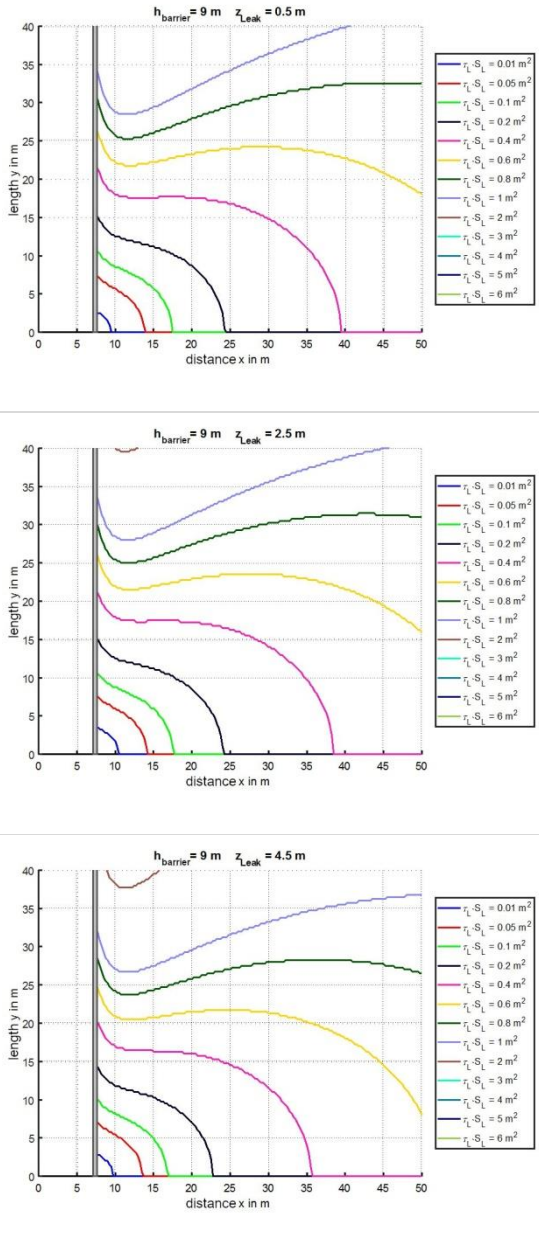


Figure 18: Calculated radius of influence for round leaks with different effective area $\tau_L \cdot S_L$; barrier height $h_{barrier}$ = 9 m; average leak height $z_{Leak}$ = 0.5 m, 2.5 m and 4.5 m. ©BASt

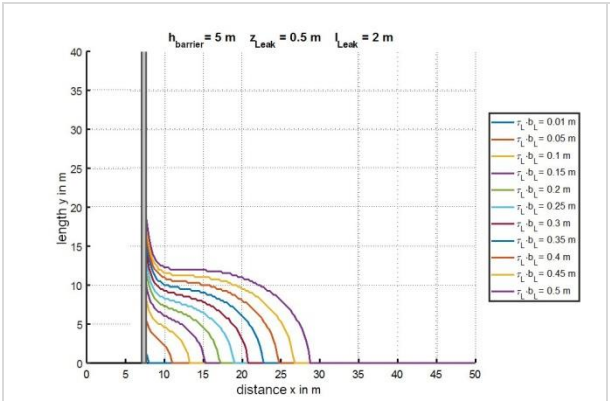


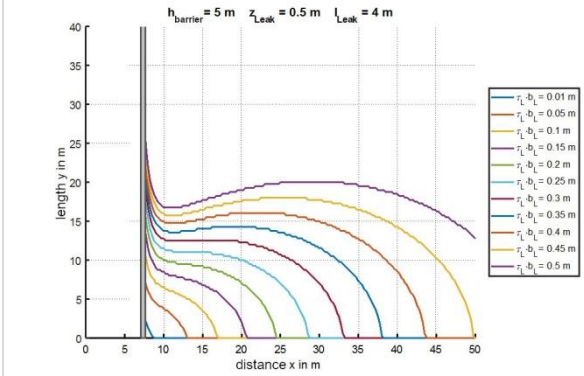


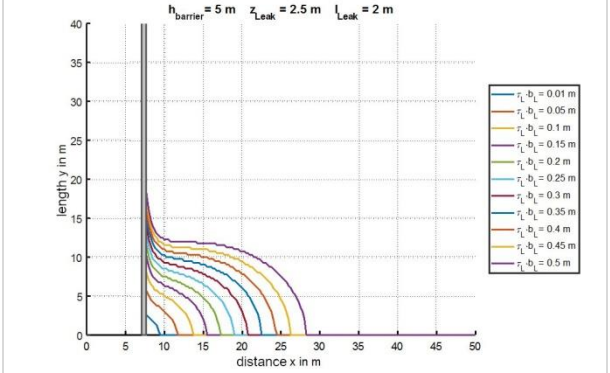


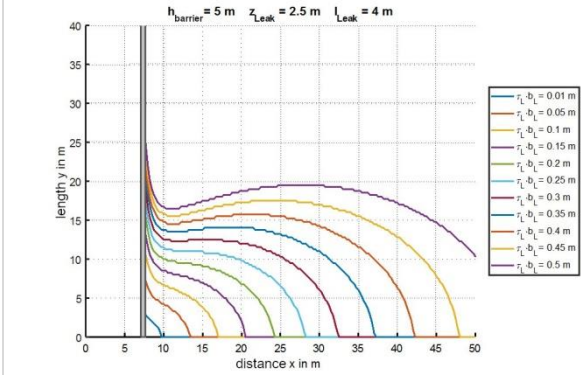


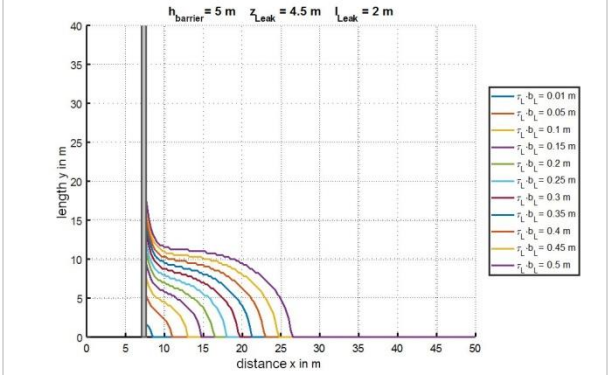


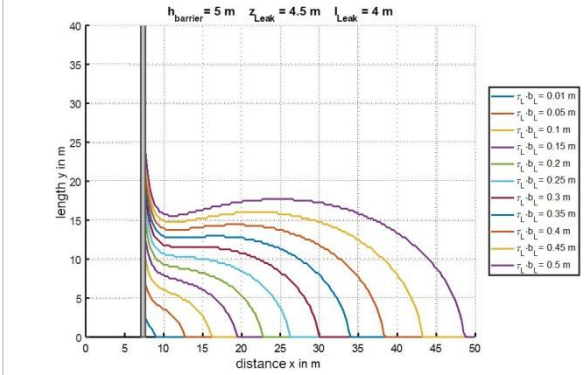


Figure 19: Calculated radius of influence for horizontal rectangular leaks of length $l_{Leak}$ = 2 m with different effective width $\tau_L \cdot b_L$; barrier height $h_{barrier}$ = 5 m; average leak height $z_{Leak}$ = 0.5 m, 2.5 m and 4.5 m. ©*BASt*

Figure 20: Calculated radius of influence for horizontal rectangular leaks of length $l_{Leak}$ = 4 m with different effective width $\tau_L \cdot b_L$; barrier height $h_{barrier}$ = 5 m; average leak height $z_{Leak}$ = 0.5 m, 2.5 m and 4.5 m. ©*BASt*

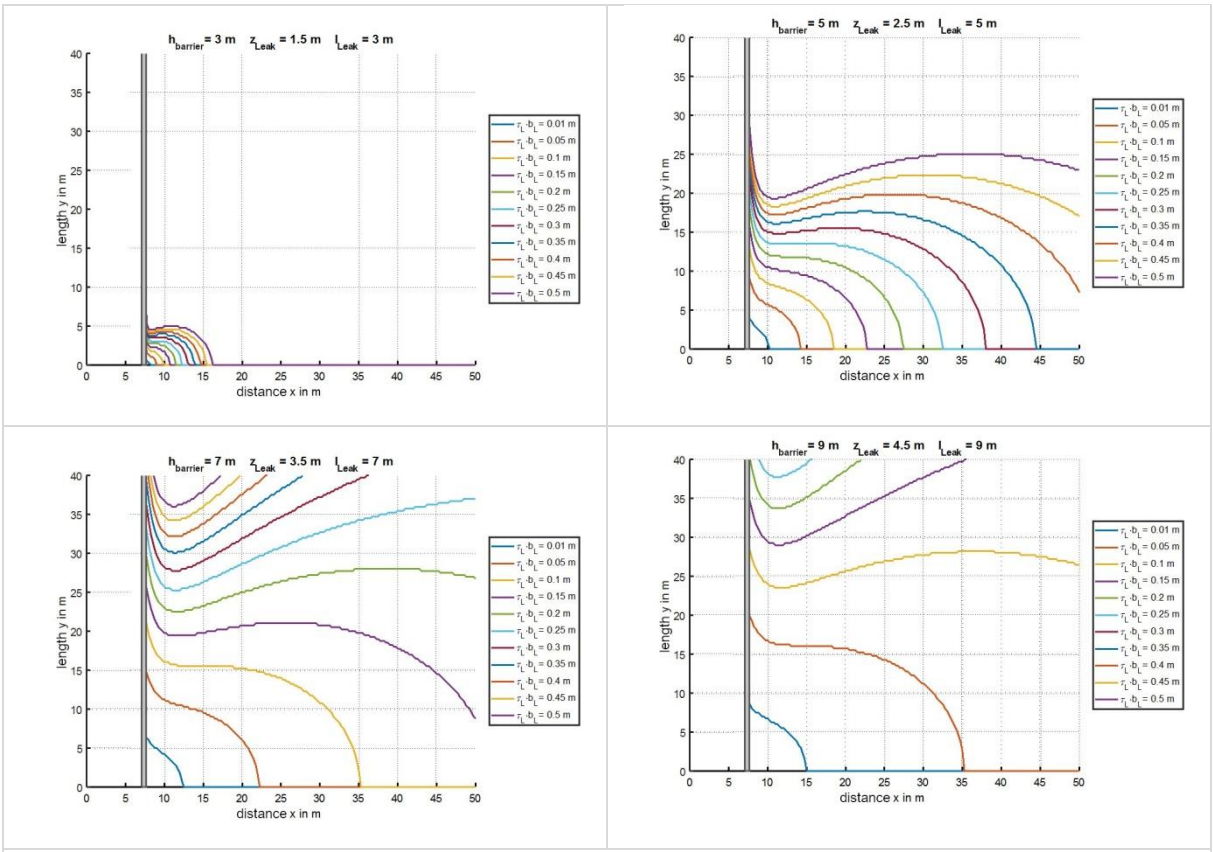


Figure 21: Calculated radius of influence for vertical rectangular leaks of length $l_{Leak} = h_{barrier}$ with different effective width $\tau_L \cdot b_L$; barrier height $h_{barrier}$ = 3 m, 5 m, 7 m and 9 m; average leak height $z_{Leak} = \frac{1}{2} h_{Wand}$. ©BASt

# 3 Overall effects of degradation on sound propagation

There are two distinct situations in which the acoustic degradation of a noise barrier can influence the total noise reduction. First, the degradation of the airborne sound insulation performance of the noise barrier can increase the noise level **behind** the noise barrier. Second, the degradation of the sound absorption performance of the noise barrier can increase the noise level **in front** of the noise barrier and, in the special case of lorries passing by close to the noise barrier, it can also increase the noise level **behind** the noise barrier. The terms "behind" and "in front" are used with respect to the side of the road traffic.

In Figure 22 two typical situations for the use of noise barriers near a source are shown.


Figure 22: Sketch of a noise barrier, acting as a (partial) reflector (left) or as a (partial) shield (right)

On the right, the noise barrier is acting as a (partial) shield. The two contributions from the diffraction above the noise barrier and the transmission through the noise barrier add energetically at the receiver. The sound transmission through the noise barrier is important. The effect of changes in the transmission loss due to degradation on the acoustical performance of a noise barrier is discussed in detail in section 3.1.

On the left, the noise barrier is acting as a (partial) reflector. In the considerations presented here, it is assumed that no transmission occurs. The two contributions from the direct source and its reflection on the barrier add energetically. The effect of changes in the reflection loss due to degradation on the acoustical performance of a noise barrier is discussed in detail in section 3.2.

## *3.1 Effect of the degradation of the transmission loss on the acoustical performance of a noise barrier*

For a noise barrier, the *insertion loss IL* is the difference of the sound pressure level without and with the noise barrier, respectively.

The *insertion loss* $IL$ of a noise barrier is defined as

$$IL = L_{pwo} - L_{pw} \quad (12)$$

where $L_{pwo} = 10 \cdot lg\left[\frac{{p_{wo}}^2}{{p_0}^2}\right] = 20 \cdot \left[\frac{p_{wo}}{p_0}\right]$ is the *sound pressure level without the barrier* and $L_{pw} = 10 \cdot lg\left[\frac{{p_w}^2}{{p_0}^2}\right] = 20 \cdot \left[\frac{p_w}{p_0}\right]$ is the *sound pressure level with the barrier*.

Here $p_0$ is the reference pressure of $2 \cdot 10^{-5}$ Pa.

The airborne sound transmission is too often neglected, but if the noise barrier is damaged or aged, the airborne sound transmission cannot be neglected any more. From here, we will consider the transmitted energy through the barrier characterized by its transmission loss.

The *transmission coefficient* is defined as

$$C_t = W_t / W_i \quad (13)$$

where $W_i$ is the *energy incident to barrier*, and $W_t$ is the *energy transmitted through the barrier.*

For the following sections, the airborne sound transmission performance of a barrier is characterised by its *sound reduction index R*[2]

$$R = -10 \cdot lg[C_t] \quad (14)$$

In the following, the sound pressure level behind a noise barrier is calculated for varying *sound reduction index R* to model the influence of the degradation of the *transmission loss* on the acoustical performance of a noise barrier.

### 3.1.1 Emission from a single traffic lane

First, the sound propagation of the sound emitted from a single traffic lane is examined. The geometry of the model is simply a single line of point sources, radiating omnidirectional. The source line is 1000 m long, and the separation between the points are 1 m each. The position of the line source is 0.5 m above the road surface, but the reflection from the road can be considered to be already included in the sound pressure level, which is arbitrarily set to 82 dB(A) for a distance of 1 m. The noise barrier is situated 8.0 m in parallel to the line source. The immission is determined for the centre of the line source and perpendicular to it. In Figure 23 the geometric situation is drawn.

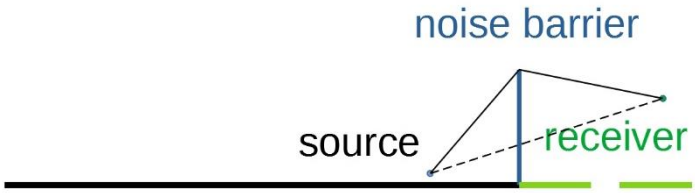


Figure 23: Sketch of the sound propagation from a single source with a noise barrier acting as a (partial) shield

The calculations of the sound propagation were carried out with the alternative method for the calculation of the A-weighted sound pressure level according to ISO 9613-2, but excluding the ground effect. The attenuation due to geometrical divergence, $A_{div}$, and the attenuation due to air absorption, $A_{atm}$, are only depending on the straight distance between source and receiver. In the presence of a noise barrier there is an extra term, $A_{bar}$, to include the screening effect of the noise barrier.

In ISO 9613-2 it is assumed, that there is no sound transmission through the noise barrier. This can be regarded as a good approximation, since in reality for newly built noise barriers the required value for the sound reduction index R is rather high, e.g. in Germany at least 24 dB [18].

In Figure 24 sound maps for heights from 2.8 m (representing the top edge of the window of the ground floor) up to 14.0 m (representing the top edge of the window of the fifth floor) and distances from 20 m up to 400 m behind a noise barrier of 4 m height are shown: on the left for the case without transmission ($R = \infty$), and on the right for the case with full transmission ($R = 0$), i.e. without barrier.

[2] The following sections use R as the airborne sound transmission characteristic, while R is measured under diffuse sound field conditions. There is a link between R and the airborne sound transmission characteristics measured under direct sound field conditions, but this is not the topic of this survey.

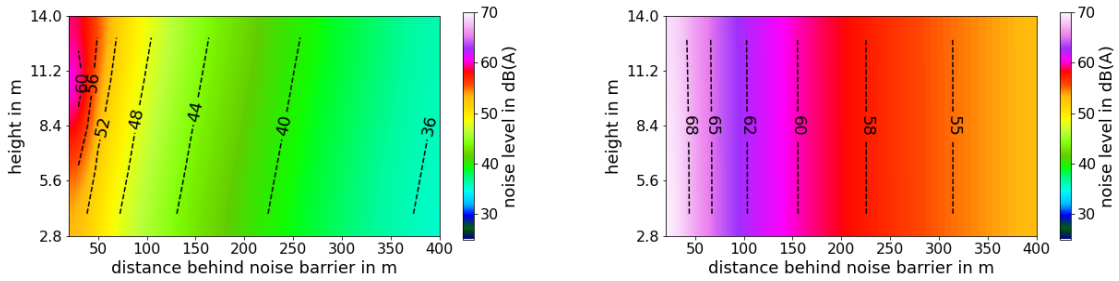


Figure 24: Sound maps at distances from 20 m up to 400 m from a line source, and at heights from 2.8 up to 14.0 m behind a noise barrier of 4 m height; single lane; left: without transmission ($R = \infty$), right: with full transmission ($R = 0$), i.e. without barrier

For further investigations, an immission line 2.8 m above ground (bottom line in Figure 24), representing the top edge of the window of the ground floor of a house on flat ground, is used. The immission line ranges from 20 m to 400 m, as measured from the source line. In Figure 25, the result of the calculations is shown.

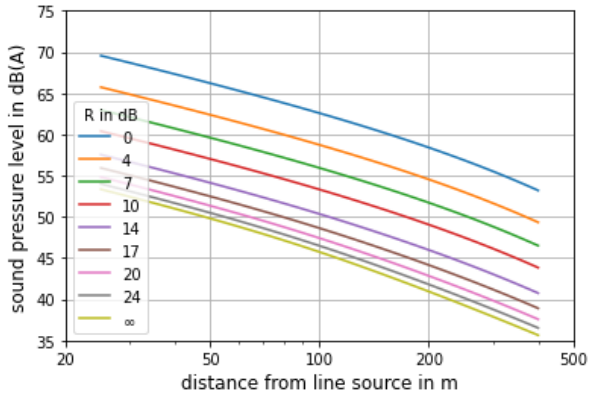


Figure 25: Sound pressure level at distances from 20 m up to 400 m from a line source, at a height of 2.8 m behind a noise barrier of 4 m height, with sound reduction index $R$ as parameter; single lane

Without transmission, $R = \infty$, the sound pressure level decays from about 55 dB(A) at 20 m distance from the source line (12 m behind the noise barrier) down to about $L_{400} = 35$ dB(A) at 400 m distance. With increasing transmission, the level behind the noise barrier is increasing. Some results for the distance of 400 m behind the noise barrier are shown in Table 2.

Table 2: Results from propagation calculations for a single source line, for a distance of 400 m from the line source behind a noise barrier of 4 m height

| $R$ in dB | $L_{400}$ in dB(A) | $\Delta L_{400}$ in dB |
|---|---|---|
| ∞ | 35.6 | 0.0 |
| 24 | 36.5 | 0.9 |
| 20 | 37.6 | 2.0 |
| 17 | 38.9 | 3.3 |
| 14 | 40.7 | 5.1 |
| 10 | 43.8 | 8.2 |
| 7 | 46.5 | 10.9 |
| 4 | 49.3 | 13.7 |
| 0 | 53.2 | 17.6 |

For the limit of $R = 24$ dB in the German regulation [18], the level in 400 m distance increases by $\Delta L_{400}$ = 0.9 dB compared to the optimum with infinite transmission loss.

Without any shielding, $R = 0$, the level increases by about 18 dB in a distance of 400 m from a line source behind a noise barrier. Note, that in this case the ground attenuation might be relevant, which is not taken into consideration here.

There is only a small dependency of the level difference, $\Delta L$, with distance; as evident from the almost parallel curves in Figure 25. Therefore, the conclusions made on the level difference at 400 m, $\Delta L_{400}$, are valid also for shorter distances behind the noise barrier, e.g. 50 m.

For an illustration of the significance of the increase in transmission, the following example is given: a noise barrier element with a height $h$ = 5.0 m and a width $w$ = 6.0 m has an area of $A = h \cdot w$ = 30 m$^2$. If the noise barrier has a sound reduction index of $R = 24$ dB, the transmission loss induced by a hole with a radius of about $r$ = 25 cm in each noise barrier element can be equivalently achieved by a horizontal slit with a width of $d_h$ = 3 cm or two vertical slits with a width of $d_v$ = 2 cm in each element. The reduction in acoustical performance for this slightly damaged noise barrier in a distance of 400 m from source line is about 1 dB. This can be compensated by an increase of the noise barrier by about 0.7 m. Hence, one can state:

**Small holes and slits in a noise barrier are no serious problem far away from a noise barrier of moderate height.**

For noise barrier heights of 2 m and of 8 m, the sound maps are shown in Figure 26.

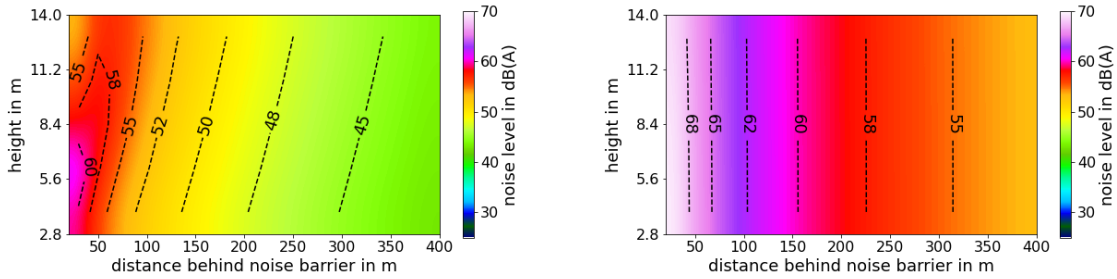


Figure 26: Sound maps at distances from 20 m up to 400 m from a line source, and at heights from 2.8 up to 14.0 m behind a noise barrier without transmission; single lane; left: height of the noise barrier is 2 m, right: height of noise barrier is 8 m

The influence of the noise barrier height on the results at an immission height of 2.8 m is shown in Figure 27.

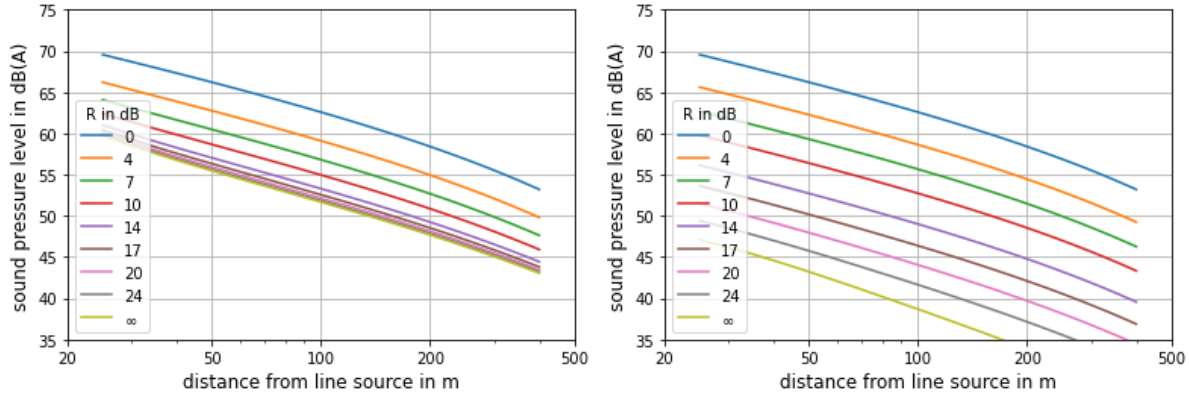


Figure 27: Sound pressure level at distances from 20 m up to 400 m from a line source, at a height of 2.8 m behind a noise barrier of 2 m (left) and 8 m (right) height, with sound reduction index $R$ as parameter; single lane

Obviously, the shielding of a 2 m wall is worse, while the shielding of an 8 m wall is better than of a 4 m wall. And, the higher the wall is, the more pronounced is the influence of an increasing sound reduction index *R*. This becomes evident from the larger spread between the curves in Figure 27.

For the example from above (slightly damaged noise barrier with a sound reduction index of $R = 20$, but with a barrier height of 8 m, the reduction of the acoustical performance at a distance of 400 m from the source line is about 1.5 dB. It is not possible to compensate this by an increase of the noise barrier: The energy transmitted through the barrier is too high to be reduced by increasing the barrier height. From this follows:

**Small holes and slits can cause serious problems behind a high noise barrier.**

In Figure 28 the level differences a distance of 400 m from a line source behind the noise barrier are displayed for noise barriers with heights of 2 m, 4 m and 8 m, respectively.

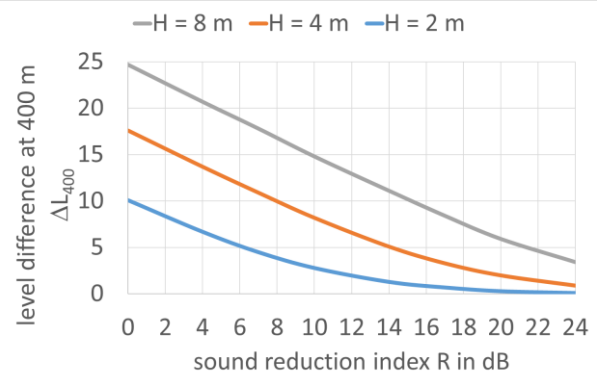


Figure 28: Sound pressure level differences at a distance of 400 m from a line source behind a noise barrier of 2 m (blue), 4 m (red) and 8 m (right) height, with sound reduction index $R$ as parameter; single lane

Small variations of the sound reduction index in the area near zero lead to large differences in the sound pressure level. This can lead to large level differences at high distances. With increasing height of the noise barrier this tendency is even more pronounced:

**The higher the noise barrier and/or the closer the houses to protect, the more important is a constant high transmission loss over the lifetime of the noise barrier. If the noise barrier is low, a high transmission loss is less important and a decrease of *the sound reduction index R* has a lesser effect on the acoustical performance of the noise barrier.**

The decrease of sound reduction index R from 24 dB to 20 dB will yield an increase of the immission level at a distance of 400 m by 0.2 dB for a noise barrier with a height of 2 m up to 2.5 dB for a noise barrier with a height of 8 m. For a smaller distance of the receiver behind the noise barrier, e.g. 50 m, the values are approximately the same.

### 3.1.2 Emission from multiple traffic lanes

So far, all the traffic has been considered to be concentrated on just one lane. In reality, especially on motorways, the traffic is split into several lanes with different amount of traffic, types of vehicles and vehicle speeds. For a typical German six-lane motorway, the data in Table 3 can be assumed for the night time. The night time is chosen, because this is the most critical time regarding the noise exposure of the population living near a motorway. The geometry of the motorway and the noise barrier acting as a (partial) shield is shown in Figure 29. It is assumed, that the traffic on both sides of the motorway is the same. As before, in a first step the calculations for the propagation were conducted for a barrier of 4 m height.

Table 3: Emission parameters for a six-lane German motorway for the night time

| Emission parameters | 1st lane | 2nd lane | 3rd lane |
|---|---|---|---|
| Distance to the noise barrier in m: near lane<br>far lane | 6.375<br>29.625 | 10.000<br>26.000 | 13.500<br>29.625 |
| Number of vehicles per hour: passenger cars<br>light good vehicles<br>heavy good vehicles | 36.4<br>44.8<br>126.0 | 218.4<br>11.2<br>14.0 | 109.2 |
| Average speed in km/h | 90.0 | 110.0 | 140.0 |
| Emission level, $L_{Aeq}$, in dB(A)/m | 88.5 | 85.3 | 81.0 |

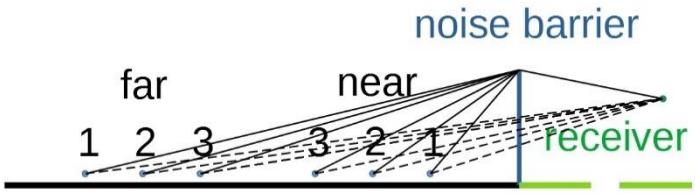


Figure 29: Sketch of the sound propagation from a typical German six-lane motorway with a noise barrier acting as a (partial) shield

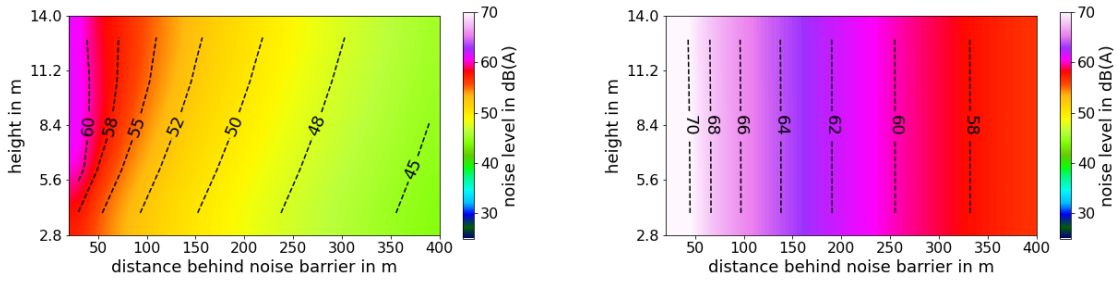


Figure 30: Sound maps at distances from 20 m up to 400 m from the nearest line source, and at heights from 2.8 up to 14.0 m behind a noise barrier of 4 m height; multiple lanes with traffic distribution; left: without transmission ($R = \infty$), right: with full transmission ($R = 0$)

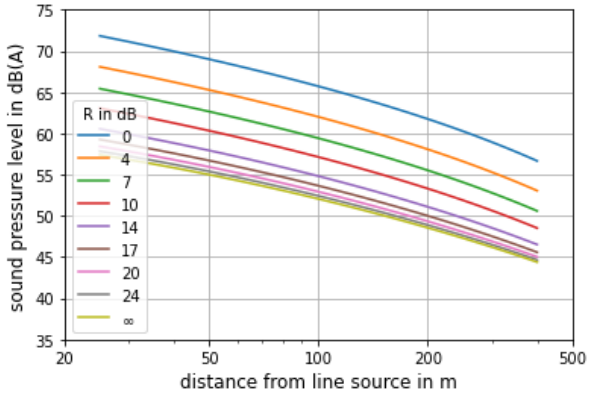


Figure 31: Sound pressure level at distances from 20 m up to 400 m from the nearest line source, at a height of 2.8 m behind a noise barrier of 4 m height, with sound reduction index $R$ as parameter; multiple lanes with traffic distribution

Again, an immission line at 2.8 m above the ground (bottom line in Figure 30) is used, see Figure 31. Compared with the situation for the single traffic lane in Figure 25, the decay of the immission level with distance is flatter. For transmissions near zero, i.e. very high sound

reduction index R, the increase of the immission level with increasing transmission is much lower than for the single source.

The reduction of the acoustical performance of a slightly damaged noise barrier at a distance of 400 m from the nearest source line is about 0.5 dB. This can be compensated by an increase of the noise barrier by about 0.2 m. One can note:

**For broad motorways, small holes and slits in a noise barrier are a lesser problem far away from a noise barrier of moderate height.**

For noise barrier heights of 2 m and of 8 m, sound maps are shown in Figure 32.

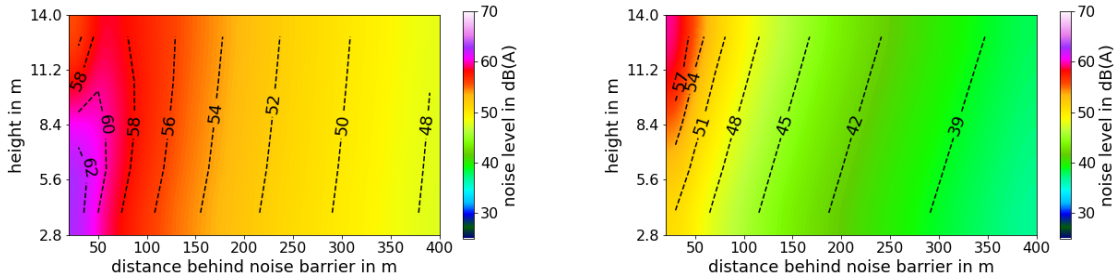


Figure 32: Sound maps at distances from 20 m up to 400 m from the nearest line source, and at heights from 2.8 up to 14.0 m behind a noise barrier without transmission; multiple lanes with traffic distribution; left: height of noise barrier is 2 m, right: height of noise barrier is 8 m

In Figure 33 the calculations for noise barrier heights of 2 m and 8 m, respectively, are shown for multiple lanes with traffic distribution. Again, the increase of the immission level with increasing transmission is much lower than for the single line source, when the traffic is compacted into a single traffic lane (compare this with Figure 27).

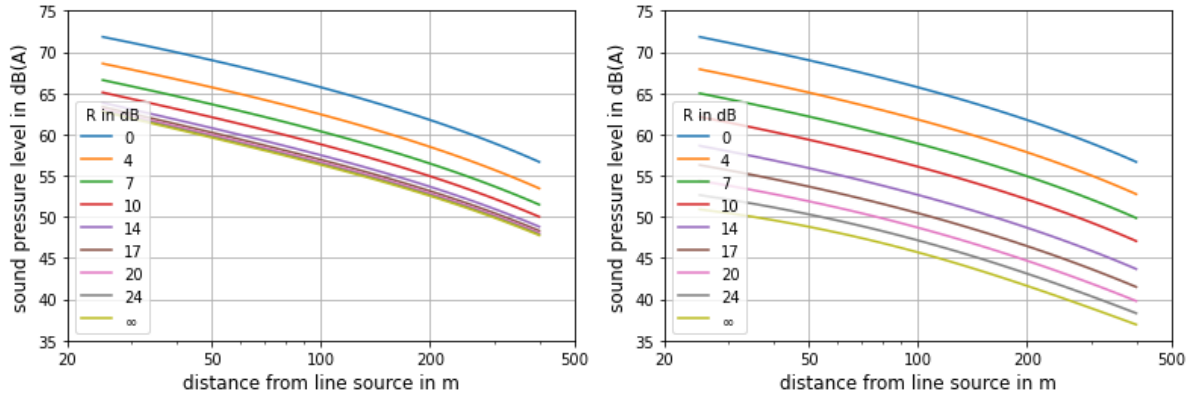


Figure 33: Sound pressure level at distances from 20 m up to 400 m from the nearest line source, at a height of 2.8 m behind a noise barrier of 2 m (left) and 8 m(right) height, with sound reduction index $R$ as parameter; multiple lanes with traffic distribution

In Figure 34 the level differences at a distance of 400 m from the nearest line source behind the noise barrier are displayed for noise barriers with heights of 2 m, 4 m and 8 m, respectively, for multiple lanes with traffic distribution.

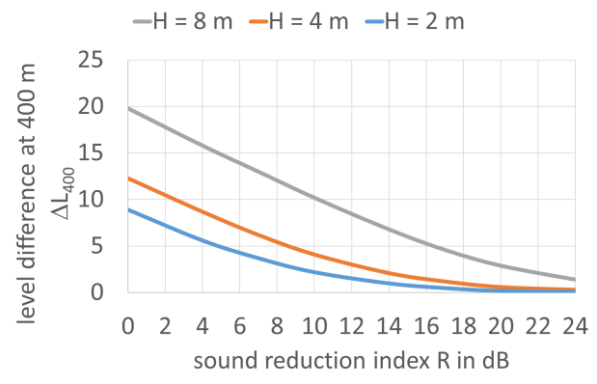


Figure 34: Sound pressure level differences at a distance of 400 m from the nearest line source behind a noise barrier of 2 m (blue), 4 m (red) and 8 m (right) height, with sound reduction index $R$ as parameter; multiple lanes with traffic distribution

The decrease of sound reduction R from 24 dB to 20 dB will yield an increase of the immission level at a distance of 400 m by 0.1 dB for a noise barrier with a height of 2 m up to 1.5 dB for a noise barrier with a height of 8 m. For a smaller distance of the receiver behind the noise barrier, e.g. 50 m, the values are approximately the same.

**For broad motorways, shielded by a noise barrier, the effect of losing acoustical efficiency by reduction of its transmission loss is not as pronounced as for small roads, but can be also substantially high.**

The reduction of the acoustical performance for a slightly damaged noise barrier at a distance of 400 m from the source line is about 1.5 dB. In contrast to Section 3.1.1, for broad motorways it is possible to compensate this by an increase of the noise barrier of 3 m.

**Small holes and slits in a noise barrier can be a serious problem behind the barrier, even for broad motorways.**

## 3.2 *Effect of the degradation of the reflection loss on the acoustical performance of a noise barrier*

The *reflection loss* $RL$[3] of an inserted object (e.g. a noise barrier) can be defined as

$$RL = L_{ps} - L_{pr} \quad (15)$$

Here $L_{ps} = 10 \cdot lg\left[\frac{{p_s}^2}{{p_0}^2}\right] = 20 \cdot \left[\frac{p_s}{p_0}\right]$ is the sound pressure level without the object and $L_{pr} = 10 \cdot lg\left[\frac{{p_r}^2}{{p_0}^2}\right] = 20 \cdot \left[\frac{p_r}{p_0}\right]$ is the reflected sound pressure level **<u>in front</u>** of the object inserted.

The reflection index RI, as defined in EN 1793-5 is an experimental measure for the reflection loss RL. In the following, the theoretical parameter RL is used.

The sound is partially reflected. Without any sound transmission, the reflected part of the sound pressure level $L_{pr}$ is the total sound pressure level $L_{ps}$ reduced by the part absorbed by the noise barrier itself. In this case it follows

[3] The following sections use RL as the sound reflection characteristic, which is characterized under diffuse sound field conditions. There is a link between RL and the sound reflection index RI measured under direct sound field conditions, but this is not the topic of this survey.

$$L_{pr} = L_{ps} - L_{pa} \quad (16)$$

Here $L_{pa} = 10 \cdot lg\left[\frac{{p_a}^2}{{p_0}^2}\right] = 20 \cdot \left[\frac{p_a}{p_0}\right]$ is the part of the sound pressure level absorbed by the object inserted.

Changes in the reflection loss play a role in three distinct situations:

(1) For the case of a single noise barrier (acting as a partial reflector), a changing reflection loss has an, somehow limited, influence on the noise level **in front** of this noise barrier (see section 3.2.1).

(2) Adding an additional second noise barrier (acting as a shield by assuming an infinite transmission loss) in parallel to the (partially) reflecting noise barrier of case (1), does influence the noise level **in front** of this (reflecting) noise barrier (see section 3.2.2).

(3) The (multiple) reflections between a noise barrier and lorries passing by have an influence on the noise level **behind** the barrier (see section 3.2.3).

As a reminder, the terms “behind” and “in front” of the noise barrier are used with respect to the side of the road traffic. In other words, by “behind” we refer to the “shielded zone” and by “in front” we refer to the “unshielded zone”. In case (2) the terms “shielded” and “unshielded” are avoided, as they are not unambiguous in the presence of a second noise barrier.

## 3.2.1 Single noise barrier

As explained above, we now consider changes of the noise level **in front** of a single noise barrier (unshielded zone) due to changes in its reflection loss. In this case, the shielded zone **behind** the noise barrier is nearly not affected and thus not investigated here.

### 3.2.1.1 Emission from a single traffic lane

As for the investigations of the transmission loss, at first the sound propagation of the sound emission from a single traffic lane is examined. The basic geometry of the model is the same as for the calculation of the transmission loss. The noise barrier acting as a (partial) reflector is situated 8.0 m in parallel to the line source. Therefore, the receiver is now on the same side of the noise barrier as the source, meaning “**in front** of the noise barrier”. In Figure 35 the geometric situation is shown.

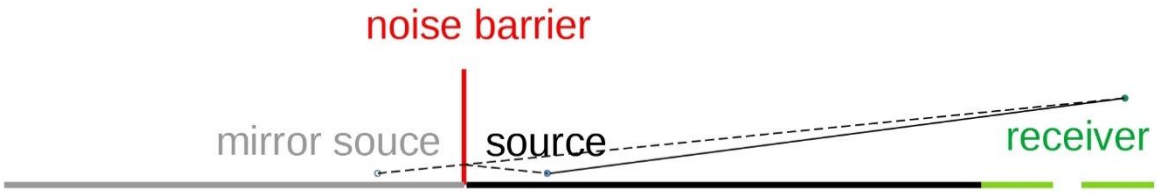


Figure 35: Sketch of the sound propagation from a single source with a noise barrier acting as a (partial) reflector

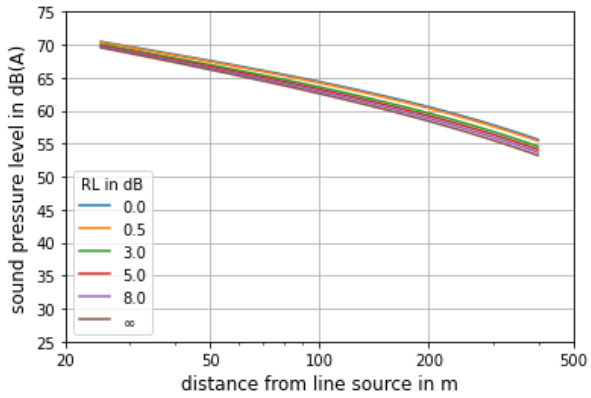


Figure 36: Sound pressure levels at distances from 20 m up to 400 m from a line source, at 2.8 m height in front of a noise barrier, with reflection loss $RL$ as parameter; single traffic lane

In Figure 36 the result of the calculations is shown. Without reflections, $RL = \infty$, the sound pressure level decays from about 69 dB(A) at 20 m distance from the line source down to about $L_{400} = 53$ dB(A) at 400 m distance. With decreasing reflection loss, the level in front of the noise barrier is slightly increasing. Some results at the distance of 400 m from the line source in front of the noise barrier are shown in Table 4.

Table 4: Results from propagation calculations for a single line source, 400 m in front of a noise barrier, without shielding barrier

| $RL$ in dB | $L_{400}$ in dB(A) | $\Delta L_{400}$ in dB |
|---|---|---|
| ∞ | 53.2 | 2.4 |
| 8.0 | 53.7 | 1.9 |
| 5.0 | 54.1 | 1.5 |
| 3.0 | 54.6 | 1.0 |
| 0.5 | 55.4 | 0.2 |
| 0.0 | 55.6 | 0.0 |

In Germany, the reflection loss assumed for a non-absorbing wall is $RL = 0.5$ dB (see [13]). For this value, the level in 400 m distance increases by $\Delta L_{400} = 0.2$ dB compared to the situation with zero reflection loss.

Without any reflection, $RL = \infty$, or in the absence of a noise barrier, the level increases by about 2.4 dB at a distance of 400 m from the line source. Note, that in the limit of infinite distance this value approximates to the value of 3.0 dB, because of the source being doubled.

#### 3.2.1.2 Emission from multiple traffic lanes

As before, the calculations for the propagation of the emission from multiple lanes were conducted for the case of a single noise barrier, acting as a (partial) reflector. The geometry of a typical German six-lane motorway is used (as in section 3.1.2) and shown in Figure 37.

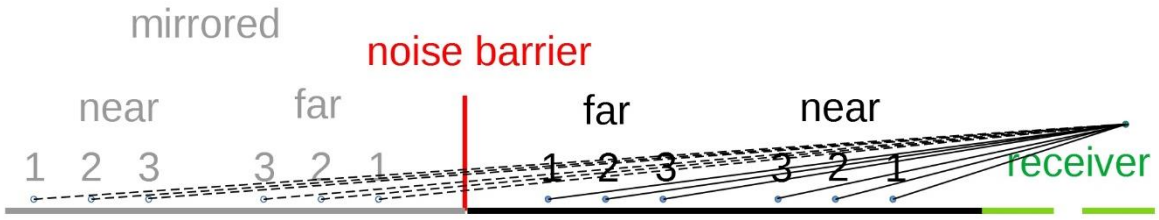


Figure 37: Sketch of a typical German six-lane motorway with a single noise barrier acting as a (partial) reflector

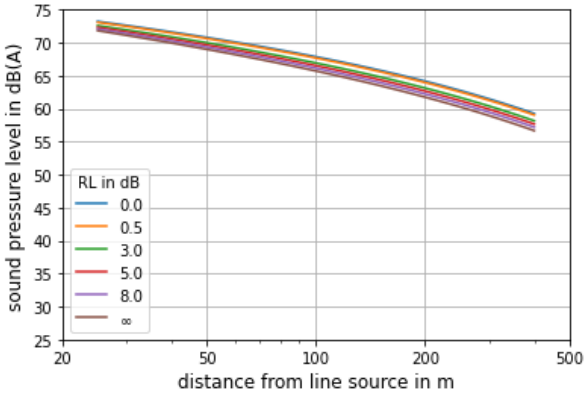


Figure 38: Sound pressure level at distances from 20 m up to 400 m from a line source, at a height of 2.8 m with reflection loss of the noise barrier $RL$ as parameter; multiple lanes with traffic distribution

In Figure 38 the results are displayed. Compared with the situation for the single traffic lane in Figure 36, the decay of the immission level with increasing distance and the dependence on $RL$ is comparable.

## 3.2.2 Two parallel noise barriers

In this section, the effect of including an additional noise barrier between source and receiver, acting as a shield, is examined. In principle, this leads also to multiple reflections between the two noise barriers. The effect investigated in this subsection deals with the influence of changes in the reflection loss of a noise barrier on the sound pressure level – in the presence of an additional (fully shielding) noise barrier parallel to the first one.

### 3.2.2.1 Emission from a single traffic lane

A sketch of the geometry with two parallel noise barriers, one acting as a (partial) reflector and one acting as a shield, is shown in Figure 39.

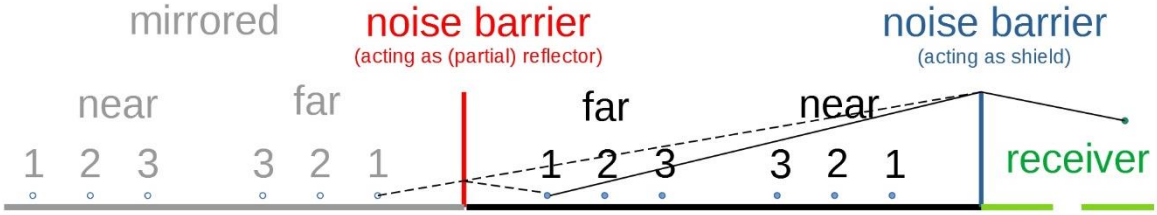


Figure 39: Sketch of the sound propagation from a single source, with two parallel noise barriers, acting as a (partial) reflector (left in red) and as a shield (right in blue)

The influence of the height of the additional noise barrier (in the following referred to as “shielding noise barrier” for simplicity) is shown in Figure 40.

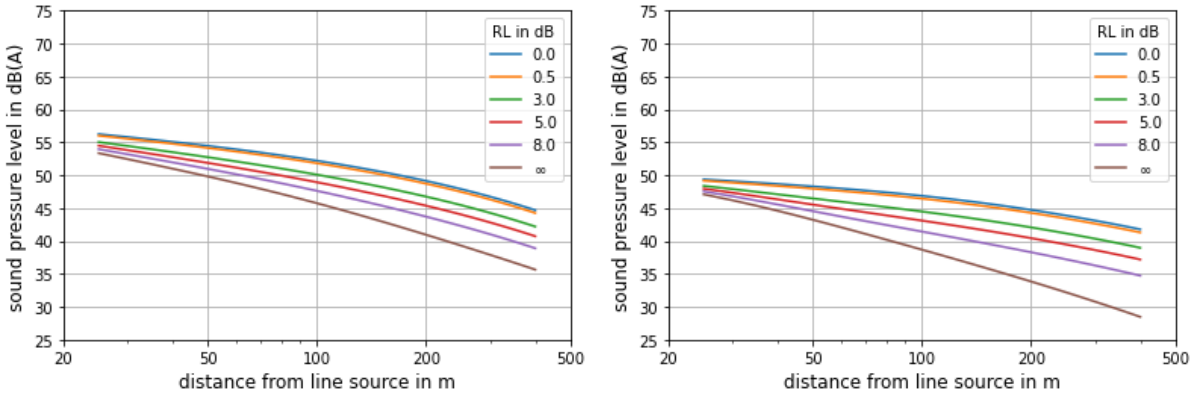


Figure 40: Sound pressure level at distances from 20 m up to 400 m from a line source, at a height of 2.8 m behind a shielding noise barrier of 4 m (left) and 8 m (right) height, with reflection loss of the (reflecting) noise barrier $RL$ as parameter; single traffic lane

Obviously, with increasing height of the shielding noise barrier, the influence of changes in the reflection loss of the (reflecting) noise barrier, e.g. an increasing reflection loss over the barrier’s lifetime due to degradation, is getting more pronounced. In Figure 41 the level differences at a distance of 400 m from a line source in front of the (reflecting) noise barrier are displayed for no shielding noise barrier and for shielding noise barriers with heights of 2 m, 4 m and 8 m, respectively.

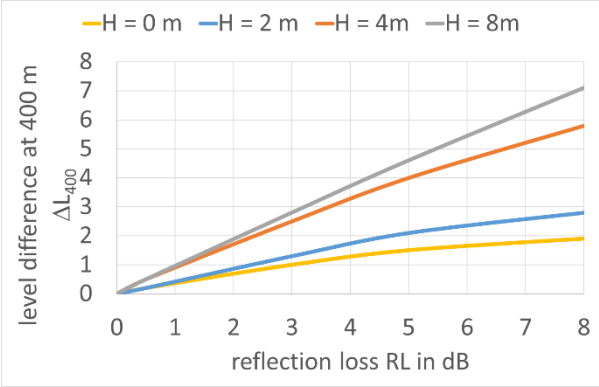


Figure 41: Sound pressure level differences at a distance of 400 m from a line source without shielding noise barrier (orange) or behind a shielding noise barrier of 2 m (blue), 4 m (red) and 8 m (black) height, respectively, with reflexion index of the (reflecting) noise barrier $RL$ as parameter; single traffic lane

Small variations of the reflection loss for large values of *RL* lead to large differences in the sound pressure level. With increasing height of the shielding noise barrier, this tendency is even more pronounced:

**The higher the shielding noise barrier, the more important is a constant high reflection loss over the lifetime of the (reflecting) noise barrier. If a shielding noise barrier is low, a high reflection loss of the (reflecting) noise barrier is not very important and a decrease of *RL* will have a lesser effect on the acoustical performance.**

A decrease of the reflection loss from 8 dB to 5 dB will yield an increase of the immission level at a distance of 400 m by 0.7 dB in the presence of an additional shielding noise barrier with a height of 2 m, and up to 2.5 dB for a shielding noise barrier with a height of 8 m.

### 3.2.2.2 Emission from multiple traffic lanes

A sketch of the geometry with two parallel noise barriers, one acting as a (partial) reflector and one acting as a shield, is shown in Figure 42 for a six-lane motorway. The dependence of the results on the height of a shielding noise barrier is shown in Figure 43.

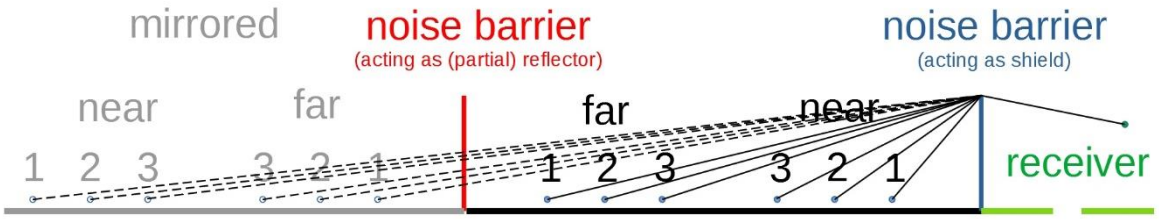


Figure 42: Sketch of the sound propagation from a six-lane motorway, with two parallel noise barriers acting as a (partial) reflector (left in red) and as a shield (right in blue)

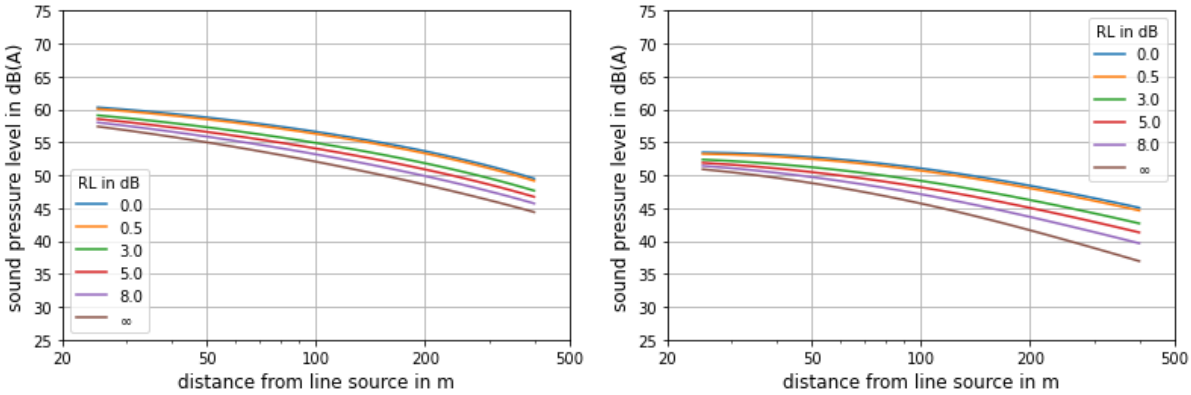


Figure 43: Sound pressure level at distances from 20 m up to 400 m from a line source, at a height of 2.8 m behind a shielding noise barrier of 4 m (left) and 8 m (right) height, with reflection loss of the (reflecting) noise barrier $RL$ as parameter; multiple lanes with traffic distribution

Compared to the situation of a single traffic lane (see Figure 40), for the case with multiple lanes the decay of the immission level with distance is much less. Hence, one can state:

**For broad motorways, the influence of losing reflection loss of a noise barrier during lifetime is less important, but increases with the height of a parallel shielding noise barrier.**

## 3.2.3 Reflections between vehicle bodies and the barrier

In certain circumstances multiple reflections occur between a noise barrier and the body of a vehicle passing by. Along railways this effect is quite common and leads to an additional noise impact. Along motorways in densely populated areas, there is sometimes no or only a small emergency lane. The emergency lane can also be opened temporarily for traffic. In these cases, the space between the vehicle and the noise barrier can be very limited. In particular, articulated lorries – consisting of a tractor unit with a dolly[4] and a semi-trailer – can lead to multiple reflections between the noise barrier and the body of the semi-trailer – especially when the body's surface is acoustically hard. The loudest sound source for these multiple reflections in this case are the near-side traction wheels of the dolly. But also, the other wheels – of the steering axel and of the trailer – give contributions to the overall noise of lorries passing by.

[4] The term "dolly" here means the coupling trailer between the tractor vehicle and the semi-trailer.

### 3.2.3.1 The source model

A typical model of an articulated lorry with a semi-trailer consists of six axels with 16 wheels. The tractor has three axels, one steering axel and two traction axels with twin tyres. The number of wheels of the tractor is ten. The dolly has three trailing axles and six wheels.

Only the six wheels closest to the noise barrier are acoustically relevant for multiple reflections. The far wheels are shielded by the other wheels, the tractor and the dolly. To simplify the model, it can be assumed that the wheels of the two traction axels are the loudest and their position can be combined to one in the middle of both. Further we can assume an omnidirectional radiation of the sound source 0.5 m above the ground.

The position of the sound source of this simple model is marked in Figure 44.

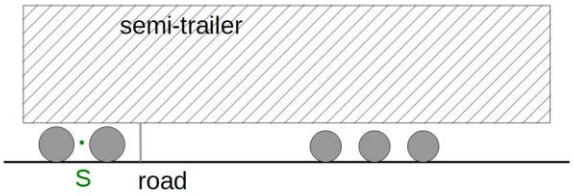


Figure 44: Position of the assumed point source “S” near the traction wheels of the dolly beneath a semi-trailer

The cartesian coordinate system used here has its origin at the position of the point source, but on the road surface, when the truck is nearest to the location of immission. The x-axis is oriented perpendicular to the noise barrier and leads through the immission point. The y-axis is oriented along the road and the z-axis is oriented upwards.

The sound propagation can be calculated by combining the simple method from ISO 9613-2 as in Section 3.1 with a mirror source model. The crucial point in the calculation is to consider the three-dimensional geometry of the sound rays. For this reason, one has to look at the cross-section of the road. In Figure 45 a semi-trailer is standing in front of a noise barrier.

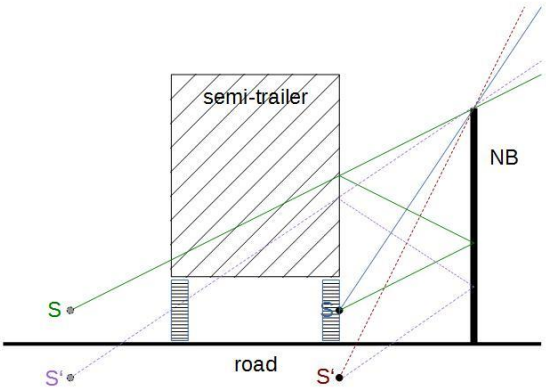


Figure 45: Cross-section of the two-dimensional model - example of multi reflection

In this example there are four sound sources. The first source is the original sound source of the traction wheels at the position [ 0.0 m | 0.0 m | 0.5 m]. The reflection of the original source at the road surface is at the position [ 0.0 m | 0.0 m | -0.5 m]. The remaining two sources are the reflections of the previous ones at the noise barrier. If the perpendicular distance between original sound source and noise barrier is labelled “d”, the coordinates are [ -2 d | 0.0 m | 0.5 m] and [ -2 d | 0.0 m | -0.5 m], respectively.

The semi-trailer is assumed to have a total height of 4 m, for this is the maximum legal height for vehicles on roads in most countries of the world. The acoustically hard body of the semi-trailer is assumed to start at a height of 1 m above the road surface, which presumably is acoustically hard as well. The first 1 m of the noise barrier is normally reflective while the upper part can be more or less absorptive, i.e. more or less non-reflective. The height of the noise barrier can vary, let us say, in the range of 2 m to 6 m.

The height for the noise barrier up to which extra noise in front of the barrier is avoided is 2.25 m, independent of the distance between semi-trailer and noise barrier. This follows directly from the intersection theorem of geometry. The minimum height for the noise barrier to avoid extra noise behind the noise barrier is 5.75 m, also independent of the distance between semi-trailer and noise barrier (see Figure 46).

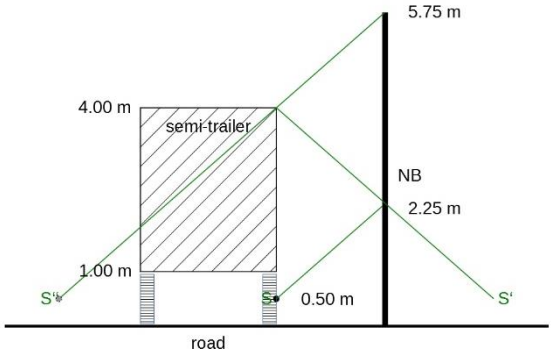


Figure 46: Cross-section of the two-dimensional model - determination of the heights of the noise barrier to avoid extra noise in front and behind the noise barrier from additional reflections

In the first step of the calculations, the positions of all the reflected sound sources are determined. To do so, the zig-zag path of the sound ray being reflected between the semi-trailer and the noise barrier is unfolded and the positions of the mirror sources are calculated. The maximum number of reflections at the semi-trailer is limited to seven, due to the geometry, independent of the distance between semi-trailer and noise barrier.

### 3.2.3.2 Increase of noise behind the noise barrier

Let us consider the case of extra noise behind the noise barrier from reflections at the semi-trailer. The height of the source is given by $h_S = 0.5$ m. The semi-trailer has a height of $h_d = 3.0$ m, starting at 2 $h_S = 1.0$ m above the road surface. With these figures, following geometric considerations, the lower height of the noise barrier, $h_l$, for the sound ray having $N$ reflections at the semi-trailer is

$$h_l = \left(N + \frac{1}{2}\right) \cdot h_S \qquad (17)$$

This equation is valid up to the maximum possible number of reflections, $N_{max} = 7$. If the noise barrier is higher than $h_l$, the number of possible reflections decreases. In this case, the following equation for the upper height of the noise barrier, $h_u$, is valid

$$h_u = \frac{2N + 1}{2N}(h_d + h_S) + h_S \qquad (18)$$

Note that the minimum height of the noise barrier is independent of the height of the semi-trailer, up to a maximum number of seven reflections.

In general, the pass-by sound level (especially for heavy vehicles) depends also on the location of the lorry, as well as its speed and length, thus on the time *t* (see report on Task 5.2).

However, a full description would require too complex simulations: to make life easier, we here consider a line source (not a moving point source) and a two-dimensional cross section.

In Table 5 the lower and upper height of the noise barrier is given for different numbers of reflections on the semi-trailer.

Table 5: Lower and upper height of the noise barrier, regarding the number of reflections on the semi-trailer

| $N$ | $h_l$ in m | $h_u$ in m |
|---|---|---|
| 1 | 0.75 | 5.75 |
| 2 | 1.25 | 4.875 |
| 3 | 1.75 | 4.583 |
| 4 | 2.25 | 4.437 |
| 5 | 2.75 | 4.35 |
| 6 | 3.25 | 4.292 |
| 7 | 3.75 | 4.25 |

From this table it is possible to determine the possible reflections at the semi-trailer for a given height, $h$, of the noise barrier, see Figure 47.

The result is a step function for the number of reflections

$$N = \begin{cases} 0 & if \quad h < 0.75\ m \\ \left\lfloor \frac{h}{h_S} - \frac{1}{2} \right\rfloor & if \quad 0.75\ m \le h < 4.25\ m \\ \left\lfloor \frac{1}{2} \cdot \frac{h_d + h_S}{h - 2h_S - h_d} \right\rfloor & if \quad 4.25\ m \le h < 5.75\ m \\ 0 & if \quad 5.75\ m \le h \end{cases}$$

Where the brackets ⌊ ⌋ denote the floor function e.g. it rounds down to the next integer.

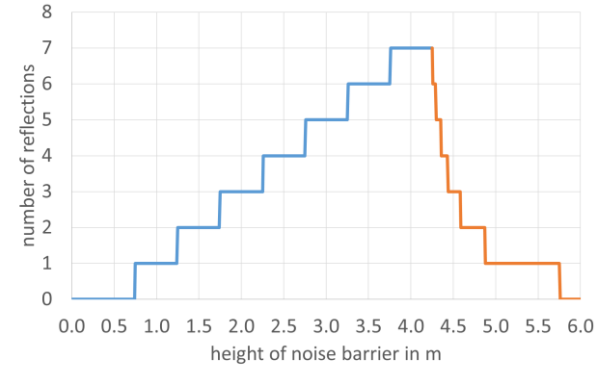


Figure 47: Number of possible reflections at the semi-trailer for a given height of the noise barrier: lower height in blue and upper height in orange

The maximum number of reflections at the semi-trailer occurs, when the height of the noise barrier is as high as the semi-trailer plus twice the height of the source, which corresponds to the total height of the lorry, i.e. 4 m. Each reflection at the semi-trailer is assumed to decrease the sound pressure level of the mirror source by an amount of 0.5 dB.

#### 3.2.3.2.1 Emission from a single traffic lane

In Figure 48 the sound maps for the fully reflective case ($RL = 0$, left) and without reflections ($RL = \infty$, right) for a noise barrier height of 4 m, for which the number of reflections at the semi-trailer is maximal, are shown.

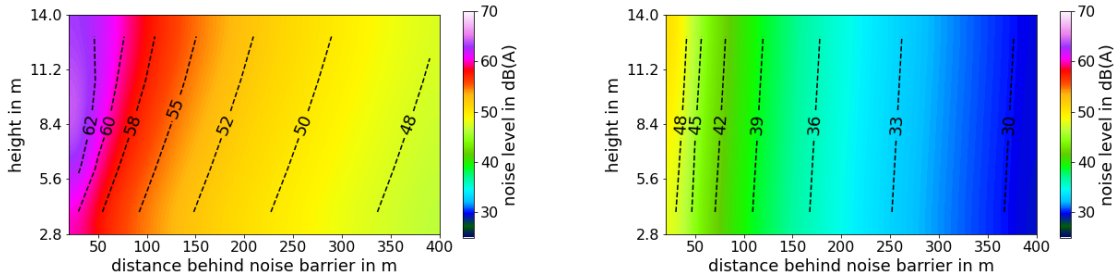


Figure 48: Sound maps at distances from 20 m up to 400 m from a line source, and at heights from 2.8 up to 14.0 m behind a noise barrier of 4 m height, multi-reflected at a semi-trailer; single lane; left: fully reflective ($RL = 0$), right: without reflections ($RL = \infty$)

In Figure 49 the results from the calculations for different values of RL for a height of 2.8 m (base line in Figure 48) are shown.

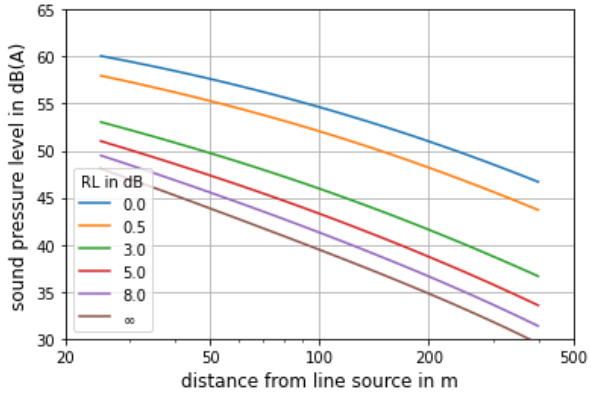


Figure 49: Sound pressure level at distances from 20 m up to 400 m from a line source, at a height of 2.8 m behind a noise barrier of 4 m height, multi-reflected at a semi-trailer, with reflection loss of the noise barrier, $RL$, as parameter; single traffic lane

The biggest influence on the sound pressure level behind a noise barrier from multiple reflections can be seen for a barrier height of around 4 m and increases with decreasing reflection loss.

The levels and level differences at 400 m distance from the source line compared to an (theoretical) infinite reflection loss are listed in Table 6 for a noise barrier with a height of 4 m.

Table 6: Results from propagation calculations for a single line source, 400 m behind a noise barrier of 4 m height, multi-reflected at a semi-trailer

| $RL$ in dB | $\rho$ | $L_{400}$ in dB(A) | $\Delta L_{400}$ in dB |
|---|---|---|---|
| ∞ | 0.0 | 29.5 | 0.0 |
| 8.0 | 0.2 | 31.3 | 1.8 |
| 5.0 | 0.3 | 33.5 | 4.0 |
| 3.0 | 0.5 | 36.6 | 7.1 |
| 0.5 | 0.9 | 43.7 | 14.2 |
| 0.0 | 1.0 | 46.7 | 17.2 |

In Figure 50 and Figure 51, the sound maps and sound pressure levels, respectively, are shown for the case of a noise barrier with a height of 3 m as well as for a noise barrier height of 5 m.

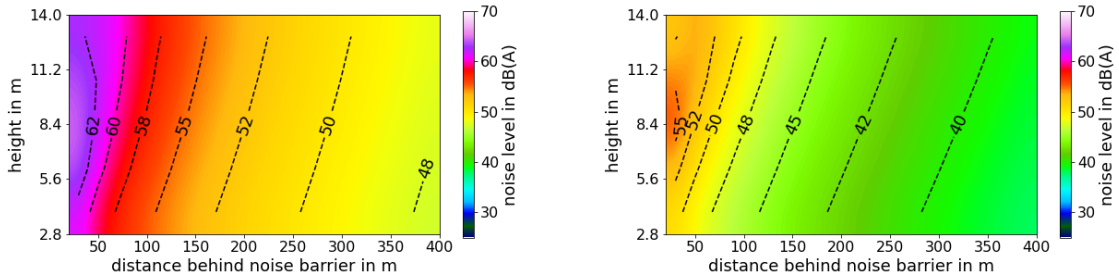


Figure 50: Sound maps at distances from 20 m up to 400 m from a line source, and at heights from 2.8 up to 14.0 m behind a noise barrier of zero reflection loss, multi-reflected at a semi-trailer; single traffic lane; left: height of noise barrier 3 m, right: height of noise barrier 5 m

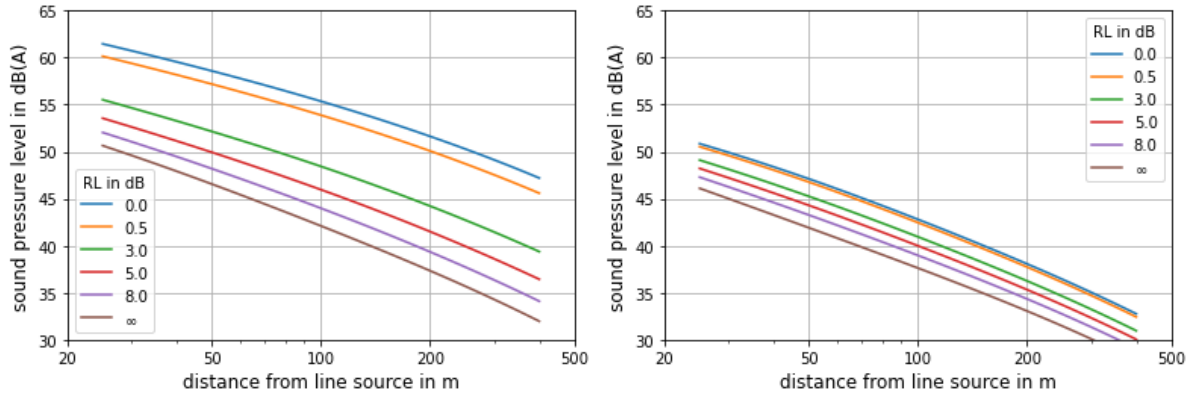


Figure 51: Sound pressure level at distances from 20 m up to 400 m from a line source, at a height of 2.8 m behind a noise barrier of 3 m height (left), and 5 m height (right), respectively, multi-reflected at a semi-trailer, with reflection loss of the noise barrier, $RL$, as parameter; single lane

For a noise barrier of 3 m height, the sound pressure level is only slightly higher than for a noise barrier with a height of 4 m. The number of possible reflections decreases from seven to five but the shielding effect increases as well. For a noise barrier of 5 m there are only two possible reflections. Therefore, and because of the better shielding ability, the sound pressure level decreases substantially. Furthermore, the dependency on the reflection loss decreases, because the number of possible reflections is low.

In Figure 52 the sound pressure level differences at 400 m from a line source behind a noise barrier are shown as a function of reflection loss.

**The difference in sound pressure level behind the noise barrier (shielded zone) increases approximately linearly with decreasing reflection loss, down to a value of about 3 dB.**

**Under the assumptions of the model presented here, the dependency of the level differences on the reflection loss in a great distance to the noise barrier is highest, when the height of the noise barrier is comparable to the height of the lorry; because in this case the number of reflections reaches its maximum of seven.**

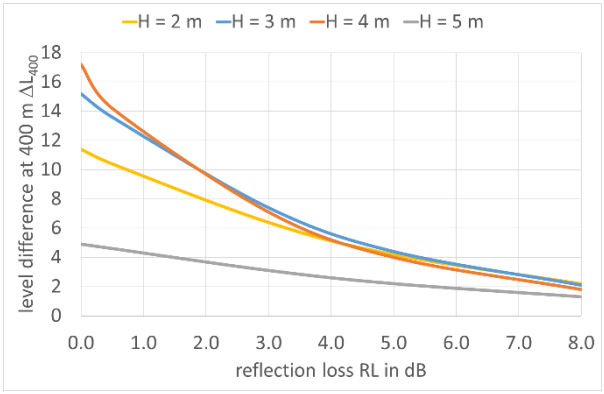


Figure 52: Sound pressure level differences at a distance of 400 m from a line source behind a noise barrier, of 2.00 m (yellow), 3.00 m (blue), 4 m (red), and 5 m (black) height, respectively, with reflection loss of noise barrier, $RL$, as parameter; single traffic lane

#### 3.2.3.2.2 Emission from multiple traffic lanes

For the calculation of the propagation of the emission from multiple lanes, the traffic distribution from section 3.1.2 is used. On the first lane, for heavy lorries multiple reflections from the position of the wheels nearest to the wall are assumed (see Figure 45), while for the rest of the traffic sources, as before, the centre of the lanes is used as emission position.

The sound maps (height-dependent) and the sound pressure level at a height of 2.8 m for a noise barrier of 4 m height are shown in Figure 53 and Figure 54, respectively.

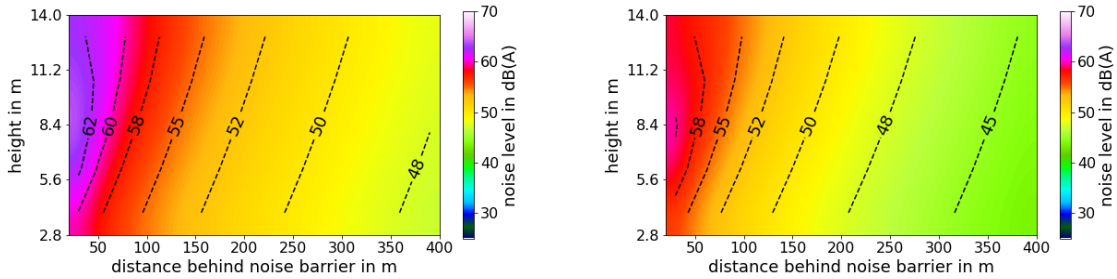


Figure 53: Sound maps at distances from 20 m up to 400 m from a line source, and at heights from 2.8 up to 14.0 m behind a noise barrier of 4 m height, multi-reflected at a semi-trailer; multiple lanes with traffic distribution; left: fully reflective ($RL = 0$), right: without reflections ($RL = \infty$)

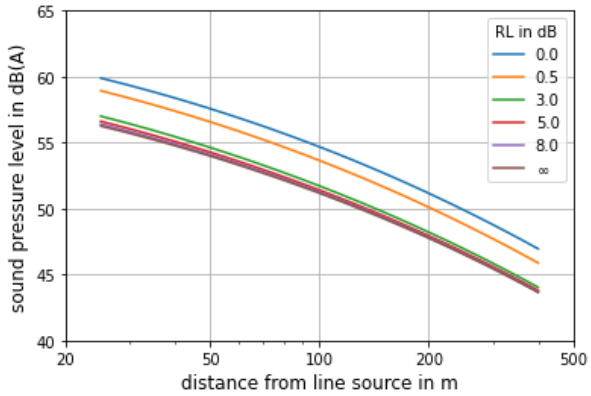


Figure 54: Sound pressure level at distances from 20 m up to 400 m from a line source, at a height of 2.8 m behind a noise barrier of 4 m height, multi-reflected at a semi-trailer, with reflection loss of the noise barrier, $RL$, as parameter; multiple lanes with traffic distribution

Compared to the results presented in Figure 49, the spread of the levels with different values for RL is much lower for the situation of multiple lanes with traffic distribution.

The level and level differences at 400 m distance from the source line closest to the noise barrier compared to an (theoretical) infinite reflection loss are listed in Table 7.

Table 7: Results from propagation calculations from multiple line sources, 400 m behind a noise barrier of 4 m height, multi-reflected at a semi-trailer

| $RL$ in dB | $\rho$ | $L_{400}$ in dB(A) | $\Delta L_{400}$ in dB |
|---|---|---|---|
| ∞ | 0.0 | 43.6 | 0.0 |
| 8.0 | 0.2 | 43.7 | 0.1 |
| 5.0 | 0.3 | 43.8 | 0.2 |
| 3.0 | 0.5 | 44.0 | 0.4 |
| 0.5 | 0.9 | 45.9 | 2.3 |
| 0.0 | 1.0 | 46.9 | 3.3 |

In Figure 55 and Figure 56 the sound maps and levels are shown for the cases of a noise barrier with a height of 3 m and 5 m.

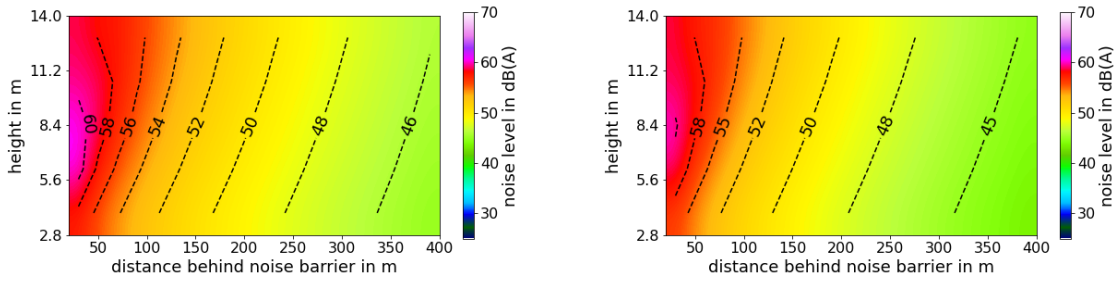


Figure 55: Sound maps at distances from 20 m up to 400 m from a line source, and at heights from 2.8 up to 14.0 m behind a noise barrier of zero reflection loss, multi-reflected at a semi-trailer; multiple lanes with traffic distribution; left: height of noise barrier 3 m, right: height of noise barrier 5 m

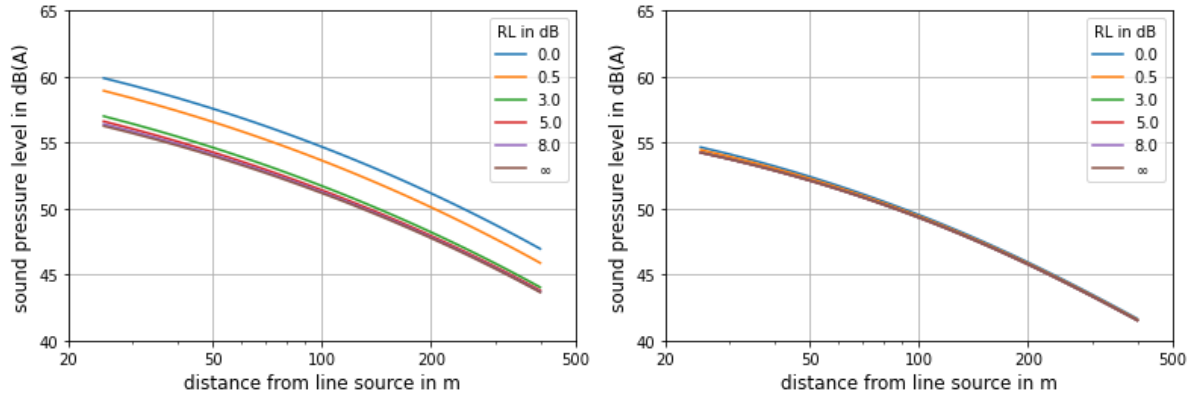


Figure 56: Sound pressure level at distances from 20 m up to 400 m from a line source, at a height of 2.8 m behind a noise barrier of 3 m height (left), and 5 m height (right), respectively, multi-reflected at a semi-trailer, with reflection loss of the noise barrier, $RL$, as parameter; multiple lanes with traffic distribution

For a noise barrier of 3 m height, the influence of the reflection loss is slightly smaller than for a barrier height of 4 m. This behaviour is even more pronounced for broad motorways. For a

noise barrier of 5 m height, the small dependence on the reflection loss vanishes nearly completely: the other line sources from the traffic distribution are much louder than the additional contribution from multiple reflections between semi-trailer and noise barrier.

**For real traffic distributions on broad motorways, reflections between noise barrier and lorry have a lower effect on the sound pressure level behind the noise barrier: only highly reflecting noise barriers have a noteworthy effect on the noise level behind the noise barrier (shielded zone).**

#### 3.2.3.3 Increase of noise in front of the noise barrier

In section 3.2.1 the effect of reflection loss on the acoustical performance in front of a single noise barrier is examined. In the following, the case of extra noise in front of the noise barrier from reflections at the semi-trailer is considered. Following the same calculations as before, it is also possible to determine the number of reflections on the semi-trailer, for a noise barrier of a given height.

If the height of the noise barrier is less than 2.25 m, there are no reflections possible (see section 3.2.3.1). If the height of the noise barrier is 3.75 m or more, exactly six reflections will occur on the semi-trailer. Between both limits, there is always a certain number of reflections on the semi-trailer possible.

The height limit $h_o$, depending on the number of possible reflections, is

$$h_o = \frac{2N-1}{2N}(h_d + h_S) + h_S \qquad (19)$$

In Table 8, $h_o$ is given for different numbers of reflections on the semi-trailer.

Table 8: Height limit $h_o$ of the noise barrier, regarding the number of possible reflections on the semi-trailer

| $N$ | $h_o$ in m |
|---|---|
| 1 | 2.25 |
| 2 | 3.125 |
| 3 | 3.417 |
| 4 | 3.563 |
| 5 | 3.65 |
| 6 | 3.708 |
| 7 | 3.75 |

From this table, it is possible to determine the possible reflections at the semi-trailer for a given height, $h$, of the noise barrier, see Figure 57.

The result is a step function for the number of possible reflections

$$N = \begin{cases} 0 & if \quad h < 2.25\ m \\ \left\lfloor \frac{1}{2} \cdot \frac{h_d + h_S}{h - 2h_S - h_d} \right\rfloor & if \quad 2.25\ m \le h < 3.75\ m \\ 0 & if \quad 3.75\ m \le h \end{cases}$$

Where the brackets ⌊ ⌋ again denote the floor function e.g. it rounds down to the next integer.

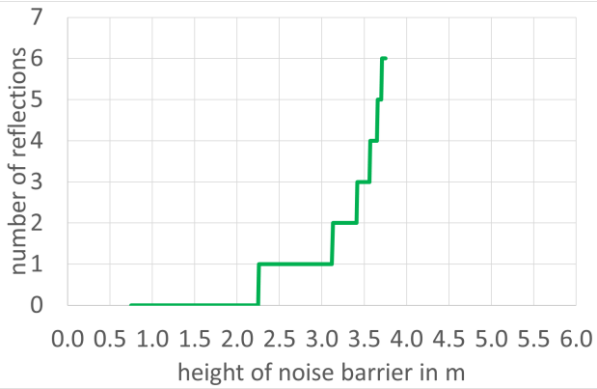


Figure 57: Number of possible reflections at the semi-trailer for a given height of the noise barrier

The maximum number of reflections at the semi-trailer occurs, when the height of the noise barrier is as high as the semi-trailer the height of the source, which is the total height of the lorry, 3.75 m. Each reflection at the semi-trailer is assumed to decrease the sound pressure level of the mirror source by an amount of 0.5 dB.

The possible number of reflections can be read from the green curve in Figure 57 for different heights of the noise barrier.

#### *3.2.3.3.1 Emission from a single lane*

The result of the calculation of the propagation of the emission from a single lane for the case of a noise barrier of 3.75 m height is shown in Figure 58.

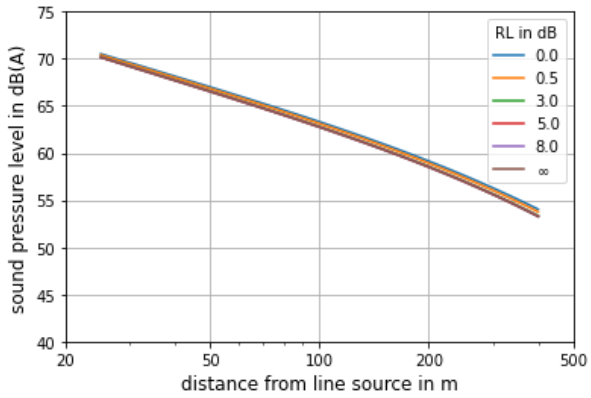


Figure 58: Sound pressure level at distances from 20 m up to 400 m from a line source, at a height of 2.8 m in front of a noise barrier of 3.75 m height, multi-reflected at a semi-trailer, with reflection loss of the noise barrier, $RL$, as parameter; single lane

In contrast to the propagation with a line source behind a noise barrier (see Figure 49) there is nearly no dependency on the reflection loss. The level divergence at 400 m distance from the line source is only 0.7 dB for zero to full reflection loss.

#### *3.2.3.3.2 Emission from multiple lanes*

The same calculations as for a single source can be done for a six-lane motorway as well. But In the situation of multiple lanes with distributed traffic on a broad motorway, the level difference shown in Figure 58 of section 3.2.3.3.2 will be even smaller, and therefore negligible. We can conclude:

**Regarding multiple reflections between semi-trailer and noise barrier, the influence of the reflection loss in front of a noise barrier (unshielded zone) is negligible.**

# 4 Summary and conclusion

In this report a theoretical description has been presented to understand and model the effect of common simple sound leaks on the sound insulation of noise barriers. The approach consists of two major parts: on the one hand, the dependence of the degree of transmission on the characteristics of the leak is derived using the model by Mechel. On the other hand, extended sound field simulations are used to calculate the reduction of the sound insulation index due to the presence of a leak with a given transmission coefficient.

From the latter, as a qualitative measure the so-called criticality condition $\xi$ is introduced, which defines a critical area behind the damaged barrier. In this area the influence of the leak is significant and relevant, whereas beyond this area the effect due to the leak is negligible.

By variation of relevant model parameters – e.g. transmission, leak surface area or width, average leak height and barrier height – a systematic batch of calculations can be carried out for round and rectangular leaks. Such a catalogue of leaks, mainly based on geometrical parameters, can serve as first practical tool for the evaluation of simple leaks. Depending on the respective area of application, an individual catalogue can be created, which covers the relevant leak types and dimensions.

In combination, the two approaches allow a good prediction of the consequences of a leak for the overall acoustic performance of a barrier: With the model by Mechel a detailed determination of the transmission of a leak (considering its filling and the character of its openings) can be carried out, which then serves as an input for the extended sound field simulations. However, regarding the inspection procedure developed in WP 3.2 and the goal to establish a simple *in-situ* assessment via visual and aural inspection, the application of Mechel's model is not suitable. In practice, a significant statement about the noise barrier's condition can be obtained via the extended sound field simulations by simply assuming a worst-case transmission. This will be discussed in more detail in WP 3.2.

The theoretical model and exemplary calculations of the radius of influence for different leak characteristics constitute the first step to relate changes in the intrinsic properties of noise barriers to changes of the overall acoustic performance; and will serve as a basis for the acoustic assessment implemented in the inspection procedure presented in WP 3.2.

In the second part of the report, a more global model has been applied to investigate the effect of the intrinsic properties of noise barriers on the sound immission level behind and in front of the noise barrier. From the calculations with a simple sound propagation model we can conclude, that the effect of losing transmission loss of noise barriers (e.g. due to aging or caused by small holes and slits) can be regarded as minor problem far away from a noise barrier of moderate height. However, for high noise barriers, changes of the transmission loss can cause a serious problem, also far away from the noise barrier. The higher the noise barrier, the more important is a constant high transmission loss over the lifetime of the noise barrier. If a noise barrier is low, a high transmission loss is not essential, and a decrease will not strongly affect the acoustical performance of the noise barrier.

Similarly, for broad motorways, small holes and slits in a noise barrier are a minor problem far away from a noise barrier of moderate height. If shielded by a noise barrier, the effect of losing acoustical efficiency due to a reduction of its transmission loss is not as pronounced as for small roads, but also substantially high. On the other hand, in the case of high noise barriers, small holes and slits have to be considered as a relevant problem far away from the barrier, even for broad motorways.

The consequences of degradations in the reflection loss of a noise barrier for its overall acoustical performance are also essential. The investigations show that with decreasing reflection loss, the level in front of the noise barrier is increasing. This increase can amount to

a maximum value of 3 dB in the limit of infinite distance of the receiver (doubling of the noise source), For multiple traffic lanes this behaviour is comparable.

In the presence of an additional noise barrier, acting as a full shield, the height of this shielding noise barrier also plays a role. The higher the additional shielding noise barrier on the other side of the road (in parallel to the original noise barrier, which acts as a (partial) reflector), the more important is a constant high reflection loss over the lifetime of the original noise barrier. In other words, if the shielding noise barrier is low, a high reflection loss of the original noise barrier is of lesser importance and a decrease of RL will not have a significant effect on its acoustical performance. Regarding multiple lanes (e.g. broad motorways), the model has shown that the influence of a diminishing reflection loss over time is less, but gains importance with increasing height of a shielding noise barrier.

Further scenario calculations show that the special case of *multiple reflections* between the semi-trailer of an articulated lorry and the noise barrier can lead to significant effects under certain conditions. In general, the pass-by sound level (especially for heavy vehicles) depends also on the temporal and the spectral dimensions (time *t* and frequency *f*).

From simple geometrical considerations, it can be concluded that a noise barrier of 5.75 m or higher has no additional effect (due to the multiple reflections) on the sound immission **behind** the noise barrier (shielded zone), whatever its reflection loss is. This result is independent of the distance between lorry and noise barrier. Moreover, it follows that if the noise barrier is lower than 2.25 m, the sound immission level **in front** (unshielded zone) of the barrier is not influenced by this kind of multiple reflections.

On the other hand, further calculations show that the difference in sound pressure level in the far field **behind** the barrier (shielded zone) increases approximately linearly with decreasing reflection loss, down to a value of about 3 dB. If the noise barrier is of comparable height with the semi-trailer, the reflection loss of the noise barrier will be relevant for the sound pressure level **behind** the noise barrier (shielded zone). Considering multiple lanes, reflections between noise barrier and lorries have a lower effect on the sound pressure level **behind** the noise barrier: only noise barriers with low reflection loss (as the usual *sound reflective barriers* are) have a noteworthy effect on the noise level **behind** the noise barrier (shielded zone).

In both cases (single lane and multiple lanes) the effect of reflections between noise barrier and lorries on the sound pressure level **in front** of the noise barrier (unshielded zone) is negligible. In general, the investigations on the interplay between the intrinsic barrier properties and the sound immission level behind and in front of the noise barrier have shown which scenarios are acoustically relevant in the case of damaged or aged barrier conditions. This helps to classify possible performance losses throughout the barrier's lifetime.

# 5 References


[1] P. Lindner, B. Hartmann, C. Schulze and J. Hübelt, “Akustische Wirksamkeit alter Lärmschutzwände (Acoustic effectivity of old noise barriers),” Berichte der Bundesanstalt für Straßenwesen - Heft V 316, Bergisch Gladbach, 2019.

[2] F. Sgard, H. Nelisse and N. Atalla, “On the modeling of the diffuse field sound transmission loss of finite thickness apertures,” *Journal of the Acoustical Society of America,* 2007.

[3] G. P. Wilson and W. W. Soroka, “Approximation to the Diffraction of Sound by a Circular Aperture in a Rigid Wall of Finite Thickness,” *Journal of the Acoustical Society of America,* 1965.

[4] A. Sauter and W. W. Soroka, “Sound transmission through rectangular slots of finite depth between reverberant rooms,” *Journal of the Acoustical Society of America,* 1970.

[5] F. P. Mechel, “The acoustic sealing of holes and slits in walls,” *Journal of Sound and Vibration,* 1986.

[6] C. C. Harrison, K. R. Fyfe and L. J. Cremers, “Insertion loss characteristics of barriers and berms,” *Journal of the Canadian Acoustical Association,* 1994.

[7] G. Watts, “Effects of sound leakage through noise barriers on screening performance,” *Applied Acoustics,* 1997.

[8] H. Y. Wong and K. M. Li, “Prediction models for sound leakage through noise barriers,” *Journal of the Acoustical Society of America,* 2000.

[9] P. Liu, S.-H. Chen and C.-Y. Wu, “Evaluation of effects of noise barrier defects on their noise reduction efficiencies,” *Joint International Conference on Computing and Decision Making in Civil and Building Engineering,* 2006.

[10] FHWA, U.S. Departement of Transportation, *FHWA Traffic Noise Model, Technical Manual,* 1998.

[11] M. Pfister, M. Gröschl, P. Reiter, R. Wehr and M. Conter, “Impact of gaps on in situ airborne sound insulation,” *Conference: 6th Congress of Alps-Adria Acoustics Assosiation,* 2014.

[12] P. Reiter, Evaluation of Noise Barriers (phD thesis), Vienna, 2018.

[13] Bundesminister für Verkehr, *RLS-90 - Richtlinien für den Lärmschutz an Straßen (Guidelines for the noise protection at roads), Ausgabe 1990, Berichtigter Nachdruck,* 1992.

[14] ISO 9613-2:1996, *Attenuation of sound during propagation outdoors - Part 2: General method of calculation,* 1997.

[15] EN 1793-3:1997, *Road traffic noise reducing devices - Test method for determining the acoustic performance - Part 3: Normalised traffic noise spectrum,* 1997.

[16] EN 1793-5:2016+AC:2018, *Road traffic noise reducing devices - Test method for determining the acoustic performance - Part 5: Intrinsic characteristics - In situ values of sound reflection under direct sound field conditions,* 2018.

[17] EN 1793-6:2018, *Road traffic noise reducing devices - Test method for determining the acoustic performance - Part 6: In situ values of airborne sound insulation under direct sound field conditions,* 2018.

[18] ZTV Lsw-06, *Zusätzliche technische Vertragsbedingungen und Richtlinien für die Ausführung von Lärmschutzwänden an Straßen (Additional technical conditions of contract and guidelines for the construction of noise barriers along roads),* Cologne: FGSV-Verlag, 2006.